



RESEARCH & DEVELOPMENT

Performance Evaluation of 29-inch and 31-inch W-beam Guardrails on Six-lane, 46-foot Median Divided Freeways

**Howie Fang, Ph.D.
Matthew Gutowski
Emre Palta
Daniil Kuvilla
Ryan Baker
Ning Li**

**Department of Mechanical Engineering & Engineering Science
The University of North Carolina at Charlotte
9201 University City Boulevard
Charlotte, NC 28223-0001**

**NCDOT Project 2014-14
FHWA/NC/2014-14
December 2015**

Technical Report Documentation Page

1. Report No. FHWA/NC/2014-14	2. Government Accession No.	3. Recipient's Catalog No.	
4. Title and Subtitle Performance Evaluation of 29-inch and 31-inch W-beam Guardrails on Six-lane, 46-foot Median Divided Freeways		5. Report Date February 18, 2015	
		6. Performing Organization Code	
7. Author(s) Howie Fang, Matthew Gutowski, Emre Palta, Daniil Kuvila, Ryan Baker, Ning Li		8. Performing Organization Report No.	
9. Performing Organization Name and Address The University of North Carolina at Charlotte 9201 University City Boulevard Charlotte, NC 28223-0001		10. Work Unit No. (TRAIS)	
		11. Contract or Grant No.	
12. Sponsoring Agency Name and Address North Carolina Department of Transportation Research and Analysis Group 1 South Wilmington Street Raleigh, North Carolina 27601		13. Type of Report and Period Covered Final Report 08/16/2013 – 11/30/2015	
		14. Sponsoring Agency Code 2014-14	
Supplementary Notes:			
<p>16. Abstract</p> <p><i>This report summarizes the research efforts of using finite element modeling and simulations to evaluate the performance of single-faced and double-faced NCDOT W-beam guardrails for different heights under MASH Test Level 3 (TL-3) impact conditions. A literature review is included on performance evaluation of W-beam guardrails as well as applications of finite element modeling and simulations in roadside safety research.</i></p> <p><i>The modeling and simulation work was conducted on fourteen single-faced and double-faced NCDOT W-beam guardrails (with placement heights of 29 and 31 inches) placed along a six-lane 46-foot median divided highway with 2.5H:1V and 4H:1V slopes. The single-faced guardrails were also evaluated with a horizontal median curvature of three degrees and the double-faced guardrails were also modeled and evaluated with a lower backside rail. The guardrails with 29- and 31-inch placement heights were impacted by a 1996 Dodge Neon and a 2006 Ford F250 at 62 mph (100 km/hour) and an impact angle of 25°. Two additional Dodge Neon simulations, one at each guardrail height (i.e., 29 and 31 inches), evaluated the single-faced guardrail without horizontal curvature with an impact speed of 70 mph (112.6 km/hour). The guardrails performance was determined by evaluating the vehicular responses based on MASH exit-box criterion, MASH evaluation criterion F, exit angles, yaw, pitch, and roll angles, transverse displacements, and transverse velocities.</i></p> <p><i>The simulation results demonstrated the effectiveness of the 29- and 31-inch single-faced and double-faced guardrails placed on a median divided freeway under MASH TL-3 impact conditions. Under small angle vehicular impacts (i.e., 25°), the guardrails with 29- and 31-inch placement heights were shown to be effective at retaining the impact vehicle but exhibited a high likelihood for tire snagging and vehicle spin-out. Finite element modeling and simulations were shown to be both effective and efficient and can be used to study crash scenarios that are difficult and/or extremely expensive to conduct with physical crash testing.</i></p>			
17. Key Words <i>W-beam; Sloped median; Horizontal curvature; Concave; Convex; Single-faced; Double-faced; Median barrier; Barrier height; 29-inch; 31-inch; Roadside safety; Highway safety; Finite element method</i>		18. Distribution Statement	
19. Security Classif. (of this report) Unclassified	20. Security Classif. (of this page) Unclassified	21. No. of Pages 141	22. Price

DISCLAIMER

The contents of this report reflect the views of the authors and not necessarily the views of the university. The authors are responsible for the facts and the accuracy of the data presented herein. The contents do not necessarily reflect the official views or policies of either the North Carolina Department of Transportation or the Federal Highway Administration. This report does not constitute a standard, specification, or regulation.

ACKNOWLEDGMENTS

This study was supported by the North Carolina Department of Transportation (NCDOT) under Project No. 2014-14. The authors would like to thank NCDOT personnel from the *Roadway Design Unit, Transportation Mobility & Safety, Highway Division 5, Project Standards and Development Unit, FHWA – NC Division, and Research and Development Unit* for the support and cooperation during the grant period.

EXECUTIVE SUMMARY

This report summarizes the research efforts of using finite element modeling and simulations to evaluate the performance of single-faced and double-faced NCDOT W-beam guardrails for different heights under MASH Test Level 3 (TL-3) impact conditions. A literature review is included on performance evaluation of W-beam guardrails as well as applications of finite element modeling and simulations in roadside safety research.

The modeling and simulation work was conducted on fourteen single-faced and double-faced NCDOT W-beam guardrails (with placement heights of 29 and 31 inches) placed along a six-lane 46-foot median divided freeway with 2.5H:1V and 4H:1V slopes. The single-faced guardrails were also evaluated with a horizontal median curvature of three degrees and the double-faced guardrails were also modeled and evaluated with a lowered backside rail. The guardrails with 29- and 31-inch placement heights were impacted by a 1996 Dodge Neon and a 2006 Ford F250 at 62 mph (100 km/hour) and an impact angle of 25°. Two additional Dodge Neon simulations, one at each guardrail height (i.e., 29 and 31 inches), evaluated the single-faced guardrail without horizontal curvature with an impact speed of 70 mph (112.6 km/hour). The guardrails performance was determined by evaluating the vehicular responses based on MASH exit-box criterion, MASH evaluation criterion F, exit angles, yaw, pitch, and roll angles, transverse displacements, and transverse velocities.

The simulation results demonstrated the effectiveness of the 29- and 31-inch single-faced and double-faced guardrails placed on a freeway median slope under MASH TL-3 impact conditions. Under small angle vehicular impacts (i.e., 25°), the guardrails with 29- and 31-inch placement heights were shown to be effective at retaining the impact vehicle but exhibited a high likelihood for tire snagging and vehicle spin-out. Finite element modeling and simulations were shown to be both effective and efficient and can be used to study crash scenarios that are difficult and/or extremely expensive to conduct with physical crash testing.

TABLE OF CONTENTS

Title Page	i
Technical Report Documentation Page	ii
Disclaimer	iii
Acknowledgments	iv
Executive Summary	v
Table of Contents	vi
List of Tables	vii
List of Figures	viii
1. Introduction	1
1.1 Background	1
1.2 Research Objectives and Tasks	2
2. Literature Review	6
2.1 Performance Evaluation of W-beam Guardrails	6
2.2 Crash Modeling and Simulations	14
3. Finite Element Modeling of Vehicles and W-beam Guardrails	22
3.1 FE Models of a Passenger Car and Pickup Truck	22
3.2 FE Model of the W-beam Guardrails	23
3.3 Simulation Setup	28
4. Simulation Results and Analysis	32
4.1 Case 1: Single-faced Guardrail Placed on a 2.5H:1V Slope	33
4.2 Case 2: Double-faced Guardrail Placed on a 2.5H:1V Slope.....	46
4.3 Case 3: Lowered Backside Double-faced Guardrail Placed on a 2.5H:1V Slope.....	66
4.4 Case 4: Single-faced Guardrail with Convex Horizontal Curvature Placed on a 2.5H:1V Slope.....	86
4.5 Case 5: Single-faced Guardrail with Concave Horizontal Curvature Placed on a 4H:1V Slope.....	97
4.6 Comparison of 29-inch and 31-inch Guardrail Splice Location	109
5. Findings and Conclusions	113
6. Recommendations	116
7. Implementation and Technology Transfer Plan	117
References	118

List of Tables

Table 3.1: Specifications of the two test vehicles used in crash simulations

Table 3.2: Simulation conditions for all cases

Table 4.1: The exit-box criterion defined in MASH

Table 4.2: Exit-box dimensions for the test vehicles of this project

Table 4.3: Simulation results of Case 1 (Single-faced Guardrail Placed on a 2.5H:1V Slope)

Table 4.4: Simulation results of Case 2 (double-faced guardrail placed on a 2.5H:1V slope)

Table 4.5: Simulation results of Case 3 (lowered backside double-faced guardrail placed on a 2.5H:1V slope)

Table 4.6: Simulation results of Case 4 (Single-faced Guardrail with Convex Horizontal Curvature Placed on a 2.5H:1V Slope)

Table 4.7: Simulation results of Case 5 (Single-faced Guardrail with Concave Horizontal Curvature Placed on a 4H:1V Slope)

Table 4.8: Vehicle redirection characteristics of single-faced guardrails with and without horizontal curvature

Table 4.9: Vehicle redirection characteristics of front-side impacts on double-faced guardrails

Table 4.10: Vehicle redirection characteristics of backside impacts on double-faced guardrails

List of Figures

Fig. 1.1: A strong-post W-beam guardrail.

Fig. 1.2: Two lines of single-faced W-beam guardrails.

Fig. 1.3: A double-faced W-beam guardrail.

Fig. 1.4: FE models of a G4(1S) guardrail, a small passenger car, and a large pickup truck.

Fig. 1.5: FE model of a single-faced W-beam guardrail placed on the shoulder near the 2.5H:1V slope and impacted by a Ford F250.

Fig. 1.6: Front-side impact on a 46-foot sloped median with 29- and 31-inch single-faced guardrails installed on a 2.5H:1V slope.

Fig. 1.7: Definition of vehicle responses.

Fig. 1.8: Front-side and backside impact on a 46-foot sloped median with 29- and 31-inch double-faced guardrails installed on a 2.5H:1V slope.

Fig. 1.9: Front-side impact on a 46-foot sloped median with horizontal curvature with 29- and 31-inch single-faced guardrails installed on a 2.5H:1V (convex curvature) and 4H:1V (concave curvature) slopes.

Fig. 3.1: FE models of the two vehicles used in crash simulations.

Fig. 3.2: FE models of the soil block around a post.

Fig. 3.3: Short-bolts on a guardrail splice.

Fig. 3.4: Splice locations for the 29- and 31-inch guardrails in the FE models.

Fig. 3.5: Profile views of the single- and double-faced guardrail FE models.

Fig. 3.6: FE model of the single-faced guardrail installed on a 2.5H:1V slope.

Fig. 3.7: FE model of the double-faced guardrail installed on a 2.5H:1V slope.

Fig. 3.8: FE model of the lowered backside double-faced guardrail installed on a 2.5H:1V slope.

Fig. 3.9: FE model of a single-faced guardrail with convex horizontal curvature installed on a 2.5H:1V slope.

Fig. 3.10: FE model of a single-faced guardrail with concave horizontal curvature installed on a 4H:1V slope.

Fig. 3.11: FE model of a front-side impact on a single-faced W-beam guardrail placed on a 2.5H:1V slope and impacted by a Ford F250.

Fig. 3.12: FE model of a front-side impact on a double-faced W-beam guardrail placed on a 2.5H:1V slope and impacted by a Ford F250.

Fig. 3.13: FE model of a backside impact on a double-faced W-beam guardrail placed on a 2.5H:1V slope and impacted by a Ford F250.

Fig. 3.14: FE model of a front-side impact on a lowered backside double-faced W-beam guardrail placed on a 2.5H:1V slope and impacted by a Ford F250.

Fig. 3.15: FE model of a backside impact on a lowered backside double-faced W-beam guardrail placed on a 2.5H:1V slope and impacted by a Ford F250.

Fig. 3.16: FE model of a front-side impact on a single-faced W-beam guardrail with convex horizontal curvature placed on a 2.5H:1V slope and impacted by a Ford F250.

Fig. 3.17: FE model of a front-side impact on a single-faced W-beam guardrail with concave horizontal curvature placed on a 4H:1V slope and impacted by a Ford F250.

Fig. 4.1: The exit-box criterion in MASH.

Fig. 4.2: A Dodge Neon impacting the front-side 29-inch single-faced guardrail on a 2.5H:1V slope.

Fig. 4.3: Yaw, pitch, and roll angles for a Dodge Neon impacting the front-side 29-inch single-faced guardrail on a 2.5H:1V slope.

Fig. 4.4: Maximum dynamic deflection of the front-side 29-inch single-faced guardrail on a 2.5H:1V slope and impacted by a Dodge Neon.

Fig. 4.5: Simulations of a Dodge Neon impacting the front-side of 29-inch single-faced guardrail on a 2.5H:1V slope.

Fig. 4.6: Transverse displacements and velocities of the Dodge Neon impacting the front-side of 29-inch single-faced guardrail on a 2.5H:1V slope at 62 mph (100 km/hour) and 25°.

Fig. 4.7: Transverse displacements and velocities of the Dodge Neon impacting the front-side of 29-inch single-faced guardrail on a 2.5H:1V slope at 70 mph (112.6 km/hour) and 25°.

Fig. 4.8: A Ford F250 impacting the front-side of 29-inch single-faced guardrail on a 2.5H:1V slope at 62 mph (100 km/hour) and 25°.

Fig. 4.9: Yaw, pitch, and roll angles of Ford F250 impacting the front-side of 29-inch single-faced guardrail on a 2.5H:1V slope at 62 mph (100 km/hour) and 25°.

Fig. 4.10: Maximum dynamic deflection of the front-side for 29-inch single-faced guardrail on a 2.5H:1V slope at 62 mph (100 km/hour) and 25° and impacted by a Ford F250.

Fig. 4.11: Simulations of Ford F250 impacting the front-side of 29-inch single-faced guardrail on a 2.5H:1V slope at 62 mph (100 km/hour) and 25°.

Fig. 4.12: Transverse displacements and velocities for the Ford F250 impacting the front-side of 29-inch single-faced guardrail on a 2.5H:1V slope at 62 mph (100 km/hour) and 25°.

Fig. 4.13: A Dodge Neon impacting the front-side single-faced of 31-inch guardrail on a 2.5H:1V slope.

- Fig. 4.14: Yaw, pitch, and roll angles of a Dodge Neon impacting the front-side single-faced 31-inch guardrail on a 2.5H:1V slope.
- Fig. 4.15: Maximum dynamic deflection for the front-side single-faced 31-inch guardrail on a 2.5H:1V slope and impacted by a Dodge Neon.
- Fig. 4.16: Simulations of the Dodge Neon impacting the front-side of single-faced 31-inch guardrail on a 2.5H:1V slope.
- Fig. 4.17: Transverse displacements and velocities for the Dodge Neon impacting the front-side of single-faced 31-inch guardrail on a 2.5H:1V slope at 62 mph (100 km/hour) and 25°.
- Fig. 4.18: Transverse displacements and velocities of a Dodge Neon impacting the front-side of single-faced 31-inch guardrail on a 2.5H:1V slope at 70 mph (112.6 km/hour) and 25°.
- Fig. 4.19: A Ford F250 impacting the front-side of single-faced 31-inch guardrail on a 2.5H:1V slope at 62 mph (100 km/hour) and 25°.
- Fig. 4.20: Yaw, pitch, and roll angles of Ford F250 impacting the front-side of single-faced 31-inch guardrail on a 2.5H:1V slope at 62 mph (100 km/hour) and 25°.
- Fig. 4.21: Maximum dynamic deflection for the front-side single-faced 31-inch guardrail on a 2.5H:1V slope at 62 mph (100 km/hour) and 25° and impacted by a Ford F250.
- Fig. 4.22: Simulations of the Ford F250 impacting the front-side of single-faced 31-inch guardrail on a 2.5H:1V slope at 62 mph (100 km/hour) and 25°.
- Fig. 4.23: Transverse displacements and velocities for a Ford F250 impacting the front-side of single-faced 31-inch guardrail on a 2.5H:1V slope at 62 mph (100 km/hour) and 25°.
- Fig. 4.24: A Dodge Neon impacting the front-side of 29-inch double-faced guardrail on a 2.5H:1V slope at 62 mph (100 km/hour) and 25°.
- Fig. 4.25: Yaw, pitch, and roll angles of a Dodge Neon impacting the front-side of 29-inch double-faced guardrail on a 2.5H:1V slope at 62 mph (100 km/hour) and 25°.
- Fig. 4.26: Maximum dynamic deflection for front-side 29-inch double-faced guardrail on a 2.5H:1V slope at 62 mph (100 km/hour) and 25° and impacted by a Dodge Neon.
- Fig. 4.27: Simulations of Dodge Neon impacting the front-side of 29-inch double-faced guardrail on a 2.5H:1V slope at 62 mph (100 km/hour) and 25°.
- Fig. 4.28: Transverse displacements and velocities for the Dodge Neon impacting the front-side of 29-inch double-faced guardrail on a 2.5H:1V slope at 62 mph (100 km/hour) and 25°.
- Fig. 4.29: A Ford F250 impacting the front-side of 29-inch double-faced guardrail on a 2.5H:1V slope at 62 mph (100 km/hour) and 25°.
- Fig. 4.30: Yaw, pitch, and roll angles for a Ford F250 impacting the front-side of 29-inch double-faced guardrail on a 2.5H:1V slope at 62 mph (100 km/hour) and 25°.

- Fig. 4.31: Maximum dynamic deflection for the front-side of 29-inch double-faced guardrail on a 2.5H:1V slope at 62 mph (100 km/hour) and 25° and impacted by a Ford F250.
- Fig. 4.32: Simulations for a Ford F250 impacting the front-side of 29-inch double-faced guardrail on a 2.5H:1V slope at 62 mph (100 km/hour) and 25°.
- Fig. 4.33: Transverse displacements and velocities for the Ford F250 impacting the front-side of 29-inch double-faced guardrail on a 2.5H:1V slope at 62 mph (100 km/hour) and 25°.
- Fig. 4.34: A Dodge Neon impacting the front-side of 31-inch double-faced guardrail on a 2.5H:1V slope at 62 mph (100 km/hour) and 25°.
- Fig. 4.35: Yaw, pitch, and roll angles of Dodge Neon impacting the front-side 31-inch double-faced guardrail on a 2.5H:1V slope at 62 mph (100 km/hour) and 25°.
- Fig. 4.36: Maximum dynamic deflection of the front-side 31-inch double-faced guardrail on a 2.5H:1V slope at 62 mph (100 km/hour) and 25° and impacted by a Dodge Neon.
- Fig. 4.37: Simulations of Dodge Neon impacting the front-side of 31-inch double-faced guardrail on a 2.5H:1V slope at 62 mph (100 km/hour) and 25°.
- Fig. 4.38: Transverse displacements and velocities of the Dodge Neon impacting the front-side of 31-inch double-faced guardrail on a 2.5H:1V slope at 62 mph (100 km/hour) and 25°.
- Fig. 4.39: A Ford F250 impacting the front-side 31-inch double-faced guardrail on a 2.5H:1V slope at 62 mph (100 km/hour) and 25°.
- Fig. 4.40: Yaw, pitch, and roll angles of Ford F250 impacting the front-side 31-inch double-faced guardrail on a 2.5H:1V slope at 62 mph (100 km/hour) and 25°.
- Fig. 4.41: Maximum dynamic deflection of the front-side 31-inch double-faced guardrail on a 2.5H:1V slope at 62 mph (100 km/hour) and 25° and impacted by a Ford F250.
- Fig. 4.42: Simulations of Ford F250 impacting the front-side 31-inch double-faced guardrail on a 2.5H:1V slope at 62 mph (100 km/hour) and 25°.
- Fig. 4.43: Transverse displacements and velocities of the Ford F250 impacting the front-side 31-inch double-faced guardrail on a 2.5H:1V slope at 62 mph (100 km/hour) and 25°.
- Fig. 4.44: A Dodge Neon impacting the backside of 29-inch double-faced guardrail on a 2.5H:1V slope at 62 mph (100 km/hour) and 25°.
- Fig. 4.45: Yaw, pitch, and roll angles of the Dodge Neon impacting the backside 29-inch double-faced guardrail on a 2.5H:1V slope at 62 mph (100 km/hour) and 25°.
- Fig. 4.46: Maximum dynamic deflection of the backside 29-inch double-faced guardrail on a 2.5H:1V slope at 62 mph (100 km/hour) and 25° and impacted by a Dodge Neon.
- Fig. 4.47: Simulations of Dodge Neon impacting the backside 29-inch double-faced guardrail on a 2.5H:1V slope at 62 mph (100 km/hour) and 25°.

- Fig. 4.48: Transverse displacements and velocities of the Dodge Neon impacting the backside 29-inch double-faced guardrail on a 2.5H:1V slope at 62 mph (100 km/hour) and 25°.
- Fig. 4.49: A Ford F250 impacting the backside 29-inch double-faced guardrail on a 2.5H:1V slope at 62 mph (100 km/hour) and 25°.
- Fig. 4.50: Yaw, pitch, and roll angles of the Ford F250 impacting the backside of 29-inch double-faced guardrail on a 2.5H:1V slope at 62 mph (100 km/hour) and 25°.
- Fig. 4.51: Maximum dynamic deflection of the backside 29-inch double-faced guardrail on a 2.5H:1V slope at 62 mph (100 km/hour) and 25° and impacted by a Ford F250.
- Fig. 4.52: Simulations of Ford F250 impacting the backside 29-inch double-faced guardrail on a 2.5H:1V slope at 62 mph (100 km/hour) and 25°.
- Fig. 4.53: Transverse displacements and velocities of the Ford F250 impacting the backside 29-inch double-faced guardrail on a 2.5H:1V slope at 62 mph (100 km/hour) and 25°.
- Fig. 4.54: A Dodge Neon impacting the backside of 31-inch double-faced guardrail on a 2.5H:1V slope at 62 mph (100 km/hour) and 25°.
- Fig. 4.55: Yaw, pitch, and roll angles of the Dodge Neon impacting the backside of 31-inch double-faced guardrail on a 2.5H:1V slope at 62 mph (100 km/hour) and 25°.
- Fig. 4.56: Maximum dynamic deflection of the backside 31-inch double-faced guardrail on a 2.5H:1V slope at 62 mph (100 km/hour) and 25° and impacted by a Dodge Neon.
- Fig. 4.57: Simulations of Dodge Neon impacting the backside 31-inch double-faced guardrail on a 2.5H:1V slope at 62 mph (100 km/hour) and 25°.
- Fig. 4.58: Transverse displacements and velocities of the Dodge Neon impacting the backside of 31-inch double-faced guardrail on a 2.5H:1V slope at 62 mph (100 km/hour) and 25°.
- Fig. 4.59: A Ford F250 impacting the backside of 31-inch double-faced guardrail on a 2.5H:1V slope at 62 mph (100 km/hour) and 25°.
- Fig. 4.60: Yaw, pitch, and roll angles of Ford F250 impacting the backside of 31-inch double-faced guardrail on
- Fig. 4.61: Maximum dynamic deflection of the backside 31-inch double-faced guardrail on a 2.5H:1V slope at 62 mph (100 km/hour) and 25° and impacted by a Ford F250.
- Fig. 4.62: Simulations of Ford F250 impacting the backside 31-inch double-faced guardrail on a 2.5H:1V slope at 62 mph (100 km/hour) and 25°.
- Fig. 4.63: Transverse displacements and velocities of the Ford F250 impacting the backside 31-inch double-faced guardrail on a 2.5H:1V slope at 62 mph (100 km/hour) and 25°.
- Fig. 4.64: A Dodge Neon impacting the front-side of the lowered backside 29-inch guardrail on a 2.5H:1V slope at 62 mph (100 km/hour) and 25°.

- Fig. 4.65: Yaw, pitch, and roll angles of Dodge Neon impacting the front-side of the lowered backside 29-inch guardrail on a 2.5H:1V slope at 62 mph (100 km/hour) and 25°.
- Fig. 4.66: Maximum dynamic deflection of the front-side of the lowered backside 29-inch guardrail on a 2.5H:1V slope at 62 mph (100 km/hour) and 25° and impacted by a Dodge Neon.
- Fig. 4.67: Simulations of the Dodge Neon impacting the front-side of the lowered backside 29-inch guardrail on a 2.5H:1V slope at 62 mph (100 km/hour) and 25°.
- Fig. 4.68: Transverse displacements and velocities of the Dodge Neon impacting the front-side of the lowered backside 29-inch guardrail on a 2.5H:1V slope at 62 mph (100 km/hour) and 25°.
- Fig. 4.69: A Ford F250 impacting the front-side of the lowered backside 29-inch guardrail on a 2.5H:1V slope at 62 mph (100 km/hour) and 25°.
- Fig. 4.70: Yaw, pitch, and roll angles of Ford F250 impacting the front-side of the lowered backside 29-inch guardrail on a 2.5H:1V slope at 62 mph (100 km/hour) and 25°.
- Fig. 4.71: Maximum dynamic deflection of the front-side of the lowered backside 29-inch guardrail on a 2.5H:1V slope at 62 mph (100 km/hour) and 25° and impacted by a Ford F250.
- Fig. 4.72: Simulations of Ford F250 impacting the front-side of the lowered backside 29-inch guardrail on a 2.5H:1V slope at 62 mph (100 km/hour) and 25°.
- Fig. 4.73: Transverse displacements and velocities of the Ford F250 impacting the front-side of the lowered backside 29-inch guardrail on a 2.5H:1V slope at 62 mph (100 km/hour) and 25°.
- Fig. 4.74: A Dodge Neon impacting the front-side of the lowered backside 31-inch guardrail on a 2.5H:1V slope at 62 mph (100 km/hour) and 25°.
- Fig. 4.75: Yaw, pitch, and roll angles of Dodge Neon impacting the front-side of the lowered backside 31-inch guardrail on a 2.5H:1V slope at 62 mph (100 km/hour) and 25°.
- Fig. 4.76: Maximum dynamic deflection of the front-side of the lowered backside 31-inch guardrail on a 2.5H:1V slope at 62 mph (100 km/hour) and 25° and impacted by a Dodge Neon.
- Fig. 4.77: Simulations of Dodge Neon impacting the front-side of the lowered backside 31-inch guardrail on a 2.5H:1V slope at 62 mph (100 km/hour) and 25°.
- Fig. 4.78: Transverse displacements and velocities of the Dodge Neon impacting the front-side of the lowered backside 31-inch guardrail on a 2.5H:1V slope at 62 mph (100 km/hour) and 25°.
- Fig. 4.79: A Ford F250 impacting the front-side of the lowered backside 31-inch guardrail on a 2.5H:1V slope at 62 mph (100 km/hour) and 25°.
- Fig. 4.80: Yaw, pitch, and roll angles of Ford F250 impacting the front-side of the lowered backside 31-inch guardrail on a 2.5H:1V slope at 62 mph (100 km/hour) and 25°.

- Fig. 4.81: Maximum dynamic deflection of the front-side of the lowered backside 31-inch guardrail on a 2.5H:1V slope at 62 mph (100 km/hour) and 25° and impacted by a Ford F250.
- Fig. 4.82: Simulations of Ford F250 impacting the front-side of the lowered backside 31-inch guardrail on a 2.5H:1V slope at 62 mph (100 km/hour) and 25°.
- Fig. 4.83: Transverse displacements and velocities of the Ford F250 impacting the front-side of the lowered backside 31-inch guardrail on a 2.5H:1V slope at 62 mph (100 km/hour) and 25°.
- Fig. 4.84: A Dodge Neon impacting the backside of the lowered backside 29-inch guardrail on a 2.5H:1V slope at 62 mph (100 km/hour) and 25°.
- Fig. 4.85: Yaw, pitch, and roll angles of Dodge Neon impacting the backside of the lowered backside 29-inch guardrail on a 2.5H:1V slope at 62 mph (100 km/hour) and 25°.
- Fig. 4.86: Maximum dynamic deflection of the backside of the lowered backside 29-inch guardrail on a 2.5H:1V slope at 62 mph (100 km/hour) and 25° and impacted by a Dodge Neon.
- Fig. 4.87: Simulations of the Dodge Neon impacting the backside of the lowered backside 29-inch guardrail on a 2.5H:1V slope at 62 mph (100 km/hour) and 25°.
- Fig. 4.88: Transverse displacements and velocities of the Dodge Neon impacting the backside of the lowered backside 29-inch guardrail on a 2.5H:1V slope at 62 mph (100 km/hour) and 25°.
- Fig. 4.89: A Ford F250 impacting the backside of the lowered backside 29-inch guardrail on a 2.5H:1V slope at 62 mph (100 km/hour) and 25°.
- Fig. 4.90: Yaw, pitch, and roll angles of Ford F250 impacting the backside of the lowered backside 29-inch guardrail on a 2.5H:1V slope at 62 mph (100 km/hour) and 25°.
- Fig. 4.91: Maximum dynamic deflection of the backside of the lowered backside 29-inch guardrail on a 2.5H:1V slope at 62 mph (100 km/hour) and 25° and impacted by a Ford F250.
- Fig. 4.92: Simulations of Ford F250 impacting the backside of the lowered backside 29-inch guardrail on a 2.5H:1V slope at 62 mph (100 km/hour) and 25°.
- Fig. 4.93: Transverse displacements and velocities of the Ford F250 impacting the backside of the lowered 29-inch guardrail on a 2.5H:1V slope at 62 mph (100 km/hour) and 25°.
- Fig. 4.94: A Dodge Neon impacting the backside of the lowered backside 31-inch guardrail on a 2.5H:1V slope at 62 mph (100 km/hour) and 25°.
- Fig. 4.95: Yaw, pitch, and roll angles of Dodge Neon impacting the backside of the lowered backside 31-inch guardrail on a 2.5H:1V slope at 62 mph (100 km/hour) and 25°.
- Fig. 4.96: Maximum dynamic deflection of the backside of the lowered backside 31-inch guardrail on a 2.5H:1V slope at 62 mph (100 km/hour) and 25° and impacted by a Dodge Neon.

- Fig. 4.97: Simulations of Dodge Neon impacting the backside of the lowered backside 31-inch guardrail on a 2.5H:1V slope at 62 mph (100 km/hour) and 25°.
- Fig. 4.98: Transverse displacements and velocities of the Dodge Neon impacting the backside of the lowered backside 31-inch guardrail on a 2.5H:1V slope at 62 mph (100 km/hour) and 25°.
- Fig. 4.99: A Ford F250 impacting the backside of the lowered backside 31-inch guardrail on a 2.5H:1V slope at 62 mph (100 km/hour) and 25°.
- Fig. 4.100: Yaw, pitch, and roll angles of Ford F250 impacting the backside of the lowered backside 31-inch guardrail on a 2.5H:1V slope at 62 mph (100 km/hour) and 25°.
- Fig. 4.101: Maximum dynamic deflection of the backside of the lowered backside 31-inch guardrail on a 2.5H:1V slope at 62 mph (100 km/hour) and 25° and impacted by a Ford F250.
- Fig. 4.102: Simulations of Ford F250 impacting the backside of the lowered backside 31-inch guardrail on a 2.5H:1V slope at 62 mph (100 km/hour) and 25°.
- Fig. 4.103: Transverse displacements and velocities of the Ford F250 impacting the backside of the lowered backside 31-inch guardrail on a 2.5H:1V slope at 62 mph (100 km/hour) and 25°.
- Fig. 4.104: A Dodge Neon impacting the front-side, convex horizontal curvature 29-inch guardrail on a 2.5H:1V slope at 62 mph (100 km/hour) and 25°.
- Fig. 4.105: Yaw, pitch, and roll angles of Dodge Neon impacting the front-side, convex horizontal curvature 29-inch guardrail on a 2.5H:1V slope at 62 mph (100 km/hour) and 25°.
- Fig. 4.106: Maximum dynamic deflection of the front-side, convex horizontal curvature 29-inch guardrail on a 2.5H:1V slope at 62 mph (100 km/hour) and 25° and impacted by a Dodge Neon.
- Fig. 4.107: Simulations of Dodge Neon impacting the front-side, convex horizontal curvature 29-inch guardrail on a 2.5H:1V slope at 62 mph (100 km/hour) and 25°.
- Fig. 4.108: Transverse displacements and velocities of the Dodge Neon impacting the front-side, convex horizontal curvature 29-inch guardrail on a 2.5H:1V slope at 62 mph (100 km/hour) and 25°.
- Fig. 4.109: A Ford F250 impacting the front-side, convex horizontal curvature 29-inch guardrail on a 2.5H:1V slope at 62 mph (100 km/hour) and 25°.
- Fig. 4.110: Yaw, pitch, and roll angles of Ford F250 impacting the front-side, convex horizontal curvature 29-inch guardrail on a 2.5H:1V slope at 62 mph (100 km/hour) and 25°.
- Fig. 4.111: Maximum dynamic deflection of the front-side, convex horizontal curvature 29-inch guardrail on a 2.5H:1V slope at 62 mph (100 km/hour) and 25° and impacted by a Ford F250.

- Fig. 4.112: Simulations of Ford F250 impacting the front-side, convex horizontal curvature, 29-inch guardrail on a 2.5H:1V slope at 62 mph (100 km/hour) and 25°.
- Fig. 4.113: Transverse displacements and velocities of the Ford F250 impacting the front-side, convex horizontal curvature, 29-inch guardrail on a 2.5H:1V slope at 62 mph (100 km/hour) and 25°.
- Fig. 4.114: A Dodge Neon impacting the front-side, convex horizontal curvature, 31-inch guardrail on a 2.5H:1V slope at 62 mph (100 km/hour) and 25°.
- Fig. 4.115: Yaw, pitch, and roll angles of Dodge Neon impacting the front-side, convex horizontal curvature, 31-inch guardrail on a 2.5H:1V slope at 62 mph (100 km/hour) and 25°.
- Fig. 4.116: Maximum dynamic deflection of the front-side, convex horizontal curvature, 31-inch guardrail on a 2.5H:1V slope at 62 mph (100 km/hour) and 25° and impacted by a Dodge Neon.
- Fig. 4.117: Simulations of Dodge Neon impacting the front-side, convex horizontal curvature, 31-inch guardrail on a 2.5H:1V slope at 62 mph (100 km/hour) and 25°.
- Fig. 4.118: Transverse displacements and velocities of the Dodge Neon impacting the front-side, convex horizontal curvature, 31-inch guardrail on a 2.5H:1V slope at 62 mph (100 km/hour) and 25°.
- Fig. 4.119: A Ford F250 impacting the front-side, convex horizontal curvature, 31-inch guardrail on a 2.5H:1V slope at 62 mph (100 km/hour) and 25°.
- Fig. 4.120: Yaw, pitch, and roll angles of Ford F250 impacting the front-side, convex horizontal curvature 31-inch guardrail on a 2.5H:1V slope at 62 mph (100 km/hour) and 25°.
- Fig. 4.121: Maximum dynamic deflection of the front-side, convex horizontal curvature, 31-inch guardrail on a 2.5H:1V slope at 62 mph (100 km/hour) and 25° and impacted by a Ford F250.
- Fig. 4.122: Simulations of Ford F250 impacting the front-side, convex horizontal curvature, 31-inch guardrail on a 2.5H:1V slope at 62 mph (100 km/hour) and 25°.
- Fig. 4.123: Transverse displacements and velocities of the Ford F250 impacting the front-side, convex horizontal curvature 31-inch guardrail on a 2.5H:1V slope at 62 mph (100 km/hour) and 25°.
- Fig. 4.124: A Dodge Neon impacting the front-side, concave horizontal curvature, 29-inch guardrail on a 2.5H:1V slope at 62 mph (100 km/hour) and 25°.
- Fig. 4.125: Yaw, pitch, and roll angles of Dodge Neon impacting the front-side, concave horizontal curvature, 29-inch guardrail on a 2.5H:1V slope at 62 mph (100 km/hour) and 25°.

- Fig. 4.126: Maximum dynamic deflection of the front-side, concave horizontal curvature, 29-inch guardrail on a 2.5H:1V slope at 62 mph (100 km/hour) and 25° and impacted by a Dodge Neon.
- Fig. 4.127: Simulations of Dodge Neon impacting the front-side, concave horizontal curvature, 29-inch guardrail on a 2.5H:1V slope at 62 mph (100 km/hour) and 25°.
- Fig. 4.128: Transverse displacements and velocities of the Dodge Neon impacting the front-side, concave horizontal curvature, 29-inch guardrail on a 2.5H:1V slope at 62 mph (100 km/hour) and 25°.
- Fig. 4.129: A Ford F250 impacting the front-side, concave horizontal curvature 29-inch guardrail on a 2.5H:1V slope at 62 mph (100 km/hour) and 25°.
- Fig. 4.130: Yaw, pitch, and roll angles of Ford F250 impacting the front-side, concave horizontal curvature, 29-inch guardrail on a 2.5H:1V slope at 62 mph (100 km/hour) and 25°.
- Fig. 4.131: Maximum dynamic deflection of the front-side, concave horizontal curvature, 29-inch guardrail on a 2.5H:1V slope at 62 mph (100 km/hour) and 25° and impacted by a Ford F250.
- Fig. 4.132: Simulations of Ford F250 impacting the front-side, concave horizontal curvature, 29-inch guardrail on a 2.5H:1V slope at 62 mph (100 km/hour) and 25°.
- Fig. 4.133: Transverse displacements and velocities of the Ford F250 impacting the front-side, concave horizontal curvature, 29-inch guardrail on a 2.5H:1V slope at 62 mph (100 km/hour) and 25°.
- Fig. 4.134: A Dodge Neon impacting the front-side, concave horizontal curvature, 31-inch guardrail on a 2.5H:1V slope at 62 mph (100 km/hour) and 25°.
- Fig. 4.135: Yaw, pitch, and roll angles of Dodge Neon impacting the front-side, concave horizontal curvature, 31-inch guardrail on a 2.5H:1V slope at 62 mph (100 km/hour) and 25°.
- Fig. 4.136: Maximum dynamic deflection of the front-side, concave horizontal curvature, 31-inch guardrail on a 2.5H:1V slope at 62 mph (100 km/hour) and 25° and impacted by a Dodge Neon.
- Fig. 4.137: Simulations of Dodge Neon impacting the front-side, concave horizontal curvature, 31-inch guardrail on a 2.5H:1V slope at 62 mph (100 km/hour) and 25°.
- Fig. 4.138: Transverse displacements and velocities of the Dodge Neon impacting the front-side, concave horizontal curvature, 31-inch guardrail on a 2.5H:1V slope at 62 mph (100 km/hour) and 25°.
- Fig. 4.139: A Ford F250 impacting the front-side, concave horizontal curvature 31-inch guardrail on a 2.5H:1V slope at 62 mph (100 km/hour) and 25°.

- Fig. 4.140: Yaw, pitch, and roll angles of Ford F250 impacting the front-side, concave horizontal curvature 31-inch guardrail on a 2.5H:1V slope at 62 mph (100 km/hour) and 25°.
- Fig. 4.141: Maximum dynamic deflection of the front-side, concave horizontal curvature 31-inch guardrail on a 2.5H:1V slope at 62 mph (100 km/hour) and 25° and impacted by a Ford F250.
- Fig. 4.142: Simulations of Ford F250 impacting the front-side, concave horizontal curvature 31-inch guardrail on a 2.5H:1V slope at 62 mph (100 km/hour) and 25°.
- Fig. 4.143: Transverse displacements and velocities of the Ford F250 impacting the front-side, concave horizontal curvature, 31-inch guardrail on a 2.5H:1V slope at 62 mph (100 km/hour) and 25°.

1. Introduction

Roadside barrier systems are important devices to ensure transportation safety; they serve the purpose of safely redirecting errant vehicles and preventing runaway vehicles from intruding into oncoming travel lanes. Over the years, different types of barriers have been developed and are categorized into rigid (e.g., concrete barriers), semi-rigid (e.g., W-beam guardrails), and flexible (e.g., cable barriers) systems. W-beam guardrails are widely used safety devices on U.S. highways. Figure 1.1 shows a strong-post W-beam guardrail that consists of a steel, W-shaped rail mounted on steel posts. W-beam guardrails usually require substantial replacement or repairs after major vehicle crashes, because even low-energy impacts can bend and damage the rails and displace the posts such that the barrier may not perform properly in a subsequent crash event.

All barrier systems used on U.S. highways are designed according to the Roadside Design Guide of the American Association of State Highway and Transportation Officials (AASHTO). They must be tested to satisfy the safety criteria specified by Manual for Assessing Safety Hardware (MASH), a replacement of the old standard – Report 350 of the National Cooperative Highway Research Program (NCHRP). The test conditions in MASH are generally more severe than those in NCHRP Report 350. For example, the two test vehicles in MASH Test Level 3 (TL-3) were changed to 1100C (1,100 kg or 2,420 lb) and 2270P (2,270 kg or 5,000 lb), representing 34% and 13.5% mass increases, respectively, over those of NCHRP Report 350. In addition, the impact angle for small vehicle was changed from 20° in NCHRP Report 350 to 25° in MASH. In addition, the language of emphasizing the importance of in-service evaluation is added to MASH. Although current barrier systems that passed the safety criteria of NCHRP Report 350 are not required to pass the corresponding MASH criteria, it is important to evaluate their performance under MASH test conditions for practical safety concerns.



Fig. 1.1: A strong-post W-beam guardrail.

1.1 Background

Forty-six feet is the minimum median width used for freeways without a concrete median barrier. For six-lane, 46-foot median divided freeways, the paved shoulder policy requires two 14-foot median shoulders, which reduce the width of the median ditch to 18 feet. For positive pavement drainage consideration, the median slopes should be changed to 4:1 or higher. As a practical solution, design engineers often place two lines of W-beam guardrails on both median shoulders (see Fig. 1.2). While preventing cross-median crashes, the two lines of guardrails create difficulty for vegetation

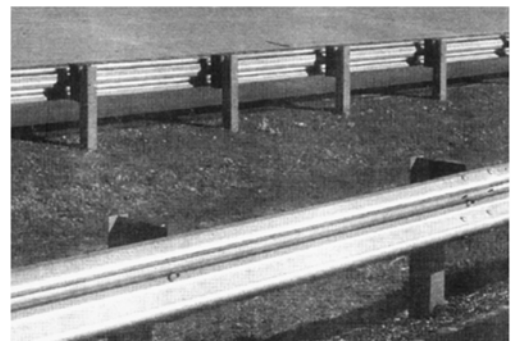


Fig. 1.2: Two lines of single-faced W-beam guardrails.

maintenance operations such as mowing. NCDOT engineers indicated that there was a strong need to investigate the possibility of replacing two single lines of guardrails with a single line of a double-faced W-beam guardrail (see Fig. 1.3). In a previous NCDOT project, the performance of the 27-in W-beam guardrails on such freeways was evaluated under the NCHRP Report 350 TL-3 conditions and two designs of double-faced guardrails were proposed. However, with the recent change on NCDOT guardrails to increase rail heights to 29 and 31 inches, both single- and double-faced guardrails with the new rail heights need to be evaluated on six-lane, 46-foot median divided freeways. In addition, the effects of horizontal curvature on 29-in and 31-in guardrails are unknown and need to be determined for appropriate installations of these guardrails. Furthermore, newly developed guardrail systems are now required to be tested under MASH test conditions, which are generally more severe than those of the NCHRP Report 350.



Fig. 1.3: A double-faced W-beam guardrail.

1.2 Research Objectives and Tasks

In this study, full-scale finite element (FE) simulations were employed to evaluate the performance of NCDOT 29- and 31-inch guardrails under MASH TL-3 test conditions. Two lines of single-faced guardrails and a single line of double-faced guardrail were evaluated on a six-lane, 46-foot median divided freeway. The effects of median horizontal curvature on these guardrails was also evaluated and compared to situations without the horizontal curvature. The research project had six major tasks as stated below.

Task 1: Literature Review and Data Collection

A comprehensive literature review was conducted on crash testing, modeling and simulations that are related, in particular, to W-beam guardrails to assist with model validation and crash simulations.

Task 2: FE Model Development and Validation

In this task, FE models of the 29- and 31-inch single- and double-faced W-beam guardrails were created. The FE model of 29-inch single-faced guardrail was developed for flat terrain in a previous project. The 31-inch single-faced guardrail for this project was modified from the 29-inch guardrail to relocate the splice location to the midspan between two posts. The 29- and 31-inch guardrail models were modified for use on a sloped median for this project; they were also used to create the models of 29- and 31-inch double-faced guardrails. The FE models of 29- and 31-inch single- and double-faced guardrails were created for the cases with a median horizontal curvature. Figure 1.4 shows the FE models of a G4(1S) guardrail, a small passenger car (1,090 kg or 2,400 lb), and a pickup truck (2,499 kg or 5,504 lb). These models were used in the simulation work for this project.



Fig. 1.4: FE models of a G4(1S) guardrail, a small passenger car, and a large pickup truck.

The FE model of the six-lane, 46-foot sloped median divided highway with 2.5H:1V slope to the left of the centerline and 4H:1V slope on the right centerline was created based on NCDOT standard designs. Figure 1.5 shows one of the simulation models in which the single-faced W-beam guardrail is placed on a 2.5H:1V slope and impacted by a 2006 Ford F250. All of the FE models were verified by NCDOT designs and validated using available simulation results and/or test data from literature.

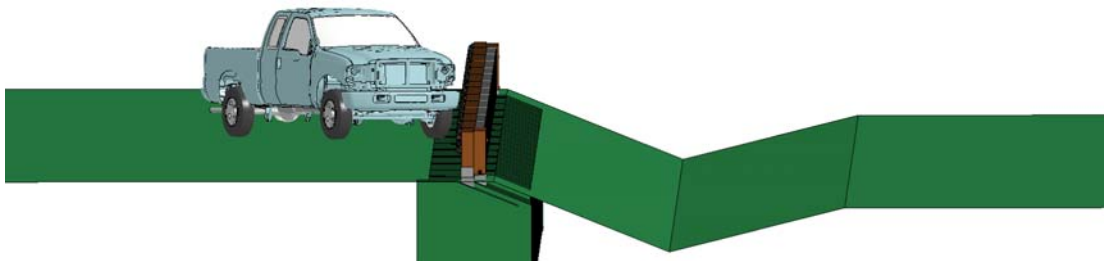


Fig. 1.5: FE model of a single-faced W-beam guardrail placed on the shoulder near the 2.5H:1V slope and impacted by a Ford F250.

Task 3: Performance Evaluation of 29- and 31-inch Single-faced W-beam Guardrails

In this task, the 29- and 31-inch single-faced W-beam guardrails were evaluated under impacts of both a small passenger car and a pickup truck. The impact speed was 62 mph (100 km/hour) and the impact angle was 25° for both vehicles, based on the MASH TL-3 impact conditions. These guardrails were placed on the shoulder near a 2.5H:1V slope of the 46-foot median (see Fig. 1.6).

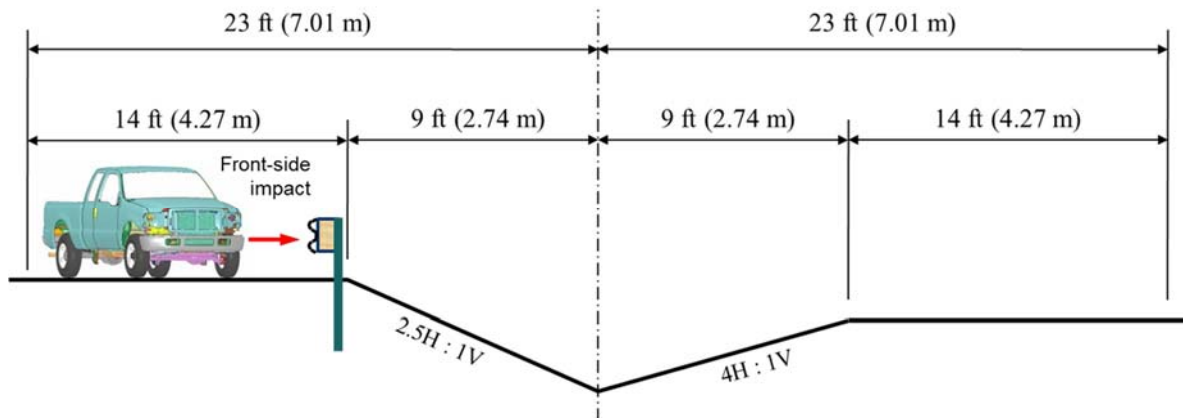


Fig. 1.6: Front-side impact on a 46-foot sloped median with 29- and 31-inch single-faced guardrails installed on a 2.5H:1V slope.

In addition, the single-faced guardrails at both rail heights were evaluated under the impact of the 1996 Dodge Neon at 70 mph (112.6 km/hour) and a 25° impact angle. In all simulations in this study, the vehicle started on the roadway and ran off the travel lane at the prescribed speed and angle towards the guardrail.

The vehicle’s response in terms of redirection, rollover, lateral displacements, and velocities were analyzed to determine the effectiveness of the 29- and 31-inch single-faced guardrail on a 2.5H:1V slope. In evaluating the vehicle’s response, the MASH exit-box criterion, Criterion N, was adopted. Additionally, the MASH Evaluation Criterion F requires that the vehicle remains upright and the maximum roll and pitch angles of the impacting vehicle do not exceed 75 degrees. Figure 1.7 shows the definition of the three rotational responses (roll, pitch, and yaw) along with the corresponding translational responses (surge, sway, and heave). The time histories of the three response parameters, i.e., roll, pitch, and yaw angles, were recorded for the entire period of simulations. The maximum roll and pitch angles were extracted and evaluated by the MASH Evaluation Criterion F. In addition to the above mentioned MASH evaluation criteria, the time histories of the vehicle’s lateral displacements and velocities were also examined for performance evaluation. The effectiveness of the 29- and 31-inch guardrails was determined based on analysis of simulation results for both small and large vehicles.

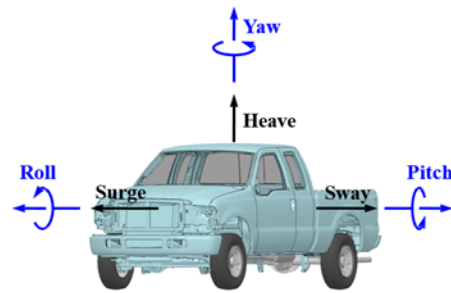


Fig. 1.7: Definition of vehicle responses.

Task 4: Performance Evaluation of 29-in and 31-in Double-faced W-beam Guardrails

In this task, the 29- and 31-inch double-faced guardrails were evaluated on a 2.5H:1V slope under both front-side and backside impacts of the Dodge Neon and Ford F250, as illustrated in Fig. 1.8. It should be noted that the backside impacts required the vehicle to traverse through the sloped median before impacting the backside rail. Previous studies indicated that the impact severity was higher on a 2.5H:1V slope than on a 4H:1V slope. Therefore, the installation of a double-faced guardrail placed on a 4H:1V slope was not considered in this study.

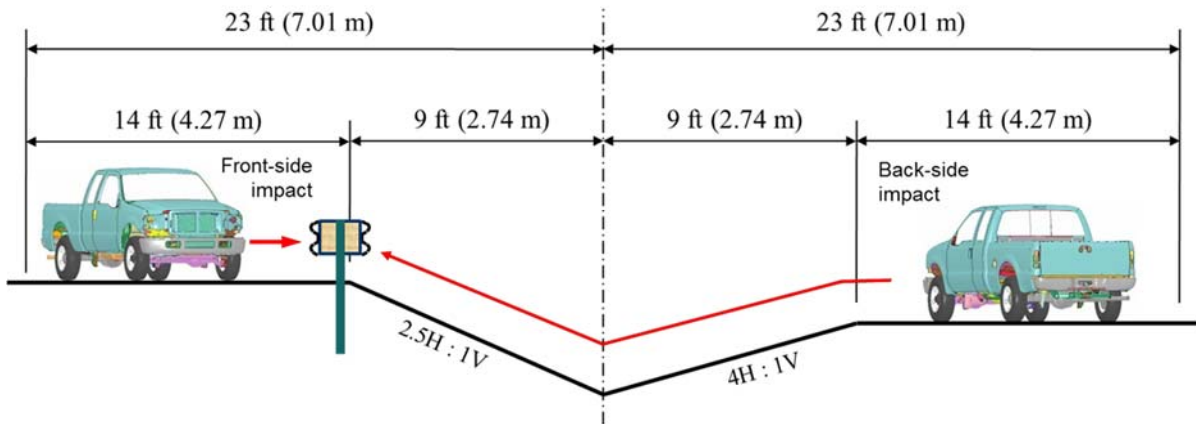


Fig. 1.8: Front-side and backside impact on a 46-foot sloped median with 29- and 31-inch double-faced guardrails installed on a 2.5H:1V slope.

For each of the 29- and 31-inch double-faced guardrails, two designs were evaluated. In the first design, the top of the backside rail was flush with the top of the front-side rail. In the second design, the backside rail was lowered by 2.1 in (53.3 mm) to ensure that the front-side and backside rails are installed at the same height relative to their grade levels (i.e. the distance from the top of the rail to the ground is either 29- or 31-inches for both front-side and backside rails). Both designs of the double-faced guardrails were evaluated under the MASH TL-3 impact conditions and their performance was evaluated and compared to determine their effectiveness. Their performance were also compared to that of the single-faced guardrails.

Task 5: Performance Evaluation of 29- and 31-inch Single-faced Guardrails on 46-foot Median with Horizontal Curvature

The effects of horizontal curvature on the performance of median barriers have been observed yet not intensively studied. In this task, the 29- and 31-inch single-faced guardrails were evaluated on a 46-foot median with horizontal curvature. Two designs of single-faced guardrails were installed, a convex horizontal curvature on a 2.5H:1V slope and a concave horizontal curvature on a 4H:1V slope as illustrated in Fig. 1.9. The impact conditions are the same as those of Task 4 and the simulation results of this task were compared to those obtained without the horizontal curvature.

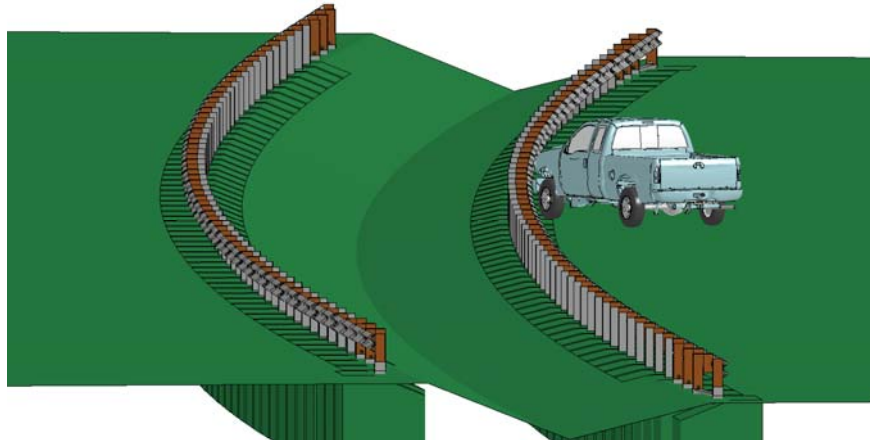


Fig. 1.9: Front-side impact on a 46-foot sloped median with horizontal curvature with 29- and 31-inch single-faced guardrails installed on a 2.5H:1V (convex curvature) and 4H:1V (concave curvature) slopes.

Task 6: Final Report

This final report provides a comprehensive summary of research activities, findings, and outcomes for this project. It synthesizes literature review, FE modeling efforts, simulation results, and the performance evaluation of 29- and 31-inch single- and double-faced W-beam guardrails on a six-lane, 46-foot median divided freeway, with and without horizontal curvature.

2. Literature Review

Median barriers have been developed and used on U.S. highway for decades. Presently, strong-post W-beam guardrails are widely used across the U.S. In this section, we provide a comprehensive summary of studies related to W-beam guardrails. The topics cover performance evaluation (in-service and crash testing) and the application of finite element (FE) modeling and simulations for highway safety research.

2.1 Performance Evaluation of Median Barriers

In the early 1960s, New York State pioneered the development of weak-post barrier systems through analytical models and full-scale vehicle crash testing. In 1965, the state's guardrail and median barrier standards were changed to include only weak-post barriers. In the early 1970s, a study by Zweden and Bryden (1977) was conducted to evaluate the field performance of the older strong-post barriers and newly-developed weak-post barriers based on New York State accident data collected from 1967 to 1970. A statistical analysis was performed to compare the performance of the investigated barrier systems based on occupant injury, vehicular response, and post-impact maintenance. This study generated a number of significant conclusions on the performance of weak- and strong-post barriers. Although there was no significant difference in fatality rates between the two barrier systems, weak-post barriers exhibited a combined fatality/serious injury rate significantly lower than that for strong-post barriers. The resulting occupant injury appeared to be linked to barrier stiffness since both barrier systems (both strong- and weak-post versions) had lower injury severity rates than other stiffer median barriers had the highest injury rates. With respect to barrier penetrations, the weak-post barriers demonstrated a lower penetration rate than the strong-post barriers, which may be due to the lack of consistency between early strong-post barrier designs. The study also indicated that barrier penetrations on the weak-post systems were typically due to the low rail heights, and that barrier end terminals (i.e., the first and the last 50 feet of the barrier) had higher rates of penetration and serious injury than the midsections. The study also related barrier damage to their stiffness: stiffer barriers (e.g., strong-post barriers) had less damage or shorter damaged sections than weaker barriers (e.g., weak-post barriers). The study also determined that despite their longer damage lengths, weak-post barriers were on average less expensive to repair than strong-post barriers.

An analysis performed in the 1970s indicated that most guardrails did not perform well when placed on 1:6 or steeper slopes. Since that time, the vehicle fleet has changed dramatically with a significant increase in light trucks and sport utility vehicles. In addition, there has been a significant change in the design of roadside barriers in recent decades. It was unclear how these changes could affect the behavior of longitudinal barriers placed on slopes. Information from the Fatality Analysis Reporting System (FARS) database of the National Highway Traffic Safety Administration (NHTSA) indicated that some cross-median crashes occurred where median barriers were in place. A full-scale crash test also showed that a passenger vehicle could penetrate a cable barrier on the backside of a depressed median.

In the early 1980s, significant changes in vehicle designs led to a large increase in the number of smaller and lighter vehicles on highways. A study (Hiss and Bryden, 1992) was initiated in 1983 by the New York State DOT to determine how impact severity on traffic

barriers was affected by vehicle size and weight, barrier type and mounting height, and roadway features. Several conclusions were drawn regarding the performance of cable, W-beam, and box-beam guardrails. For cable and W-beam median barriers, however, the sample sizes were too small to assess their performance due to their limited use and exposure to possible accidents.

Ross and Sicking (1984) investigated the impact performance of longitudinal barriers when placed on sloped terrain using both crash tests and the Highway-Vehicle-Object Simulation Model (HVOSM) computer program. In the study, they determined typical conditions to place longitudinal barriers on sloped terrain and evaluated the impact behavior of widely used barrier systems. Guidelines were developed for the selection and placement of barriers on sloped terrain. It was found from the study that W-beam and Thrie-beam guardrails were more sensitive to the terrain slopes than cable barriers.

In the study conducted by Ross et al. (1993), uniform procedures were developed for evaluating the safety performance of candidate roadside hardware systems, including longitudinal barriers, crash cushions, breakaway supports, truck-mounted attenuators, and work zone traffic control devices. The report from this study, the National Cooperative Highway Research Program (NCHRP) Report 350, was adopted as the standard guideline for evaluating the safety performance of roadside safety devices until it was replaced by the new standard, Manual for Assessing Safety Hardware (MASH), in 2009. The evaluation of devices in NCHRP 350 was facilitated through three main criteria: structural adequacy, occupant risk, and post-impact vehicle trajectory. Structural adequacy referred to how well the device performed its intended task (i.e. a guardrail preventing a vehicle from striking a shielded object). The occupant risk criteria attempted to quantify the probability of severe occupant injury. The post-impact vehicle trajectory was adopted to ensure that the device would not cause subsequent harm (i.e. a vehicle being unsafely redirected back into traffic). The guidelines recognized the infinite number of roadside hardware installations and crash configurations. Therefore, standardized installation configurations and practical worst-case impact scenarios were used to provide a basis for comparing the performance of similar devices. A matter of particular note was, the multi-service level concept that provided six different test levels (TLs) to allow for more or less stringent performance evaluation (ideally depending on the ultimate usage/placement of the hardware).

With respect to cross-median crashes, the NCHRP Report 350 was the standard by which median barriers were tested before the new standard, MASH, was developed. Although the report specified six different test levels, the warrants for devices satisfying an individual test level was outside the scope of the document and left to the judgment of the transportation agency implementing the hardware. Generally speaking, devices tested to the lower test levels (i.e., TL-1 and TL-2) were mostly used on roadways with smaller traffic volume and lower travel speeds and devices tested to the higher levels (TL-3 to TL-6) were typically used on roadways with a larger volume and higher speeds. Note that the 2000P, 2000-kg (4,409-pound), test vehicle was used to evaluate the strength and redirecting capabilities of longitudinal barriers up to and including test level three. For the 2000P test vehicle, all impacts were performed at 25° and at 31, 44, and 62 mph (50, 70, and 100 km/hour) for test levels 1, 2, and 3, respectively.

In the NCHRP Project 22-14, “Improvement of the Procedures for the Safety Performance Evaluation of Roadside Features,” updates were incorporated to the NCHRP Report 350 based on assessments at TL-3 conditions, which was the basic level used for devices on the *National Highway System*. In the report published by Mak and Bligh (2002), the effects of higher impact speeds and additional impact angles were considered for TL-3 conditions. These additional parameters were considered due to the fact that a number of states had changed maximum speed limits on some of their highways to 75 mph (121 km/hour) and not all crashes were occurring at an impact angle of 25°. These parameters often caused a concern on the stability of the test vehicle instead of containment capability. The report determined that increasing the impact speed to 68.4 mph (110 km/hour) would have significant effects on many of the existing roadside safety devices. Although some barriers could be modified to accommodate the higher impact speed with minor modifications, some other barriers would require major changes, and yet some barriers might never be able to accommodate the higher impact speed due to other design constraints. Increasing the impact speed could result in a whole new generation of roadside safety hardware. In return, the higher impact speed would only cover an additional 2.8% of the crashes and increase the percentage of covered crashes (i.e., crashes with impact speeds equal to or less than the design test speed) from approximately 90% to 92.7%. The reduction of the impact angle from 25° to 20° posed a number of arguments including the possibility for existing W-beam guardrail systems having difficulty containing vehicles at the higher impact speeds. It was emphasized that the selection of impact conditions was more of a policy decision than a technical issue to be resolved when updating the NCHRP Report 350 guidelines.

In the early 1990s, the Traffic Engineering Branch of the North Carolina Department of Transportation (NCDOT) conducted a study of accidents on North Carolina’s interstate highways in which vehicles crossed the median and entered the opposing travel lanes (Lynch et al. 1993). The study analyzed accidents that occurred during the time period from April 1, 1988 through October 31, 1991. The objectives of this study were to identify interstate locations with unusually high cross-median accidents, to determine possible safety improvements, to develop a priority listing of these locations with recommended improvements, and to develop a model for identifying potentially dangerous locations on North Carolina interstate highways. Data collected in the study showed that 751 cross-median crashes took place in North Carolina, resulting in 105 fatalities. These crashes represented three percent of total crashes but 32% of total fatalities on interstate highways during the study period. One of the outcomes of this study was the recommendation to construct median barriers at 24 sections of interstate highways in North Carolina.

Using data collected from Connecticut, Iowa, and North Carolina from 1997 to 1999, Ray and Weir (2001) performed an in-service performance evaluation of four guardrail systems: the G1 cable guiderail, G2 weak-post W-beam guardrail, and the G4(1S) and G4(1W) strong-post W-beam guardrails. The study particularly focused on estimating the number of unreported collisions and the true distribution of occupant injuries. The collision performance was measured in terms of collision characteristics, occupant injury, and barrier damage. Within the sample size limitations of the data collected in the study, no statistically significant difference was found on the performance of the guardrails in the three states, and there was no difference between the performance of G1 and G2 guardrails and between G1

and G4(1W) guardrails. However, occupant injuries were found less common in collisions with a G1 cable guardrail than in collisions with G4(1S) or both G4 types combined.

Ray et al. (2003) reviewed literature on in-service evaluations and identified previously found effective methods. The in-service performance of common barriers and terminals was examined by collecting data in the following three areas: crash, maintenance, and inventory information. A procedure manual for planning and conducting in-service evaluations of roadside hardware was developed based on the methods used and the lessons learned in the evaluation study. The manual was subsequently used as a guide for an in-service evaluation project performed in Washington State by a different research team and modified based on their experiences and recommendations.

In the work by Bligh and Mak (1999), crashworthiness of roadside features across vehicle platforms were evaluated. The impact performances of roadside safety features were typically evaluated through full-scale crash tests with two vehicles selected from the extremes of the passenger vehicle fleet in terms of weight and size. The implicit assumption was that if a roadside safety device successfully passed the test requirements for vehicles at the extremes of the fleet, it would perform satisfactorily for all other vehicles in between. Since many vehicle parameters could influence the performance during impacts, this assumption may or may not be valid. The safety performances of roadside features for various passenger car platforms and light-truck subclasses were evaluated in the study, which consisted of evaluations of the frequency and severity of roadside crashes for these generic platforms and subclasses by using recent crash data from the Fatal Accident Report System, the General Estimates System, and the Highway Safety Information System.

A new median barrier guideline was developed for Texas to assist highway engineers in the evaluation of median barrier needs, with the intention of achieving the highest practical level of median safety (Miaou et al. 2005; Bligh et al. 2006). In this work, statistical crash models for various types of median-related crashes were developed based on an analysis of crash data in Texas. Using estimates from the frequency and severity models and crash costs used by Texas Department of Transportation, an economic analysis of the median barrier need was performed. Guidelines for installing median barriers on divided, access-controlled freeways were developed as a function of average annual daily traffic and median width. Guidance to assist engineers evaluating median barriers needed on existing highway facilities was also developed based on the mean cross-median crash rate.

Under the guidelines of NCHRP Project 22-9, "Improved Methods for the Cost-Effectiveness Evaluation of Roadside Safety Features," Mak and Sicking (2003) developed the Roadside Safety Analysis Program (RSAP). The main objective of Project 22-9 was to develop an improved cost effective analysis procedure for assessing roadside safety improvements. The RSAP incorporated two integrated programs: the Main Analysis Program, which contained the cost-effectiveness procedure and algorithms, and the User Interface Program, which provided a user friendly environment for data input and review of program results. The cost-effectiveness procedure incorporated in RSAP was based on the concept of incremental benefit/cost analysis. In 2009, NCHRP Project 22-27, "Roadside Safety Analysis Program (RSAP) Update," was started to assist the AASHTO Technical Committee on Roadside Safety to develop the next edition of the AASHTO Roadside Design

Guide. The objectives of this project were to rewrite the software, update the manuals, improve the user interface, and update the embedded default data tables of the RSAP (NCHRP 22-27, 2012).

Donnell et al. (2002) reviewed the methods used to assess median safety on interstates and expressways in Pennsylvania, upon observations of cross-median collisions (CMCs) on highways where median barriers were not warranted by the Pennsylvania DOT design policy. A critical literature review and assessment of median safety practices for various state DOTs were conducted, and qualitatively assessed median safety practices were used to provide input for quantitative data collection. Negative binomial regression models were used to model CMC frequencies on earth-divided highways. The qualitative results from the study suggested that three-strand cable barriers, strong-post W-beam guardrails, or concrete barriers were recommended as median barriers and were warranted by site conditions. The quantitative results showed that CMCs were rare events and that nearly 15% involved fatalities and 72% involved nonfatal injuries. Additional findings concluded that CMC rates at earth-divided highways decreased as the median width increased, that CMCs appeared more likely to occur downstream of interchange entrance ramps, and that CMCs were more likely to involve adverse pavement surface conditions (e.g., wet or icy) than other crashes.

In a project funded by the New Jersey DOT, Gabler et al. (2005) evaluated the post-impact performance of two median barrier systems in New Jersey: a three-strand cable median barrier system and a modified Thrie-beam median barrier system. FE modeling was adopted as a major means for the investigation. The project also included field investigation of crashes into the subject barriers and a survey of the median barrier experience of other state DOTs. This study concluded that Thrie-beam median barrier was capable of containing and redirecting passenger vehicles, as well as a limited number of heavy vehicles. The Thrie-beam median barrier also reduced the incidence of higher severity cross-median collisions but increased the number of less severe collisions.

In a subsequent study also funded by the New Jersey DOT, Gabler and Gabauer (2006) investigated the fatalities and injuries in accidents involving W-beam guardrails on New Jersey highways. The study found that the guardrails generally performed well in vehicular crashes and only accounted for 1.5% of total highway fatalities. This study also found that occupant injuries in guardrail crashes were not a major issue unless the vehicle had a rollover: three-fourths of all occupants exposed to guardrail crashes suffered no injuries. Some of the issues related to the guardrail performance were also identified. For example, the study found that over half of all the fatal collisions with guardrails involved secondary events, i.e., either a second impact or a rollover. It was also found that 14% of all fatal crashes on guardrails resulted in a rollover, and that light trucks had a significantly greater chance of vaulting and/or rollover than other vehicles when colliding with the guardrail.

The placement of median barriers on sloped medians imposed a significant challenge to retaining the desired performance as seen on flat terrains. The performance tests specified by NCHRP Report 350 and MASH were all based on flat terrain conditions, though terrain conditions can have a significant effect on the barrier's impact performance (AASHTO 2011). Median slopes can affect the performance of the barrier, because the vehicle may

engage the barrier in a significantly different manner than on flat terrain. In NCHRP Project 17-14, “Improved Guidelines for Median Safety,” researchers attempted to develop guidelines for using a median barrier and selecting median widths/slopes (Hughes, 2004). Unfortunately, the collection of data needed for this project proved to be very expensive and the data limitations hampered the strength of the recommendations. The project results have not been incorporated into practice, but should be very beneficial to future research.

Abu-Odeh et al. (2008) investigated the sensitivity of W-beam guardrail placement in front of and on a median slope steeper than 2H:1V. This study focused on the post length and post placement parameters when evaluated under the conditions and criteria of NCHRP Report 350 TL-3. Bogie tests were performed and simulated with FE as sensitivity analyses to determine the guardrail placement along the slope. It was determined the guardrail should be placed 1 ft (0.3 m) off the slope break with a post spacing of 3.125 ft (0.95 m) and a full scale crash test was performed with a pickup truck. Although the vehicle was contained and redirected, it rolled over after impact failing the criteria of NCHRP Report 350 conditions.

To avoid some of the obstacles that NCHRP 17-14 faced, the NCHRP 22-21 focused on typical cross-section designs for a construction or reconstruction project rather than on the exact cross-section design at a particular point. The typical cross-section designs were determined early in the design process before adjustments were made to account for variations along the alignment (e.g., horizontal and vertical curves, interchanges and intersections, and special drainage requirements). The Project 22-21 was started on January 2006 and was completed in April 2011. In 2014, Graham et al. (2014) released, “NCHRP Report 794: Median Cross-Section Design for Rural Divided Highways”. The report contains guidance on the interrelationships between median width, median slope, and the use of median barrier on crash risk and severity. Practitioners can then use the collected data to evaluate the safety implications of various median cross-section designs, including barrier type and placement guidelines (NCHRP 22-22, 2010), so that a cost-effective design can be achieved. The NCHRP 22-22, “Placement of Traffic Barriers on Roadside and Median Slopes,” has been extended to NCHRP 22-22(02) “Effectiveness of Traffic Barriers on Non-Level Terrain” to conduct simulation modeling in accordance with the approved plan developed in NCHRP 22-22 and verify the results by conducting crash testing. The results of NCHRP 22-22(02) are to be incorporated into the final product of NCHRP 22-21 (2011).

In 2009, MASH was published to supersede the old roadside safety standard, NCHRP Report 350. MASH presents uniform guidelines for crash testing permanent and temporary highway safety features and recommends evaluation criteria to assess test results. MASH does not supersede any guidelines for the design of roadside safety hardware, which are contained within the AASHTO *Roadside Design Guide*. As of January 1, 2011, the Federal Highway Administration (FHWA) has required that all new product designs be tested using MASH test criteria for use on the National Highway System. A few of the significant changes from NCHRP Report 350 to MASH include:

- The weight of the small car test vehicle was increased from 1,800 lbs. (820C) to 2,420 lbs. (1100C)
- The impact angle of the small test vehicle was increased from 20° to 25°

- The weight of the pickup truck test vehicle was increased from 4,400 lbs. (2000P) to 5,000 lbs. (2270P)
- The mass of the single unit truck in TL-4 was increased from 18,000 lbs. (8,000 kg) to 22,000 lbs. (10,000 kg) and the impact speed was increased from 50 mph (80 km/hour) to 56 mph (90 km/hour).

In 2010, the FHWA released a memorandum to provide guidance to all state DOTs on the installation heights of G4(1S) strong-post W-beam guardrail systems on the National Highway System (NHS) (Nicol, 2010). The standard 27-inch guardrail was no longer able to meet the superseded NCHRP Report 350 or the current MASH TL-3 criteria; therefore, a new minimum guardrail height was recommended from prior crash test data of seven full scale crash tests and three FE simulations. Although 16 states had made revisions to the minimum installation height of a G4(1S) guardrail to 27-¾ inches, the FHWA recommends the State DOTs consider a 31-inch guardrail design.

A study was conducted to analyze the severity of median barrier crashes using data from 2000 – 2004 on rural divided Interstate highways and expressways with longitudinal median barrier in North Carolina (Hu and Donnell 2010). The criteria used for the analysis included median barrier type, the barrier's offset distance from the edge of the travel lane, roadway segment characteristics, roadway surface conditions, driver and vehicle characteristics, median barrier placement, and median cross-slope data. The major conclusion of this study was that less severe crash outcomes pertained to those on cable median barriers when compared to concrete barriers and W-beam guardrail. It was also observed that the barrier's offset distance from the travel lane was associated with a lower probability of severe crash outcomes and that cable barriers placed on steep median slopes were associated with an increased probability of severe crashes.

In 2010, Hampton et al. (2010) conducted crash tests and FE analysis on already damaged sections of the G4(1S) W-beam guardrails. The FEA work will be discussed in depth in subsequent sections. The testing of already damaged barrier systems had not previously been conducted. Two crash tests were performed by the MGA Research Corporation for the NCHRP Project 22-23, "Criteria for Restoration of Longitudinal Barriers," to evaluate the performance of guardrails with pre-prescribed rail and post deflections. The first crash test was conducted at 30 mph (48.3 km/hour) with an impact angle of 25° and resulted in a 36 ft (10.97 m) damaged section of barrier with a maximum deflection of 1.21 ft (0.37 m). The second crash test was performed in the damaged location; however, the results were undesirable. The barrier provided little to no resistance to the impacting vehicle, which vaulted over the barrier. These results were due to a failed link present in the barrier that separated the post from the rail. The study concluded that a deflection of 0.92 ft (0.279 m) or more on the post and rail would result in the vehicle vaulting over the median barrier.

Gabauer et al. (2010) also conducted research on the G4(1S) guardrail performance with minor damage already done to sections. There were five types of damage that were assessed using pendulum impacts: vertical tear, horizontal tear, splice damage, twisted blockout, and missing blockout. W-beam rupture was observed in tests with vertical tear damage due to the tear causing a stress concentrator and was recommended to be repaired with high priority.

There was no evidence of rail rupture near the location of a horizontal tear, but there was an observed splice failure at the higher speed test. The recommendation for a horizontal tear is that tears less than 12 inches and 0.5 inches in width do not significantly affect the performance of the barrier and should be repaired with medium priority. The splice damage was simulated with one of the bolts having lost all bearing capacity and had a performance indistinguishable from the undamaged barrier. The recommended repair priority for a single compromised bolt is medium with a high priority for more than one bolt. A twisted blockout had little to no effect on the performance of the barrier and was recommended to have a low repair priority. The performance of the barrier with a missing blockout was marginal to unacceptable for the higher speed tests with a medium priority for repair. Further investigations with full-scale crashes would help evaluate vehicle trajectory and stability due to limitations of just pendulum tests.

Ochoa and Ochoa (2011) completed a study to optimize guardrail barriers for rural roadways in the U.S., Europe, and some developing countries. In order to optimize the W-beam guardrail, the main methods for identifying failures had to be defined and considered. In the conventional strong-post W-beam guardrails, the relatively high release load varied by approximately 360% and was further compounded by another 40% due to variations in the yield strength of guardrail panels. A physics-based guardrail analysis was performed to determine the solution of optimizing the release load in relation to post section properties. This optimization was accomplished by introducing an improved fastening system that incorporated a separate deformable release member to consistently provide a predefined release load of around 1,700 lbs. (7,565 N) with a maximum variation of 20%. The versatile W-beam guardrail incorporating these improvements was successfully crash tested and accepted by FHWA at NCHRP Report 350 test levels and at MASH TL-3 conditions.

In 2011, AASHTO published the new *Roadside Design Guide*, which presented a synthesis of current information and operating practices related to roadside safety. The guide was intended to be used as a resource document from which individual highway agencies could develop standards and policies. It was focused on safety treatments that could minimize the likelihood of serious injuries when a motorist leaves the roadway. The 2011 edition was updated to include hardware systems that had been tested to meet the evaluation criteria contained in the NCHRP Report 350. It also included an outline of the most current evaluation criteria contained in MASH.

In 2012, Findley et al. (2012) at the Institute of Transportation Research and Education, North Carolina State University, conducted a statewide structural and safety investigation on the performance of weathered steel beam guardrails (WSBG) in North Carolina. This study was prompted when New Hampshire found that the WSBG deteriorates at a much faster rate compared to the galvanized steel guardrail (GSG) in the northeast due to the harsher weather conditions. The study concluded that in all test sites across North Carolina, there were no structural concerns about using WSBG in the state. Additionally, the research results suggested a lower percentage of injury collisions associated with WSBG installations than the GSG installations at comparison sites. However, this study used a small sample size and further investigation would need to be made for a more robust comparison.

Alluri et al. (2012) evaluated the safety performance of the G4(1S) guardrail system installed on both limited and non-limited access facilities in Florida. The effectiveness of the guardrail was measured by the percentage of vehicles prevented from crossing the guardrail during a crash. During the years 2006-2010, there were a total of 7,290 crashes involving the G4(1S) guardrail on limited access facilities and 1,384 on non-limited access facilities. For the limited access facilities, 95.3% of the vehicles were prevented from crossing over the guardrail, which broke down into 97.5% for cars and 91.6% for light trucks (included vans and trucks with four rear tires). If you separate median and roadside guardrail locations, then 95.5% of all vehicles were prevented from crossing over at median locations and 94.5% at roadside locations. Medium and heavy trucks were found to have significantly lower crossover percentages, around 78%, due to the guardrail system not being designed for those vehicle types. The severity of crossover crashes was found to be higher than that of non-crossover crashes, with over-rides being the most severe. The non-limited access facilities had similar findings as guardrails installed in median locations had a higher prevention percentage.

Researchers at the Midwest Roadside Safety Facility (MwRSF) performed a study on the safety performance of the Midwest Guardrail System (MGS) with no blockout. This revised design could possibly be used at locations where the required 12-inch blockout would not work and an alternative was required. They successfully crash tested the non-proprietary design of the MGS with 31 inch of rail height using a passenger car and a pickup truck under MASH TL-3 conditions (Schrum et al. 2013). The results of this report suggested that the MGS with no blockout could be used on roadways where the width of the blockout was a limiting factor and the standard MGS with blockouts was recommended for other locations.

In 2013, Abu-Odeh et al. (2013) at Texas A&M Transportation Institute investigated the redesign of a G4(1S) double-faced W-beam guardrail system that was originally published in NCHRP Project 22-14(03): “Evaluation of Existing Roadside Safety Hardware Using Updated Criteria – Technical Report.” The guardrail system design presented in Project 22-14(03) was a 27-inch guardrail which was unable to pass the MASH TL-3 impacts. The redesigned guardrail system was raised to a guardrail height of 31-inches and had the splice relocated from the post. FE simulations were used prior to full scale testing that indicated the redesigned barrier system would pass the MASH evaluation criteria. The full scale crash tests used a sedan sized vehicle and a pickup truck under MASH TL-3 impact conditions. Both crash tests passed the evaluation criteria and the MASH compliant modified double-faced W-beam guardrail system was now an option for state DOTs to implement if needed.

2.2 Crash Modeling and Simulations

Mackerle (2003) provided a bibliography that included 271 references published between 1998 and 2002 on crash simulations using FEA and on impact-induced injuries. This bibliography categorized the references into four different topic areas: 1) Crash and impact simulations where occupants were not included; 2) Impact-induced injuries; 3) Human surrogates; and 4) Injury protection. Topics in the first area included crashworthiness of aircrafts and helicopters, automobiles, and vehicle rail structures. The second area of research utilized two major types of models for humans, the crash dummy and real human body models. Research topics in this area were mainly on biomechanics and impact analyses for

various human injuries. Topics on human surrogates focused on the development FE models of hybrid and other types of human dummies. These dummy models were used to obtain dynamic responses of the whole human body during impacts, which were difficult to measure experimentally. In the area of injury protection, FEA were utilized to simulate and analyze injury protection systems such as seat belts, air bags, and collapsible structures to reduce serious or fatal injuries. The references included in Mackerle's bibliography were generally useful to the work on FE crash simulations; however, only a few references under injury protection were related to roadside safety.

Most publicly available FE models of vehicles and roadside safety structures were developed at the FHWA National Crash Analysis Center (NCAC) at George Washington University. Since the 1990s, significant efforts have been put on the development of FE models for crash analysis. Most of these models are available as LS-DYNA input files from NCAC's website (NCAC web1). A list of references on these modeling efforts and the simulation work performed at NCAC is also available from NCAC's website (NCAC web2).

The modeling and simulation efforts from NCAC can be found in several representative works. Marzougui et al. (2000) developed the FE model of an F-shaped portable concrete barrier (PCB) and validated the model with full-scale crash test data. With the proven fidelity and accuracy of the modeling methodology, the models for two modified PCB designs were created and used in FE simulations to evaluate their safety performance. A third design was then developed based on the simulation results and its performance was analyzed. In the work by Zaouk et al. (2000a, 2000b), a detailed FE model of a 1996 Plymouth Neon was developed. The three dimensional geometric data of each component was obtained by using a passive digitizing arm and then imported into a preprocessor for mesh generation, part connections, and material properties assignment. Tensile tests were conducted on specimens to obtain the material properties of the various sheet metal components. The body-in-white model was used in the simulation of a frontal impact and the results were compared with test data to evaluate the accuracy and validity of the model.

Kan et al. (2001) developed an integrated FE model that included the vehicular structure, interior components, an occupant (Hybrid III dummy), and an airbag for crashworthiness evaluation. The integrated model was then used in a case study to demonstrate the potential benefit of the integrated simulation and analysis approach. This approach which would further improve the engineering practice with cost savings, while also producing more accurate and consistent analysis results. Marzougui et al. (2004) developed a detailed suspension model and incorporated it into the previously developed FE model of a Chevrolet C2500 pickup truck (Zaouk et al. 1997). Pendulum tests were conducted at the FHWA Federal Outdoor Impact Laboratory (FOIL) and the test data were compared with simulation results of deformations, displacements, and accelerations at various locations. Crash simulations were performed using the upgraded vehicle model and the results were compared with crash data from previously conducted full-scale tests.

To facilitate the use of FE simulations to evaluate roadside safety structures at higher test levels specified by NCHRP Report 350, Mohan et al. (2007) improved and validated a previously developed model of a 1996 Ford F800 single unit truck. This 18,000-lb (8,172-kg)

truck was used as the standard TL-4 vehicle in NCHRP Report 350. Simulations were performed using the improved model and the results were compared with those from a full-scale crash test. The global kinematics and the acceleration time histories of the truck from simulations were found to correlate well with the test data. The research also suggested considering frictions between the tires and barrier and between the tires and ground so as to correlate well on the vehicle's yaw.

In a study by Marzougui et al. (2007), the FE model of a W-beam guardrail was developed and validated using full-scale crash test data. The model was shown to give an accurate representation of the real system based on comparison of the vehicle's roll and yaw angles. Using the validated model, they performed four simulations of a passenger truck impacting the W-beam guardrails with different rail heights. The simulation results showed that the effectiveness of the barrier to redirect a vehicle could be compromised when the rail height was lower than the recommended value.

Researchers from the roadside safety group at Worcester Polytechnic Institute utilized FE models in a number of roadside safety studies. Ray (1996a) analyzed the data from full-scale crash tests and developed a criterion using statistical parameters to assess the repeatability of a full-scale crash test. The evaluated simulation results were also compared to crash test data. Ray (1996b) reviewed the history of using FEA in roadside safety research and presented the vehicle, occupant, and roadside hardware models that had been developed to date. Ray and Patzner (1997) developed a nonlinear FE model of a modified eccentric loader breakaway cable terminal (MELT) that was common for W-beam guardrails and used it in simulating a full-scale crash test involving a small passenger car. Based on a comparison of simulation results with crash test data, and the FE model was recommended to be used in the evaluation of new design alternatives. Plaxico et al. (1997) developed a 3D FE model of a modified Thrie-beam and simulated the impact of a compact vehicle. The computational model was then calibrated with data from an actual field test that was previously conducted as part of a full-scale crash test program carried out under the auspices of FHWA. Plaxico et al. (1998) developed the FE model of a breakaway timber post and soil system used in the breakaway cable terminal (BCT) and the modified eccentric loader BCT. Simulation results were compared and found to correlate well to data from physical tests. In the work of Patzner et al. (1999), they examined the effects of post strength and soil strengths on the overall performance of the MELT terminal system using a nonlinear FE model. A matrix of twelve simulations of particular full-scale crash test scenarios was used to establish the combinations of post and soil strengths from which favorable situation(s) could be identified. This parametric study showed that certain combinations of soil and post strengths could increase the hazardous possibilities of wheel snagging, pocketing, or rail penetration, while other combinations produced more favorable results.

Plaxico et al. (2000) compared the impact performance of two strong-post W-beam guardrails, the G4(2W) and G4(1W). After validating the FE model for the G4(2W) guardrail with data from a full-scale crash test, the FE model of the G4(1W) guardrail was developed. The two guardrails were compared with respect to deflection, vehicle redirection, and occupant risk factors. The two systems were found to perform similarly in collisions and satisfied the requirements of the NCHRP Report 350 for the Test 3-11 conditions. Using LS-

DYNA simulations and laboratory experiments, Plaxico et al. (2003) investigated the failure mechanism of the bolted connection of a W-beam rail to a guardrail post, which could have a significant effect on the performance of a guardrail system. A computationally efficient and accurate FE model of the rail-to-post connection was developed for use in the performance evaluation of guardrail systems using LS-DYNA. Orengo et al. (2003) presented a method to model tire deflation in LS-DYNA simulations along with examples of the use of this improved model. The simulation results showed that deflated tires had significantly different behaviors from those of inflated tires as observed in real world crashes and in full-scale crash tests. A vehicles' kinematics were found to be strongly coupled to the behaviors of deflated tires. Therefore, modeling such behaviors is critical to roadside hardware simulations. In a separate study by Ray et al. (2004), LS-DYNA simulations were used to determine if an extruded aluminum bridge rail would pass the full-scale crash tests for TL-3 and TL-4 conditions of NCHRP Report 350. The simulation results, which were supported by a subsequent AASHTO load and resistance factor design (LRFD) analysis, indicated a high likelihood of passing the crash tests.

FE simulations have also been used by researchers at the Midwest Roadside Safety Facility (MwRSF). Reid (1996) utilized FEA to study the influence of material properties on automobile crash structures and attempted to develop crashworthiness guidelines for design engineers. In one of his later works, Reid (1998) demonstrated through the use of two simple examples, contact definition and damping, how potential modeling issues could easily be overlooked in FE impact simulations. He also suggested ways to check for modeling errors and how to make improvements. In the work of Reid and Bielenberg (1999), FE simulations were performed for a bullnose median barrier crashed by a 4,405-lbs (2000-kg) pickup truck to determine the cause of failure and to obtain a potential solution to the problem. In a collaborative work to improve the FE model of a Chevrolet C2500 pickup truck (Reid and Marzougui 2002; Tiso et al. 2002), structural modeling methods were introduced for model improvement through refining meshes, using more sophisticated material models, adding details to simplified components, and improving connections between components. Suspension modeling, which was critical to the correct vehicle dynamic responses, was also investigated in this collaborative work and a new model was successfully developed with significant improvements.

To educate roadside safety engineers and promote the use of simulations, Reid (2004) summarized ten years of the simulation efforts on the development of new roadside safety accessories performed at the MwRSF. In the work of Reid and Hiser (2004), they studied the friction effects between solid elements and for component connections, as well as their interactions in crash modeling and analysis. In their work on modeling bolted connections that allowed for slippage, Reid and Hiser (2005) investigated two modeling techniques that were based on discrete-spring clamping and stressed clamping using deformable elements. The simulation results for both models compared well with test data, with the stressed clamping model using deformable elements having better accuracy accompanied with a significantly increased computational cost. Hiser and Reid (2005) also investigated improved FE modeling methods for slip base structures, which could have a considerable potential for reducing the amount of crash resistance and thus occupant injury. They developed and evaluated two bolt preloading methods, with one using discrete spring elements and the other

using pre-stressed solid elements. Similar to their findings in the work of modeling hook-bolts, they found that the method using solid elements was more accurate than that using discrete spring elements when the impact conditions became more severe. The results showed that the slip base model was acceptable in both end-on impact and length of need impact simulations.

In 2009, Reid et al. (2009) investigated the potential of increasing the suggested flare rates for strong-post W-beams to reduce guardrail installation lengths, which would result in decreased guardrail construction, maintenance costs, and impact frequency. Both computer simulations and full-scale crash tests were used in the evaluation of increased flare rates up to, and including, 5H:1V. Simulation results indicated that the conventional G4(1S) guardrail modified to incorporate a routed wood blockout could not successfully meet NCHRP Report 350 crash test criteria when installed at any flare rates steeper than the recommended 15H:1V in the Roadside Design Guide. Their study also showed that the MGS could meet NCHRP Report 350 impact criteria when installed at a 5H:1V flare rate, yet with greater impact severities observed from the tests than anticipated. The research also indicated that whenever roadside or median slopes are relatively flat (10H:1V or less), increasing the flare rate on guardrail installations became practical and had some major advantages including significantly reducing the guardrail lengths and associated costs. The study, however, did not give any indications of W-beam performance on steeper slopes.

FE simulations were also found in the work of other researchers in roadside safety research. Whitworth et al. (2004) evaluated the crashworthiness of a modified W-beam guardrail using detailed FE models of a guardrail and a Chevrolet C2500 pickup truck. The simulation results were compared and found to be in agreement with crash test data in terms of roll and yaw angles. Simulations were also performed to evaluate the effects of rail mounting height and routed/non-routed blockouts, on the crashworthiness and safety performance of the system. In the work of Bligh et al. (2004), FEA was utilized to develop new roadside features to address three roadside safety issues. An alternative design to the popular T6 tubular W-beam bridge rail was developed to address problems with vehicle instability observed in full-scale crash testing. A retrofit connection to Texas DOT's grid-slot portable concrete barrier was developed to limit dynamic barrier deflections to levels that were more practical for work zone deployments. Finally, crashworthy mow strip configurations were developed for use when vegetation controls around guard fence systems were desired to reduce the cost and risk associated with hand mowing.

Computer simulations were also used by international researchers on roadside safety research. Using LS-DYNA simulations, Atahan (2002) analyzed a strong-post W-beam guardrail system that failed in a previously conducted full-scale crash test. After identifying the cause of failure and incorporating necessary improvements, a new W-beam guardrail was developed and showed improved performance based on simulation results. Atahan (2003) also studied the performance of the G2 steel weak-post W-beam guardrail system installed at the slope-break point on non-leveled terrains using LS-DYNA simulations. The simulation results showed that there was a risk of increased vehicle instability when the roadside slope adjacent to the W-beam guardrail became steeper than 6H:1V.

Using LS-DYNA simulations, Fang et al. (2010) conducted a study to evaluate the performance of three types of barriers on sloped medians: a single-faced W-beam guardrail, two designs of double-faced W-beam guardrails, and a low-tension cable barrier. The three types of barriers were evaluated under vehicular impacts at multiple speeds and impact angles. The simulation results suggested that the effectiveness of the W-beam guardrails and cable barriers could be reduced on sloped medians compared to their performance on flat terrain as specified in NCHRP Report 350. It was observed from all barrier types that the frequency and severity of vehicle rollover rose with increased impact angles. This observation was shown to be true for the single-faced W-beam guardrail, both designs of the double-faced W-beam guardrails, and cable barriers. It was also observed that the performance of the barriers investigated in this project exceeded the TL-3 requirements of NCHRP Report 350, considering the large median slopes (4H:1V and 2.5H:1V) and having higher impact speeds than the standard impact conditions.

Dorcely and McKyes (2010) theoretically investigated the interactions between barrier posts and soil near the crown of a slope. The theoretical results matched smoothly to the case where the slope was far away from the post and predicted a gradual reduction of maximum horizontal soil resistance by up to 60% when a post was installed near the crown of a slope. By installing the post to a greater depth, the resistance of a post could be increased. The theoretical increase of depth by 36% almost doubled the maximum horizontal post resistance. It was found to be critical that a post be surrounded by heavily compacted soil, which can lead to a horizontal resistance four times that of lightly compacted soil. The surface roughness of the post, such as a concrete post, was also found to almost double the horizontal resistance versus that of a smooth surfaced post. These results would be further justified by conducting follow-up studies using FE simulations and crash tests.

Vehicular impact height is one of the important parameters in evaluating the performance of barrier systems. The vehicle's impact height can vary depending on the trajectory of the vehicle along the median and the lateral offset of the barrier. Ferdous et al. (2011) analyzed the performances of the modified G4(1S) W-beam guardrail, modified Thrie-beam guardrail, Midwest Guardrail System, and modified weak post W-beam guardrail using LS-DYNA. Each model was validated based on the results obtained from existing crash tests. Using vehicle models from NCHRP Report 350, the override and under-ride limits for each guardrail model were identified. The performance limit of each barrier was determined by parametrically varying the vehicle impact height to determine at what point the override or rollover for the pickup truck and under-ride for the small passenger car would occur.

In 2012, Marzougui et al. (2012) investigated some barrier systems that passed the NCHRP Report 350 requirements but failed to pass the MASH requirements to determine if the barrier systems could be retrofitted with various modifications to improve the performance. These modifications were conducted on six G9 Thrie-beam guardrails and three G4(1S) W-beam guardrails using FE simulations. The simulation results showed that with the proposed modifications, the guardrails that originally failed to pass the MASH requirements were able to retain the vehicle under MASH TL-3 conditions and to reduce the propensity to vault over the guardrails.

Hampton et al. (2013) evaluated the performance of strong-post W-beam guardrails with missing posts under impact conditions specified by the NCHRP Report 350. The effects of missing posts on the guardrails performance were quantitatively evaluated using FE simulations of crash tests under impacts of a 4,409-lbs (2,000-kg) pickup truck. Simulations in which one, two, or three posts were removed from the guardrails were conducted with varying points of impact to evaluate the effects of missing posts. The FE simulation results demonstrated that guardrails missing even one post could have remarkably decreased performance under vehicular impacts due to wheel snagging. It was also observed that both the maximum deflection and maximum rail tension were greatly increased as more posts were removed from the guardrail. The overall conclusion of the study was that even if one post was missing, the guardrail performance could be significantly reduced and post replacement should be a high-priority repair for guardrail maintenance.

Ferdous et al. (2013) furthered the research from NCHRP Project 22-22 to include numerical simulations to evaluate the performance of commonly used traffic barriers on roadside and median slopes. The modified G4(1S) W-beam guardrail, modified Thrie-beam guardrail, Midwest guardrail system, and modified weak-post W-beam guardrail were selected for evaluation. The barriers were placed on both the foreslope and backslope when testing the truck model, while placing them near the bottom of the ditch for the small-car test. The modified G4(1S) system was found to have the lowest override limit due to its lower rail mounting height of 28 inches. This system was also prone to more vehicle post-snagging due to the narrower blockouts than that of the Midwest guardrail system. For the truck, placing the W-beam farther up the slope towards the shoulder produced results that were expected to pass the safety evaluation criteria and an increase in the median slope would require the W-beam to be even farther up. Since the NCHRP Report 350 guidelines were used in this study results are expected to change if MASH guidelines are adhered to.

Mongiardini and Reid (2013) investigated relevant phenomena in simulation models that would help create a more accurate representation of the kinematics and dynamics of an actual full-scale crash test. Modifications to the steering system, tire size, and bumper failure were analyzed. A properly working steering system was found to have an insignificant role due to the deformation of the suspension A-arm at impact inducing a steering effect, as well as the tires being forced to slide over the ground. Although the bumper usually plays a relatively minimal role in a full-scale crash test, the definition of a failure mechanism for the front bumper was found to be crucial for simulating the vehicle kinematics. Without this failure mechanism the bumper restricted the wheel from steering properly when it contacted the barrier post. This caused the tire to roll over the second post hit during impact, thus limiting the proper redirection of the vehicle. Similarly, the correct modeling of tire size was essential for simulating the interaction between the wheel and posts.

Abu-Odeh et al. (2013) evaluated post placement positioning when the rail is over the slope breaking point. Even though the AASHTO Roadside Design Guide recommends posts to be installed two feet in front of a slope break, there are often restrictive environmental conditions, such as mountainous terrain, where this is not feasible. The simulations indicated that a 31 inch W-beam guardrail system with 8 foot long posts, spaced 6.25 feet apart on centers met MASH TL-3 criteria. These simulations placed the guardrail system a foot down

from the slope break on a 2H:1V slope and the posts were placed off splice. Full-scale crash tests were used to confirm the simulation results.

Marzougui et al. (2015) used FE simulations and applied vehicle dynamic tools to assess the trajectories of vehicles leaving the traffic lane on curved, superelevated roadway sections. The research was intended to develop a better understanding of the influence of various roadway curvatures, superelevation, shoulder/roadside designs, and barrier features. In addition, the safety performance of the barrier's dynamic response to the vehicle impacts were assessed. The study included two vehicles, three impact angles, three impact velocities, and six roadway designs with curvature and superelevation. A conclusion drawn from the results indicated that barriers with increased height and deflection zone should be used for sharper curves and the higher levels of superelevation. Although this research is still ongoing due to inability to draw conclusive results, additional research is occurring to develop further recommendations for the selection and placement of barriers on curved and superelevated roadways.

FE simulations, particularly conducted with LS-DYNA, have been used increasingly more in roadside safety research. In addition to the abovementioned references, FHWA published several manuals on using LS-DYNA material models and evaluation of these models (Lewis 2004; Murray et al. 2005; Murray 2007; Reid et al. 2004). These references can also be useful in the crash modeling work using LS-DYNA (LSTC, 2013).

3. Finite Element Modeling of Vehicles and W-beam Guardrails

The simulation work of this study involved finite element (FE) models of two vehicles (a 1996 Dodge Neon and a 2006 Ford F250) and five NCDOT W-beam guardrail configurations, each with 29- and 31-inch placement heights. The FE models of five guardrails were created in this project: 1) single-faced guardrail installed on a 2.5H:1V slope; 2) double-faced guardrail installed on a 2.5H:1V slope; 3) double-faced guardrail, with a lowered backside rail, installed on a 2.5H:1V slope; 4) single-faced guardrail with a convex horizontal curvature installed on a 2.5H:1V slope; and 5) single-faced guardrail with a concave horizontal curvature installed on a 4H:1V slope. All of these configurations were evaluated using crash simulations in which the two vehicles impacted the guardrails at 62 mph (100 km/hour) and at a 25° impact angle. Two additional simulations were conducted for configuration one using the 1996 Dodge Neon impacting the two single-faced guardrails at an impact speed of 70 mph (112.6 km/hour) and at a 25° impact angle.

In all simulation cases, the vehicle departed the travel lane at the prescribed speed and angle before hitting the guardrail. The impact speed was defined in the vehicle’s travel direction, and the impact angle was defined as the angle between the vehicle’s travel direction and the guardrail’s longitudinal direction.

3.1 FE Models of a Passenger Car and Pickup Truck

The FE models of the two vehicles used in this project were a 1996 Dodge Neon passenger car and a 2006 Ford F250 pickup truck, as shown in Fig. 3.1. Table 3.1 gives the specifications of the two vehicles relevant to this study.

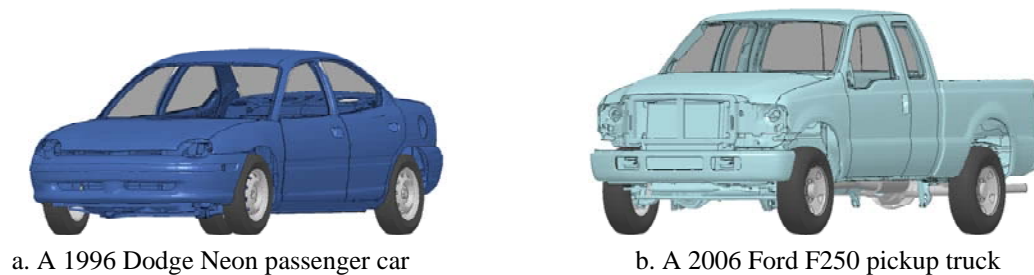


Fig. 3.1: FE models of the two vehicles used in crash simulations.

Table 3.1: Specifications of the two test vehicles used in crash simulations

Specification	Test Vehicle	
	1996 Dodge Neon	2006 Ford F250
Curb weight *	2,403 lb (1,090 kg)	5,504 lb (2,499 kg)
Overall length	171.8 in (4.36 m)	226.4 in (5.75 m)
Overall width	67.5 in (1.71 m)	79.9 in (2.03 m)
Overall height	52.8 in (1.34 m)	76.5 in (1.94 m)
Ground clearance	5.7 in (145 mm)	8.3 in (211 mm)

* The curb weight is the weight of the vehicle with all standard equipment and amenities, but without any passengers, cargo or any other separately loaded items.

The FE model of the 1996 Dodge Neon had a total of 339 parts that were discretized into 283,683 nodes and 270,727 elements (2,852 solid, 92 beam, 267,775 shell, and 8 discrete elements). Ten different constitutive models were used, including the piecewise linear plasticity model defined for most steel components, the rigid model for mounting hardware, the elastic model for the tires and other rubber components, the Blatz-Ko rubber model for nearly incompressible rubber cushions, the viscous damping model for the shock absorbers, the low-density foam model for the radiator core, the spot-weld model for sheet metal connections, the null material model defined for contact purposes, the linear elastic spring model for the spring-damper connection of the front suspension, and the crushable foam model for the bumper energy absorber. Hourglass control was used on components that could potentially experience large deformations. The FE model of the Dodge Neon was originally developed at NCAC and validated with the NHTSA's New Car Assessment Program (NCAP) Frontal-Impact Test 2320 (NCAC, 2007a).

The FE model of the 2006 Ford F250 was composed of a total of 746 parts that were discretized into 737,986 nodes and 735,895 elements (25,905 solid, 2,305 beam, 707,656 shell, and 29 discrete elements). Eleven different constitutive models were used, including the piecewise linear plasticity model defined for most steel components, the rigid model for mounting hardware, the elastic model for the tires and other rubber components, the linear and nonlinear elastic spring model for the suspension springs, the viscous damping model for the shock absorbers, the low-density foam model for the radiator core, the spot-weld model for sheet metal connections, the viscoelastic model for radiator support mounts, the Blatz-Ko rubber model for nearly incompressible rubber cushions, and the null material model for contact purposes. Hourglass control was used on various components that could potentially experience large deformations. The FE model of the Ford F250 was originally developed at NCAC and validated with the NHTSA's NCAP Frontal-Impact Test 5820 (NCAC, 2008).

3.2 FE Models of the W-beam Guardrails

The FE model of the single-faced G4(1S) strong-post W-beam guardrail was originally developed at NCAC and validated using full-scale crash tests at Texas A&M Transportation Institute under NCHRP Report 350's TL-3 conditions (NCAC, 2007b). The FE model contained six different constitutive models: the piecewise linear plasticity model for steel components, the elastic model for the wood blockouts and terminal posts, the soil and foam model for the soils around posts, the rigid model for the bolts, nuts, and road surface, the nonlinear elastic spring model for the bolt-tensioning spring in the long-bolts (used to attach the rails and wood blockouts to the posts), and the null material model for contact purposes.

In the original NCAC model, the soil around each post was a cylindrical block that was suitable for flat-terrain conditions. For W-beam guardrails installed on the shoulder of sloped median, the boundary of the cylindrical soil blocks would not match to the borderlines. In this study, the guardrail model including the soil foundations was obtained from a previous NCDOT research project (Fang et al., 2010; Fang et al., 2013) in which an FE model of a square soil foundation was developed for use on flat terrains. The square soil model, which used the same material model and properties as the original NCAC soil model, was compared and found identical to the circular soil model using simulations of a vehicular crash test. For the model of guardrails placed on a sloped median, the soil model was further modified to

match the grade of the sloped median. Figure 3.2 shows the original NCAC soil model, the square-shaped soil model, and the sloped median soil model developed for this project.

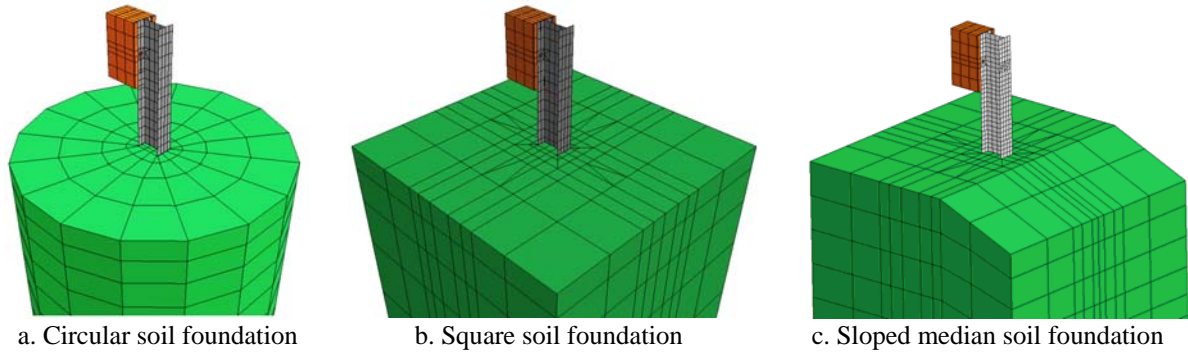


Fig. 3.2: FE models of the soil block around a post.

In addition to modifications on the soil model, modeling issues such as initial penetrations among the components were found in the original guardrail model and were resolved in the FE models of this project. The revised models were found to have improved numerical stability and accuracy of the simulations with the elimination of penetrations and the use of sophisticated contact algorithms. To reduce the computational cost of the simulations and further improve the numerical stability, the guardrail models were simplified on the bolt connections of the rail splices. Figure 3.3 illustrates the location of a guardrail splice where two sections of W-beam rails are joined and secured by eight short-bolts. In the original guardrail model, these short-bolts incorporated a failure mechanism that could separate the bolt and nut upon reaching the failure point (defined by a threshold value of the force). While realistic and capable of emulating the bolt’s behavior, these bolt connections were modeled with their individual components and thus were computationally expensive. It was determined through simulation testing that these short-bolts would never reach their failure point under the impact conditions used in this project, i.e., MASH TL-3 impact conditions. Therefore, the failure mechanism was removed from the short-bolts to simplify the component models. It should be noted that contacts were defined between the short-bolts and the rails so the bolts could still rip out of the holes where the bolts were placed. This modification along with resolutions to other contact issues (e.g., initial penetrations due to mismatched geometries) were found to significantly improve the FE model’s stability and efficiency.

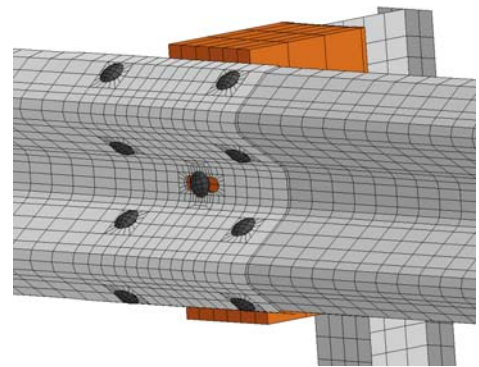


Fig. 3.3: Short-bolts on a guardrail splice.

Another modification made to the guardrail models was the reposition of splice locations from the 29-inch guardrail to the 31-inch guardrail. The splice for the 29-inch guardrail was located at the post; whereas, for the 31-inch guardrail, the splice was located at the mid-span between two adjacent posts (see Fig. 3.4). Since all simulations had an impact location at the post, the severity of impacting the splice location was also investigated.

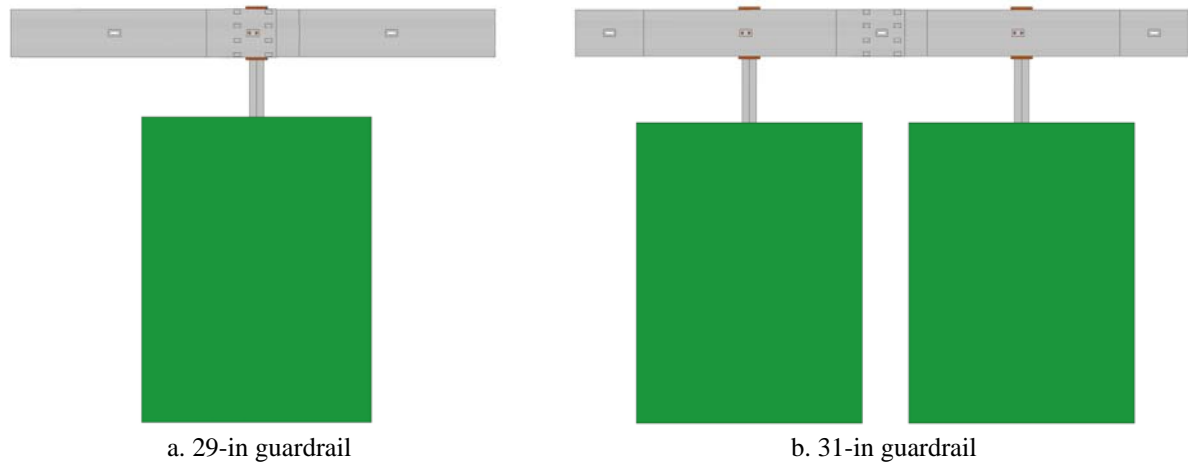


Fig. 3.4: Splice locations for the 29- and 31-inch guardrails in the FE models.

Figure 3.5 shows profile views of the first three guardrail models: the single-faced guardrail, a double-faced guardrail with both front-side and backside rails flash with the top of the post, and a double-faced guardrail with the backside rail lowered by 2.1 in (53.3 mm) considering the lowered grade on the slope. All of the three guardrails were installed on a 2.5H:1V slope.

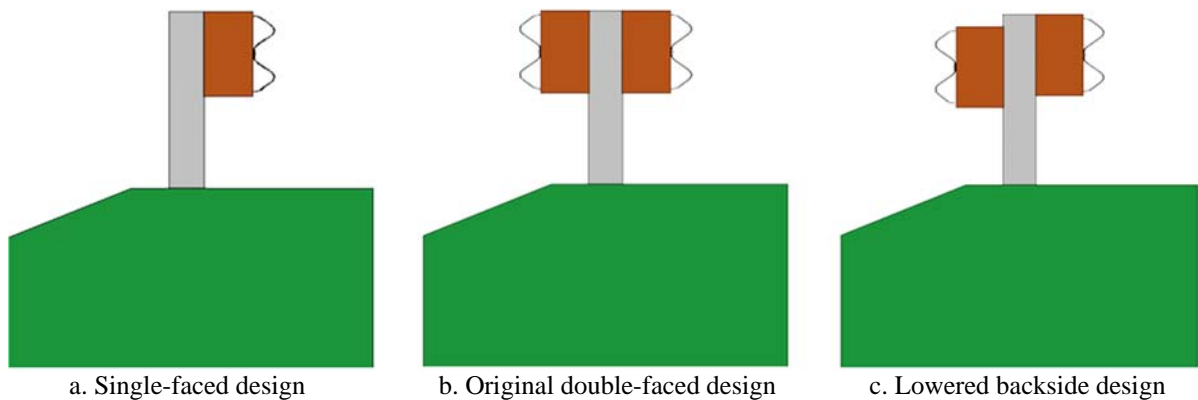


Fig. 3.5: Profile views of the single- and double-faced guardrail FE models.

The FE model of a single guardrail segment (i.e., one guardrail length with two posts), once effectively modified, was duplicated to create the entire 400-ft (122-m) section of the guardrails required for this study. This duplication of the guardrail section was done with an in-house code developed to replicate not only the parts, nodes, elements, and material properties, but also the contact definitions defined between each pair of parts. The program was also capable of merging the ends of adjacent segments with proper numbering and contact definitions. With this program, the guardrail model was generated by duplicating the single guardrail segment to the required length-of-need section and connecting both ends to the terminal sections obtained from the original guardrail model. Figures 3.6, 3.7, and 3.8 illustrate the full FE models a single-faced, a double-faced, and a lowered backside double-faced guardrails, respectively, placed on a 2.5H:1V slope of a six-lane 46-foot median divided freeway.

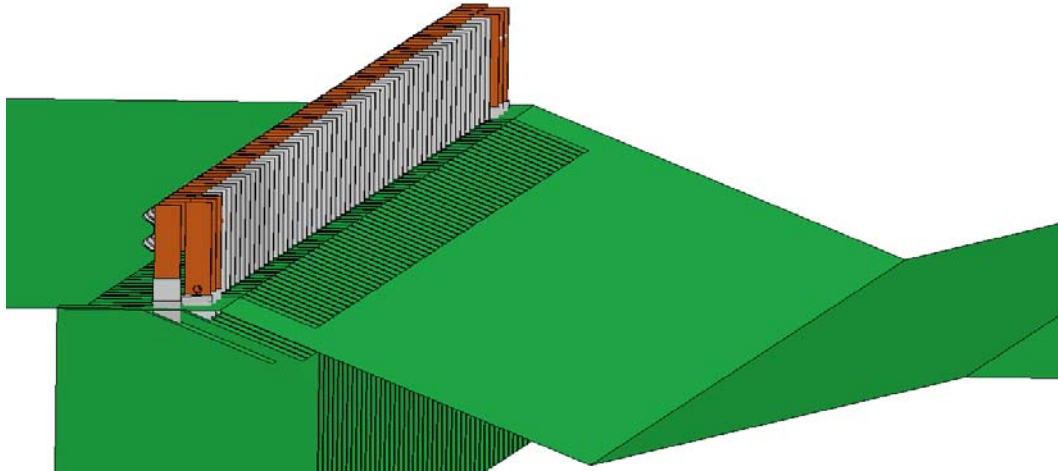


Fig. 3.6: FE model of the single-faced guardrail installed on a 2.5H:1V slope.

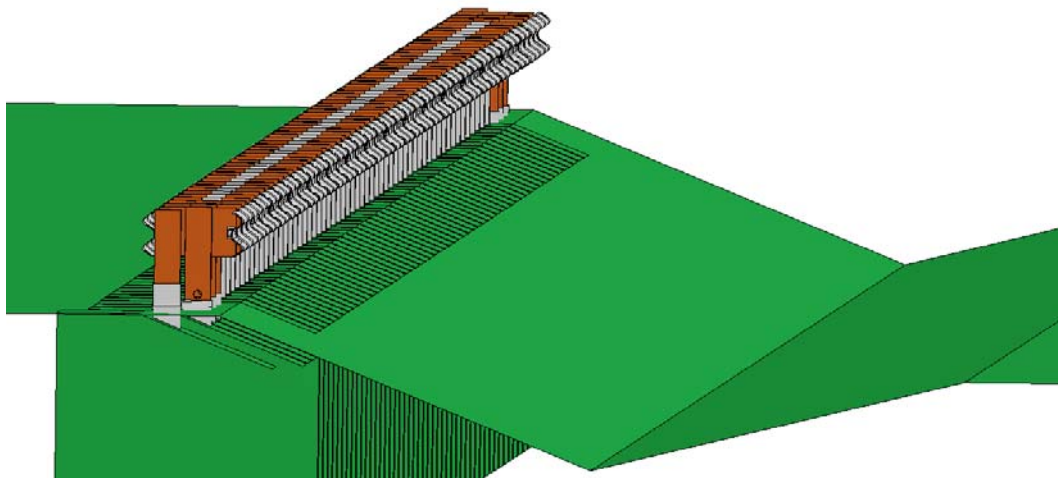


Fig. 3.7: FE model of the double-faced guardrail installed on a 2.5H:1V slope.

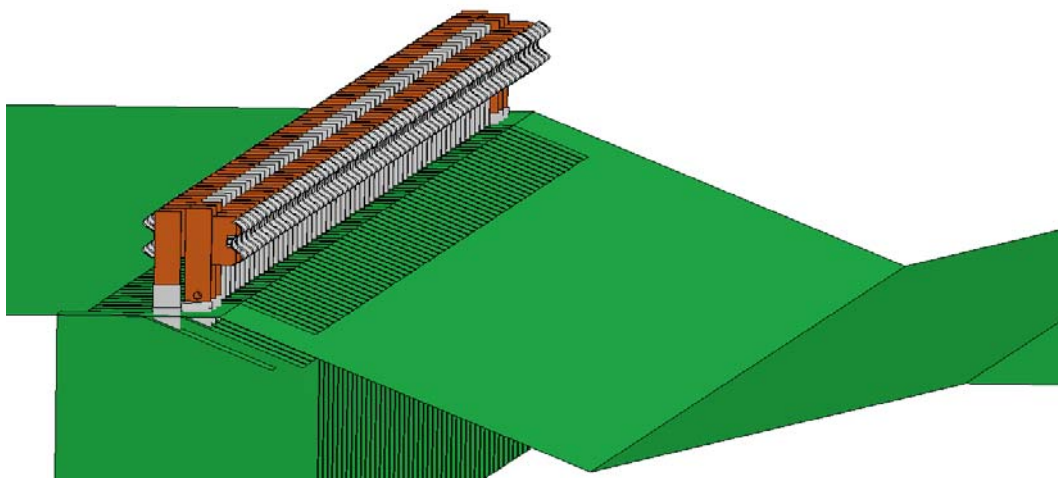


Fig. 3.8: FE model of the lowered backside double-faced guardrail installed on a 2.5H:1V slope.

The remaining two guardrail configurations utilized a single-faced guardrail with the addition of a horizontal curvature. The curvature across the length-of-need barrier section had a radius of curvature of 1,910 ft (582 m), which was equivalent to a 3° curvature. The single-faced guardrail with a convex curvature (i.e., the rail on the convex side of the curve), was installed on a 2.5H:1V slope as seen in Fig. 3.9. The single-faced guardrail with a concave curvature was installed on a 4H:1V slope as seen below in Fig. 3.10.

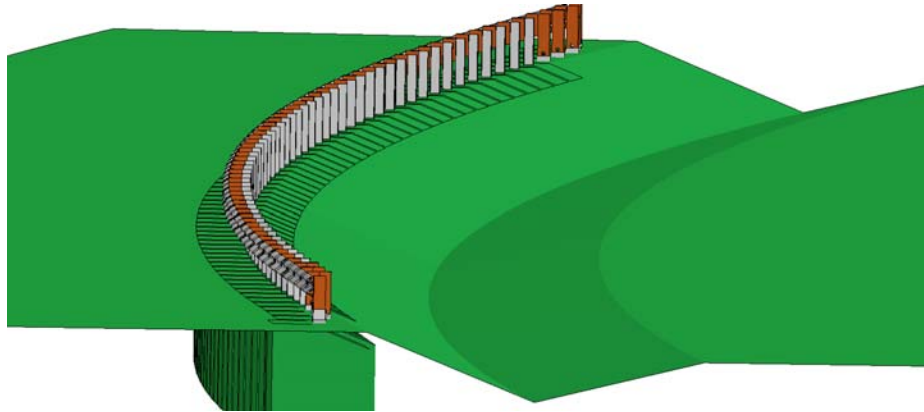


Fig. 3.9: FE model of a single-faced guardrail with convex horizontal curvature installed on a 2.5H:1V slope.

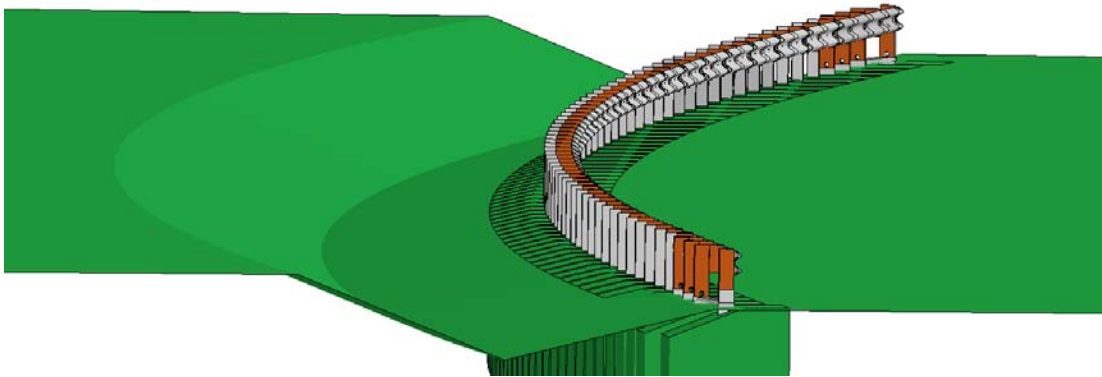


Fig. 3.10: FE model of a single-faced guardrail with concave horizontal curvature installed on a 4H:1V slope.

Simulations of the vehicles crashing into roadside barriers imposed significant challenges to the numerical models due to the large, nonlinear deformations and the large numbers of components contacting each other. For example, in the simulations of the Ford F250 crashing into the W-beam guardrail, the W-beam rails and the vehicle's fender experienced severe deformations. The vehicle's wheel, fender, bumper cover, suspension, and a number of other parts were in contact with the guardrail post, rail, and blockout. These contacts needed to be handled by selecting the appropriate contact algorithms to eliminate the unrealistic penetrations of the elements. Otherwise, the simulations would encounter great numerical difficulties, resulting in premature termination and unrealistic behaviors of the vehicle and/or guardrail (e.g., the vehicle being entangled with the guardrail components). The FE model of the Dodge Neon experienced a similar issue with elements on the bumper cover penetrating the guardrail and becoming entangled due to a contact definition that was used in the original model but inappropriate for the simulations of this project. The contact definition between

the vehicle's bumper and the guardrail was changed to resolve these contact issues. Before running simulations for this project, simulations were conducted using the Ford F250 and the Dodge Neon to ensure appropriate contacts being defined for all parts in the guardrail and the vehicles.

3.3 Simulation Setup

The five guardrail models, each with two rail heights of 29 and 31 inches, were combined with the two vehicle models to conduct the simulation work of this study. The simulation work was divided into five major categories based on guardrail model:

- 1) Case 1: Single-faced Guardrail Placed on a 2.5H:1V Slope
Front-side impacts on 29- and 31-inch guardrails were evaluated.
- 2) Case 2: Double-faced Guardrail Placed on a 2.5H:1V Slope
Front-side and backside impacts on 29- and 31-inch guardrails were evaluated.
- 3) Case 3: Lowered Backside Double-faced Guardrail Placed on a 2.5H:1V Slope
Front-side and backside impacts on 29- and 31-inch guardrails were evaluated.
- 4) Case 4: Single-faced Guardrail with Convex Horizontal Curvature Placed on a 2.5H:1V Slope
Front-side impacts on 29- and 31-inch guardrails were evaluated.
- 5) Case 5: Single-faced Guardrail with Concave Horizontal Curvature Placed on a 4H:1V Slope
Front-side impacts on 29- and 31-inch guardrails were evaluated.

Figure 3.11 shows the full simulation model for front-side impacts on the single-faced guardrails in Case 1. Figures 3.12 and 3.13 show the full simulation models for the front-side and backside impacts on the double-faced guardrails, respectively, in Case 2. Figures 3.14 and 3.15 show the full simulation models for the front-side and backside impacts on the lowered backside double-faced guardrails, respectively, Case 3. Figures 3.16 show the simulation model for front-side impacts on the single-faced guardrails with a convex horizontal curvature in Case 4. Figures 3.17 show the simulation model for front-side impacts on the single-faced guardrails with a concave horizontal curvature in Case 5. Figures 3.11 through 3.17 all show examples of a Ford F250 impacting a 29-inch guardrail at a speed of 62 mph (100 km/hour) and an impact angle of 25°.

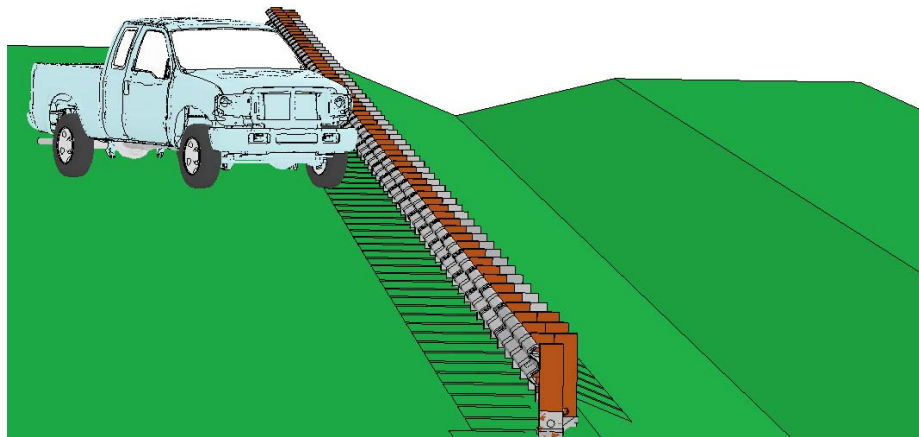


Fig. 3.11: FE model of a front-side impact on a single-faced W-beam guardrail placed on a 2.5H:1V slope and impacted by a Ford F250.

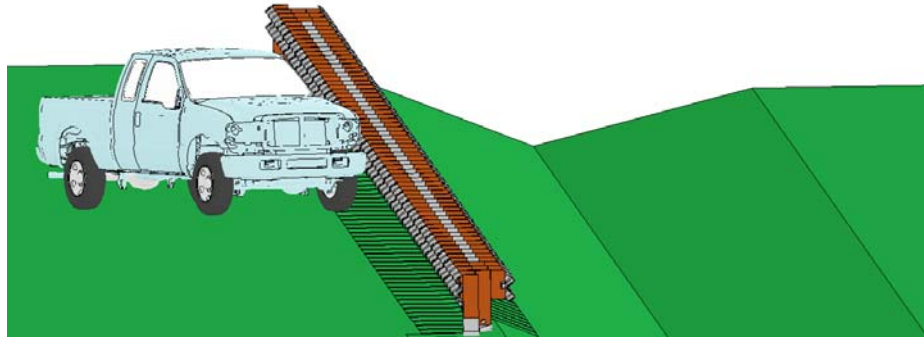


Fig. 3.12: FE model of a front-side impact on a double-faced W-beam guardrail placed on a 2.5H:1V slope and impacted by a Ford F250.

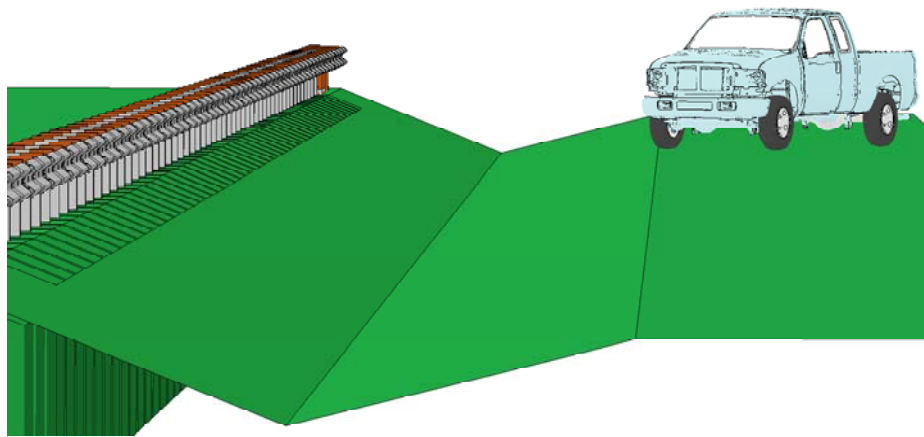


Fig. 3.13: FE model of a backside impact on a double-faced W-beam guardrail placed on a 2.5H:1V slope and impacted by a Ford F250.

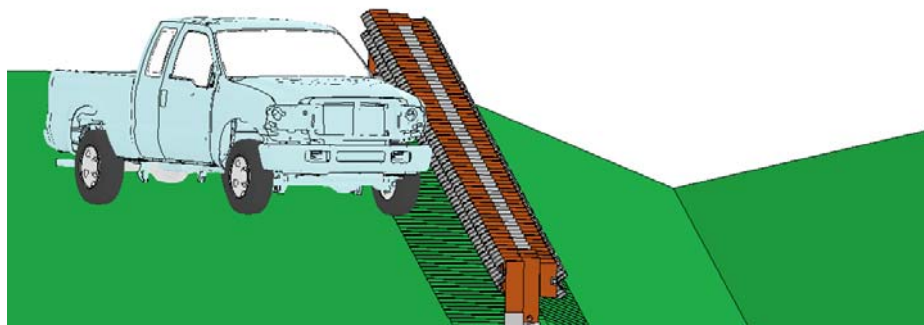


Fig. 3.14: FE model of a front-side impact on a lowered backside double-faced W-beam guardrail placed on a 2.5H:1V slope and impacted by a Ford F250.

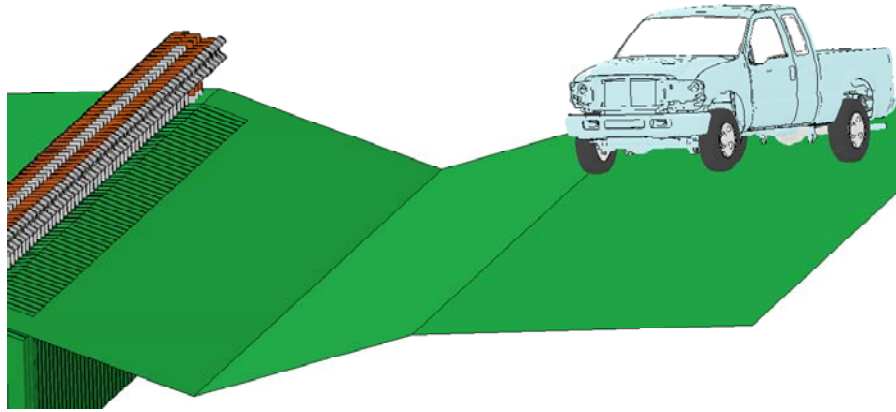


Fig. 3.15: FE model of a backside impact on a lowered backside double-faced W-beam guardrail placed on a 2.5H:1V slope and impacted by a Ford F250.

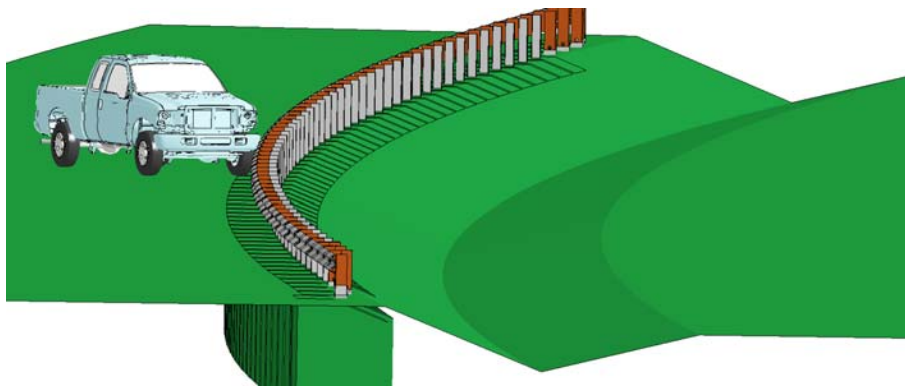


Fig. 3.16: FE model of a front-side impact on a single-faced W-beam guardrail with convex horizontal curvature placed on a 2.5H:1V slope and impacted by a Ford F250.

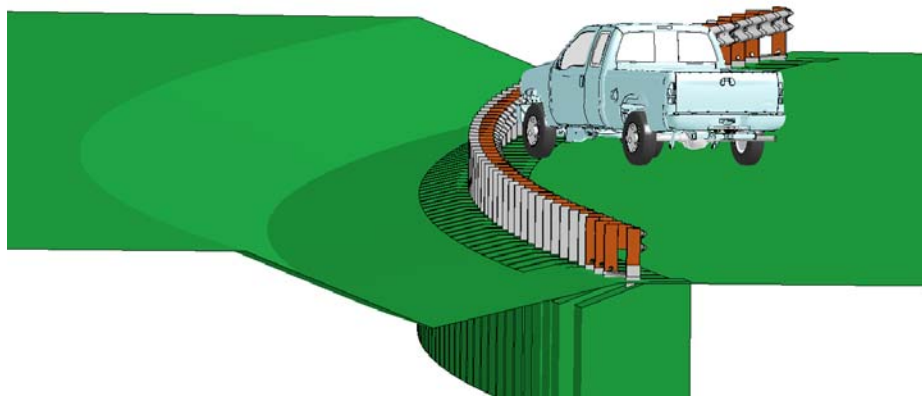


Fig. 3.17: FE model of a front-side impact on a single-faced W-beam guardrail with concave horizontal curvature placed on a 4H:1V slope and impacted by a Ford F250.

Table 3.2 summarizes the simulation conditions for all five cases. The impact speed was 62 mph (100 km/hour) for all of simulation cases except for the two additional simulations in

Case 1 in which the Dodge Neon impacted the 29- and 31-inch single-faced guardrails at an impact speed of 70 mph (112.6 km/hour).

Table 3.2: Simulation conditions for all cases

Case No.	Guardrail Model	Guardrail Heights	Impacting Side	Impacting Vehicles	Impact Speed	Impact Angle
1	Single-faced guardrail placed on a 2.5H:1V slope	29 & 31 inch	Front-side	Ford F250	62 mph	25°
				Dodge Neon	62 mph	25°
					70 mph	25°
2	Double-faced guardrail placed on a 2.5H:1V slope	29 & 31 inch	Front-side & Backside	Ford F250 & Dodge Neon	62 mph	25°
3	Lowered backside double-faced guardrail placed on a 2.5H:1V slope	29 & 31 inch	Front-side & Backside	Ford F250 & Dodge Neon	62 mph	25°
4	Single-faced guardrail with a convex horizontal curvature placed on a 2.5H:1V slope	29 & 31 inch	Front-side	Ford F250 & Dodge Neon	62 mph	25°
5	Single-faced guardrail with a concave horizontal curvature placed on a 4H:1V slope	29 & 31 inch	Front-side	Ford F250 & Dodge Neon	62 mph	25°

Based on Table 3.2, Case 1 required a total of six simulations (two guardrail heights, two vehicles, plus two additional cases at a higher impact speed). Cases 2 and 3 each had a total of eight simulations since they were impacted from both the front-side and backside at two guardrail heights and using two vehicles. Cases 4 and 5 each had four simulations and there were a total of 30 simulation runs for this study. The simulation results will be presented and analyzed in the next chapter of this report.

4. Simulation Results and Analysis

The FE simulation results for the five cases in Table 3.2 are presented in this section. The performance of the guardrails under vehicular impacts were evaluated using vehicular responses classified by the MASH exit-box criterion. The simulation results of the vehicles' yaw, pitch, and roll angles as well as transverse displacements and velocities were also examined to provide a comprehensive understanding of vehicular responses.

The exit-box criterion was designed to determine vehicle redirection characteristics based on certain vehicular responses after impacting a longitudinal barrier. Figure 4.1 illustrates the definition of the exit-box, which begins at the point of the vehicle's last contact point with the barrier's initial face location. The size of the exit-box (i.e., the side lengths A and B of the rectangular area) is determined by the type and size of the impacting vehicle. Table 4.1 gives the definition of the dimensions A and B in the MASH exit-box criterion.

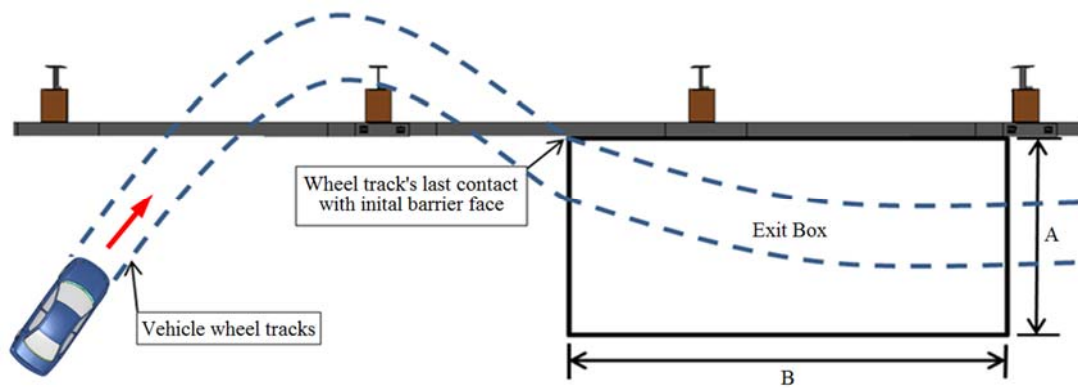


Fig. 4.1: The exit-box criterion in MASH.

Table 4.1: The exit-box criterion defined in MASH

Vehicle Type	Exit-box Dimension	
	A	B
Cars or Pickup Trucks	$7.2 + V_w + 0.16V_L$ (ft)	32.8 ft (10 m)
Other Vehicles	$14.4 + V_w + 0.16V_L$ (ft)	65.6 ft (20 m)

In Table 4.1, V_w and V_L stand for the vehicle's width and length, respectively. According to the exit-box criterion, if all four wheels of the vehicle remain inside the exit-box for the distance B , the case is considered to be a safe redirect. Another scenario, which is categorized as safe by the MASH evaluation criterion N , is if the vehicle remains in contact with the guardrail while reducing velocity to zero. When this scenario is present, no exit-box is required. Although the exit-box criterion is a useful tool for determining the post-impact vehicular trajectories, use of this criterion alone is not sufficient to determine if the vehicle has been safely redirected. In addition, a large exit angle and/or spin-out, which may be caused by pocketing and/or snagging of the vehicle on the guardrail posts, may still be present even for a case determined as a safe redirect by the exit-box criterion.

The exit-box dimensions for the Dodge Neon and Ford F250 were obtained using the formula in Table 4.1 and the vehicle data in Table 3.1 and used to assess the post-impact vehicular responses from the simulation results. Table 4.2 shows the exit-box dimensions for both vehicles.

Table 4.2: Exit-box dimensions for the test vehicles of this project

Vehicle	Exit-box Dimension	
	A	B
1996 Dodge Neon	15.1 ft (4.6 m)	32.8 ft (10.0 m)
2006 Ford F250	16.9 ft (5.15 m)	32.8 ft (10.0 m)

Due to the outcome of the post-impact trajectory of a large number of simulations in this project, the traditional method of calculating the exit angle (subtracting the impact angle from the vehicle yaw angle when guardrail-to-vehicle interaction ends) would not yield beneficial information. For this reason, as well as drawing more meaningful conclusions from simulation results, the exit angle was calculated by adding the vehicle yaw angle to the impact angle unless otherwise specifically stated. The exceptions occur for impact cases referenced in Figs. 4.40, 4.45, 4.55, and 4.140 for which the exit angle was calculated using the traditional method and stated in result discussions of each simulation case.

4.1 Case 1: Single-faced Guardrail Placed on a 2.5H:1V Slope

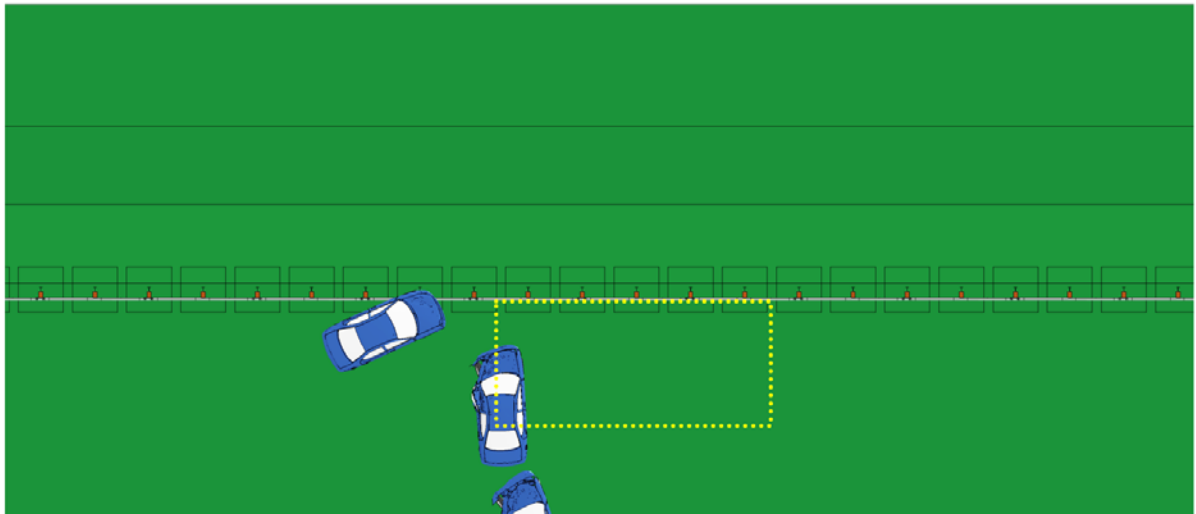
In this case, the 29- and 31-inch single-faced guardrails were evaluated when placed on a 2.5H:1V slope and impacted by both the Dodge Neon and Ford F250. An impact angle of 25° was used in the evaluation. The impact speed used in all simulations in Case 1, except two, was 62 mph (100 km/hour). The other impact speed was 70 mph (112.6 km/hour). Table 4.3 gives a summary of the simulation results that were used to evaluate guardrail performance in terms of vehicular responses.

Table 4.3: Simulation results of Case 1 (Single-faced Guardrail Placed on a 2.5H:1V Slope)

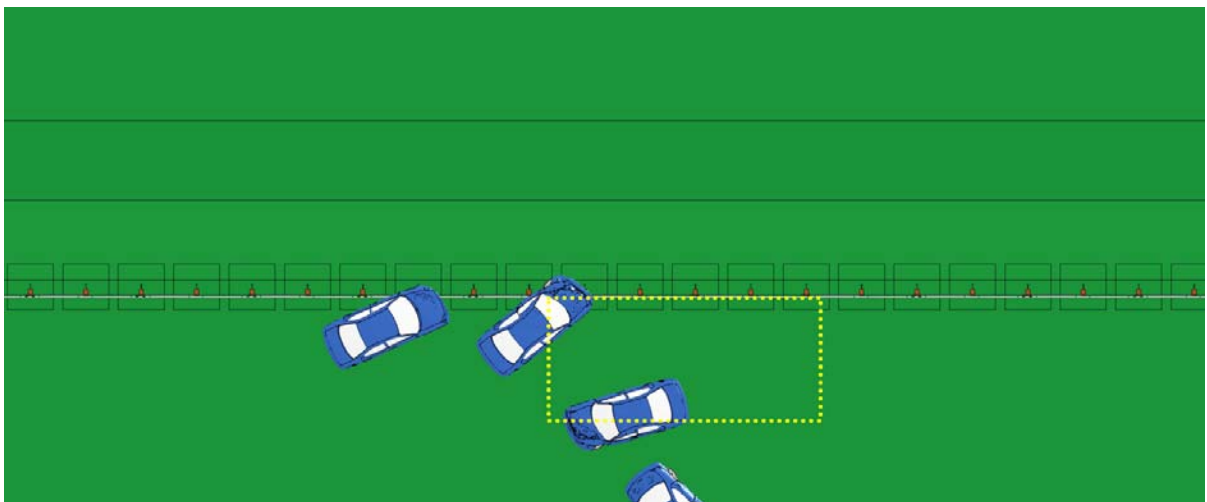
Impact Side	Guardrail Height	Test Vehicle	Impact Velocity	Simulation Results
Front-side	29 inch	Dodge Neon	62 mph (100 km/hour)	The vehicle failed the exit-box criterion caused by vehicle spin-out and a large exit angle
			70 mph (112.6 km/hour)	The vehicle failed the exit-box criterion caused by vehicle spin-out and a large exit angle
		Ford F250	62 mph (100 km/hour)	The vehicle failed the exit-box criterion caused by vehicle spin-out and a large exit angle
	31 inch	Dodge Neon	62 mph (100 km/hour)	The vehicle failed the exit-box criterion caused by vehicle spin-out and a large exit angle
			70 mph (112.6 km/hour)	The vehicle failed the exit-box criterion caused by vehicle spin-out and a large exit angle
		Ford F250	62 mph (100 km/hour)	The vehicle failed the exit-box criterion caused by vehicle spin-out and a large exit angle

4.1.1 The 29-inch single-faced Guardrail – Front-side Impact

Figure 4.2 shows the top view of vehicle trajectories for the Dodge Neon impacting at 62 mph (100 km/hour) and 70 mph (112.6 km/hour) and 25° into the 29-inch single-faced guardrail placed on a 2.5H:1V slope. The W-beam guardrail is shown in its original undeformed shape and the exit-box, placed at the last point of contact of the vehicle's wheel tracks to the initial guardrail face, is shown by the yellow dotted rectangle. It was observed that the vehicle experienced tire snagging on the guardrail post, causing vehicle spin-out with a large exit angle for both impacts. According to the MASH exit-box criterion, the vehicle was not retained inside the exit-box before traversing its length in both impacts. Both cases failed the exit-box criterion.



a. At 62 mph (100 km/hour) and 25°



b. At 70 mph (112.6 km/hour) and 25°

Fig. 4.2: A Dodge Neon impacting the front-side 29-inch single-faced guardrail on a 2.5H:1V slope.

The yaw, pitch, and roll angles of the Dodge Neon in both the 62 mph (100 km/hour) and 70 mph (112.6 km/hour) impacts are shown in Fig. 4.3. Due to vehicle wheel snagging and spin-out, the exit angle could not be determined by simply subtracting the impact angle from the yaw angle as done for a safe redirection. Rather, the exit angle was calculated by adding the impact angle to the yaw angle at exit to extract more meaningful comparisons from the results. For all the subsequent simulations, the exit angles are calculated the same way as this case, unless explicitly stated prior to the exit angle calculation for a specific simulation. The exit angle of the Dodge Neon simulation at 62 mph (100 km/hour) was determined to be 48°, which was calculated by adding the impact angle (i.e., 25°) to the yaw angle at exit (i.e., 23°). The exit angle of the Dodge Neon simulation at 70 mph (112.6 km/hour) was determined to be 62°, which was calculated by adding the impact angle (i.e., 25°) to the yaw angle at exit (i.e., 37°). The vehicles were not safely redirected due to the continuous spin after prematurely leaving the exit-box as indicated by the increasing yaw angles. From the time histories of the yaw angles in Fig. 4.3, it can be seen that the Dodge Neon was first redirected (during the first 0.25 seconds, indicated by the negative yaw angles) and then started to rotate in the opposite direction while losing contact with the guardrail. This positive rotation went on even after the vehicles lost contact with the guardrail, resulting in large exit angles. It was observed from the simulation results that the Dodge Neon partially under-rode the guardrail and directly crashed into the posts in both impacts, causing pocketing and snagging on the front part of the vehicles. The roll and pitch angles of both cases were less than twenty degrees in either positive or negative direction. They passed the MASH evaluation criterion F, which specified a maximum 75° roll or pitch angle.

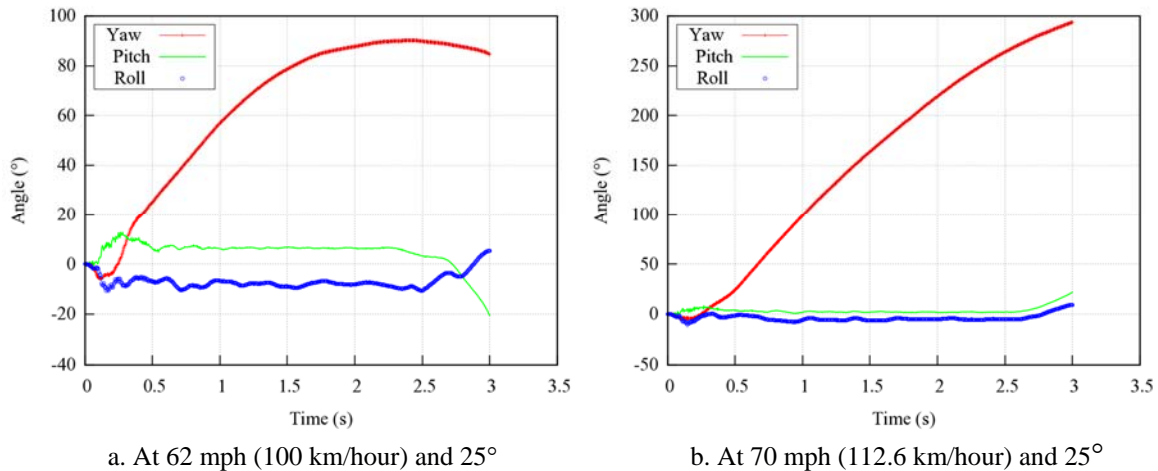
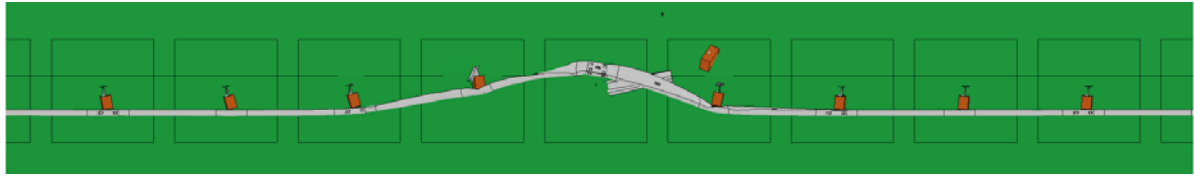
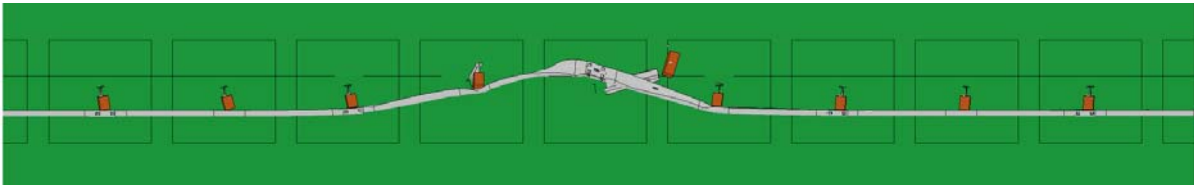


Fig. 4.3: Yaw, pitch, and roll angles for a Dodge Neon impacting the front-side 29-inch single-faced guardrail on a 2.5H:1V slope.

Once the vehicle impacted the guardrail, the measured maximum deflection of the guardrail during the impact was defined as the maximum dynamic deflection according to MASH. Figure 4.4 shows the maximum dynamic deflections for guardrails under impacts by the Dodge Neon at 62 mph (100 km/hour) and 70 mph (112.6 km/hour). Figures 4.4a and 4.4b had maximum dynamic deflections of 2.46 ft (0.75 m) and 2.56 ft (0.78 m), respectively. It can be seen that the damaged guardrail sections are small and localized. This serves as an indication of relatively low-severity impact from the small car.

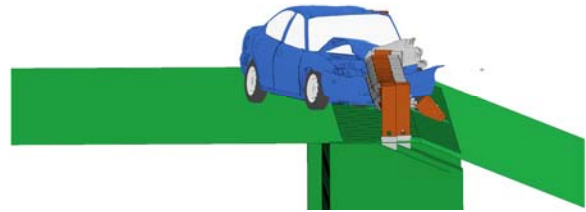
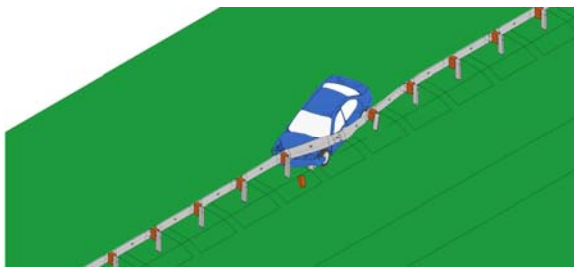


a. At 62 mph (100 km/hour) and 25°

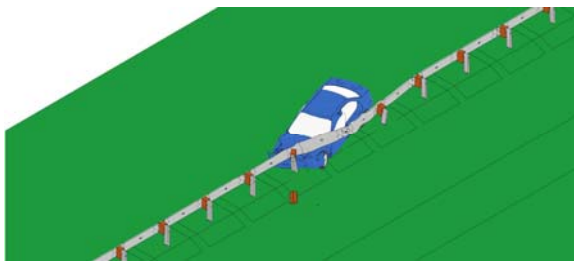


b. At 70 mph (112.6 km/hour) and 25°

Fig. 4.4: Maximum dynamic deflection of the front-side 29-inch single-faced guardrail on a 2.5H:1V slope and impacted by a Dodge Neon.



a. At 62 mph (100 km/hour) and 25°



b. At 70 mph (112.6 km/hour) and 25°

Fig. 4.5: Simulations of a Dodge Neon impacting the front-side of 29-inch single-faced guardrail on a 2.5H:1V slope.

Figure 4.5 shows the detailed views of vehicle-barrier interactions for both impact speeds. It can be seen from Fig. 4.5b that both the vehicle and barrier experienced slightly more severe deformations than in Fig. 4.5a, due to the increased impact speed. Figures 4.6 and 4.7 show the time histories of transverse displacements and velocities, respectively, measured at the center of gravity (CG) point of the vehicle in the 62 mph (100 km/hour) and 70 mph (112.6 km/hour) impacts. The transverse velocities, exit-box criterion, along with the exit angle, could all be used to determine if a redirection was safe or subjected to a possible secondary

collision. For example, if the transverse velocity of a redirected vehicle remained large, the redirection could be followed by a secondary collision if the exit angle was also large. For the case of the Dodge Neon, the transverse velocities were both approximately 8 mph (3.6 m/s) towards the travel lane. The small transverse velocities could possibly cause a secondary impact due to the large exit angles from the vehicle spin-out.

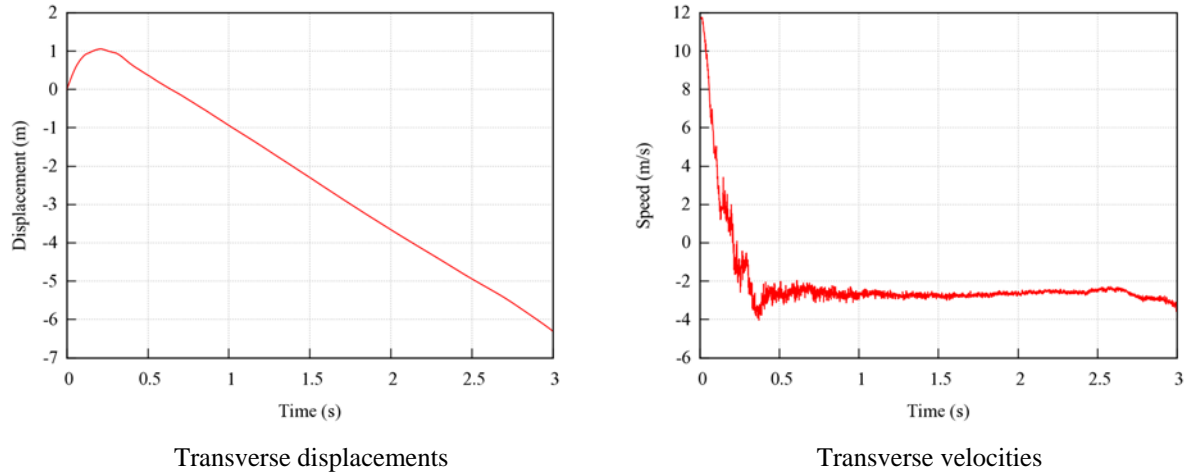


Fig. 4.6: Transverse displacements and velocities of the Dodge Neon impacting the front-side of 29-inch single-faced guardrail on a 2.5H:1V slope at 62 mph (100 km/hour) and 25°.

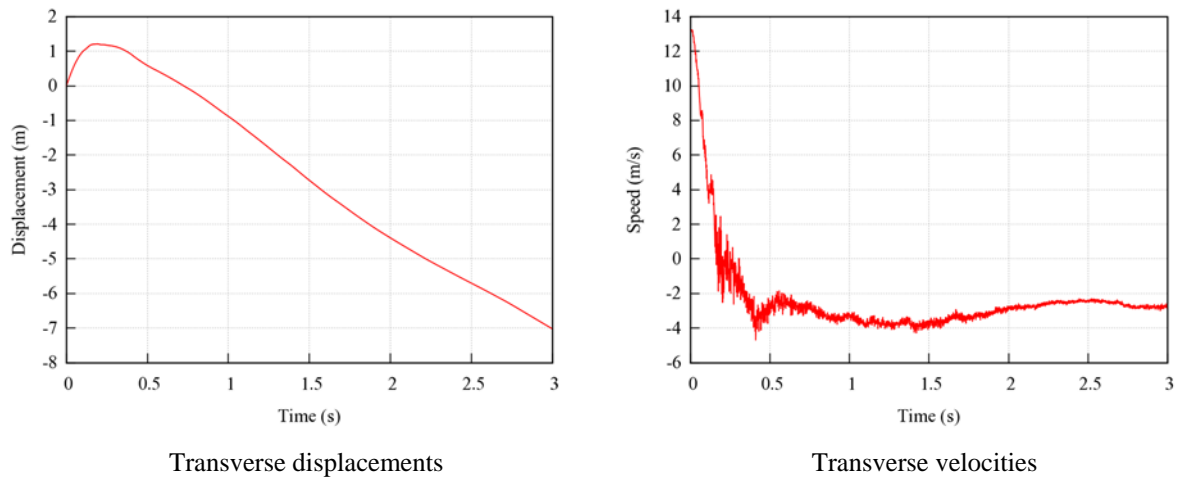


Fig. 4.7: Transverse displacements and velocities of the Dodge Neon impacting the front-side of 29-inch single-faced guardrail on a 2.5H:1V slope at 70 mph (112.6 km/hour) and 25°.

Under impacts of the Ford F250 at 62 mph (100 km/hour), the 29-inch single-faced W-beam guardrail placed on a 2.5H:1V slope was found to cause a vehicle spin-out. Figure 4.8 shows the top view of the vehicle trajectory of the Ford F250 along with the exit-box. Similar to the case of the Dodge Neon impact (Fig. 4.2), the W-beam guardrail is shown in its original undeformed shape. The exit-box shown by the yellow dotted rectangle is placed at the last point of contact of the vehicle's wheel tracks to the initial guardrail face. It can be seen that the vehicle experienced tire snagging and exhibited spin-out with a large exit angle failing the MASH exit-box criterion.

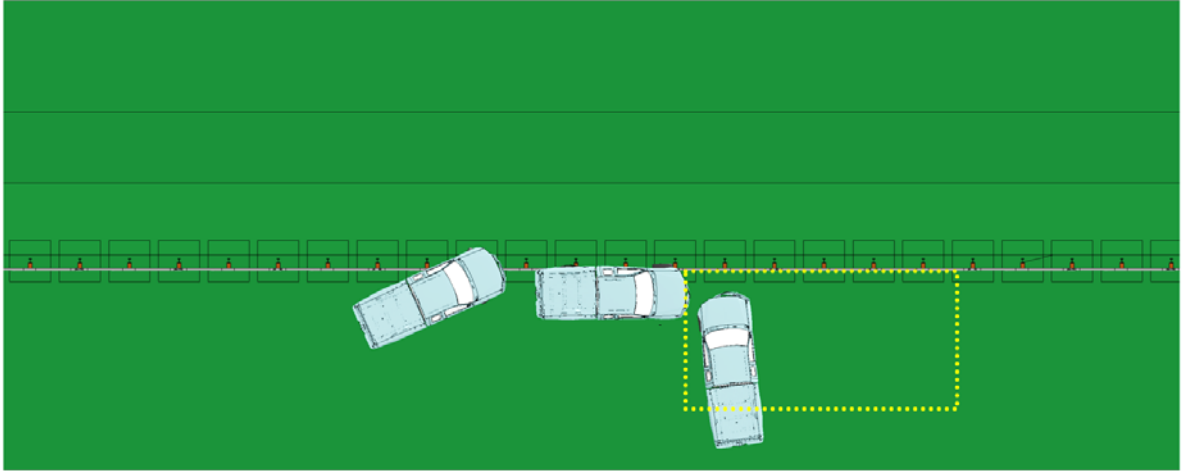


Fig. 4.8: A Ford F250 impacting the front-side of 29-inch single-faced guardrail on a 2.5H:1V slope at 62 mph (100 km/hour) and 25°.

The yaw, pitch, and roll angles of the Ford F250 is shown in Figure 4.9. The exit angle of the impact was determined to be 48° same as the case of the Dodge Neon impacting the guardrail at 62 mph (100 km/hour). In addition, the roll and pitch angles in the Ford F250 impact were less than fifteen degrees in either the positive or negative direction and thus passed the MASH evaluation criterion F, which specified a maximum 75° roll or pitch angle.

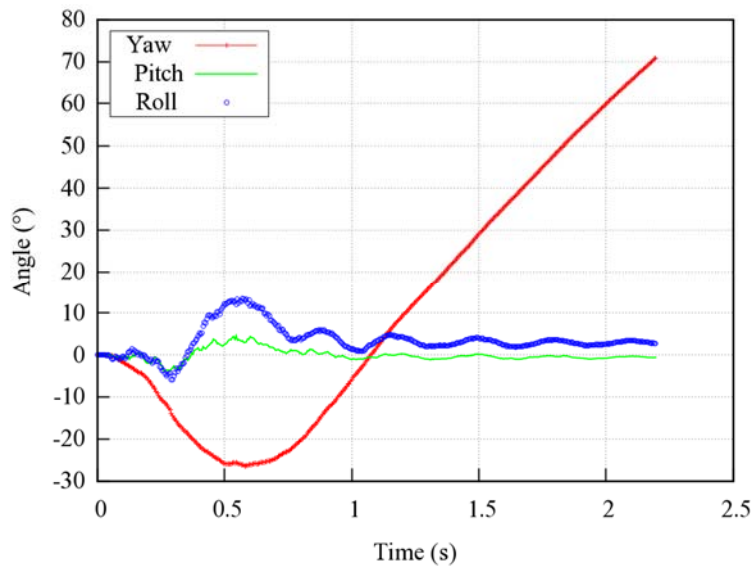


Fig. 4.9: Yaw, pitch, and roll angles of Ford F250 impacting the front-side of 29-inch single-faced guardrail on a 2.5H:1V slope at 62 mph (100 km/hour) and 25°.

Figure 4.10 shows the 29-inch guardrail at maximum dynamic deflection of 3.97 ft (1.21 m) under the impact of the Ford F250 at 62 mph (100 km/hour) and 25°. It can be seen that the maximum dynamic deflection of the guardrail under the Ford F250 was significantly larger than that for the Dodge Neon impacts. This increased deformation was attributed to the larger vehicle size and mass of the Ford F250 compared to the Dodge Neon.

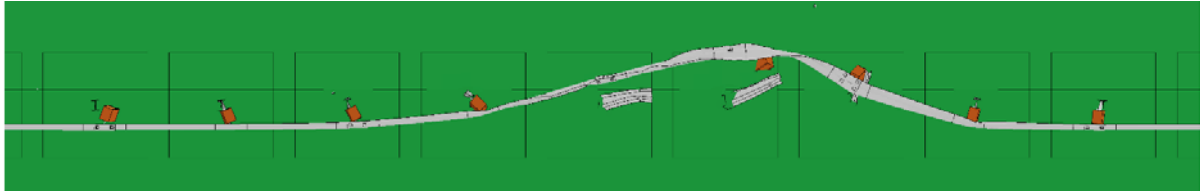


Fig. 4.10: Maximum dynamic deflection of the front-side for 29-inch single-faced guardrail on a 2.5H:1V slope at 62 mph (100 km/hour) and 25° and impacted by a Ford F250.

Figure 4.11 shows detailed views of the vehicle-barrier interaction for the impact by the Ford F250. In the front-side impact on the 29-inch single-faced guardrail, the vehicle's bumper cover and wheel fender engaged well with the guardrail; however, the guardrail post was caught behind the vehicle's tire and resulted in a vehicle spin-out. Due to its high profile, the Ford F250 had better engagement with the guardrail than the Dodge Neon, which partially went under the W-beam rail in the preceding two impacts. All three simulations resulted in vehicle spin-out. Figure 4.12 shows the time histories of transverse displacements and velocities measured at the CG point for the Ford F250 in this impact scenario. The transverse velocity was approximately 4 mph (1.8 m/s) towards the travel lane, indicating a relatively small chance of being involved in a secondary collision.

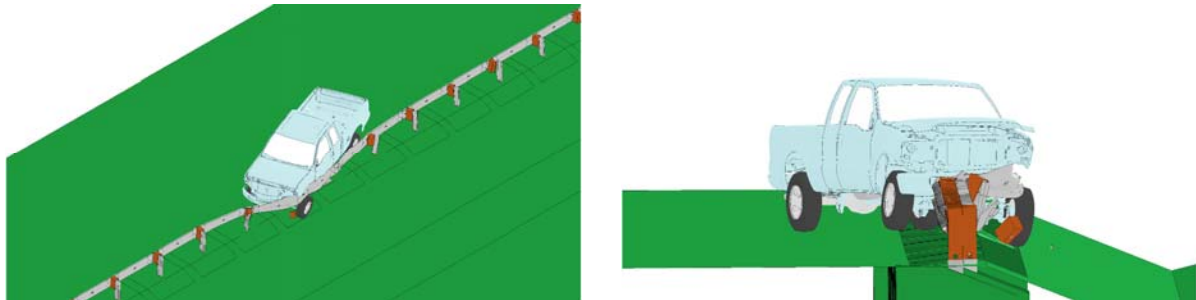


Fig. 4.11: Simulations of Ford F250 impacting the front-side of 29-inch single-faced guardrail on a 2.5H:1V slope at 62 mph (100 km/hour) and 25°.

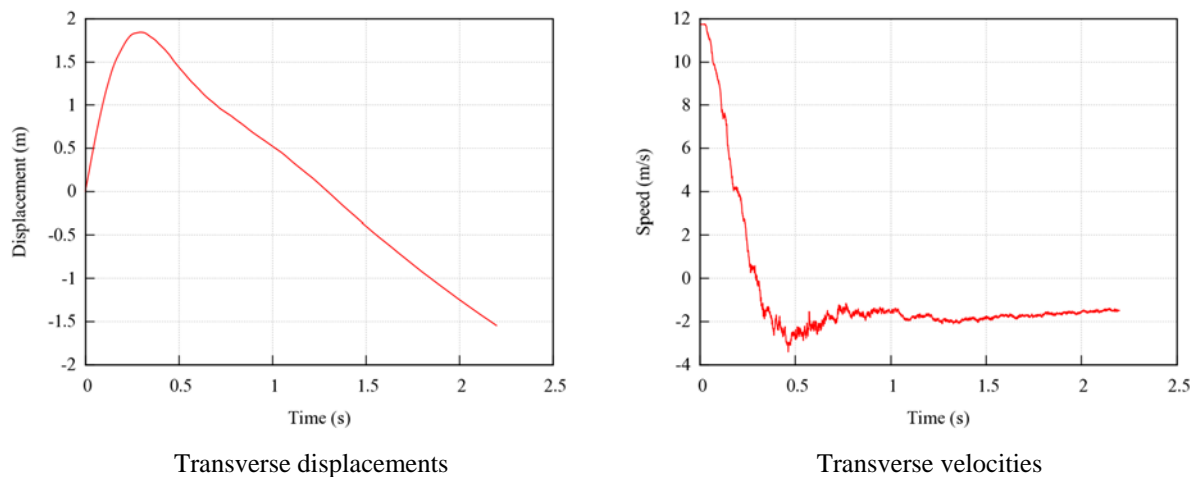
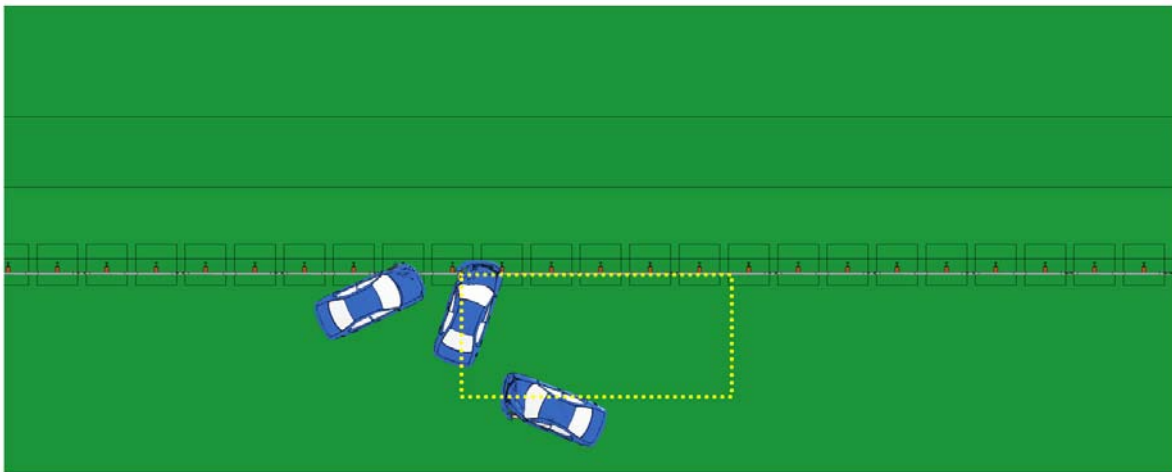


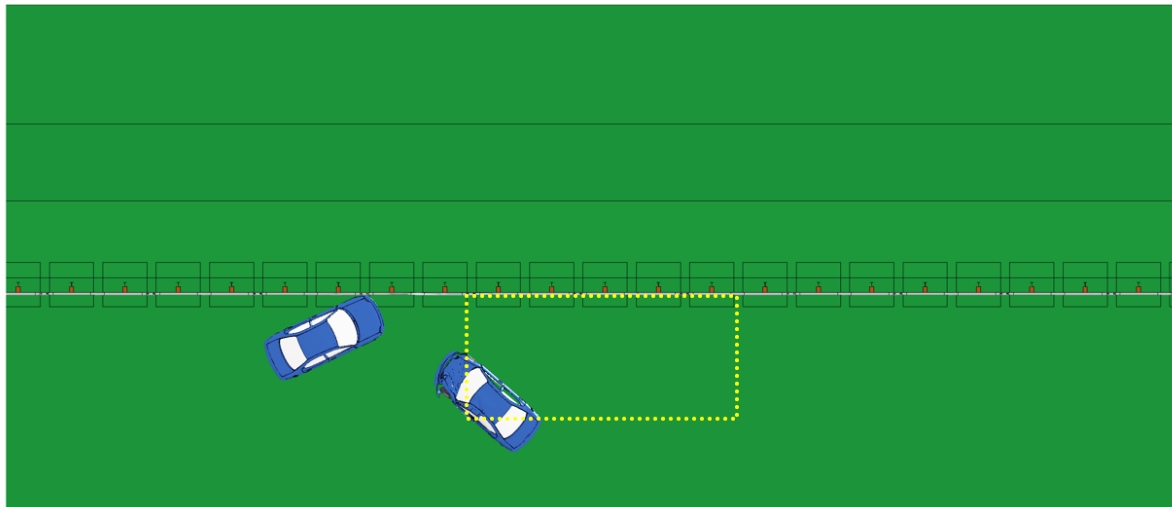
Fig. 4.12: Transverse displacements and velocities for the Ford F250 impacting the front-side of 29-inch single-faced guardrail on a 2.5H:1V slope at 62 mph (100 km/hour) and 25°.

4.1.2 The Single-faced 31-inch Guardrail – Front-side Impact

Figure 4.13 shows the top views of vehicle trajectories for the Dodge Neon impacting the 31-inch guardrail at 62 mph (100 km/hour) and 70 mph (112.6 km/hour) and 25°, respectively. The W-beam guardrail, placed on a 2.5H:1V slope, is shown in its original undeformed shape along with the exit-box shown by the yellow dotted rectangle. Upon impacting the single-faced 31-inch guardrail, the Dodge Neon snagged on a guardrail post and spun about the post in both simulations. This wheel snagging was mainly due to the relatively low vehicle profile that caused the vehicle to partially underride the guardrail and impact the post. The results in Figure 4.13 show that the MASH exit-box criterion was not satisfied for either impact by the Dodge Neon at 62 mph (100 km/hour) or at 70 mph (112.6 km/hour). The vehicle experienced spin-out and could possibly reenter the travel lane.



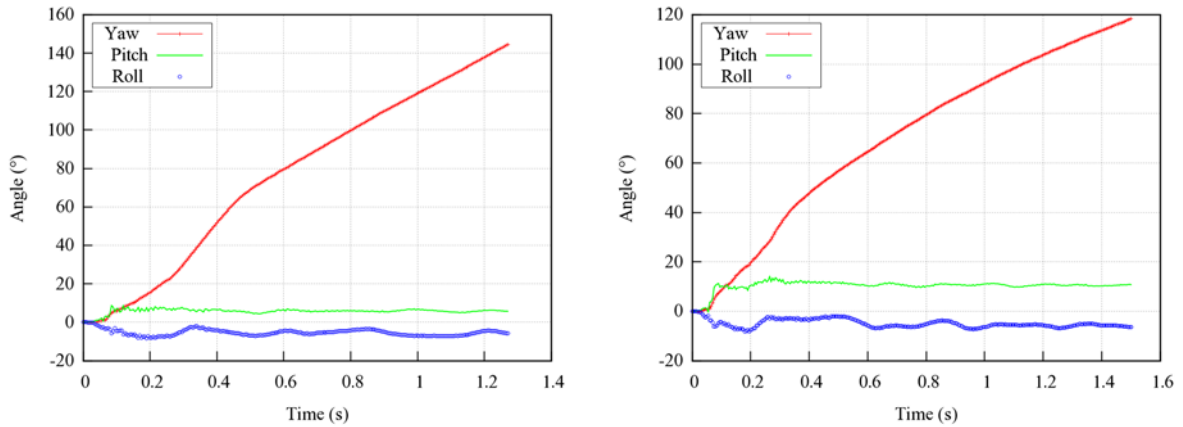
a. At 62 mph (100 km/hour) and 25°



b. At 70 mph (112.6 km/hour) and 25°

Fig. 4.13: A Dodge Neon impacting the front-side single-faced of 31-inch guardrail on a 2.5H:1V slope.

The yaw, pitch, and roll angles of the Dodge Neon in both the 62 mph (100 km/hour) and 70 mph (112.6 km/hour) impacts are shown in Fig. 4.14. The exit angle of the 62 mph (100 km/hour) impact was determined to be 83° by adding the impact angle (i.e., 25°) to the yaw angle at exit (i.e., 58°). For the 70 mph (112.6 km/hour) impact, the exit angle was determined to be 80° with a yaw angle of 55° at exit. The steadily increasing yaw angles in Figures 4.14a and 4.14b indicate a continuous spin-out of the vehicle away from the guardrail. The roll and pitch angles of both cases were approximately ten degrees in either positive or negative direction; satisfying the MASH evaluation criterion F.

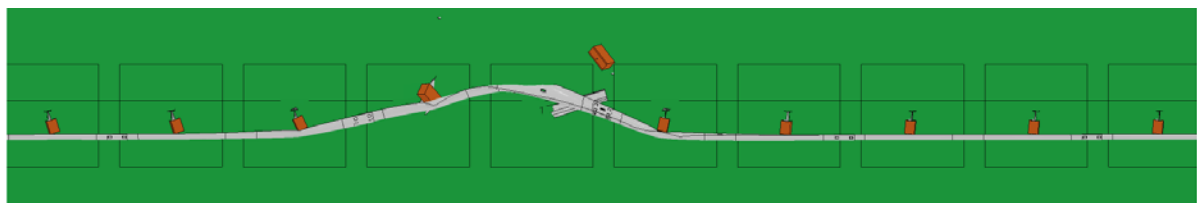


a. At 62 mph (100 km/hour) and 25°

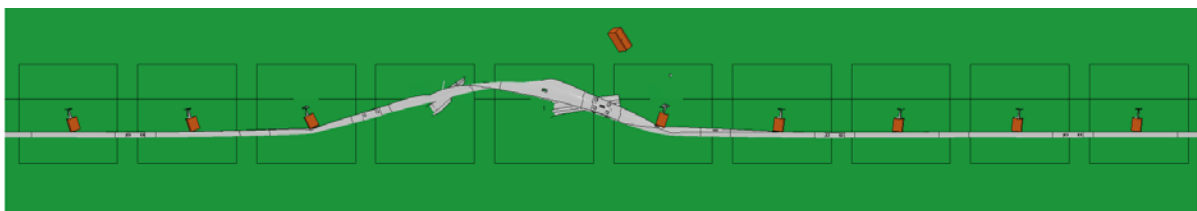
b. At 70 mph (112.6 km/hour) and 25°

Fig. 4.14: Yaw, pitch, and roll angles of a Dodge Neon impacting the front-side single-faced 31-inch guardrail on a 2.5H:1V slope.

The maximum dynamic deflections of the single-faced 31-inch guardrail under impacts by the Dodge Neon are shown in Fig. 4.15. The maximum dynamic deflection of the guardrail in the 70 mph (112.6 km/hour) impact (Fig. 4.15b) was 2.79 ft (0.85 m), which is slightly larger than the 2.49 ft (0.76 m) deflection in the 62 mph (100 km/hour) impact (Fig 4.15a).



a. At 62 mph (100 km/hour) and 25°



b. At 70 mph (112.6 km/hour) and 25°

Fig. 4.15: Maximum dynamic deflection for the front-side single-faced 31-inch guardrail on a 2.5H:1V slope and impacted by a Dodge Neon.

Compared to the 29-inch single-faced guardrail, the maximum dynamic deflections of the single-faced 31-inch guardrail were only slightly larger. At both guardrail heights, the guardrail had very small engagement with the vehicle's bumper cover and fender. The Dodge Neon, at both impact speeds, intruded under the rail, engaged the rail on the hood, and dragged the rail forward, resulting in a large but localized transverse deflection of the guardrail.

Figure 4.16 shows detailed views of the vehicle-barrier interaction for the impacts on the 31-inch single-faced guardrail by the Dodge Neon at 62 mph (100 km/hour) and 70 mph (112.6 km/hour). In both impacts, due to the vehicle's low front profile and higher impact velocity, the guardrail did not engage with the vehicle's bumper cover and wheel fender. As a result, the vehicle intruded under the guardrail and snagged on a post which caused vehicle spin-out with large exit angles.

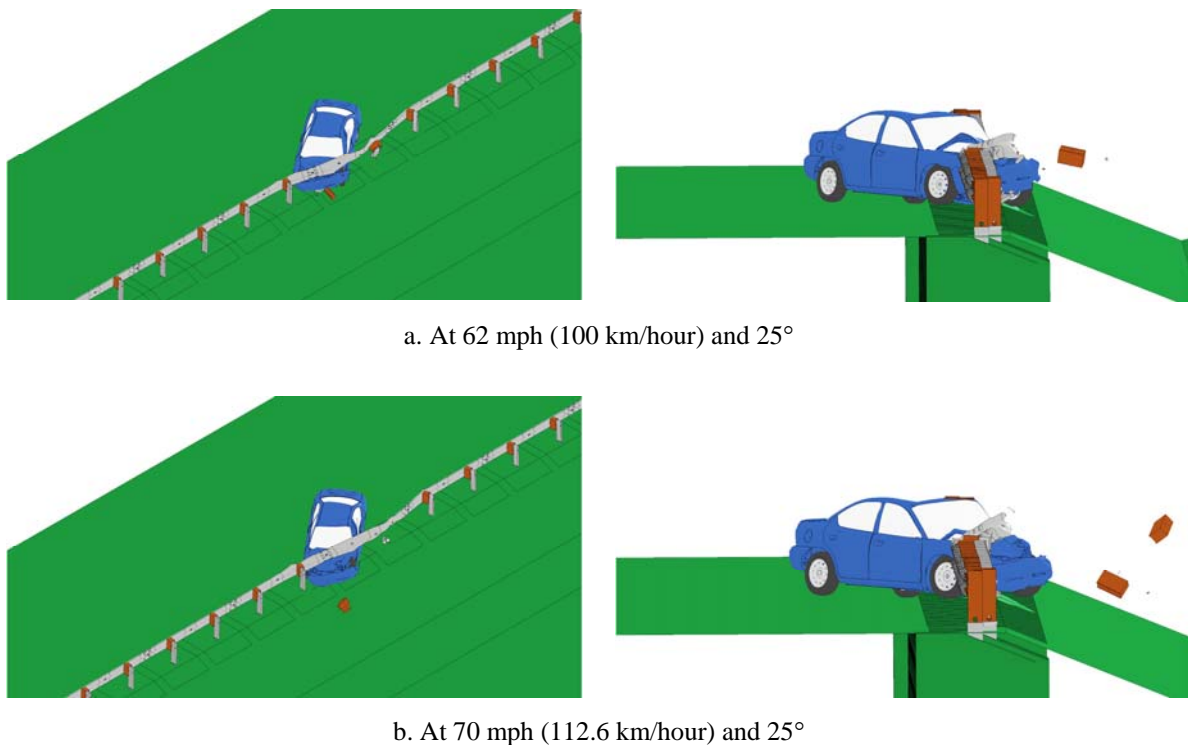


Fig. 4.16: Simulations of the Dodge Neon impacting the front-side of single-faced 31-inch guardrail on a 2.5H:1V slope.

Figures 4.17 and 4.18 show the time histories of transverse displacements and velocities measured at the CG point of the Dodge Neon in the 62 mph (100 km/hour) and 70 mph (112.6 km/hour) impacts, respectively. The post-impact transverse velocities of the 62 mph (100 km/hour) and 70 mph (112.6 km/hour) simulations were approximately 12 mph (5.5 m/s) and 6 mph (2.7 m/s), respectively. For the 62 mph (100 km/hour) impact, since the vehicle snagged on the guardrail and spun around a post, it would be possible to get involved in a secondary collision with the residual velocity left after impact. For the 70 mph (112.6 km/hour) impact, the transverse velocity was approximately 6 mph towards the travel lane, indicating a relatively small chance of getting involved in a secondary collision.

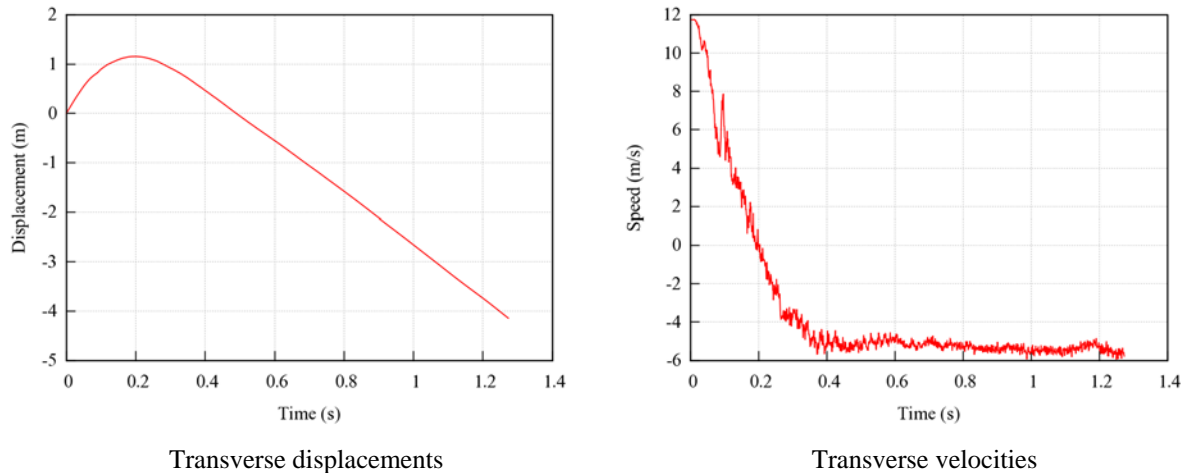


Fig. 4.17: Transverse displacements and velocities for the Dodge Neon impacting the front-side of single-faced 31-inch guardrail on a 2.5H:1V slope at 62 mph (100 km/hour) and 25°.

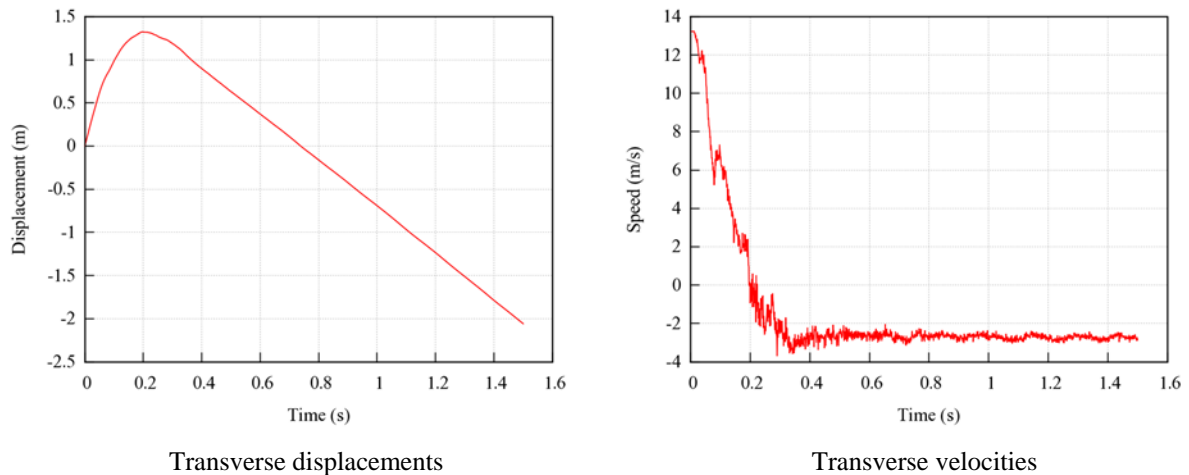


Fig. 4.18: Transverse displacements and velocities of a Dodge Neon impacting the front-side of single-faced 31-inch guardrail on a 2.5H:1V slope at 70 mph (112.6 km/hour) and 25°.

Figure 4.19 shows the top view vehicle trajectory of the Ford F250 impacting the 31-inch single-faced guardrail at 62mph (100 km/hour) and 25° impact angle. The W-beam guardrail, placed on a 2.5H:1V slope, is shown in its original undeformed shape along with the exit-box shown by the yellow dotted rectangle. In this case, the Ford F250 left the exit-box from the bottom-left corner caused by tire snagging and vehicle spin-out, thus not meeting the MASH exit-box criterion. Since the vehicle’s length was 18.87 ft (5.75 m) and the shoulder was 14 ft (4.27 m) wide, the tail end of the vehicle had begun to reenter the travel lane.

The yaw, pitch, and roll angles of the Ford F250 is shown in Fig. 4.20. The exit angle was determined to be 65° by adding the impact angle (i.e., 25°) to the yaw angles at exit (i.e., 40°). The steadily increasing positive yaw angle indicates a counter-clockwise rotation of the vehicle away from the guardrail. The roll and pitch angles in this impact were less than 15 degrees in either positive or negative direction and thus passed the MASH evaluation criterion F, which specified a maximum 75° roll or pitch angle.

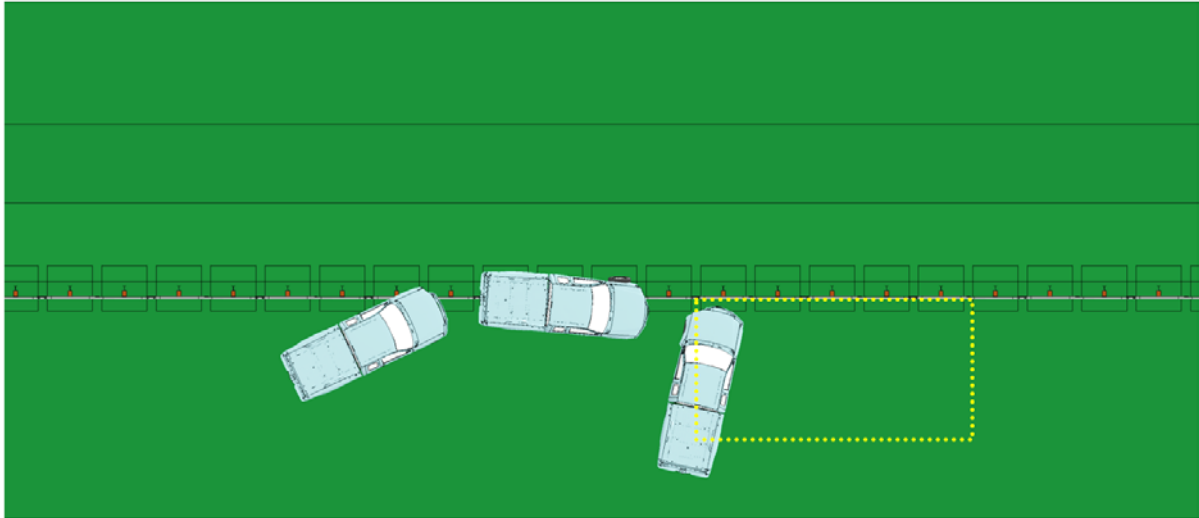


Fig. 4.19: A Ford F250 impacting the front-side of single-faced 31-inch guardrail on a 2.5H:1V slope at 62 mph (100 km/hour) and 25°.

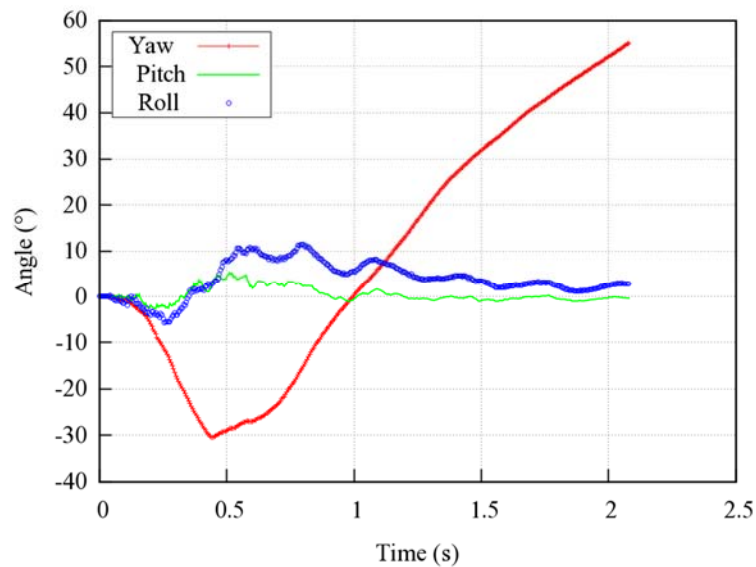


Fig. 4.20: Yaw, pitch, and roll angles of Ford F250 impacting the front-side of single-faced 31-inch guardrail on a 2.5H:1V slope at 62 mph (100 km/hour) and 25°.

Figure 4.21 shows the maximum dynamic deflection of the 31-inch single-faced guardrail impacted by the Ford F250 at 62 mph (100 km/hour) and 25°. The maximum dynamic deflection of the guardrail was 3.9 ft (1.19 m). Although this deflection was rather severe, it was relatively localized to the impact location. Figure 4.22 shows detailed views of the vehicle-barrier interaction at an instant when the maximum dynamic deflection occurred. In the front-side impact on the 31-inch single-faced guardrail, the vehicle's bumper cover and wheel fender engaged well with the guardrail; however, the guardrail post was caught behind the vehicle's tire and resulted in the vehicle spin-out.

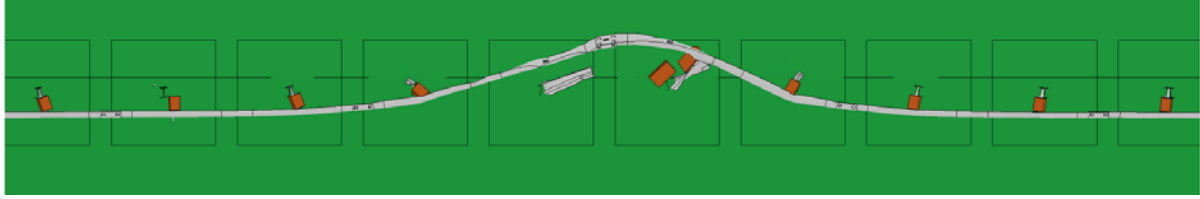


Fig. 4.21: Maximum dynamic deflection for the front-side single-faced 31-inch guardrail on a 2.5H:1V slope at 62 mph (100 km/hour) and 25° and impacted by a Ford F250.

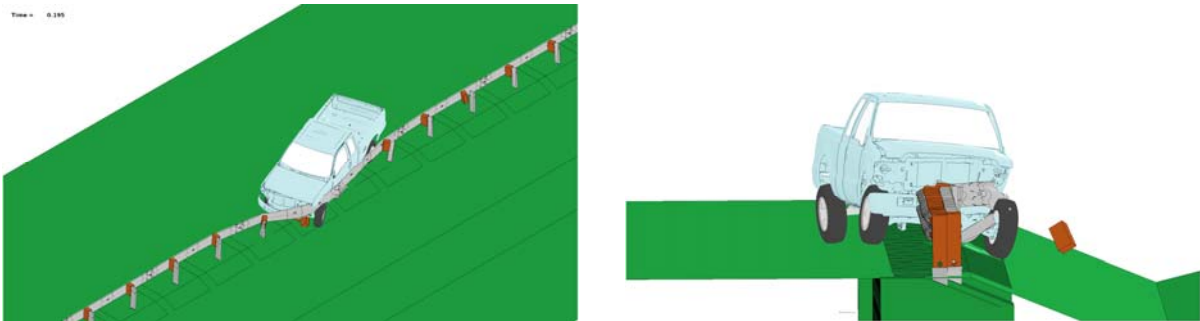


Fig. 4.22: Simulations of the Ford F250 impacting the front-side of single-faced 31-inch guardrail on a 2.5H:1V slope at 62 mph (100 km/hour) and 25°.

Figure 4.23 shows the time histories of transverse displacements and velocities measured at the CG point for the Ford F250 with an impact at 62 mph (100 km/hour) and 25°. The transverse velocity was approximately 1.5 mph (0.7 m/s) towards the travel lane at the end of the simulation. Considering the exit-box criterion, exit angle, and transverse velocity, the Ford F250 had a high potential of reentering further into the travel lane and being involved in a secondary collision.

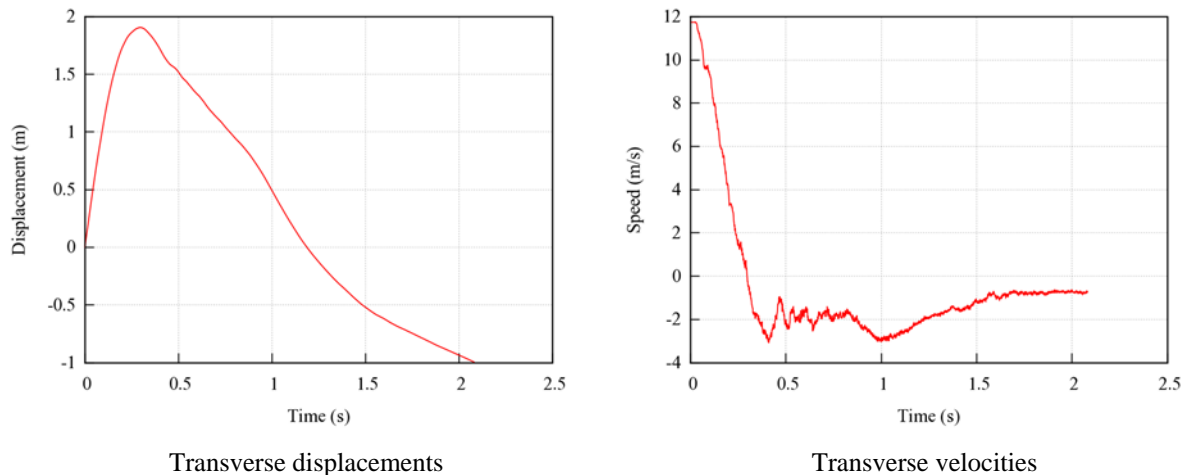


Fig. 4.23: Transverse displacements and velocities for a Ford F250 impacting the front-side of single-faced 31-inch guardrail on a 2.5H:1V slope at 62 mph (100 km/hour) and 25°.

4.2 Case 2: Double-faced Guardrail Placed on a 2.5H:1V Slope

In this case, the effectiveness of replacing two lines of single-faced guardrail installed on both sides of a sloped median with a single line of double-faced guardrail was investigated. The double-faced guardrail design in this case had the front-side and backside rails installed at the same elevation. Therefore, the backside ground-to-rail height was slightly higher than the placement height due to the slope of the median. The double-faced guardrails were installed on a 2.5H:1V slope at placement heights of 29 and 31 inches and evaluated under the impacts of both a Dodge Neon and Ford F250. Two impact sides were tested: the front-side and backside impacts. The backside impact was defined as the vehicle traversing through the sloped median before impacting the backside of the double-faced guardrail. An impact speed of 62 mph (100 km/hour) was used in all simulations. Table 4.4 gives a summary of the guardrail performance in terms of vehicular responses.

Table 4.4: Simulation results of Case 2 (double-faced guardrail placed on a 2.5H:1V slope)

Impact side	Guardrail Height	Test Vehicle	Simulation Results
Front-side	29 inch	Dodge Neon	The vehicle failed the exit-box criterion caused by vehicle spin-out and a large exit angle
		Ford F250	The vehicle remained in contact with guardrail due to tire snagging on guardrail post
	31 inch	Dodge Neon	The vehicle failed the exit-box criterion caused by vehicle spin-out and a large exit angle
		Ford F250	The vehicle was redirected but failed the exit-box criterion with a low exit angle
Backside	29 inch	Dodge Neon	The vehicle passed the exit-box criterion and was safely redirected
		Ford F250	The vehicle failed the exit-box criterion caused by vehicle spin-out and a large exit angle
	31 inch	Dodge Neon	The vehicle passed the exit-box criterion and was safely redirected
		Ford F250	The vehicle failed the exit-box criterion caused by vehicle spin-out and a large exit angle

4.2.1 The 29-inch Double-faced Guardrail – Front-side Impact

Figure 4.24 shows the top view vehicle trajectory of the Dodge Neon impacting the front-side rail of the 29-inch double-faced guardrail at 62 mph (100 km/hour) and 25°. The W-beam guardrail, placed on a 2.5H:1V slope, is shown in its original undeformed shape along the exit-box shown by the yellow dotted rectangle. Upon impacting guardrail, the Dodge Neon snagged on and spun about a guardrail post. Due to the relatively low vehicle profile, under riding occurred and caused the vehicle to experience tire snagging and disconnected from the guardrail with a high exit angle. The Dodge Neon did not traverse through the width of the exit-box, therefore, the MASH exit-box criterion was not satisfied.

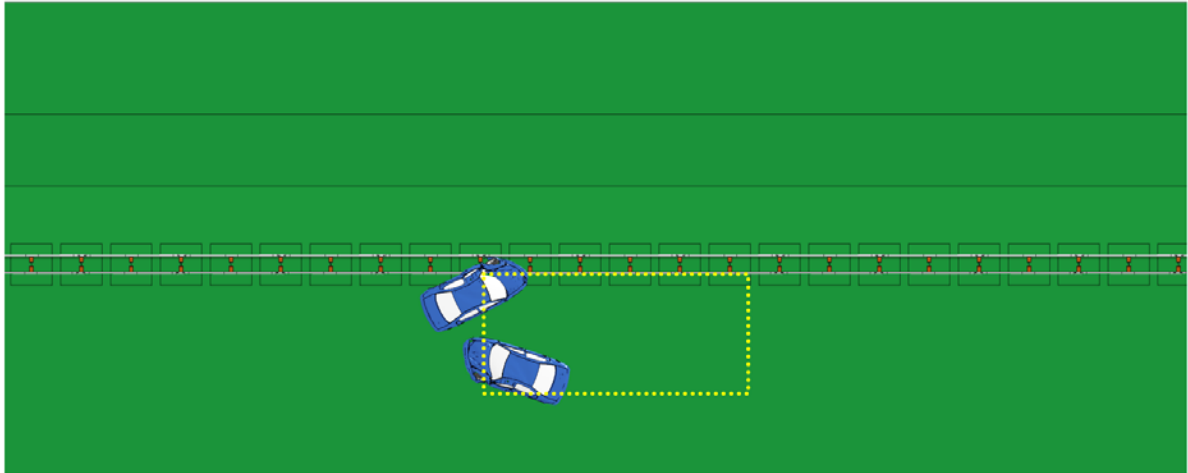


Fig. 4.24: A Dodge Neon impacting the front-side of 29-inch double-faced guardrail on a 2.5H:1V slope at 62 mph (100 km/hour) and 25°.

The yaw, pitch, and roll angles of the Dodge Neon is shown in Fig. 4.25. The exit angle of the vehicle was determined to be 66° by adding the 41° yaw angle at exit and the 25° impact angle. The steadily increasing positive yaw angle indicated a counter-clockwise rotation of the vehicle away from the guardrail. The roll and pitch angles in this impact were less than twenty degrees in either positive or negative direction and thus passed the MASH evaluation criterion F , which specified a maximum 75° roll or pitch angle.

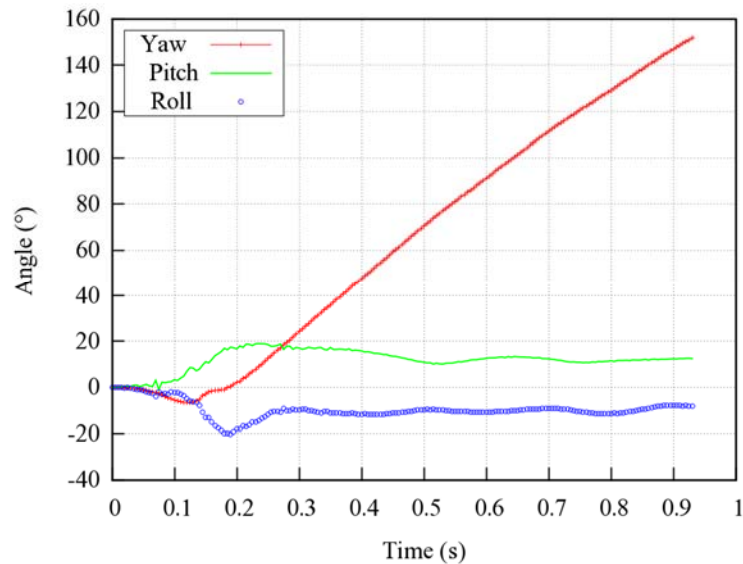


Fig. 4.25: Yaw, pitch, and roll angles of a Dodge Neon impacting the front-side of 29-inch double-faced guardrail on a 2.5H:1V slope at 62 mph (100 km/hour) and 25°.

Figure 4.26 shows the maximum dynamic deflection of the 29-inch double-faced guardrail under impact by the Dodge Neon at 62 mph (100 km/hour) and 25°. The maximum dynamic deflection of the guardrail was 1.97 ft (0.6 m) on the front-side rail, i.e., the impacted rail. Compared to the 29-inch single-faced guardrail under impact by the Dodge Neon (see Fig.

4.4a), the 29-inch double-faced guardrail had a significantly lower maximum dynamic deflection. Figure 4.27 shows detailed views of vehicle-barrier interaction during impact on the 29-inch double-faced guardrail. At the 29-inch rail height, the guardrail had very little engagement with the vehicle's bumper cover and fender due to the vehicle's low front profile. The Dodge Neon intruded under the rail, engaged with the rail on the hood of the vehicle, dragged the rail forward, and snagged on a post. This resulted in a localized deflection of the guardrail without a successful vehicle redirection.

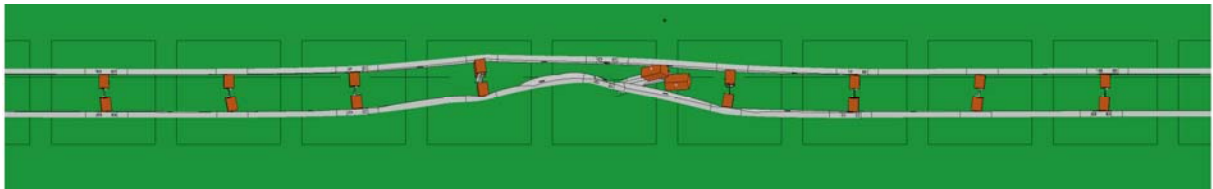


Fig. 4.26: Maximum dynamic deflection for front-side 29-inch double-faced guardrail on a 2.5H:1V slope at 62 mph (100 km/hour) and 25° and impacted by a Dodge Neon.

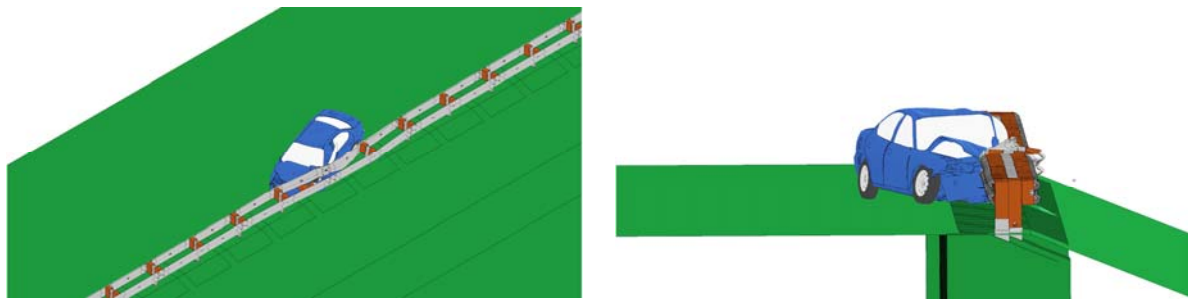


Fig. 4.27: Simulations of Dodge Neon impacting the front-side of 29-inch double-faced guardrail on a 2.5H:1V slope at 62 mph (100 km/hour) and 25°.

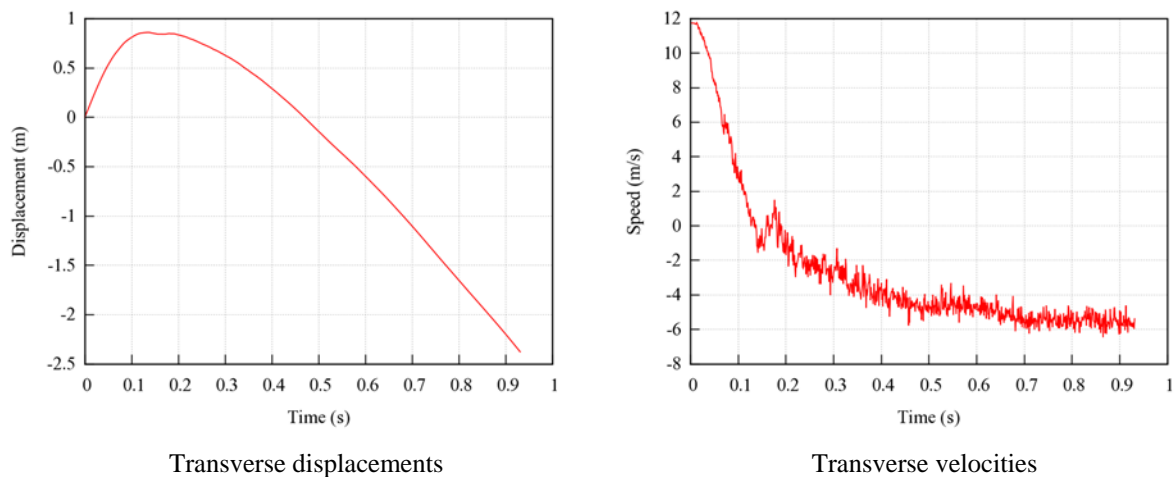


Fig. 4.28: Transverse displacements and velocities for the Dodge Neon impacting the front-side of 29-inch double-faced guardrail on a 2.5H:1V slope at 62 mph (100 km/hour) and 25°.

Figure 4.28 shows the time histories of transverse displacements and velocities measured at the CG point for the Dodge Neon impacting the guardrail at 62 mph (100 km/hour) and 25°. The transverse velocity of the vehicle was approximately 11 mph (5 m/s), indicating a moderate chance of moving towards the travel lane. In this case, since the vehicle was snagged on the guardrail and spun around a post, it would likely be involved in a secondary collision due to the fact that the MASH exit-box criterion was not met. The results in Figs. 4.24 to 4.28 indicated that the front-side impact on the 29-inch double-faced guardrail placed on a 2.5H:1V slope could safely retain the vehicle on the impacting side, but not eliminate the chance of causing a secondary collision due to vehicle spinning.

For the 29-inch double-faced W-beam guardrail impacted by a Ford F250, Fig. 4.29 shows the vehicle trajectory while impacting the front-side rail. Since the vehicle impacted the guardrail and spun around the post but did not lose contact with the guardrail (in its original position) during the entire case, the exit-box was not needed for this case. According to MASH (2009), “The ideal after-collision vehicular trajectory performance goal for all features should be that the vehicle trajectory and final stopping position should not intrude into the adjacent or opposing traffic stream.” For this case, the MASH evaluation criterion *N* was met since an acceptable post-impact behavior could be achieved with the vehicle being decelerated to a stop while maintaining vehicle-barrier contact. Even though the exit-box criterion was not applicable, the case can be determined as safe without the chance of causing a secondary collision.

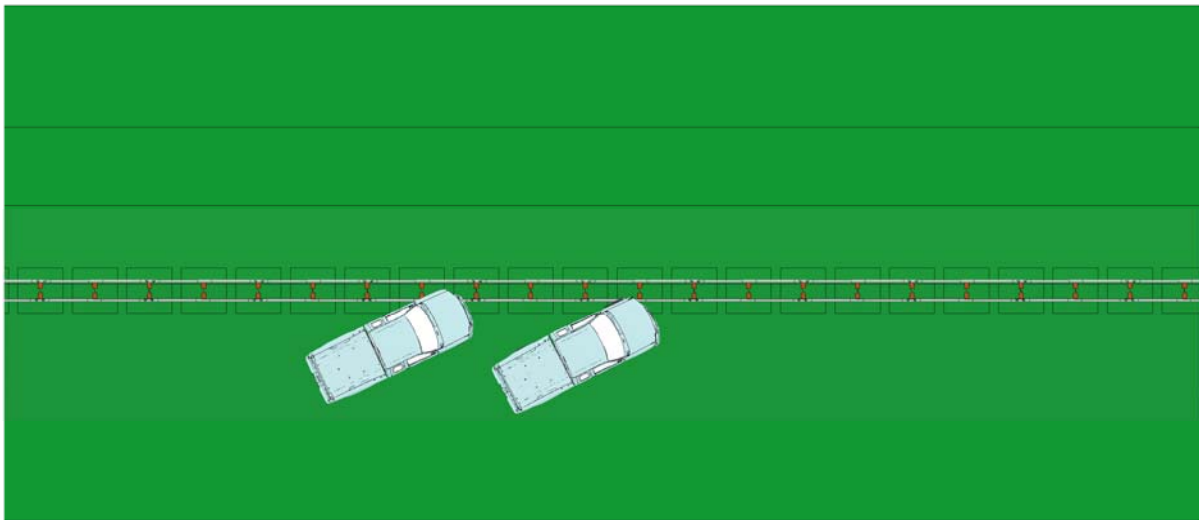


Fig. 4.29: A Ford F250 impacting the front-side of 29-inch double-faced guardrail on a 2.5H:1V slope at 62 mph (100 km/hour) and 25°.

The yaw, pitch, and roll angles of the Ford F250 in the front-side impact on the 29-inch double-faced guardrail is shown in Fig. 4.30. Since the vehicle did not lose contact with the guardrail, an exit angle could not be calculated. The roll and pitch angles in this impact were less than seven degrees in either positive or negative direction and thus passed the MASH evaluation criterion *F* that specified a maximum 75° roll or pitch angle.

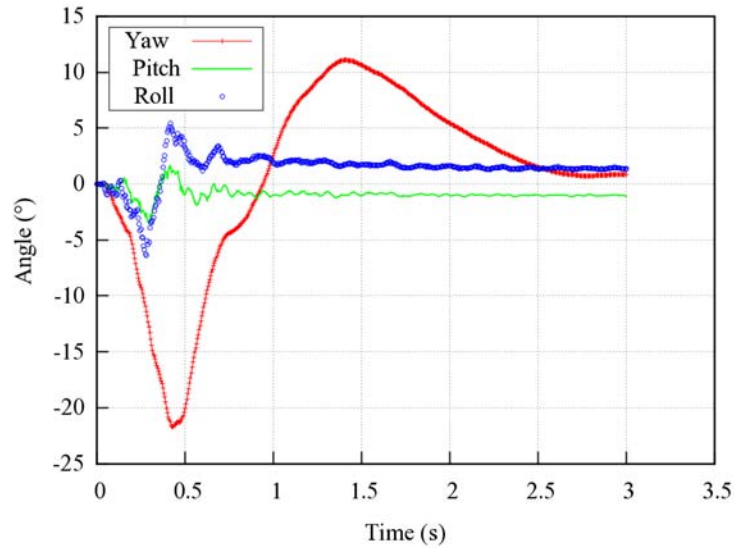


Fig. 4.30: Yaw, pitch, and roll angles for a Ford F250 impacting the front-side of 29-inch double-faced guardrail on a 2.5H:1V slope at 62 mph (100 km/hour) and 25°.

The maximum dynamic deflection of the 29-inch double-faced guardrail was measured to be 3.74 ft (1.14 m) on the impacted front-side rail (see Fig. 4.31). The transverse deflection of the double-faced guardrail was more severe than that of the single-faced guardrail under impact by the Ford F250. This was because the double-faced guardrail absorbed most impact energy as compared to redirecting the vehicle with minimal contact in the case of the single-faced guardrail. The guardrail slipped behind the vehicle’s tire after the front-left fender was damaged upon initial impact, as can be seen in Fig. 4.32.

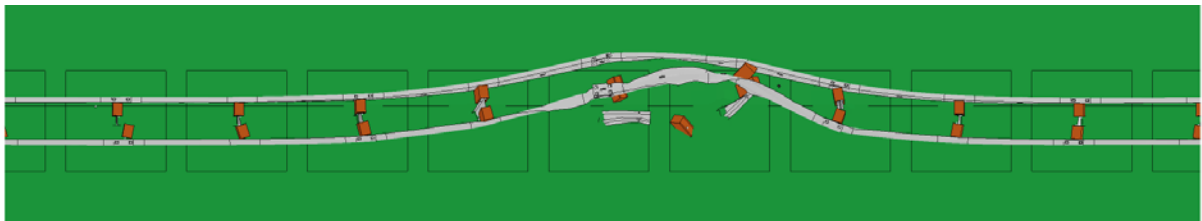


Fig. 4.31: Maximum dynamic deflection for the front-side of 29-inch double-faced guardrail on a 2.5H:1V slope at 62 mph (100 km/hour) and 25° and impacted by a Ford F250.

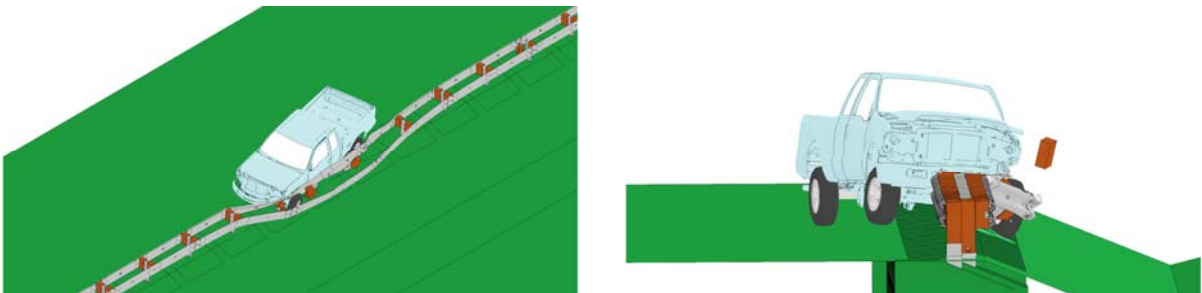


Fig. 4.32: Simulations for a Ford F250 impacting the front-side of 29-inch double-faced guardrail on a 2.5H:1V slope at 62 mph (100 km/hour) and 25°.

Figure 4.33 shows the time histories of transverse displacements and velocities measured at the CG point of the Ford F250 impacting the guardrail at 62 mph (100 km/hour) and 25°. The transverse velocity was reduced to zero because of the remaining vehicle-barrier contact. In this case, the Ford F250 had no chance of getting involved in a secondary collision.

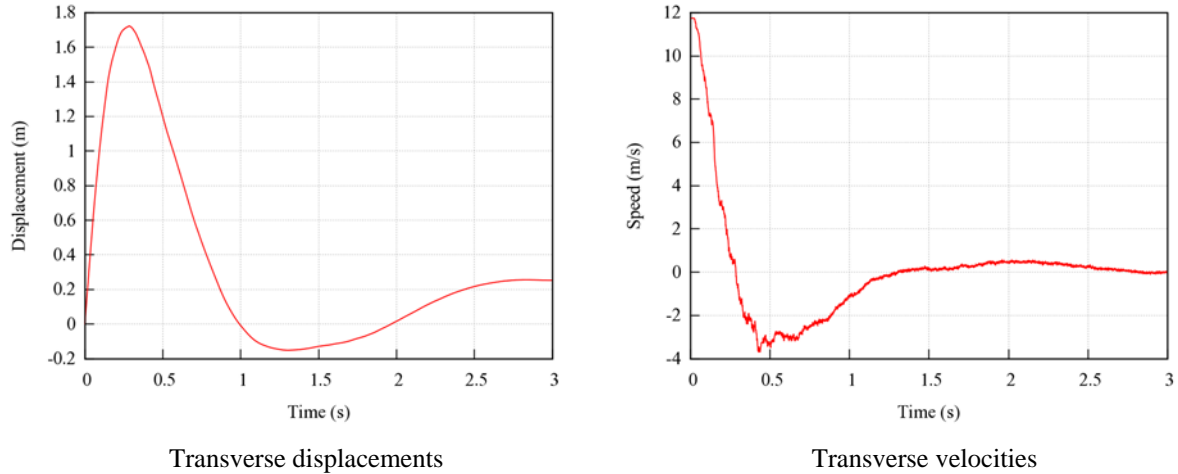


Fig. 4.33: Transverse displacements and velocities for the Ford F250 impacting the front-side of 29-inch double-faced guardrail on a 2.5H:1V slope at 62 mph (100 km/hour) and 25°.

4.2.2 The 31-inch Double-faced Guardrail – Front-side Impact

The 31-inch double-faced guardrail was also evaluated under impacts by both vehicles, i.e., the Dodge Neon and Ford F250. Figure 4.34 shows the top-view vehicle trajectory of the Dodge Neon impacting the front-side rail of the 31-inch double-faced guardrail at 62 mph (100 km/hour) and 25°. The W-beam guardrail, placed on a 2.5H:1V slope, is shown in its original, undeformed shape along with the exit-box shown by the yellow dotted rectangle.

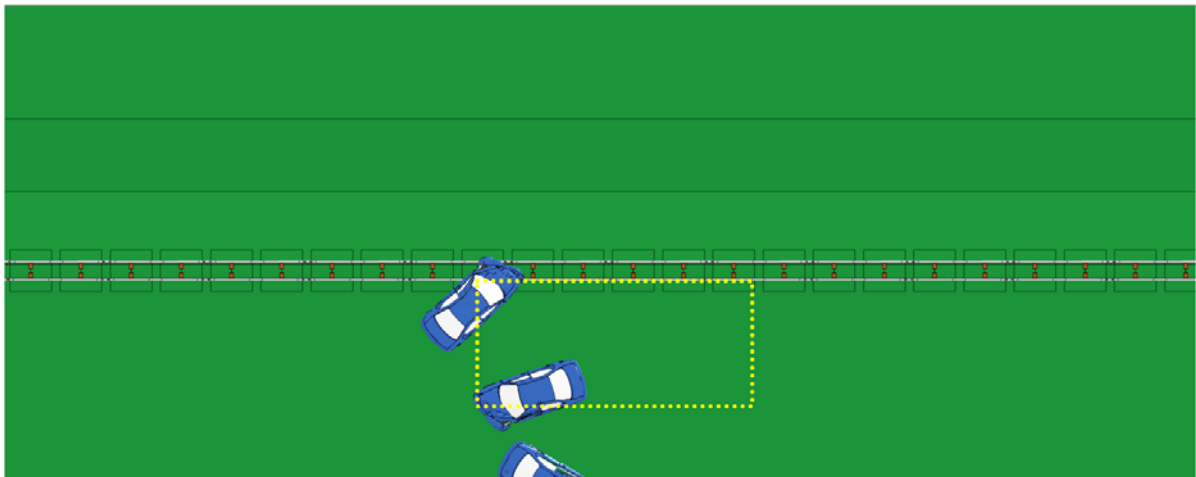


Fig. 4.34: A Dodge Neon impacting the front-side of 31-inch double-faced guardrail on a 2.5H:1V slope at 62 mph (100 km/hour) and 25°.

Upon impacting the front-side of the guardrail, the Dodge Neon snagged on a post and spun about the post. The post-impact trajectory of the vehicle was a continuous spin-out with a large exit angle. It can be seen from Fig. 4.34 that the MASH exit-box criterion was not satisfied and the vehicle was redirected almost perpendicular to the guardrail. This post-impact trajectory exhibits a high probability of being involved in a secondary collision.

The yaw, pitch, and roll angles of the Dodge Neon are shown in Fig. 4.35. The exit angle of the impact was determined to be 72° by adding the 25° impact angle to the 47° yaw angle at exit. The continuously increasing yaw angle indicated a counter-clockwise rotation of the vehicle away from the guardrail. The roll and pitch angles in this impact were less than twenty degrees in either positive or negative direction and thus passed the MASH evaluation criterion F , which specified a maximum 75° roll or pitch angle.

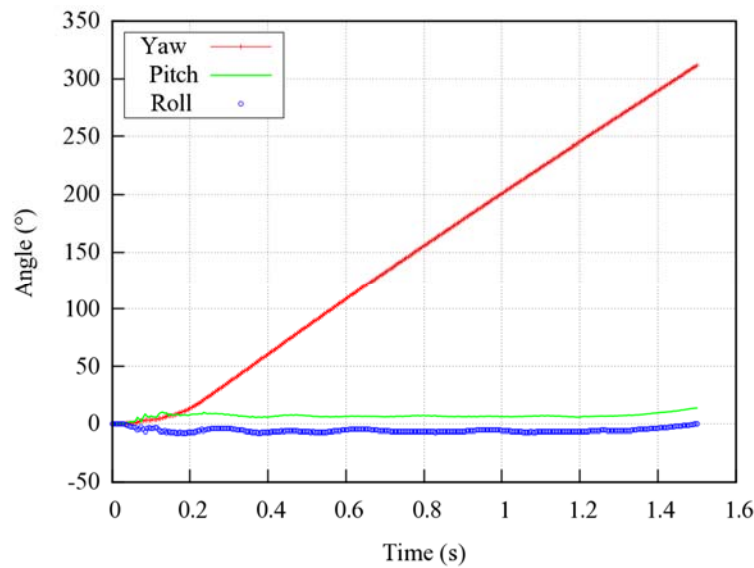


Fig. 4.35: Yaw, pitch, and roll angles of Dodge Neon impacting the front-side 31-inch double-faced guardrail on a 2.5H:1V slope at 62 mph (100 km/hour) and 25° .

The maximum dynamic deflection of the 31-inch double-faced guardrail impacted on the front-side by the Dodge Neon at 62 mph (100 km/hour) and 25° is shown in Fig. 4.36. The maximum dynamic deflection of the guardrail in this impact was determined to be 2.36 ft (0.72 m) on the impacted rail. The maximum dynamic deflection of the 31-inch guardrail was four inches more than that on the 29-inch double-faced guardrail impacted by the Dodge Neon at the same impact speed and angle (see Fig. 4.26a).

Figure 4.37 shows the detailed views of vehicle-barrier interaction on the 31-inch double-faced guardrail impacted by the Dodge Neon. Due to the vehicle's low front profile, the rail of the 31-inch guardrail did not have much engagement with the vehicle's bumper cover and wheel fender. Therefore, the vehicle intruded under the guardrail and snagged on a post, which caused the vehicle to spin-out with a large exit angle.

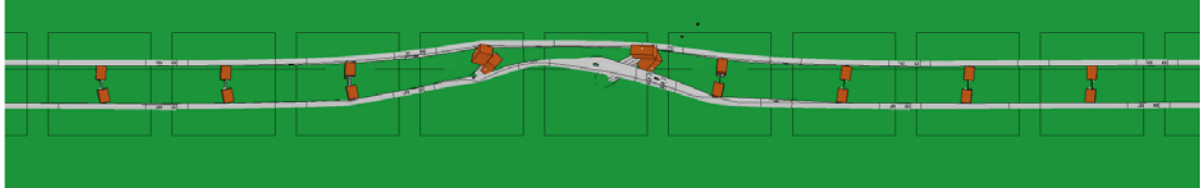


Fig. 4.36: Maximum dynamic deflection of the front-side 31-inch double-faced guardrail on a 2.5H:1V slope at 62 mph (100 km/hour) and 25° and impacted by a Dodge Neon.

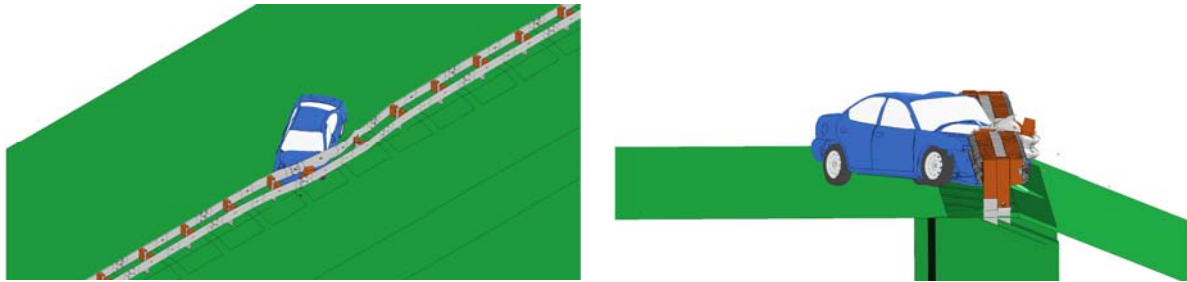


Fig. 4.37: Simulations of Dodge Neon impacting the front-side of 31-inch double-faced guardrail on a 2.5H:1V slope at 62 mph (100 km/hour) and 25°.

Figure 4.38 shows the time histories of transverse displacements and velocities measured at the CG point of the Dodge Neon impacting the front-side of the double-faced guardrail. The transverse velocity of the vehicle was approximately 10 mph (4.5 km/hour) indicating a possibility of further displacement towards the travel lane. In this case, the vehicle snagged on the guardrail and spun around a post before disengaging with the guardrail with a large exit angle. The simulation results showed that the MASH exit-box criterion was not met and the vehicle could be involved in a secondary collision.

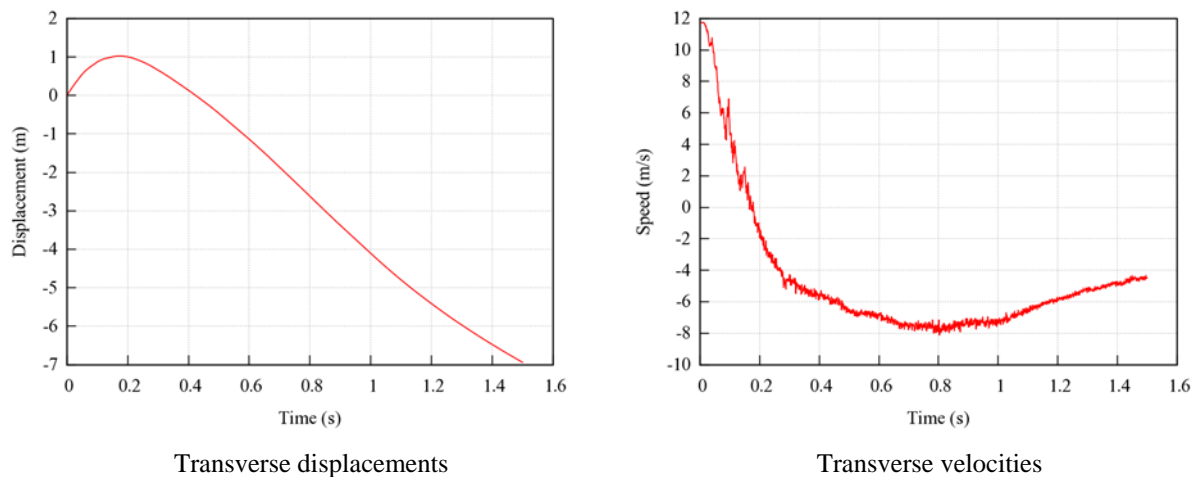


Fig. 4.38: Transverse displacements and velocities of the Dodge Neon impacting the front-side of 31-inch double-faced guardrail on a 2.5H:1V slope at 62 mph (100 km/hour) and 25°.

Figure 4.39 shows the top view vehicle trajectory of the Ford F250 impacting the 31-inch double-faced guardrail from the front-side at 62mph (100 km/hour) and 25°. The W-beam

guardrail, placed on a 2.5H:1V slope, is shown in its original undeformed shape along with the exit-box shown by the yellow dotted rectangle. The MASH exit-box criterion was not satisfied because the vehicle did not traverse the full length of the exit-box before leaving the box. Due to the low exit angle of the post-impact trajectory, the chances of a secondary collision was relatively low even though the exit-box criterion was not met.

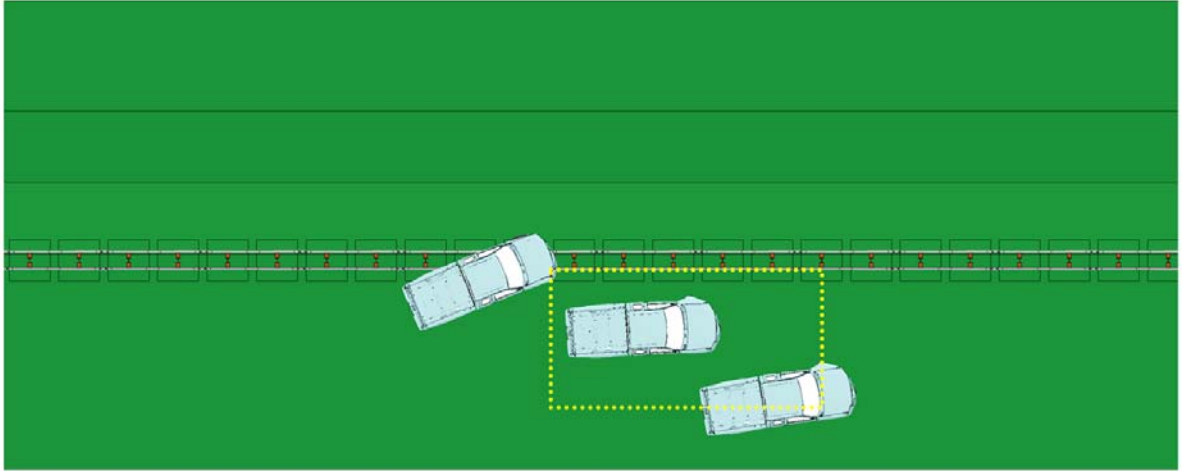


Fig. 4.39: A Ford F250 impacting the front-side 31-inch double-faced guardrail on a 2.5H:1V slope at 62 mph (100 km/hour) and 25°.

The yaw, pitch, and roll angles of the Ford F250 are shown in Fig. 4.40. Since the vehicle was redirected by the guardrail instead of snagging on a post, the exit angle was determined to be 4° by subtracting the 25° impact angle from the 29° yaw angle at exit. The roll and pitch angles were less than seven degrees in either positive or negative direction and thus passed the MASH evaluation criterion F , which specified a maximum 75° roll or pitch angle.

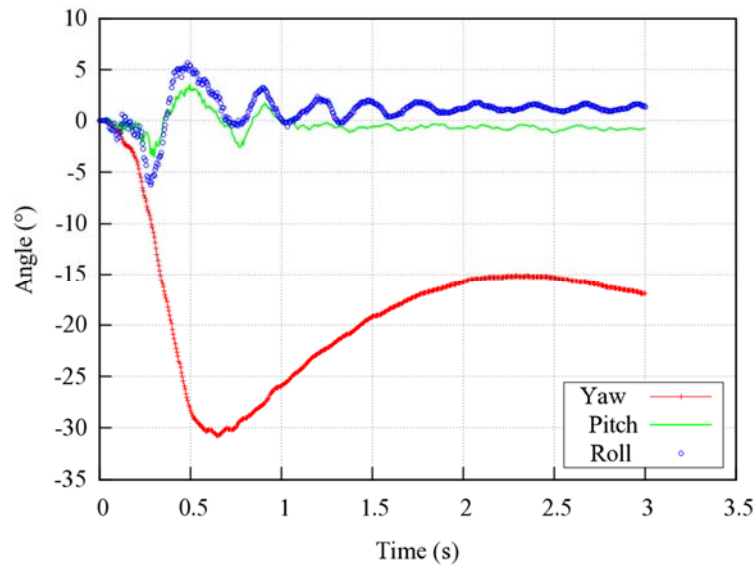


Fig. 4.40: Yaw, pitch, and roll angles of Ford F250 impacting the front-side 31-inch double-faced guardrail on a 2.5H:1V slope at 62 mph (100 km/hour) and 25°.

Figure 4.41 shows the maximum dynamic deflection of the 31-inch double-faced guardrail impacted by the Ford F250 at 62 mph (100 km/hour) and 25°. The maximum dynamic deflection was determined to be 3.87 ft (1.14 m) on the impacted rail. This was comparable to the front-side impact by the Ford F250 on the single-faced guardrail. The vehicle had good interaction with the guardrail and was redirected with a low exit angle, as seen in Fig. 4.42.

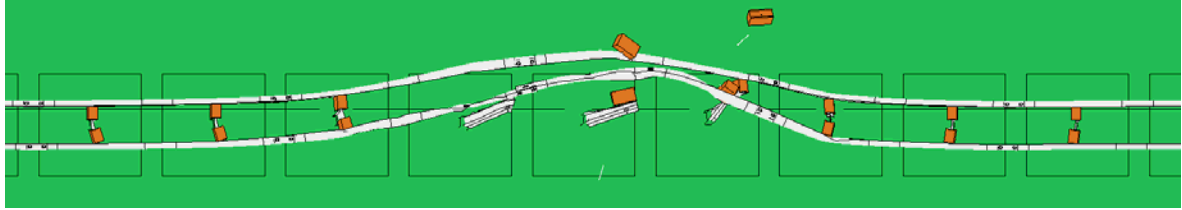


Fig. 4.41: Maximum dynamic deflection of the front-side 31-inch double-faced guardrail on a 2.5H:1V slope at 62 mph (100 km/hour) and 25° and impacted by a Ford F250.

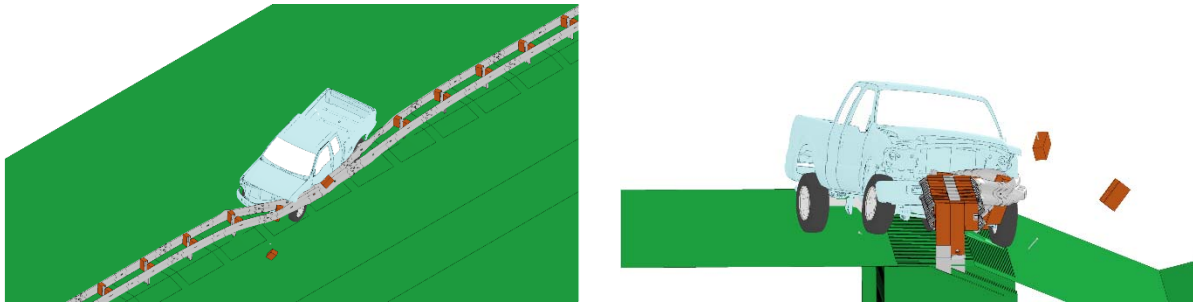


Fig. 4.42: Simulations of Ford F250 impacting the front-side 31-inch double-faced guardrail on a 2.5H:1V slope at 62 mph (100 km/hour) and 25°.

Figure 4.43 shows the time histories of transverse displacements and velocities measured at the CG point of the Ford F250 impacting the 31-inch double-faced guardrail. The transverse velocity was determined to be approximately 2 mph (1 m/s) towards the travel lane. Considering the exit-box criterion, exit angle, and transverse velocity, the Ford F250 would have a relatively small chance of getting involved in a secondary collision.

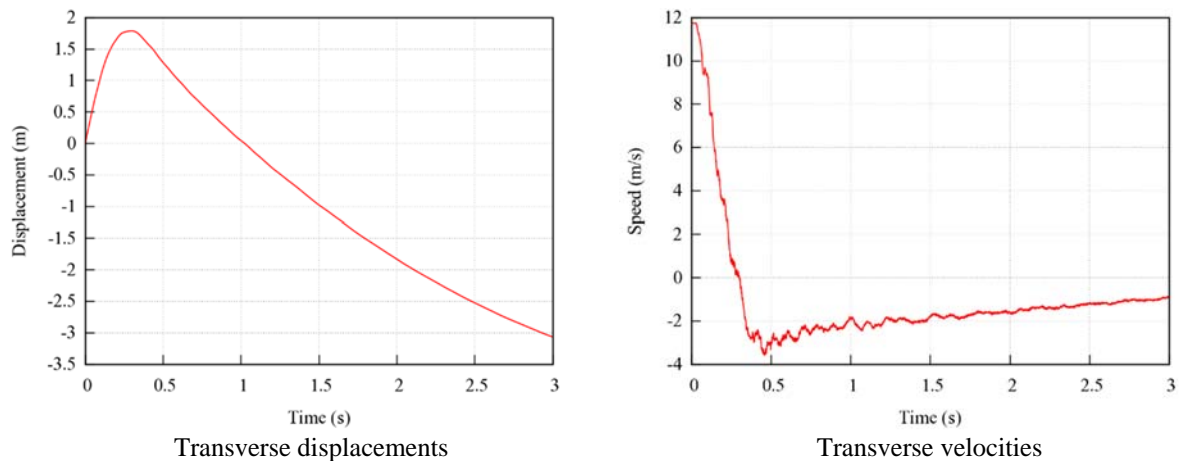


Fig. 4.43: Transverse displacements and velocities of the Ford F250 impacting the front-side 31-inch double-faced guardrail on a 2.5H:1V slope at 62 mph (100 km/hour) and 25°.

4.2.3 The 29-inch Double-faced Guardrail – Backside Impact

In these simulations, the vehicle was placed on the flat shoulder next to a 4H:1V slope. Starting from the vehicle's initial location, the vehicle traverses through both median slopes before impacting the backside rail of the 29-inch double-faced guardrail.

Figure 4.44 shows the top-view vehicle trajectory of the Dodge Neon impacting the backside rail of the 29-inch double-faced guardrail at 62 mph (100 km/hour) and 25°. The W-beam guardrail, placed on a 2.5H:1V slope, is shown in its original undeformed shape along with the exit-box shown by the yellow dotted rectangle.

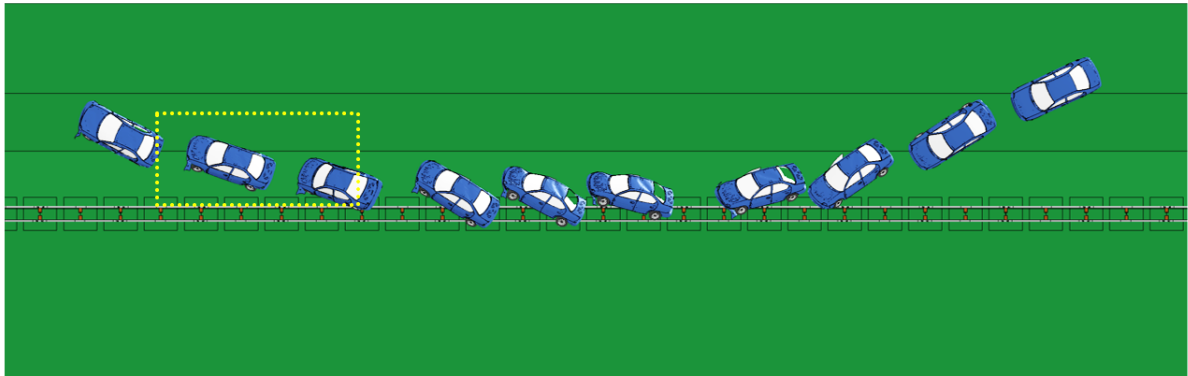


Fig. 4.44: A Dodge Neon impacting the backside of 29-inch double-faced guardrail on a 2.5H:1V slope at 62 mph (100 km/hour) and 25°.

Upon impacting the backside rail of the 29-inch double-faced guardrail, the Dodge Neon became airborne for a short amount of time. The rear left wheel contacted the guardrail upon touching the ground so the exit-box was placed at this location and the vehicle traversed the full length of the box before exiting. Since the post-impact trajectory of this case satisfied the MASH exit-box criterion, the case can be categorized as a safe redirection. The reason that the vehicle became airborne after impacting the guardrail was due to the compressed and expanding suspension while traversing the sloped median.

The yaw, pitch, and roll angles of the Dodge Neon impacting the backside of the 29-inch double-faced guardrail at 62 mph (100 km/hour) and 25° are shown in Fig. 4.45. Since the vehicle was redirected by the guardrail instead of snagging on a post, the exit angle was calculated by subtracting the impact angle from the yaw angle at the last point of contact with the guardrail. The exit angle of this impact was determined to be 2° by subtracting the impact angle (i.e., 25°) from the yaw angle at exit (i.e., 27°). The roll and pitch angles were higher than the previous cases but were still within the range of a maximum 75° roll or pitch angle specified by the MASH evaluation criterion *F*. The roll angles were less than 18° and 55° in the positive and negative directions, respectively, and the pitch angles were less than 22° and 35° in the positive and negative directions, respectively.

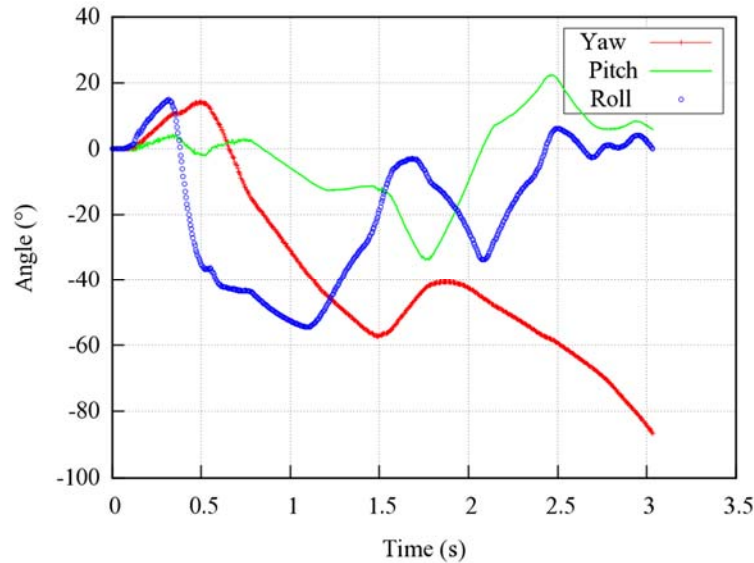


Fig. 4.45: Yaw, pitch, and roll angles of the Dodge Neon impacting the backside 29-inch double-faced guardrail on a 2.5H:1V slope at 62 mph (100 km/hour) and 25°.

The maximum dynamic deflection of the backside impact on the 29-inch double-faced guardrail impacted by the Dodge Neon at 62 mph (100 km/hour) and 25° is shown in Fig. 4.46. It was determined that the maximum dynamic deflection of the guardrail in this case was 0.98 ft (0.3 m) on the backside rail (i.e., the impacted rail). This maximum deflection was the smallest among all the cases examined in the entire study. This small deflection can be attributed to the vehicle vaulting into the air upon impacting the guardrail. The initial vehicle-barrier contact was with the vehicle’s front bumper cover followed by the front-left tire riding up the face of the guardrail. As seen in Fig. 4.46, the backside rail (top rail in the figure) is rotated up along the longitudinal axis due to vaulting of the vehicle.

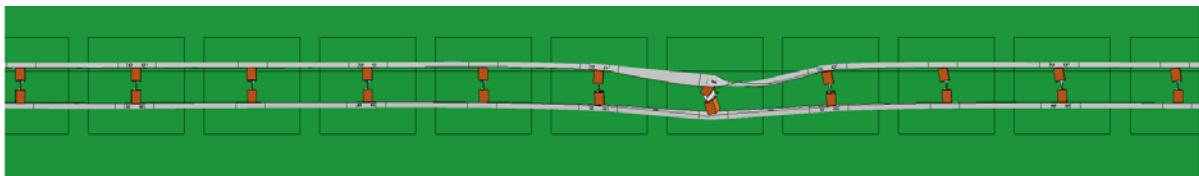


Fig. 4.46: Maximum dynamic deflection of the backside 29-inch double-faced guardrail on a 2.5H:1V slope at 62 mph (100 km/hour) and 25° and impacted by a Dodge Neon.

Figure 4.47 shows detailed views of the vehicle-barrier interaction during impacts by the Dodge Neon on the backside rail of the 29-inch double-faced guardrail. In this impact, due to the compressed and expanding suspension when traversing the sloped median, the vehicle’s bumper cover and wheel fender were in initial contact with backside rail, followed by the front-left tire riding up the rail of the 29-inch double-faced guardrail. Figure 4.47 depicts a state shortly after the initial impact and shows the vehicle partially airborne while riding up the face of the guardrail.



Fig. 4.47: Simulations of Dodge Neon impacting the backside 29-inch double-faced guardrail on a 2.5H:1V slope at 62 mph (100 km/hour) and 25°.

Figure 4.48 show the time histories of transverse displacements and velocities measured at the CG point of the Dodge Neon impacting the backside of the 29-inch double-faced guardrail. The transverse velocity of the vehicle upon leaving contact with the guardrail after touchdown was approximately 9 mph (4 m/s). In this case, since the vehicle met the MASH exit-box criterion and was traversing in the sloped median after impact, it was unlikely to get involved in a secondary collision. The results in Figs. 4.44 to 4.48 indicated that the backside rail of the 29-inch double-faced guardrail could safely redirect a small car that impacted the guardrail at an impact angle of 25°.

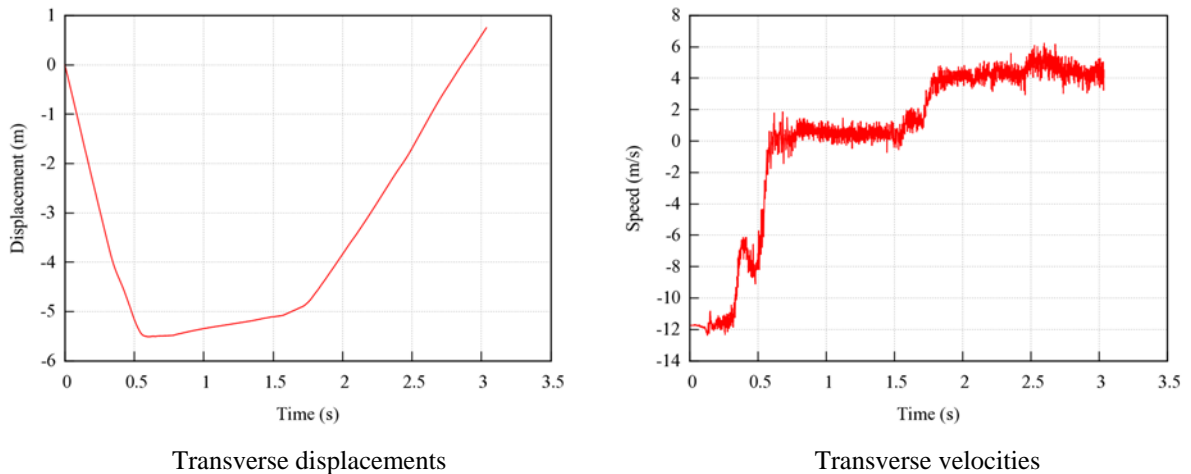


Fig. 4.48: Transverse displacements and velocities of the Dodge Neon impacting the backside 29-inch double-faced guardrail on a 2.5H:1V slope at 62 mph (100 km/hour) and 25°.

Figure 4.49 shows the top view vehicle trajectory of the Ford F250 impacting the backside rail of the 29-inch double-faced guardrail at 62mph (100 km/hour) and 25°. The W-beam guardrail, placed on a 2.5H:1V slope, is shown in its original undeformed shape along with the exit-box shown by the yellow dotted rectangle. Upon impacting the guardrail, the Ford F250 experienced tire snagging on a guardrail post. This tire snagging resulted in the vehicle rotating around the post, disengaging from the guardrail, and leaving the exit-box prematurely with a large exit angle and a continuous spin. The yaw, pitch, and roll angles of the vehicle in this impact are shown in Fig. 4.50. The exit angle was determined to be 107°, by adding the impact angle (i.e., 25°) to the yaw angle at exit (i.e., 82°). The continuously growing yaw angle indicated a counter-clockwise rotation of the vehicle away from the guardrail. The roll and pitch angles were less than thirty degrees in either positive or negative

direction and thus passed the MASH evaluation criterion F, which specified a maximum 75° roll or pitch angle.

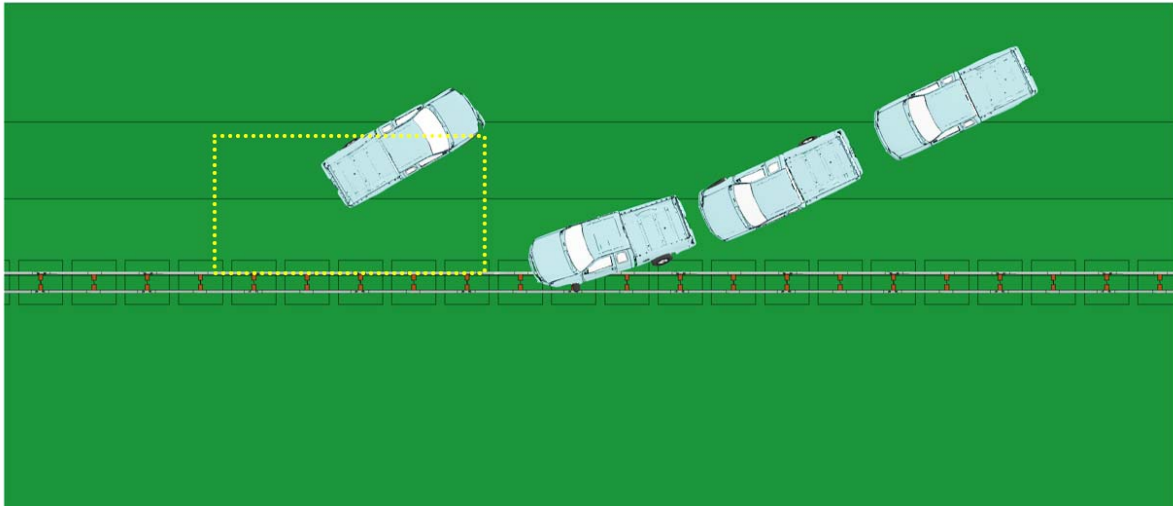


Fig. 4.49: A Ford F250 impacting the backside 29-inch double-faced guardrail on a 2.5H:1V slope at 62 mph (100 km/hour) and 25° .

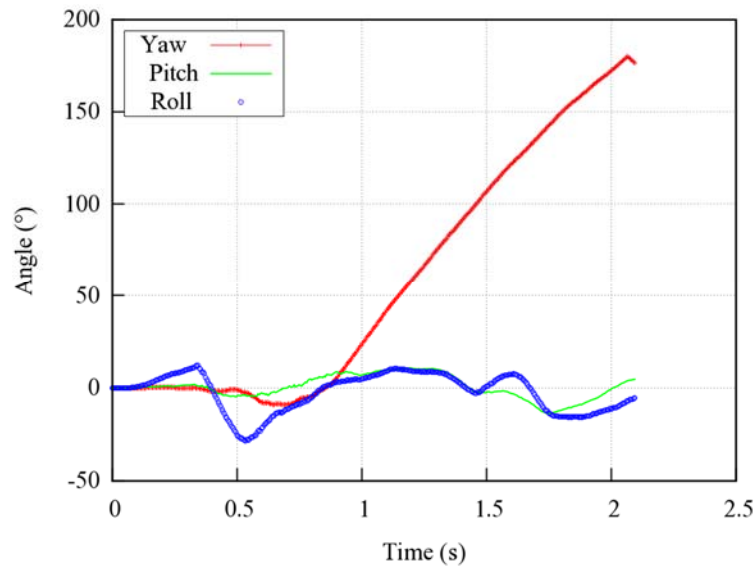


Fig. 4.50: Yaw, pitch, and roll angles of the Ford F250 impacting the backside of 29-inch double-faced guardrail on a 2.5H:1V slope at 62 mph (100 km/hour) and 25° .

The maximum dynamic deflection of the 29-inch double-faced guardrail impacted by the Ford F250 on the backside at 62 mph (100 km/hour) and 25° is shown in Fig. 4.51. The maximum dynamic deflection of the guardrail in this case was 2.17 ft (0.66 m) measured on the impacted rail. In this case, the vehicle had good interaction with the guardrail at the beginning of the impact (see Fig. 4.52), but experienced subsequent tire snagging on a guardrail post and spun out in a trajectory away from the guardrail.

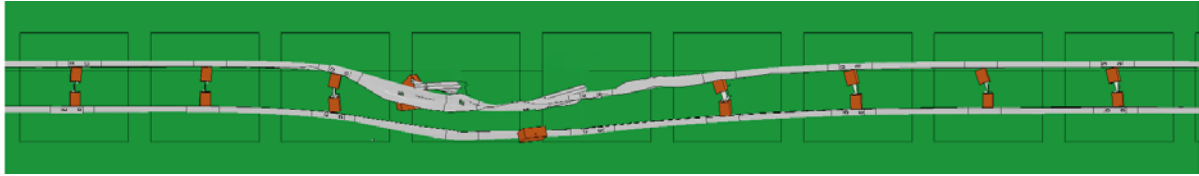


Fig. 4.51: Maximum dynamic deflection of the backside 29-inch double-faced guardrail on a 2.5H:1V slope at 62 mph (100 km/hour) and 25° and impacted by a Ford F250.

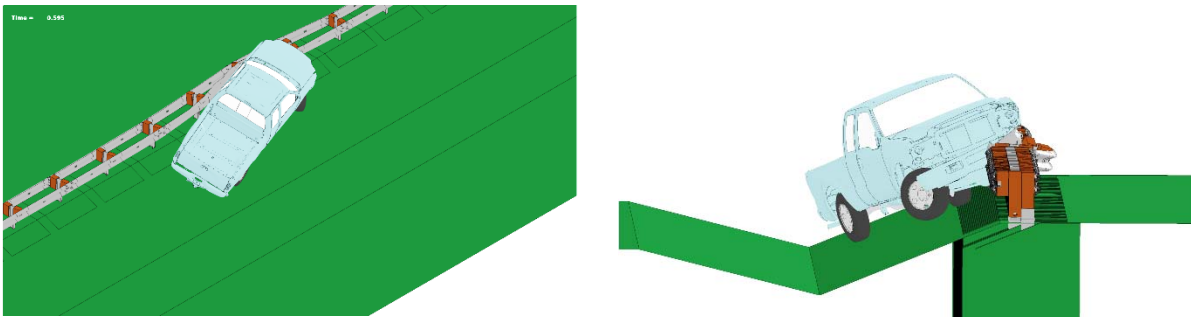


Fig. 4.52: Simulations of Ford F250 impacting the backside 29-inch double-faced guardrail on a 2.5H:1V slope at 62 mph (100 km/hour) and 25°.

Figure 4.53 shows the time histories of transverse displacements and velocities measured at the CG point of the Ford F250 impacting the backside of the 29-inch double-faced guardrail. The transverse velocity was approximately 5 mph (2.2 m/s) into the sloped median towards the travel lane. Considering the width of the sloped median and the low transverse velocity, the Ford F250 have a relatively small chance of getting involved in a secondary collision.

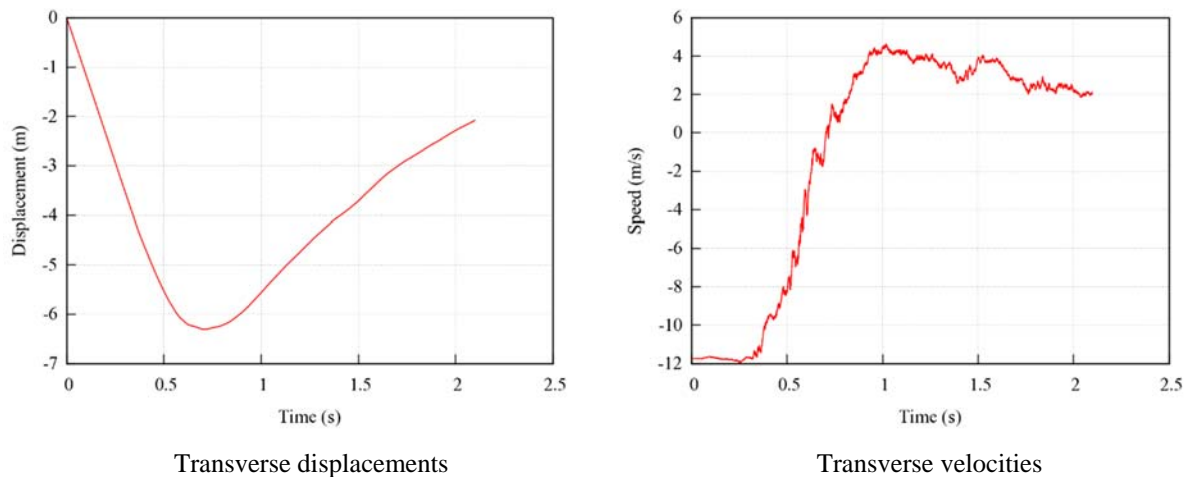


Fig. 4.53: Transverse displacements and velocities of the Ford F250 impacting the backside 29-inch double-faced guardrail on a 2.5H:1V slope at 62 mph (100 km/hour) and 25°.

4.2.4 The 31-inch Double-faced Guardrail – Backside Impact

In these simulations, the vehicle was placed on the flat shoulder next to a 4H:1V slope. Starting from the vehicle's initial location, the vehicle traversed through both sides of the

sloped median before impacting the backside rail of the 31-inch double-faced guardrail. Figure 4.54 shows the top view vehicle trajectory of the Dodge Neon impacting the backside rail of the 31-inch double-faced guardrail at 62 mph (100 km/hour) and 25°. The W-beam guardrail, placed on a 2.5H:1V slope, is shown in its original undeformed shape and the exit-box is shown by the yellow dotted rectangle. Upon impacting the guardrail, the Dodge Neon was successfully redirected by the guardrail and passed the MASH exit-box criterion.

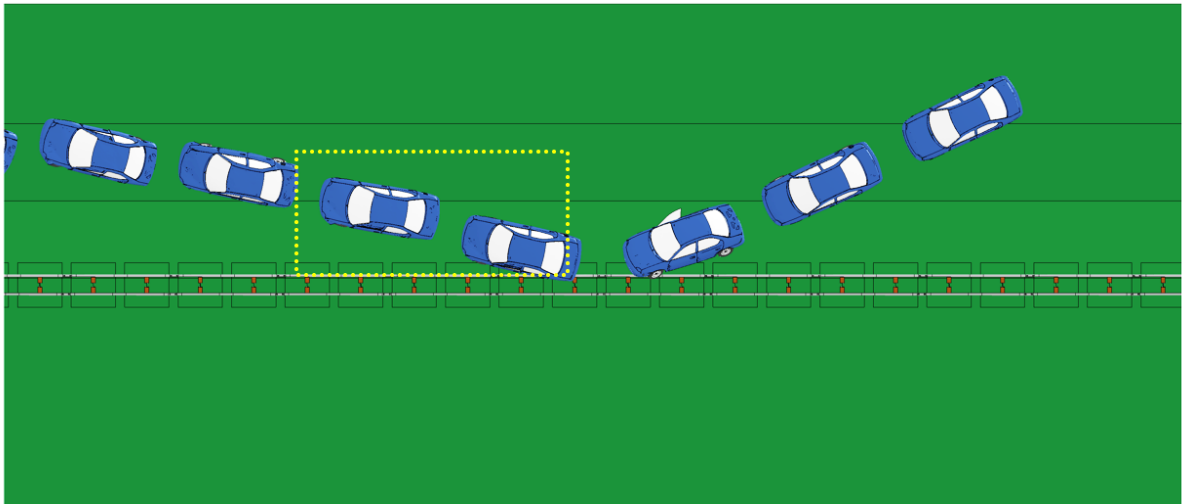


Fig. 4.54: A Dodge Neon impacting the backside of 31-inch double-faced guardrail on a 2.5H:1V slope at 62 mph (100 km/hour) and 25°.

The yaw, pitch, and roll angles of the Dodge Neon impacting the backside rail of the 31-inch double-faced guardrail is shown in Fig. 4.55. Since the vehicle was redirected by the guardrail instead of snagging on a post, the exit angle was determined to be 13° by subtracting the impact angle (i.e., 25°) from the yaw angle (i.e., 38°) at the last point of contact with the guardrail. The roll and pitch angles were less than thirty five degrees in either positive or negative direction and thus passed the MASH evaluation criterion F , which specified a maximum 75° roll or pitch angle.

Figure 4.56 shows the maximum dynamic deflection of the backside rail on the 31-inch double-faced guardrail impacted by the Dodge Neon at 62 mph (100 km/hour) and 25°. The maximum dynamic deflection of the guardrail in this case was 1.21 ft (0.37 m) on the impacted rail. Compared to the backside impact of the 29-inch double-faced guardrail by the Dodge Neon (see Fig. 4.46), the 31-inch guardrail had a slightly larger maximum dynamic deflection yet successfully redirected the vehicle with a smaller exit angle. At 31-inch rail height on a 2.5H:1V slope, the guardrail had very good engagement with the vehicle's bumper cover and fender, allowing the guardrail to redirect the vehicle with localized damage to the guardrail. Figure 4.57 shows the detailed views of vehicle-barrier interactions while the Dodge Neon impacts the 31-inch double-faced guardrail at 62 mph (100 km/hour) and 25°. It can be seen from Fig. 4.57 that the vehicle engaged well with the guardrail and that the vehicle had an airborne trajectory after traversing the sloped median.

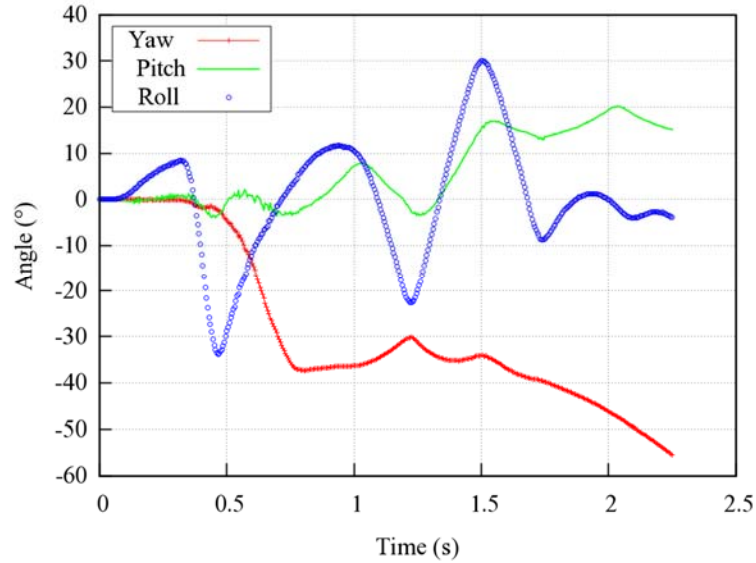


Fig. 4.55: Yaw, pitch, and roll angles of the Dodge Neon impacting the backside of 31-inch double-faced guardrail on a 2.5H:1V slope at 62 mph (100 km/hour) and 25°.

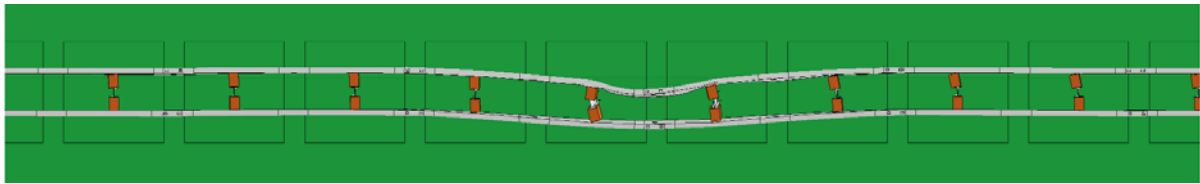


Fig. 4.56: Maximum dynamic deflection of the backside 31-inch double-faced guardrail on a 2.5H:1V slope at 62 mph (100 km/hour) and 25° and impacted by a Dodge Neon.

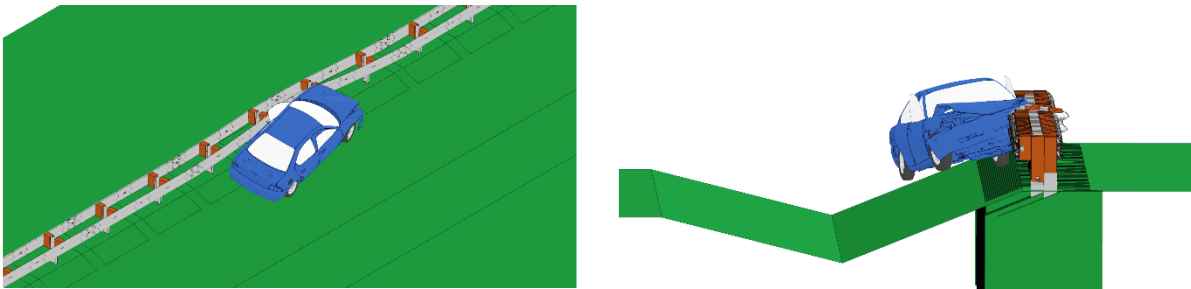


Fig. 4.57: Simulations of Dodge Neon impacting the backside 31-inch double-faced guardrail on a 2.5H:1V slope at 62 mph (100 km/hour) and 25°.

Figure 4.58 show the time histories of transverse displacements and velocities measured at the CG point of the Dodge Neon impacting the backside of the 31-inch double-faced guardrail. The transverse velocity of the vehicle was approximately 4 mph (1.8 m/s) towards the travel lane, indicating a low probability of further displacement. In this case, the vehicle was successfully redirected with a low exit angle meeting the MASH exit-box criterion; it was unlikely to cause a secondary collision. The results in Figs. 4.54 to 4.58 indicated that the 31-inch double-faced guardrail placed on a 2.5H:1V slope could safely redirect a small vehicle that impacted the guardrail at 62 mph (100 km/hour) and at an impact angle of 25°.

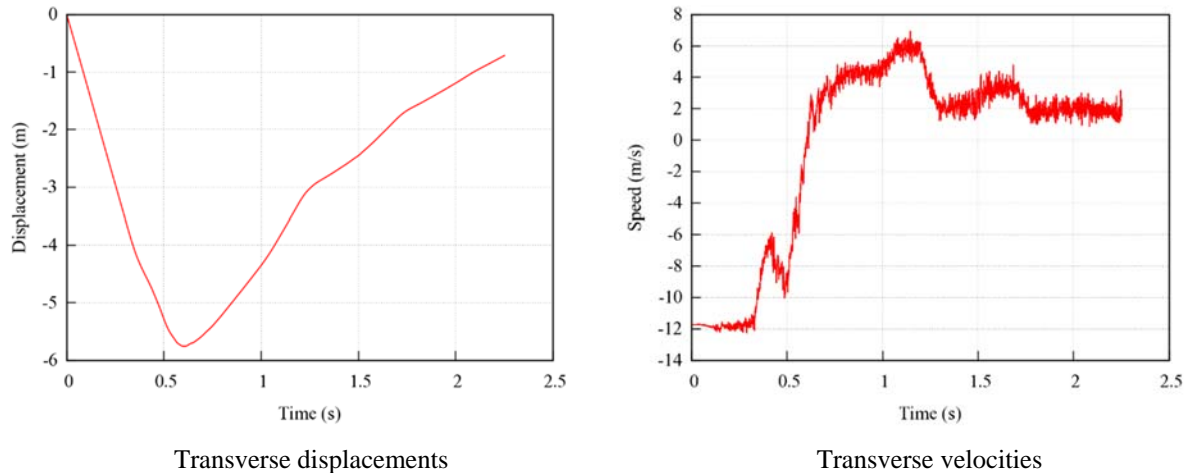


Fig. 4.58: Transverse displacements and velocities of the Dodge Neon impacting the backside of 31-inch double-faced guardrail on a 2.5H:1V slope at 62 mph (100 km/hour) and 25°.

Figure 4.59 shows the top view vehicle trajectory of the Ford F250 impacting the backside rail of the 31-inch double-faced guardrail at 62mph (100 km/hour) and 25°. The W-beam guardrail, placed on a 2.5H:1V slope, is shown in its original undeformed shape along with the exit-box shown by the yellow dotted rectangle. Upon impacting the guardrail, the vehicle experienced tire snagging on a guardrail post, rotated around the guardrail post, and spun out of the exit box. The vehicle disengaged from the guardrail with a large exit angle and failed to meet the MASH exit-box criterion.

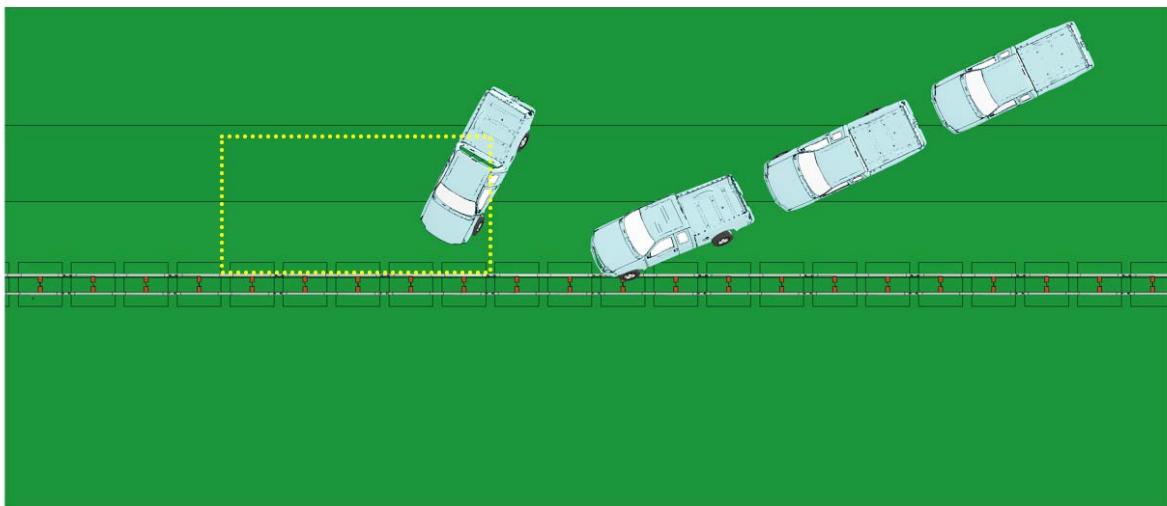


Fig. 4.59: A Ford F250 impacting the backside of 31-inch double-faced guardrail on a 2.5H:1V slope at 62 mph (100 km/hour) and 25°.

The yaw, pitch, and roll angles of the Ford F250 impacting the backside rail of the 31-inch double-faced guardrail is shown in Fig. 4.60. The exit angle was determined to be 52°, by adding the impact angle (i.e., 25°) to the yaw angle at exit (i.e., 27°). The continuously growing yaw angle indicated a counter-clockwise rotation of the vehicle away from the

guardrail. The roll and pitch angles in this impact was less than thirty degrees in either positive or negative direction and thus passed the MASH evaluation criterion F , which specified a maximum 75° roll or pitch angle.

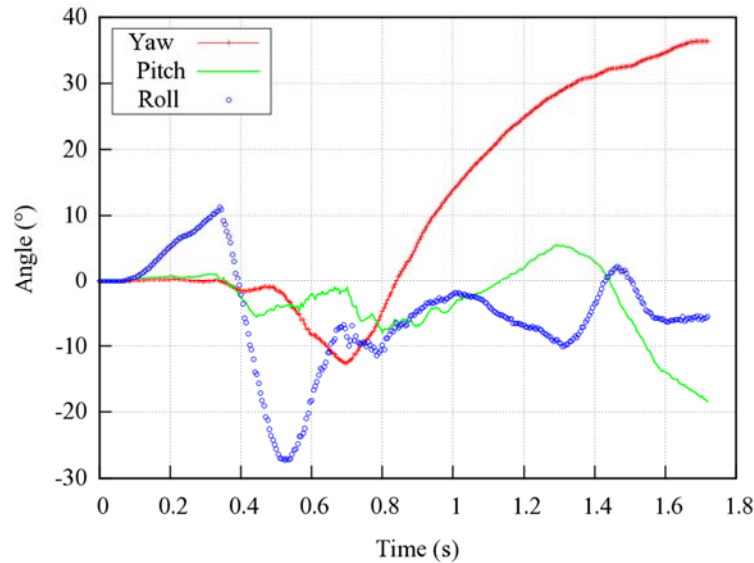


Fig. 4.60: Yaw, pitch, and roll angles of Ford F250 impacting the backside of 31-inch double-faced guardrail on a 2.5H:1V slope at 62 mph (100 km/hour) and 25° .

The maximum dynamic deflection of the 31-inch double-faced guardrail impacted by the Ford F250 from backside at 62 mph (100 km/hour) and 25° is shown in Fig. 4.61. The maximum dynamic deflection of the guardrail in this case was 2.69 ft (0.82 m) on the impacted rail. Similar to the comparison between the 29- and 31-inch double-faced guardrails impacted by the Dodge Neon, the 31-inch guardrail impacted by the Ford F250 also had more severe deformation and a larger maximum dynamic deflection than the 29-inch guardrail. As seen in Fig. 4.62, the vehicle had good interaction with the guardrail but was subsequently caught on a guardrail post and disengaged from the guardrail with spin-out and a continuously increasing yaw angle.

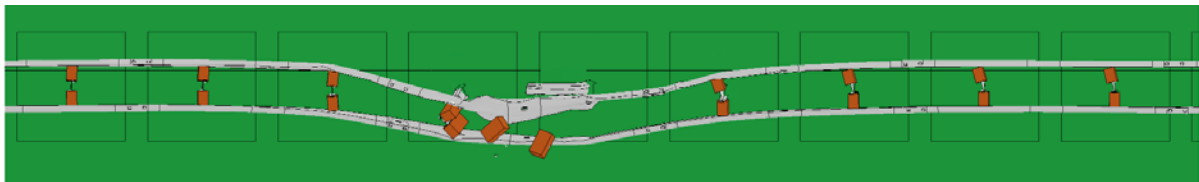


Fig. 4.61: Maximum dynamic deflection of the backside 31-inch double-faced guardrail on a 2.5H:1V slope at 62 mph (100 km/hour) and 25° and impacted by a Ford F250.

Figure 4.63 show the time histories of transverse displacements and velocities measured at the CG point of the Ford F250 impacting the backside of the 31-inch double-faced guardrail. For this impact, the transverse velocity of the vehicle was approximately 7 mph (3 m/s), indicating a low probability of further displacement towards the travel lane would occur.

Considering the low transverse velocity and post-impact vehicular responses, the Ford F250 was retained within the median so it is unlikely it would be involved in a secondary collision.

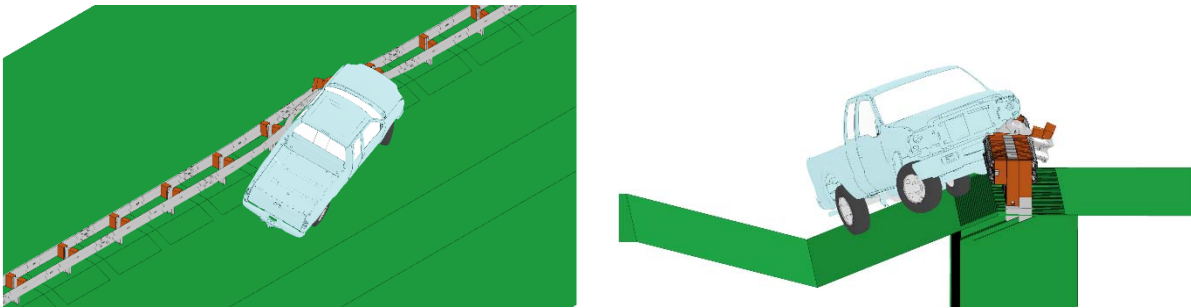


Fig. 4.62: Simulations of Ford F250 impacting the backside 31-inch double-faced guardrail on a 2.5H:1V slope at 62 mph (100 km/hour) and 25°.

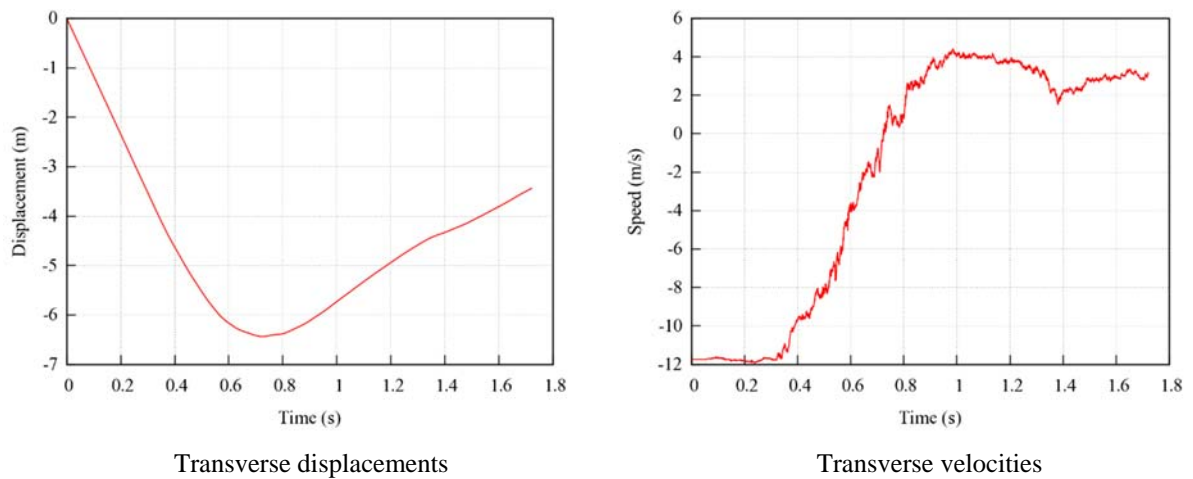


Fig. 4.63: Transverse displacements and velocities of the Ford F250 impacting the backside 31-inch double-faced guardrail on a 2.5H:1V slope at 62 mph (100 km/hour) and 25°.

4.3 Case 3: Lowered Backside Double-faced Guardrail Placed on a 2.5H:1V Slope

Similar to Case 2, the double-faced guardrails with a lowered backside rail were placed on a 2.5H:1V slope at the placement heights of 29 and 31 inches and evaluated under impacts of both the Dodge Neon and Ford F250. In this case, the backside rail was lowered by 2.1 in (53.3 mm) to account for the slope on the backside so as to achieve the same ground-to-guardrail height as the front-side rail. Two impact sides were tested: the front-side impact and the backside impact for all the double-faced guardrail. In the backside impact, the vehicle traverses through the sloped median before impacting the backside of the double-faced guardrail. An impact speed of 62 mph (100 km/hour) was used in all simulations. Table 4.5 gives a summary of the guardrail performance in terms of vehicular responses.

Table 4.5: Simulation results of Case 3 (lowered backside double-faced guardrail placed on a 2.5H:1V slope)

Impact side	Guardrail Height	Test Vehicle	Simulation Results
Front-side	29 inch	Dodge Neon	The vehicle failed the exit-box criterion caused by vehicle spin-out and a large exit angle
		Ford F250	The vehicle failed the exit-box criterion caused by vehicle spin-out and a large exit angle
	31 inch	Dodge Neon	The vehicle failed the exit-box criterion caused by vehicle spin-out and a large exit angle
		Ford F250	The vehicle failed the exit-box criterion caused by vehicle spin-out and a large exit angle
Backside	29 inch	Dodge Neon	The vehicle failed to remain upright
		Ford F250	The vehicle failed to remain upright
	31 inch	Dodge Neon	The vehicle failed to remain upright
		Ford F250	The vehicle failed the exit-box criterion caused by vehicle spin-out and a large exit angle

4.3.1 The 29-inch Double-faced Guardrail with a Lowered Backside Rail – Front-side Impact

Figure 4.64 shows the top view vehicle trajectory of the Dodge Neon impacting the 29-inch double-faced guardrail with a lowered backside rail on a 2.5H:1V slope. The guardrail was impacted by the vehicle from the front-side at 62 mph (100 km/hour) and 25°. The W-beam guardrail is shown in its original undeformed shape and the exit-box is shown by the yellow dotted rectangle. Upon impacting front-side rail of the 29-inch double-faced guardrail, the

Dodge Neon snagged on a guardrail post and spun around the post losing contact with the guardrail with a large exit angle and continuously spinning towards the travel lane.

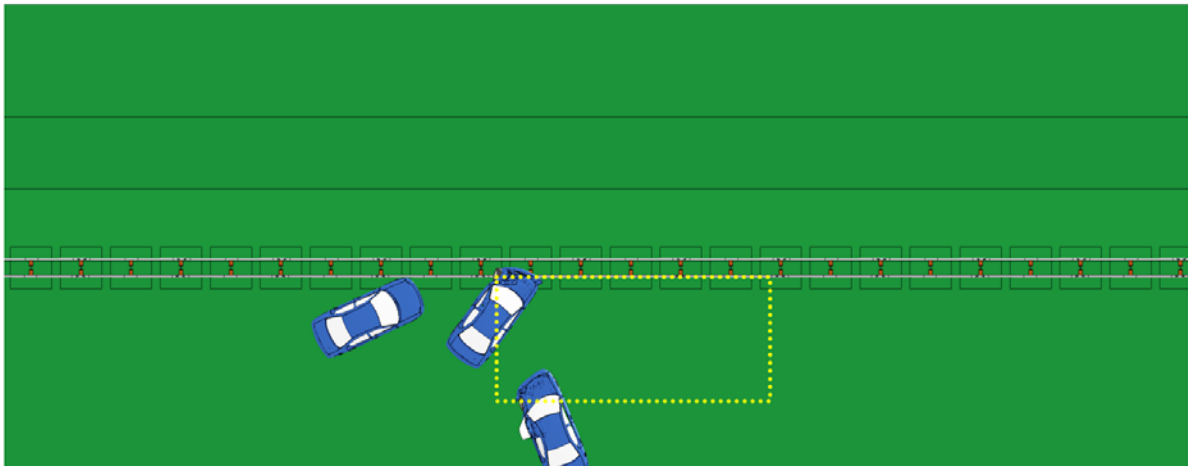


Fig. 4.64: A Dodge Neon impacting the front-side of the lowered backside 29-inch guardrail on a 2.5H:1V slope at 62 mph (100 km/hour) and 25°.

The yaw, pitch, and roll angles of the Dodge Neon during the impact of the 29-inch lowered backside double-faced guardrail is shown in Fig. 4.65. The exit angle was determined to be 52° by adding the 25° impact angle to the yaw angle at exit (i.e., 27°). The increasing positive yaw angle indicates a counter-clockwise rotation of the vehicle after losing contact with the guardrail. The roll and pitch angles in this impact was less than twenty degrees in either positive or negative direction and thus passed the MASH evaluation criterion *F*, which specified a maximum 75° roll or pitch angle.

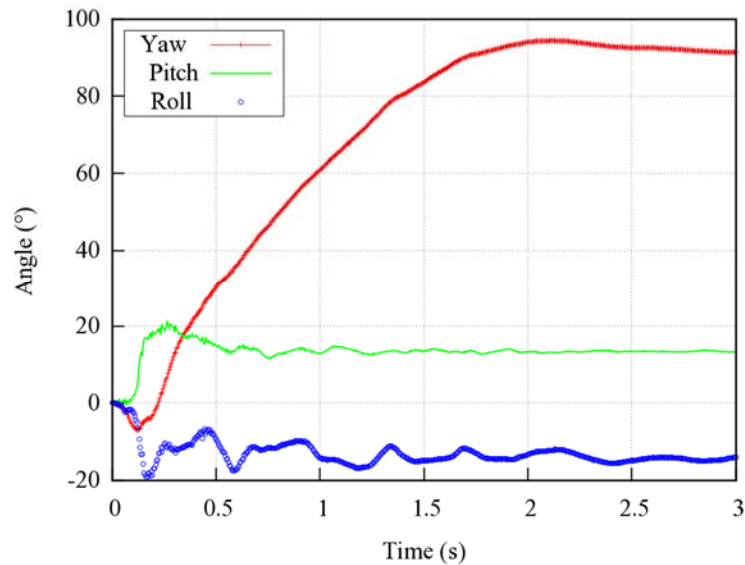


Fig. 4.65: Yaw, pitch, and roll angles of Dodge Neon impacting the front-side of the lowered backside 29-inch guardrail on a 2.5H:1V slope at 62 mph (100 km/hour) and 25°.

Figure 4.66 shows the maximum dynamic deflection of the 29-inch lowered backside double-faced guardrail impacted by the Dodge Neon from the front-side at 62 mph (100 km/hour) and 25°. The maximum dynamic deflection of the guardrail in this case was 2 ft (0.61 m) measured on the impacted rail. Compared to the 29-inch double-faced guardrail in Case 2 (see Fig. 4.26), the 29-inch lowered backside double-faced guardrail had similar maximum dynamic deflection under the impact of the Dodge Neon. The guardrail had very small engagement with the vehicle's bumper cover and fender. The Dodge Neon intruded under the rail, engaged with the rail on the hood, and dragged the rail forward, resulting in a localized transverse deflection of the guardrail.

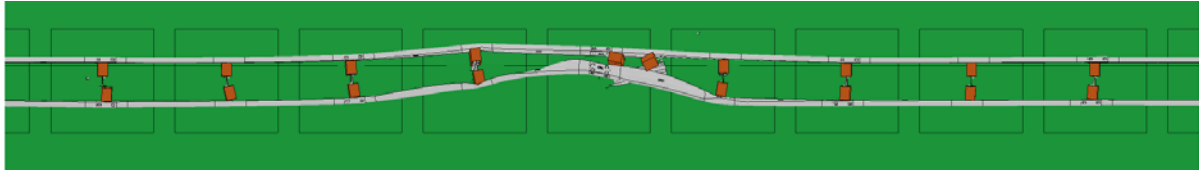


Fig. 4.66: Maximum dynamic deflection of the front-side of the lowered backside 29-inch guardrail on a 2.5H:1V slope at 62 mph (100 km/hour) and 25° and impacted by a Dodge Neon.

Figure 4.67 shows the detailed views of vehicle-barrier interactions while the Dodge Neon impacts the front-side rail of the 29-inch lowered backside double-faced guardrail at 62 mph (100 km/hour) and 25°. In this impact, due to the vehicle's low front profile, the rail of the 29-inch guardrail did not have much engagement with the vehicle's bumper cover and wheel fender. Therefore, the vehicle intruded under the guardrail, engaged with the guardrail on its hood, and snagged on a post, resulting in vehicle spin-out with a large exit angle.

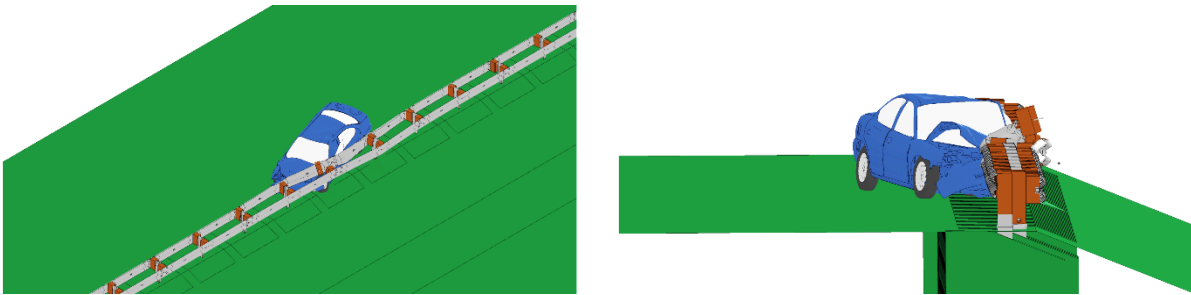


Fig. 4.67: Simulations of the Dodge Neon impacting the front-side of the lowered backside 29-inch guardrail on a 2.5H:1V slope at 62 mph (100 km/hour) and 25°.

Figure 4.68 shows the time histories of transverse displacements and velocities measured at the CG point of the Dodge Neon impacting the front-side rail of the 29-inch lowered backside double-faced guardrail. For this impact, the transverse velocity of the vehicle was approximately 4 mph (1.8 m/s), indicating a small chance of further displacement towards the travel lane. In this case, since the vehicle disengaged from the guardrail with a continuous spin and a large exit angle, there is the probability the vehicle would enter the travel lane and be involved in a secondary collision.

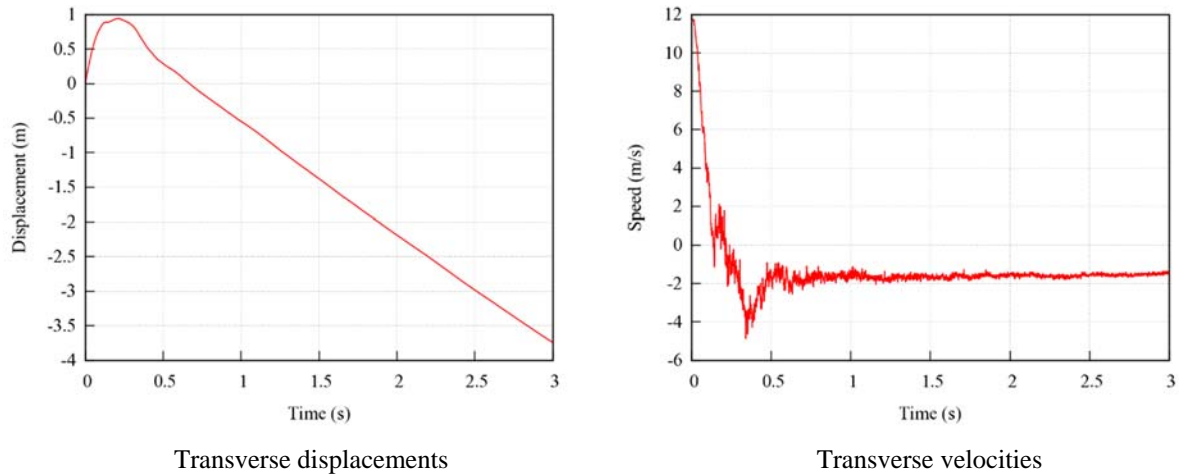


Fig. 4.68: Transverse displacements and velocities of the Dodge Neon impacting the front-side of the lowered backside 29-inch guardrail on a 2.5H:1V slope at 62 mph (100 km/hour) and 25°.

Figure 4.69 shows the top view vehicle trajectory of the Ford F250 impacting the front-side rail of the 29-inch lowered backside double-faced guardrail at 62mph (100 km/hour) and 25°. The W-beam guardrail, placed on a 2.5H:1V slope, is shown in its original undeformed shape along with the exit-box shown by the yellow dotted rectangle. Upon impacting the guardrail, the vehicle experienced spin-out caused by tire snagging on a guardrail post. The vehicle then rotated around the guardrail post and disengaged from the guardrail with a large exit angle and failed to meet the MASH exit-box criterion.

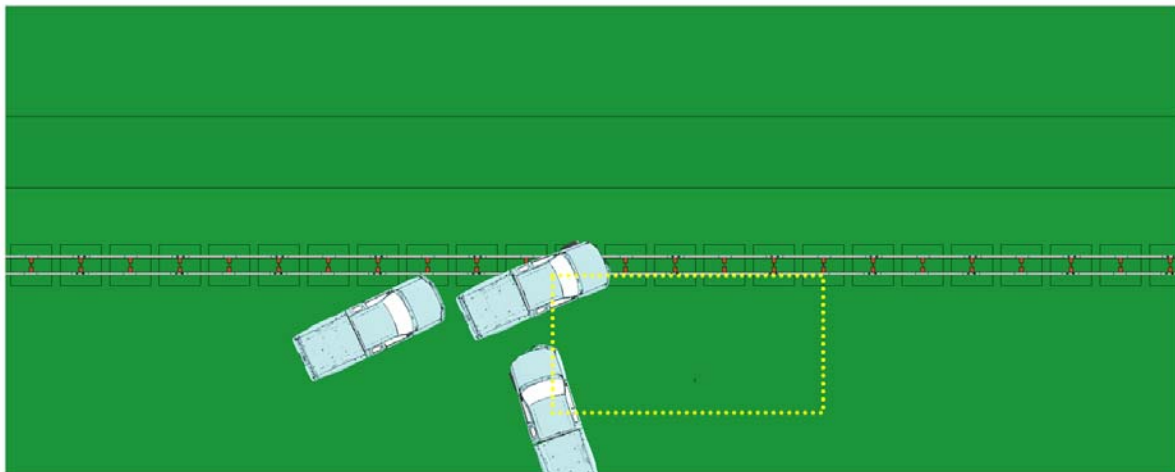


Fig. 4.69: A Ford F250 impacting the front-side of the lowered backside 29-inch guardrail on a 2.5H:1V slope at 62 mph (100 km/hour) and 25°.

The yaw, pitch, and roll angles of the Ford F250 impacting the front-side rail of the 29-inch lowered backside double-faced guardrail is shown in Fig. 4.70. The exit angle was determined to be 55° by adding the 25° impact angle to the yaw angle at exit (i.e., 30°). The steadily increasing positive yaw angle indicates a counter-clockwise rotation of the vehicle away from the guardrail. The roll and pitch angles in this impact was less than ten degrees in either positive or negative direction and thus passed the MASH evaluation criterion *F*.

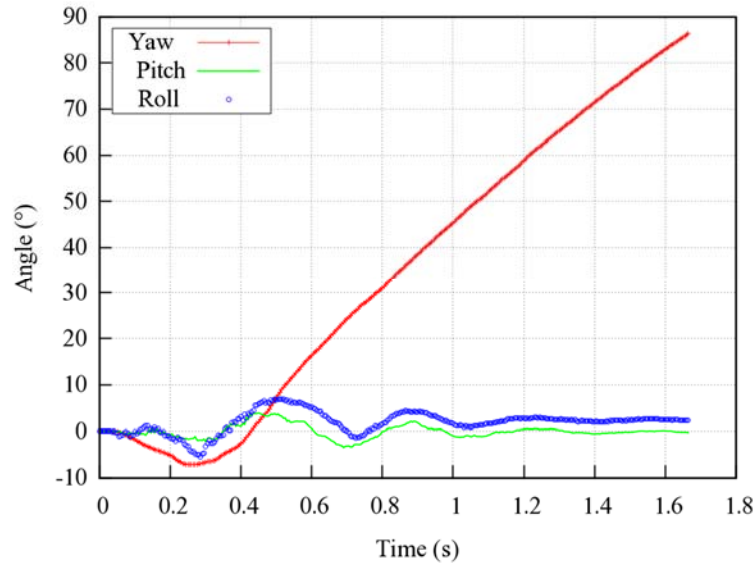


Fig. 4.70: Yaw, pitch, and roll angles of Ford F250 impacting the front-side of the lowered backside 29-inch guardrail on a 2.5H:1V slope at 62 mph (100 km/hour) and 25°.

Figure 4.71 shows the maximum dynamic deflection of the 29-inch lowered backside double-faced guardrail impacted by the Ford F250 at 62 mph (100 km/hour) and 25°. The maximum dynamic deflection of the guardrail in this case was 3.51 ft (1.07 m) on the impacted rail. The visual damage to both rails of the double-faced guardrail was more severe than the previous simulations in this study. The guardrail had a much longer damaged section in this case. It can be seen from Fig. 4.72 that the vehicle had a good interaction with the guardrail but later experienced tire snagging and vehicle spin-out.

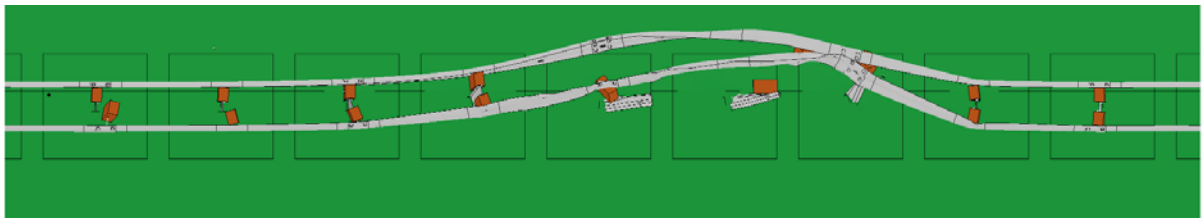


Fig. 4.71: Maximum dynamic deflection of the front-side of the lowered backside 29-inch guardrail on a 2.5H:1V slope at 62 mph (100 km/hour) and 25° and impacted by a Ford F250.

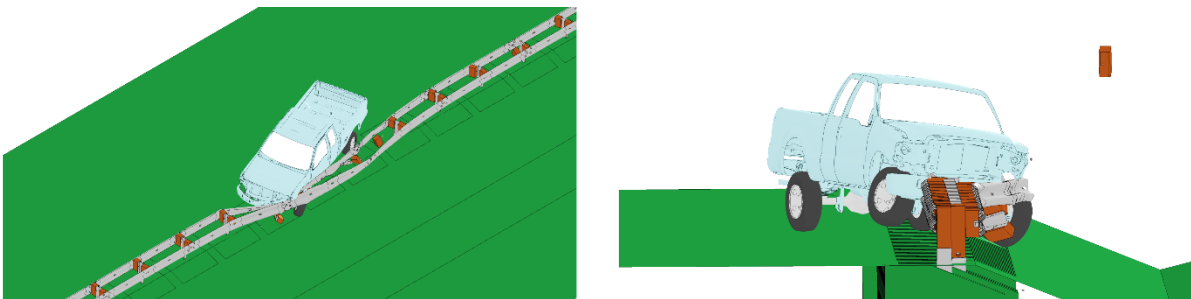


Fig. 4.72: Simulations of Ford F250 impacting the front-side of the lowered backside 29-inch guardrail on a 2.5H:1V slope at 62 mph (100 km/hour) and 25°.

Figure 4.73 shows the time histories of transverse displacements and velocities measured at the CG point of the Ford F250 impacting the front-side rail of the 29-inch lowered backside double-faced guardrail. The transverse velocity of the vehicle was approximately 9 mph (4 m/s) towards the travel lane. Considering the large exit angle, and post-impact transverse velocity, the Ford F250 would have a relatively high chance of causing a secondary collision.

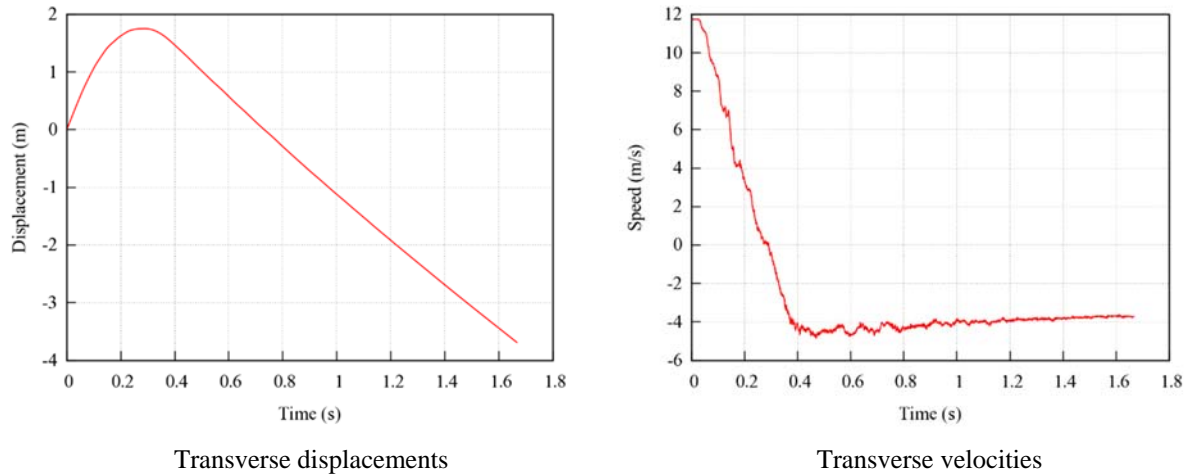


Fig. 4.73: Transverse displacements and velocities of the Ford F250 impacting the front-side of the lowered backside 29-inch guardrail on a 2.5H:1V slope at 62 mph (100 km/hour) and 25°.

4.3.2 The 31-inch Double-faced Guardrail with a Lowered Backside Rail – Front-side Impact

Figure 4.74 shows the top view vehicle trajectory of the Dodge Neon impacting the front-side rail of the 31-inch lowered backside double-faced guardrail at 62 mph (100 km/hour) and 25°. The W-beam guardrail, placed on a 2.5H:1V slope, is shown in its original undeformed shape and the exit-box is shown by the yellow dotted rectangle. Due to the vehicle’s low profile and the higher guardrail height, upon impacting the guardrail, the vehicle under-rode the rail and experienced tire snagging on a guardrail post followed by vehicle spin-out with a large exit angle, failing to meet the MASH exit-box criterion.

The yaw, pitch, and roll angles of the Dodge Neon impacting the front-side rail of the 29-inch lowered backside double-faced guardrail is shown in Fig. 4.75. The exit angle was determined to be 94° by adding the 25° impact angle to the yaw angle at exit (i.e., 69°). The steadily increasing positive yaw angle indicates a counter-clockwise rotation of the vehicle away from the guardrail. The roll and pitch angles in this impact was less than thirty degrees in either positive or negative direction and thus passed the MASH evaluation criterion *F*.

The maximum dynamic deflection of the 31-inch lowered backside double-faced guardrail impacted by the Dodge Neon is shown in Fig. 4.76. The maximum dynamic deflection in this case was 2.23 ft (0.68 m) on the impacted rail. At the 31-inch rail height, the guardrail had very small engagement with the vehicle’s bumper cover and fender, instead the majority of the impact occurred with the vehicle’s hood. The Dodge Neon intruded under the rail, engaged with the rail on its hood, and dragged the rail forward, resulting in a relatively small and localized deflection of the guardrail.

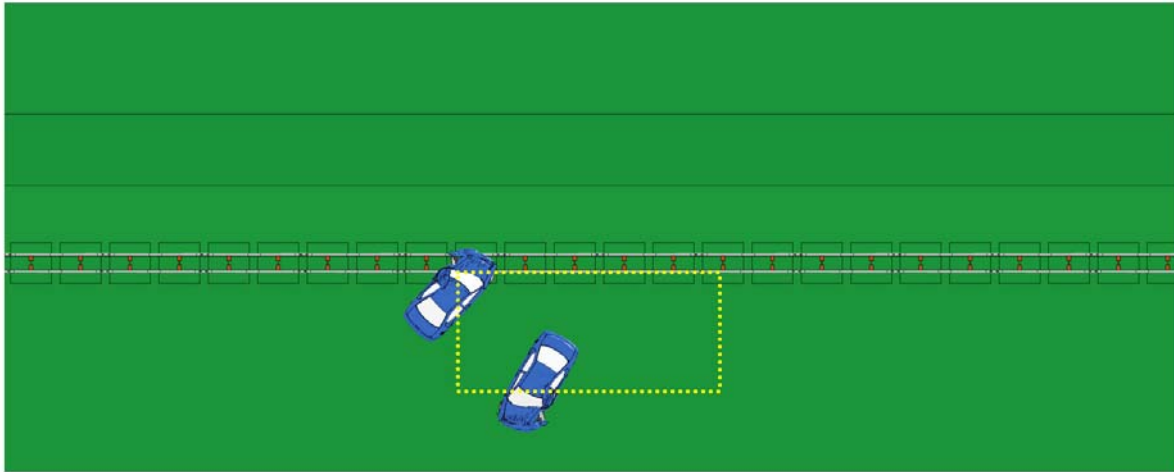


Fig. 4.74: A Dodge Neon impacting the front-side of the lowered backside 31-inch guardrail on a 2.5H:1V slope at 62 mph (100 km/hour) and 25°.

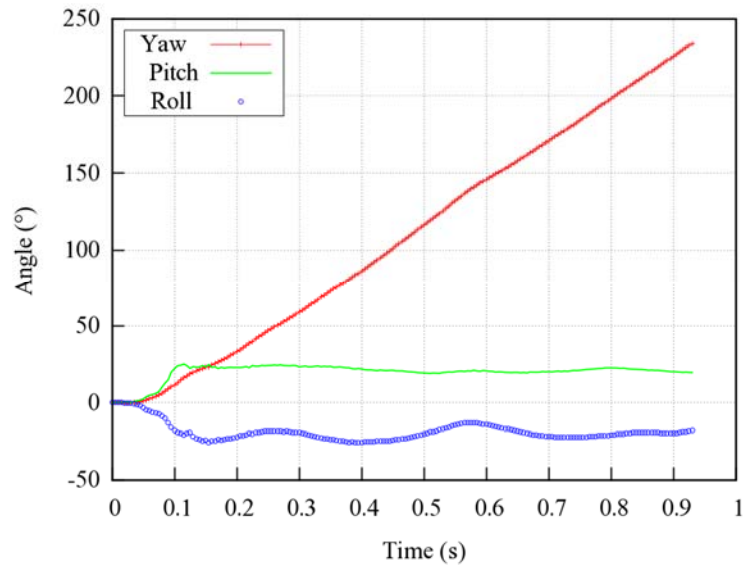


Fig. 4.75: Yaw, pitch, and roll angles of Dodge Neon impacting the front-side of the lowered backside 31-inch guardrail on a 2.5H:1V slope at 62 mph (100 km/hour) and 25°.

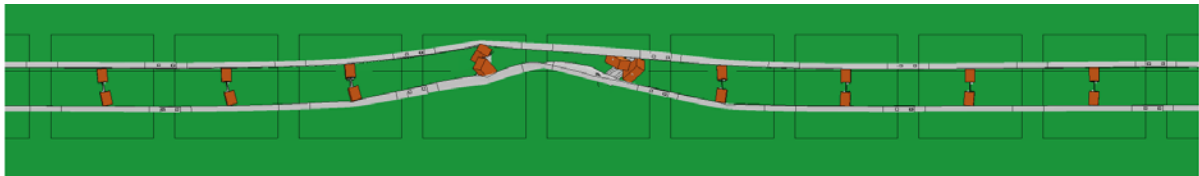


Fig. 4.76: Maximum dynamic deflection of the front-side of the lowered backside 31-inch guardrail on a 2.5H:1V slope at 62 mph (100 km/hour) and 25° and impacted by a Dodge Neon.

Figure 4.77 shows the detailed views of vehicle-barrier interactions with the Dodge Neon impacting the front-side rail of the lowered backside 31-inch double-faced guardrail. In this

impact, due to the vehicle's low front profile, the vehicle did not engage the guardrail on its bumper cover and wheel fender. Therefore, the vehicle intruded under the guardrail and snagged on a post, resulting in vehicle spin-out towards the traffic lane.

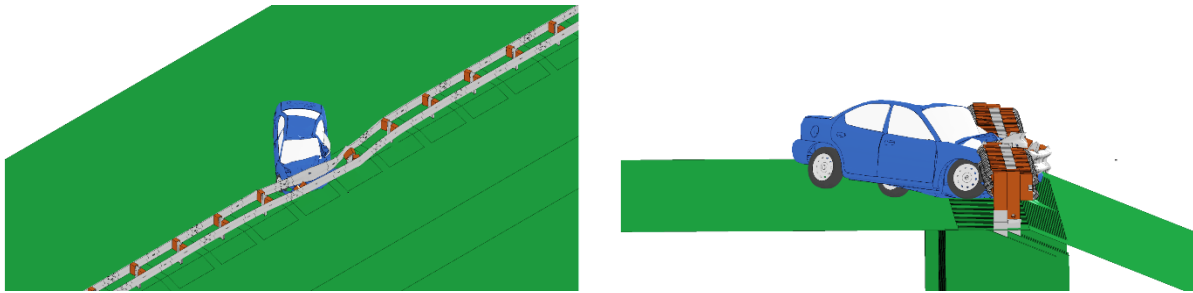


Fig. 4.77: Simulations of Dodge Neon impacting the front-side of the lowered backside 31-inch guardrail on a 2.5H:1V slope at 62 mph (100 km/hour) and 25°.

Figure 4.78 shows the time histories of transverse displacements and velocities measured at the CG point of the Dodge Neon impacting the front-side rail of the 31-inch lowered backside double-faced guardrail. The transverse velocity of the vehicle was approximately 14 mph (6.7 m/s) while spinning away from the guardrail, indicating a high probability of traversing back towards the travel lane and causing a secondary collision.

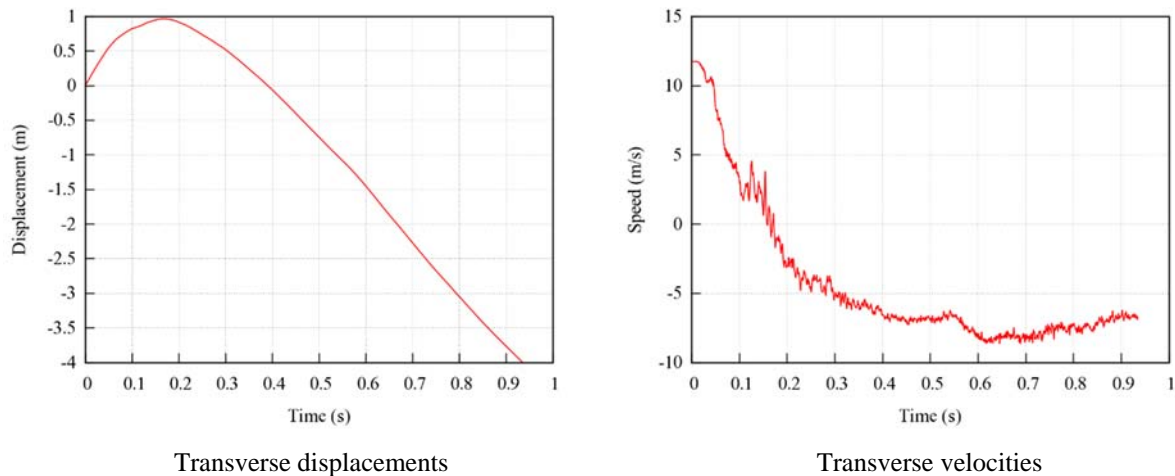


Fig. 4.78: Transverse displacements and velocities of the Dodge Neon impacting the front-side of the lowered backside 31-inch guardrail on a 2.5H:1V slope at 62 mph (100 km/hour) and 25°.

Figure 4.79 shows the top view vehicle trajectory of the Ford F250 impacting the lowered backside 31-inch double-faced guardrail from front-side at 62mph (100 km/hour) and 25°. The W-beam guardrail, placed on a 2.5H:1V slope, is shown in its original undeformed shape along with the exit-box shown by the yellow dotted rectangle. Upon impacting the guardrail, the vehicle experienced tire snagging on a guardrail post and then rotated around the guardrail post, resulting in a spin-out and disengaging from the guardrail with a large exit angle and failed to meet the MASH exit-box criterion.

The yaw, pitch, and roll angles of the Ford F250 in this front-side impact on the lowered backside 31-inch double-faced guardrail is shown in Fig. 4.80. The exit angle was determined to be 67° by adding the 25° impact angle to the yaw angle at exit (i.e., 42°). The steadily increasing yaw angle indicates a counter-clockwise rotation of the vehicle away from the guardrail. The roll and pitch angles in this impact was less than ten degrees in either positive or negative direction and thus passed the MASH evaluation criterion F , which specified a maximum 75° roll or pitch angle.

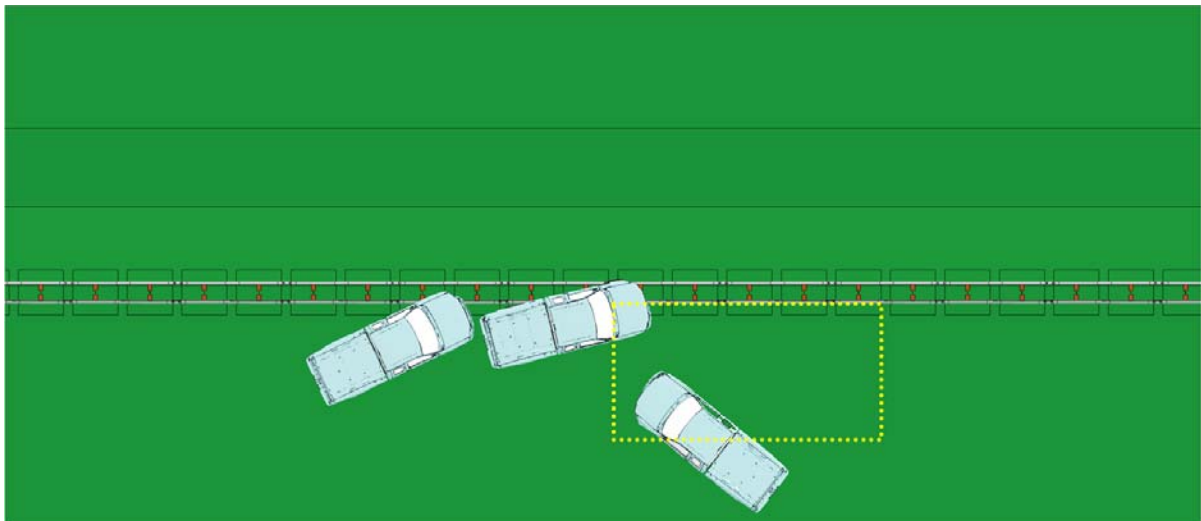


Fig. 4.79: A Ford F250 impacting the front-side of the lowered backside 31-inch guardrail on a 2.5H:1V slope at 62 mph (100 km/hour) and 25° .

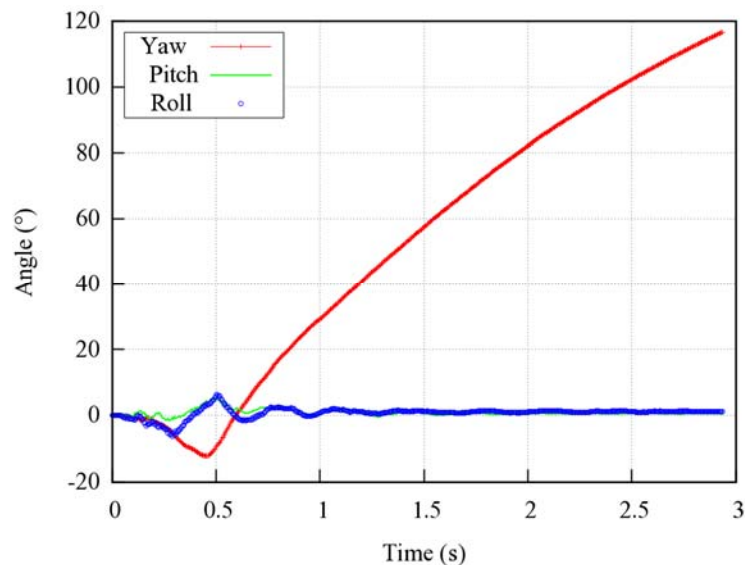


Fig. 4.80: Yaw, pitch, and roll angles of Ford F250 impacting the front-side of the lowered backside 31-inch guardrail on a 2.5H:1V slope at 62 mph (100 km/hour) and 25° .

Figure 4.81 shows the maximum dynamic deflection of the front-side rail on the lowered backside 31-inch double-faced guardrail impacted by the Ford F250 at 62 mph (100

km/hour) and 25° . The maximum dynamic deflection of the guardrail in this case was 3.9 ft (1.19 m) on the impacted rail. The visual damage to both rails of the double-faced guardrail was more severe in this simulation as compared to the 29-inch double-faced guardrail impacted by the Ford F250. The 31-inch guardrail had a relatively large section of damaged rails, posts and wood blockouts. The vehicle had good initial interaction with the guardrail but later experienced tire snagging, as can be seen from the detailed view of vehicle-guardrail interaction shown in Fig. 4.82.

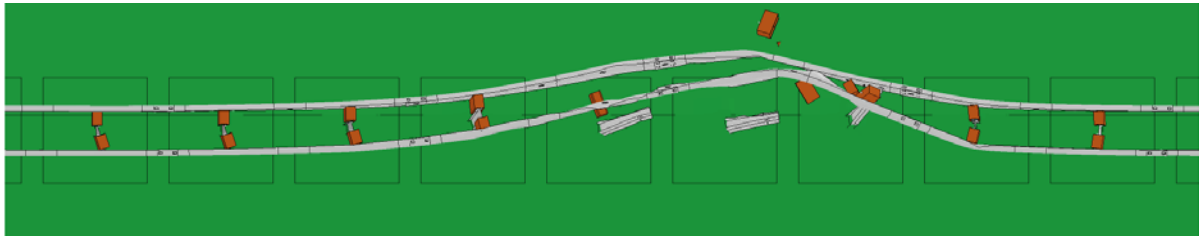


Fig. 4.81: Maximum dynamic deflection of the front-side of the lowered backside 31-inch guardrail on a 2.5H:1V slope at 62 mph (100 km/hour) and 25° and impacted by a Ford F250.

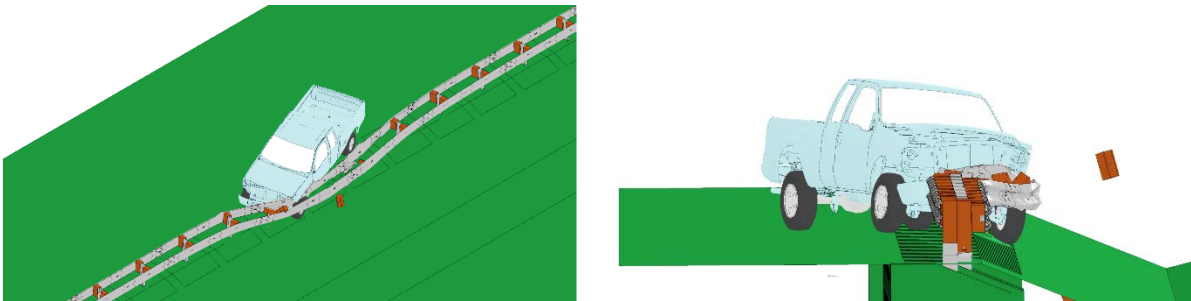


Fig. 4.82: Simulations of Ford F250 impacting the front-side of the lowered backside 31-inch guardrail on a 2.5H:1V slope at 62 mph (100 km/hour) and 25° .

Figure 4.83 shows the time histories of transverse displacements and velocities measured at the CG point of the Ford F250 impacting the lowered backside 31-inch double-faced guardrail. The transverse velocity of the vehicle was approximately 2 mph (0.9 m/s) while spinning away from the guardrail, indicating a low probability of further displacement towards the travel lane. Considering the failed exit-box criterion, high exit angle, but relatively low transverse velocity, the Ford F250 would have a relatively small chance of causing a secondary collision as the vehicle travels towards the travel lane.

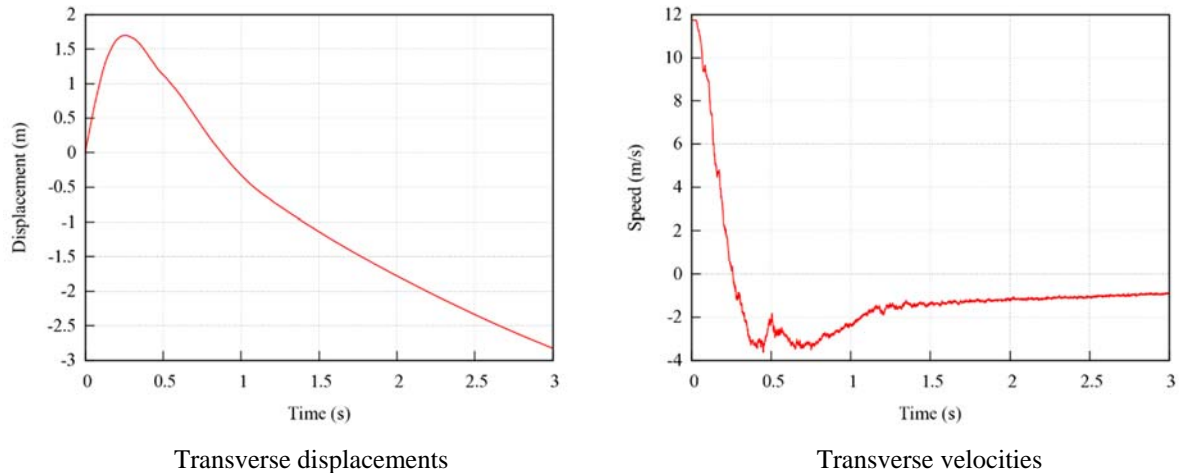


Fig. 4.83: Transverse displacements and velocities of the Ford F250 impacting the front-side of the lowered backside 31-inch guardrail on a 2.5H:1V slope at 62 mph (100 km/hour) and 25°.

4.3.3 The 29-inch Double-faced Guardrail with a Lowered Backside Rail – Backside Impact

In these simulations, the vehicle was placed on the shoulder next to a 4H:1V slope of the median and started traversing through both median slopes before impacting the backside rail of the lowered backside 29-inch double-faced guardrail. Figure 4.84 shows the top view vehicle trajectory of the Dodge Neon impacting backside rail of the 29-inch double-faced guardrail at 62 mph (100 km/hour) and 25°. The W-beam guardrail, placed on a 2.5H:1V slope, is shown in its original undeformed shape. Upon impacting the guardrail, the Dodge Neon failed to remain upright and flipped over towards the median ditch. Since the vehicle flipped, the MASH exit-box criterion was not used. The vehicle overturning in this scenario can be attributed to the vehicles compressed and expanding suspension while traversing the sloped median before impacting the lowered backside rail.

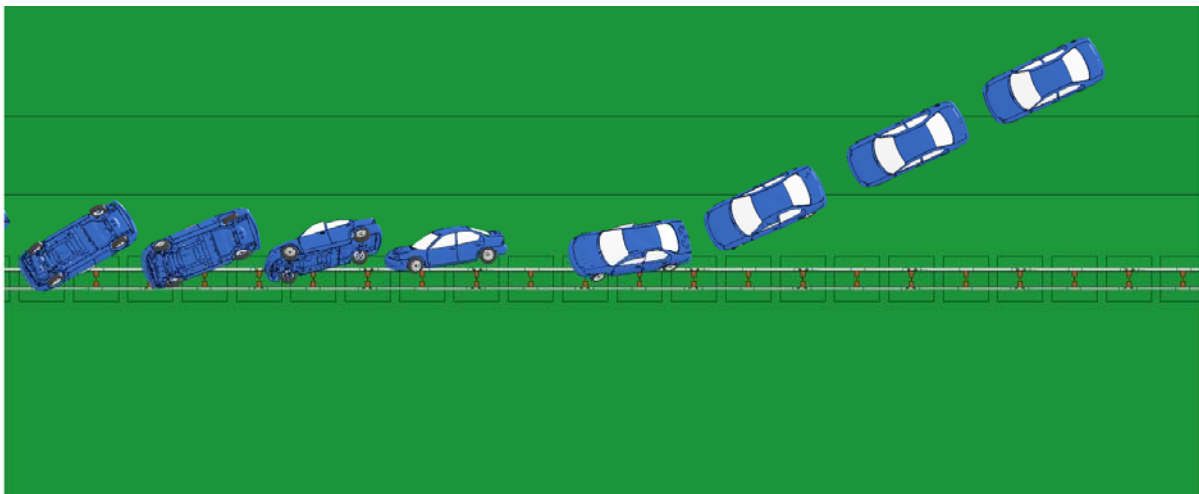


Fig. 4.84: A Dodge Neon impacting the backside of the lowered backside 29-inch guardrail on a 2.5H:1V slope at 62 mph (100 km/hour) and 25°.

The yaw, pitch, and roll angles of the Dodge Neon impacting the lowered backside rail of the 29-inch double-faced guardrail is shown in Fig. 4.85. Due to the vehicle's flipping over after impacting the guardrail, no exit angle was calculated in this scenario. The roll angle in this simulation also failed the MASH evaluation criterion F , which specified a maximum 75° roll or pitch angle.

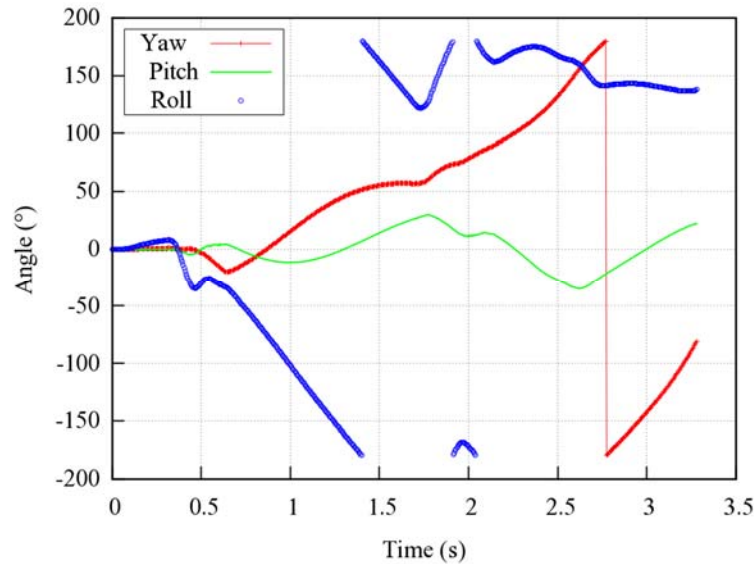


Fig. 4.85: Yaw, pitch, and roll angles of Dodge Neon impacting the backside of the lowered backside 29-inch guardrail on a 2.5H:1V slope at 62 mph (100 km/hour) and 25°.

The maximum dynamic deflection of the 29-inch double-faced guardrail impacted by the Dodge Neon at 62 mph (100 km/hour) and 25° is shown in Fig. 4.86. The maximum dynamic deflection of the guardrail in this case was 1.05 ft (0.32 m) on the impacted rail. The guardrail had very small engagement with the vehicle's bumper cover and fender, instead, the vehicle rode up the face of the guardrail, resulting in a small maximum dynamic deflection and localized rail deformation.



Fig. 4.86: Maximum dynamic deflection of the backside of the lowered backside 29-inch guardrail on a 2.5H:1V slope at 62 mph (100 km/hour) and 25° and impacted by a Dodge Neon.

Figure 4.87 shows the detailed views of vehicle-barrier interactions while the Dodge Neon impacts the lowered backside rail of the 29-inch double-faced guardrail. In this impact, due to the compression and expansion of suspension while traversing the median, the vehicle became airborne after impact. The backside rail of the 29-inch guardrail did not have much engagement with the vehicle's bumper cover and wheel fender. Instead, the vehicle rode up the face of the guardrail and flipped around the long axis of the vehicle.



Fig. 4.87: Simulations of the Dodge Neon impacting the backside of the lowered backside 29-inch guardrail on a 2.5H:1V slope at 62 mph (100 km/hour) and 25°.

Figure 4.88 shows the time histories of transverse displacements and velocities measured at the CG point of the Dodge Neon impacting the lowered backside rail of the 29-inch double-faced guardrail. The transverse velocity of the vehicle was approximately 7 mph (3 m/s) while failing to remain upright. In this case, although the vehicle flipped over, the guardrail was able to retain the vehicle on the impacting side of the guardrail and eliminate the possibility of penetrating into oncoming travel lanes. The results in Figs. 4.84 to 4.88 indicated that the lowered backside rail of the 29-inch double-faced guardrail placed on a 2.5H:1V slope exhibit the potential for vehicle roll-over with a small sedan sized vehicle impacting the guardrail at 62 mph (100 km/hour) and 25°.

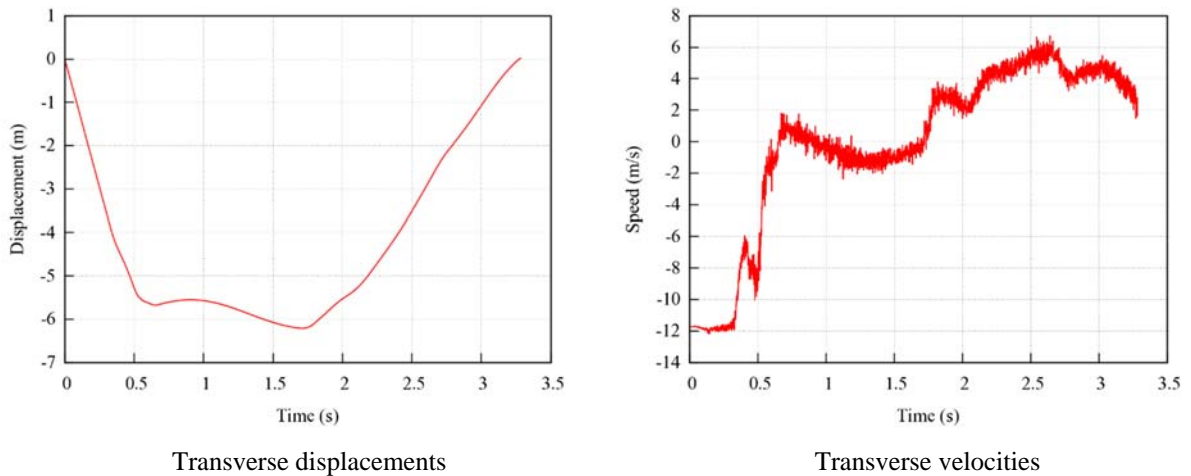


Fig. 4.88: Transverse displacements and velocities of the Dodge Neon impacting the backside of the lowered backside 29-inch guardrail on a 2.5H:1V slope at 62 mph (100 km/hour) and 25°.

Figure 4.89 shows the top view vehicle trajectory of the Ford F250 impacting the 29-inch double-faced guardrail from the backside at 62 mph (100 km/hour) and 25°. The W-beam guardrail, placed on a 2.5H:1V slope, is shown in its original undeformed shape. Upon impacting the lowered backside rail of the 29-inch double-faced guardrail, the Ford F250 failed to remain upright and flipped over after impacting the rail. Since the vehicle flipped, the MASH exit-box criterion was not used. The vehicle overturning in this scenario can be attributed to the vehicles compressed and expanding suspension while traversing the sloped median before impacting the lowered backside guardrail.

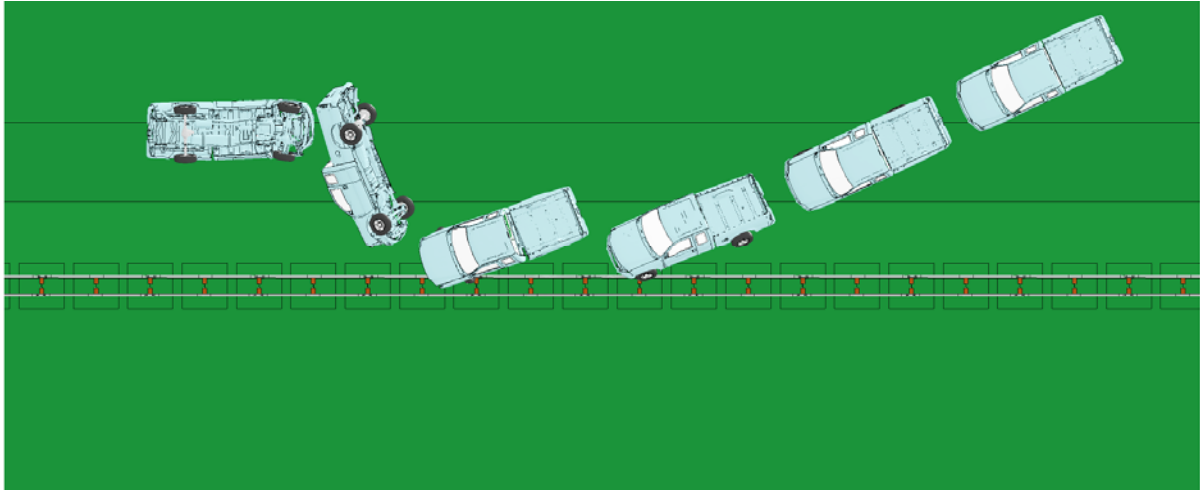


Fig. 4.89: A Ford F250 impacting the backside of the lowered backside 29-inch guardrail on a 2.5H:1V slope at 62 mph (100 km/hour) and 25°.

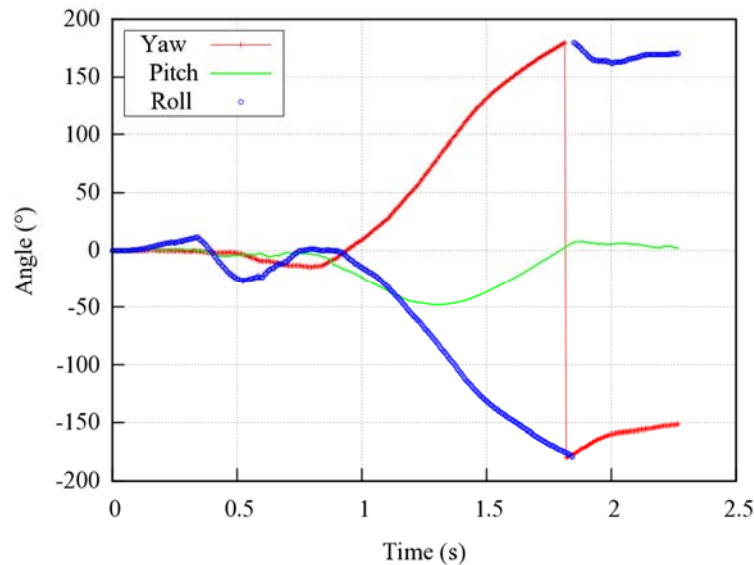


Fig. 4.90: Yaw, pitch, and roll angles of Ford F250 impacting the backside of the lowered backside 29-inch guardrail on a 2.5H:1V slope at 62 mph (100 km/hour) and 25°.

The yaw, pitch, and roll angles of the Ford F250 impacting the 29-inch double-faced guardrail is shown in Fig. 4.90. Due to the vehicle flipping over after impacting the guardrail, no exit angle was calculated in this scenario. The roll angle in this simulation also failed the MASH evaluation criterion F , which specified a maximum 75° roll or pitch angle.

The maximum dynamic deflection of the 29-inch double-faced guardrail impacted by the Ford F250 at 62 mph (100 km/hour) and 25° is shown in Fig. 4.91. The maximum dynamic deflection of the guardrail in this case was 2.76 ft (0.84 m) on the impacted rail.



Fig. 4.91: Maximum dynamic deflection of the backside of the lowered backside 29-inch guardrail on a 2.5H:1V slope at 62 mph (100 km/hour) and 25° and impacted by a Ford F250.

Figure 4.92 shows the detailed views of vehicle-barrier interactions while the Ford F250 impacts the lowered backside rail of the 29-inch double-faced guardrail. In this impact, due to the compression and expansion of the suspension while traversing through the median slopes, the vehicle became airborne after impact. The rail of the 29-inch guardrail did not have much engagement with the vehicle's bumper cover and wheel fender. Instead, vehicle's wheel was caught on a guardrail post and the roll angle began to increase steadily, resulting in vehicle flipping over around the long axis while rotating away from the guardrail.

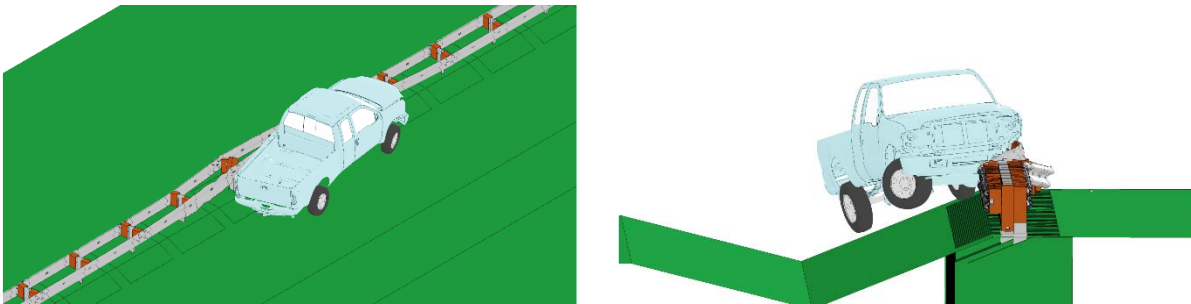


Fig. 4.92: Simulations of Ford F250 impacting the backside of the lowered backside 29-inch guardrail on a 2.5H:1V slope at 62 mph (100 km/hour) and 25°.

Figure 4.93 shows the time histories of transverse displacements and velocities measured at the CG point of the Ford F250 impacting the 29-inch double-faced guardrail from the backside. The transverse velocity of the vehicle was approximately zero after failing to remain upright. In this case, although the vehicle flipped over, the guardrail was able to retain the vehicle on the impacting side of the guardrail and eliminate the possibility of penetrating into oncoming traffic lanes. The results in Figs. 4.89 to 4.93 indicated that the lowered backside 29-inch double-faced guardrail had a potential for causing vehicle roll-over with a pick-up truck sized vehicle impacting the guardrail at 62 mph (100 km/hour) and 25°.

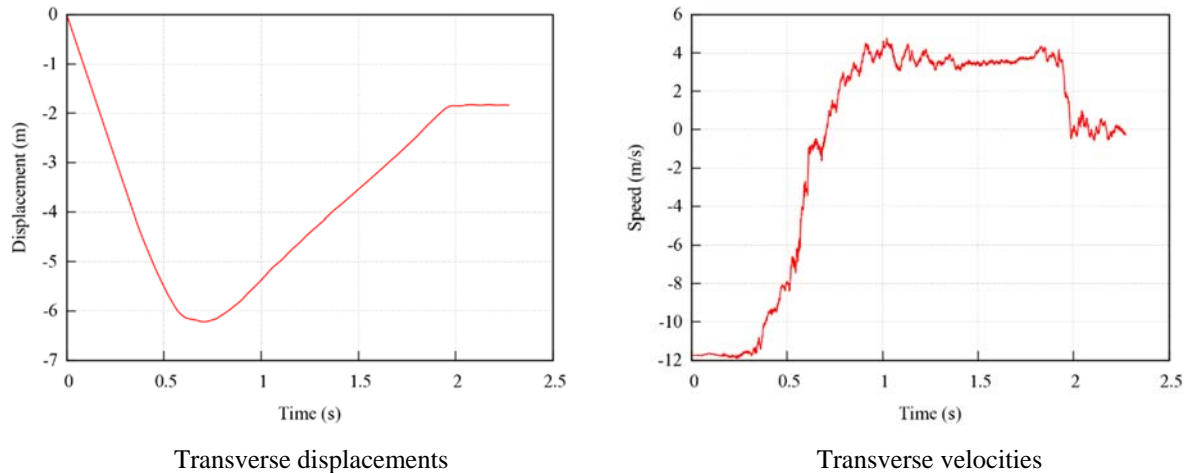


Fig. 4.93: Transverse displacements and velocities of the Ford F250 impacting the backside of the lowered 29-inch guardrail on a 2.5H:1V slope at 62 mph (100 km/hour) and 25°.

4.3.4 The 31-inch Double-faced Guardrail with a Lowered Backside Rail – Backside Impact

In these cases, the vehicle was placed on the shoulder next to a 4H:1V slope of the sloped median and started traversing through both sides of the sloped median before impacting the backside rail of the 31-inch double-faced guardrail.

Figure 4.94 shows the top view vehicle trajectory of the Dodge Neon impacting the 31-inch double-faced guardrail at 62 mph (100 km/hour) and 25°. The W-beam guardrail, placed on a 2.5H:1V slope, is shown in its original undeformed shape. Upon impacting the lowered backside rail of the 31-inch double-faced guardrail, the Dodge Neon failed to remain upright and flipped over after impacting the rail. Therefore, the MASH exit-box criterion was not used. The vehicle overturning in this case can be attributed to the vehicle’s compressed and expanding suspension while traversing the sloped median before impacting the guardrail.

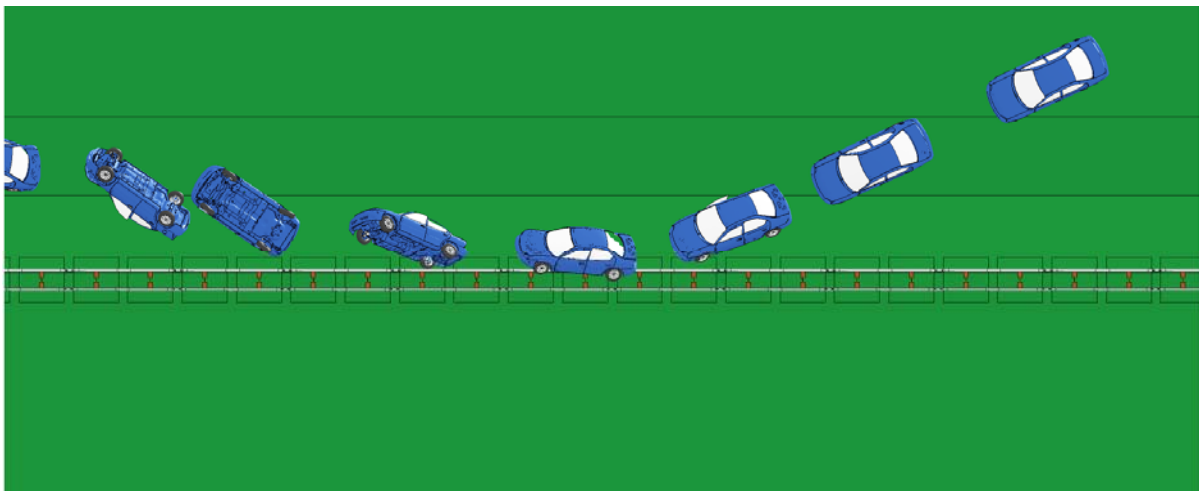


Fig. 4.94: A Dodge Neon impacting the backside of the lowered backside 31-inch guardrail on a 2.5H:1V slope at 62 mph (100 km/hour) and 25°.

The yaw, pitch, and roll angles of the Dodge Neon impacting the 31-inch double-faced guardrail is shown in Fig. 4.95. Due to the vehicle failing to remain upright after impacting the guardrail, no exit angle was calculated in this scenario. The roll angle in this simulation also failed the MASH evaluation criterion F , which specified a maximum 75° roll or pitch angle. The steadily increasing roll angle signified the vehicle’s flipping about the long axis of the vehicle (i.e., a “barrel roll”).

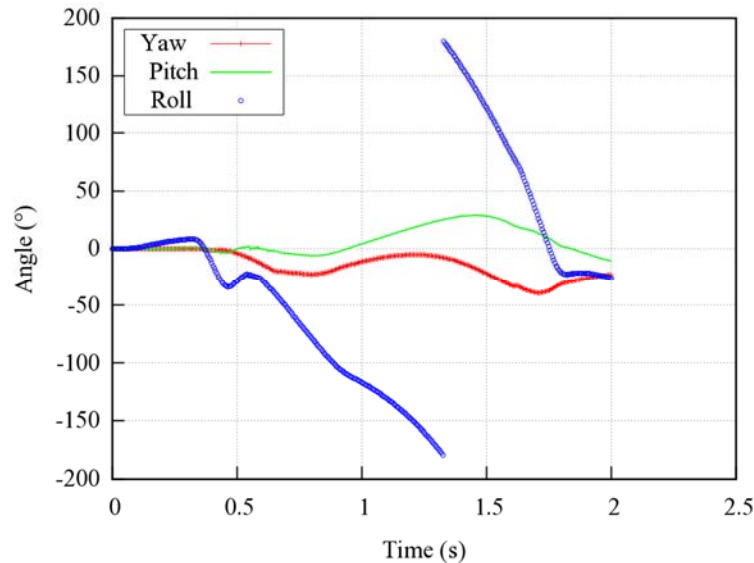


Fig. 4.95: Yaw, pitch, and roll angles of Dodge Neon impacting the backside of the lowered backside 31-inch guardrail on a 2.5H:1V slope at 62 mph (100 km/hour) and 25° .

The maximum dynamic deflection of the lowered backside rail on the 31-inch double-faced guardrail impacted by the Dodge Neon at 62 mph (100 km/hour) and 25° is shown in Fig. 4.96. The maximum dynamic deflection of the guardrail in this case was 1.38 ft (0.42 m) on the impacted rail. The guardrail had very small engagement with the vehicle’s bumper cover and fender. Instead, the vehicle’s tire rode up the face of the guardrail and launched the vehicle with a steadily increasing roll angle.



Fig. 4.96: Maximum dynamic deflection of the backside of the lowered backside 31-inch guardrail on a 2.5H:1V slope at 62 mph (100 km/hour) and 25° and impacted by a Dodge Neon.

Figure 4.97 shows the detailed views of vehicle-barrier interactions while the Dodge Neon impacts the 31-inch double-faced guardrail. In this impact, due to the compression and expansion of vehicle suspension while traversing the sloped median, the vehicle became airborne upon impacting the lowered backside rail of the 31-inch guardrail. The vehicle thus rode up the guardrail and flipped over towards the median ditch with a steadily increasing roll angle.

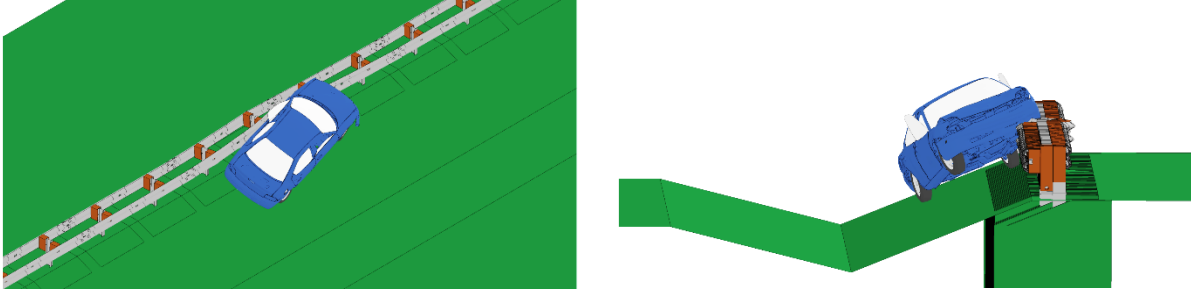


Fig. 4.97: Simulations of Dodge Neon impacting the backside of the lowered backside 31-inch guardrail on a 2.5H:1V slope at 62 mph (100 km/hour) and 25°.

Figure 4.98 shows the time histories of transverse displacements and velocities measured at the CG point of the Dodge Neon impacting the lowered backside rail of the 31-inch double-faced guardrail. The transverse velocity of the vehicle was approximately 2 mph (0.9 m/s) after failing to remain upright. In this case, although the vehicle flipped over, the guardrail was able to retain the vehicle on the impacting side of the guardrail and eliminated the possibility of penetrating into the oncoming travel lanes. The results in Figs. 4.94 to 4.98 indicated that the lowered backside rail of the 31-inch double-faced guardrail placed on a 2.5H:1V slope exhibited the potential for vehicle roll-over with a small sedan sized vehicle impacting the guardrail at 62 mph (100 km/hour) and 25°.

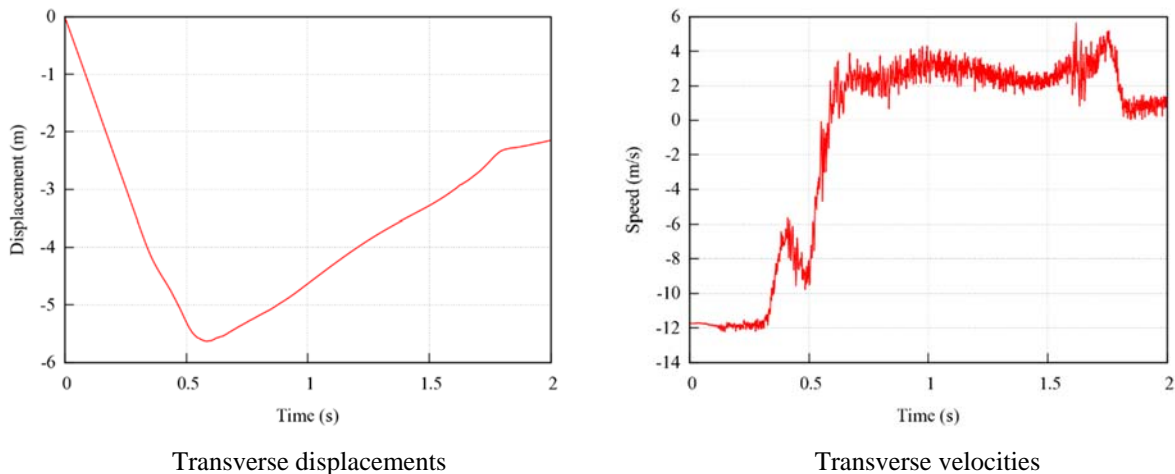


Fig. 4.98: Transverse displacements and velocities of the Dodge Neon impacting the backside of the lowered backside 31-inch guardrail on a 2.5H:1V slope at 62 mph (100 km/hour) and 25°.

Figure 4.99 shows the top view vehicle trajectory of the Ford F250 impacting the lowered backside rail of the 31-inch double-faced guardrail at 62 mph (100 km/hour) and 25°. The W-beam guardrail, placed on a 2.5H:1V slope, is shown in its original undeformed shape and the exit-box is shown by the yellow dotted rectangle. Upon impacting the lowered backside rail of the 31-inch double-faced guardrail, the Ford F250 experienced tire snagging on a guardrail post and rotated around the guardrail post, resulting in a vehicle spin-out while disengaging from the guardrail. The vehicle went out of the exitbox prematurely with a large exit angle and failed to meet the MASH exit-box criterion.

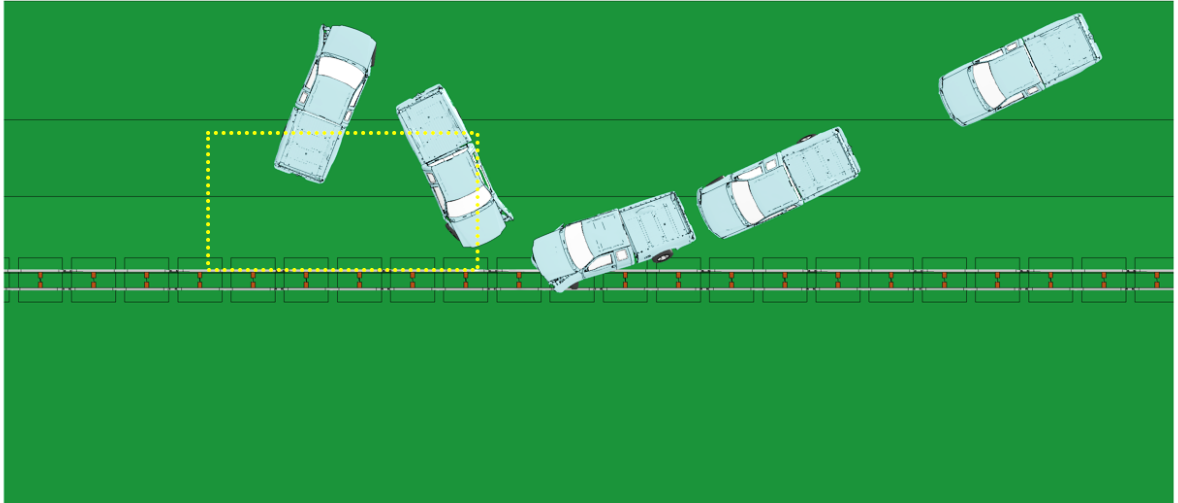


Fig. 4.99: A Ford F250 impacting the backside of the lowered backside 31-inch guardrail on a 2.5H:1V slope at 62 mph (100 km/hour) and 25°.

The yaw, pitch, and roll angles of the Ford F250 impacting the 31-inch double-faced guardrail is shown in Fig. 4.100. The exit angle was determined to be 69° by adding the 25° impact angle to the yaw angle at exit (i.e., 44°). The steadily increasing yaw angle indicates a counter-clockwise rotation of the vehicle away from the guardrail. The jump from positive to negative yaw angle at about 1.7 seconds indicates the vehicle made a complete revolution. The roll and pitch angles in this impact was less than thirty degrees in either positive or negative direction and thus passed the MASH evaluation criterion *F*.

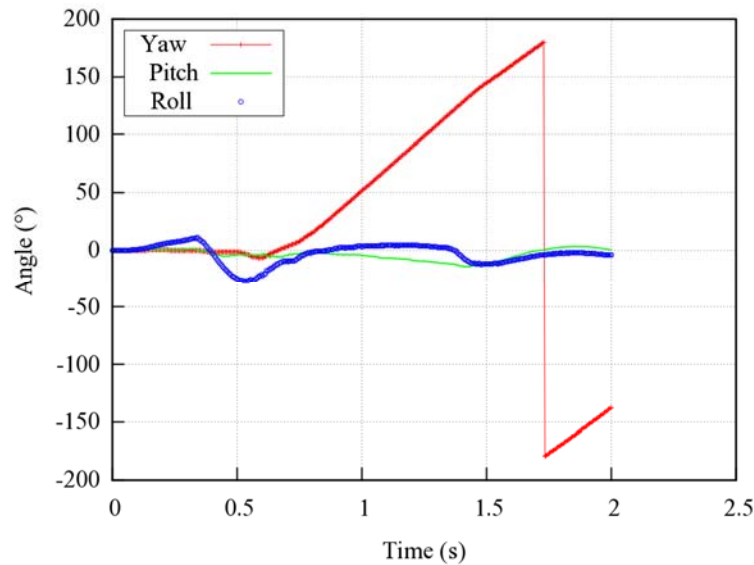


Fig. 4.100: Yaw, pitch, and roll angles of Ford F250 impacting the backside of the lowered backside 31-inch guardrail on a 2.5H:1V slope at 62 mph (100 km/hour) and 25°.

Figure 4.101 shows the maximum dynamic deflection of the 31-inch double-faced guardrail impacted by the Ford F250 at 62 mph (100 km/hour) and 25°. The maximum dynamic

deflection of the guardrail in this case was 2.99 ft (0.91 m) on the impacted rail. Figure 4.102 shows the state at which the maximum dynamic deflection occurs, the vehicle had a good initial interaction with the guardrail but later experienced tire snagging.

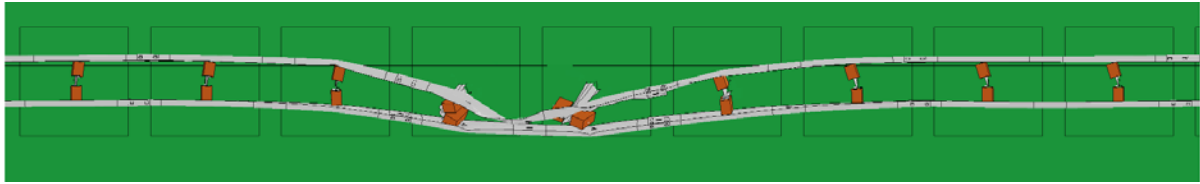


Fig. 4.101: Maximum dynamic deflection of the backside of the lowered backside 31-inch guardrail on a 2.5H:1V slope at 62 mph (100 km/hour) and 25° and impacted by a Ford F250.

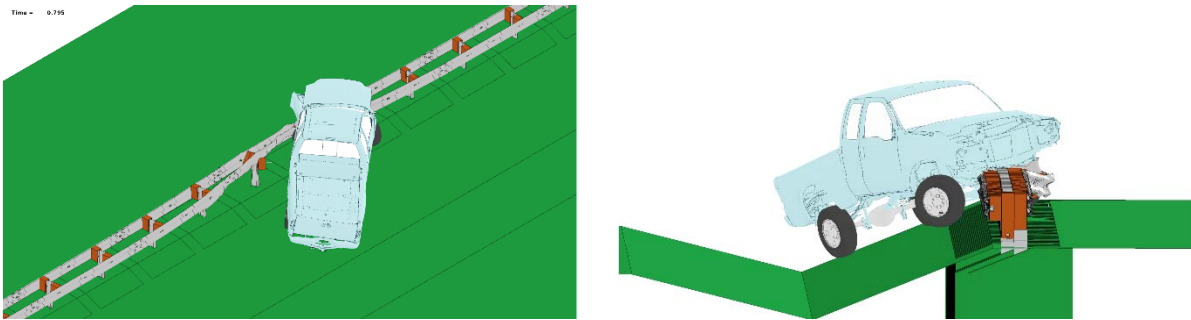


Fig. 4.102: Simulations of Ford F250 impacting the backside of the lowered backside 31-inch guardrail on a 2.5H:1V slope at 62 mph (100 km/hour) and 25°.

Figure 4.103 shows the time histories of transverse displacements and velocities measured at the CG point of the Ford F250 impacting the 31-inch double-faced guardrail. The transverse velocity of the vehicle was approximately 8 mph (3.6 m/s). Considering the moderate post-impact transverse velocity and the width of the sloped median, the Ford F250 would have a relatively small chance of getting involved in a secondary collision.

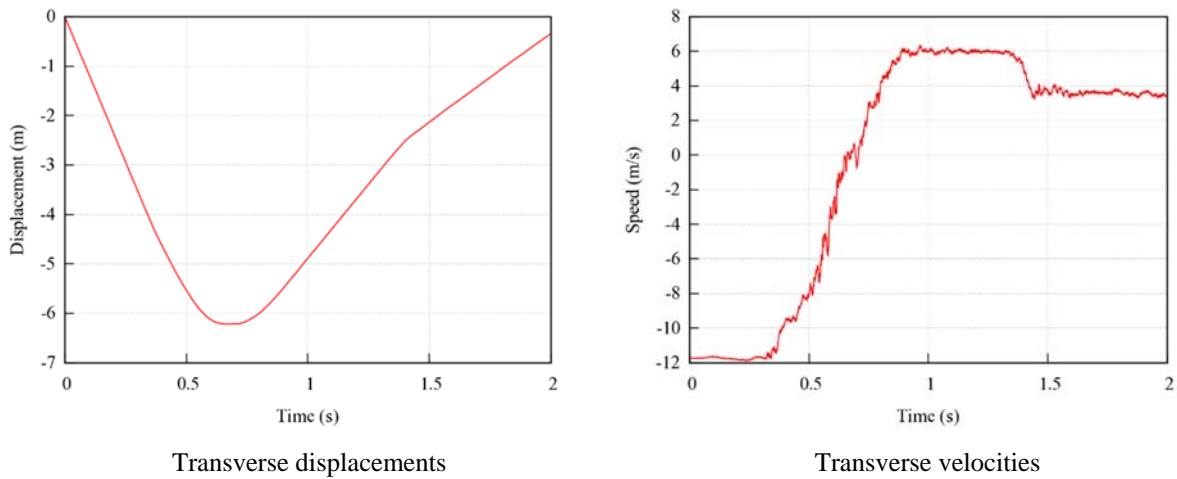


Fig. 4.103: Transverse displacements and velocities of the Ford F250 impacting the backside of the lowered backside 31-inch guardrail on a 2.5H:1V slope at 62 mph (100 km/hour) and 25°.

4.4 Case 4: Single-faced Guardrail with Convex Horizontal Curvature Placed on a 2.5H:1V Slope

In this case, the 29- and 31-inch single-faced guardrails with convex horizontal curvature were evaluated when placed on a 2.5H:1V slope and impacted by both the Dodge Neon and Ford F250. An impact speed of 62 mph (100 km/hour) and a 25° impact angle were used in all simulations in Case 4. Table 4.6 gives a summary of the simulation results that were used to evaluate guardrail performance in terms of vehicular responses.

Table 4.6: Simulation results of Case 4 (Single-faced Guardrail with Convex Horizontal Curvature Placed on a 2.5H:1V Slope)

Impact side	Guardrail Height	Test Vehicle	Simulation Results
Front-side	29 inch	Dodge Neon	The vehicle failed the exit-box criterion caused by vehicle spin-out and a large exit angle
		Ford F250	The vehicle remained in contact with guardrail due to tire snagging on guardrail post
	31 inch	Dodge Neon	The vehicle failed the exit-box criterion caused by vehicle spin-out and a large exit angle
		Ford F250	The vehicle remained in contact with guardrail due to tire snagging on guardrail post

4.4.1 The 29-inch Single-faced Guardrail with convex horizontal curvature – Front-side Impact

Figure 4.104 shows the top view vehicle trajectory of the Dodge Neon impacting the 29-inch single-faced guardrail with convex horizontal curvature at 62 mph (100 km/hour) and 25°. The W-beam guardrail, placed on a 2.5H:1V slope, is shown in its original undeformed shape and the exit-box is shown by the yellow dotted rectangle. It can be seen that the vehicle experienced tire snagging on the guardrail post, causing vehicle spin-out with a large exit angle. According to the MASH exit-box criterion, since the vehicle left the exit-box before traversing the length of the exit-box, the exit-box criterion was not met.

The yaw, pitch, and roll angles for the Dodge Neon in this impact are shown in Fig. 4.105. The exit angle was determined to be 60° by adding the 25° impact angle to the yaw angle at exit (i.e., 35°). The steadily increasing yaw angle indicates a counter-clockwise rotation of the vehicle away from the guardrail. The vehicle was not safely redirected due to the continuous spin after prematurely leaving the exit-box as indicated by the increasing yaw angle. From the time history of the yaw angle in Fig. 4.105, it can be seen that the Dodge Neon was first redirected (during the first 0.3 seconds, indicated by the negative yaw angles) and then started to rotate in the opposite direction while losing contact with the guardrail. This rotation went on even after the vehicles lost contact with the guardrail, resulting in a

large exit angle. It was observed from the simulation results that the Dodge Neon partially under-rode the guardrail and crashed directly on a post, causing pocketing and snagging on the front part of the vehicle. The roll and pitch angles were less than twenty five degrees in either positive or negative direction which passed the MASH evaluation criterion F , which specified a maximum 75° roll or pitch angle.

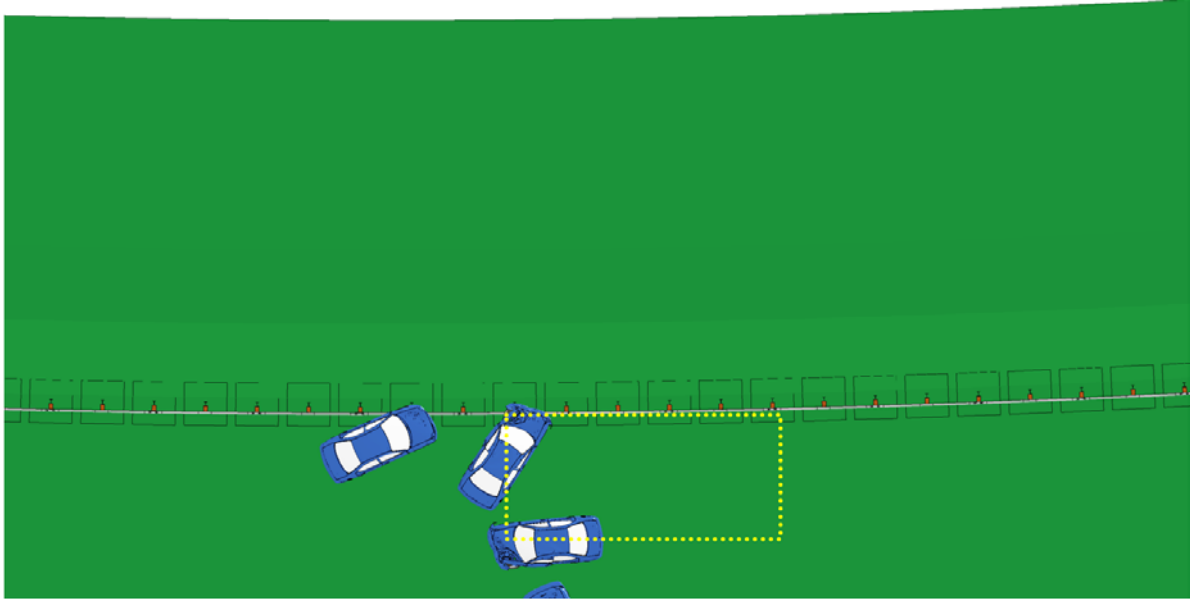


Fig. 4.104: A Dodge Neon impacting the front-side, convex horizontal curvature 29-inch guardrail on a 2.5H:1V slope at 62 mph (100 km/hour) and 25° .

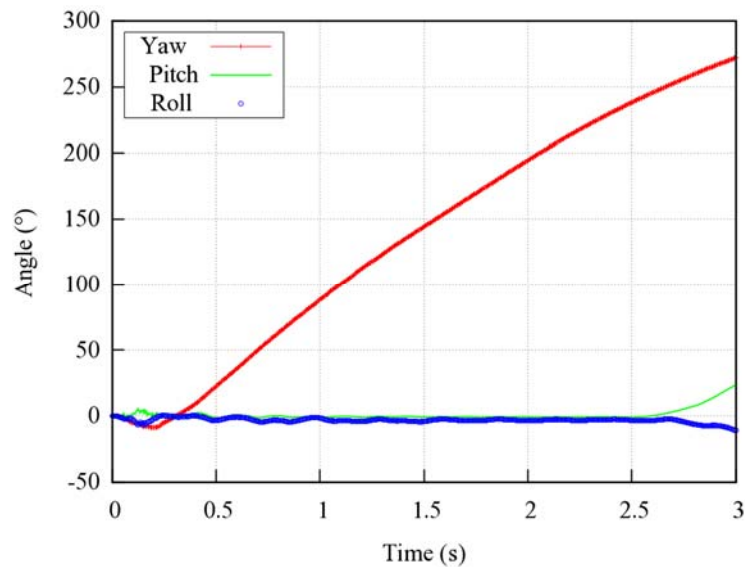


Fig. 4.105: Yaw, pitch, and roll angles of Dodge Neon impacting the front-side, convex horizontal curvature 29-inch guardrail on a 2.5H:1V slope at 62 mph (100 km/hour) and 25° .

Figure 4.106 shows the maximum dynamic deflection of the 29-inch single-faced guardrail with convex horizontal curvature impacted by the Dodge Neon at 62 mph (100 km/hour) and

25°. The maximum dynamic deflection of the guardrail in this case was 2.10 ft (0.64 m). Compared to the 29-inch single-faced guardrail without horizontal curvature impacted by the Dodge Neon (see Fig. 4.4a), the maximum dynamic deflection in this case was slightly smaller but the vehicle had a larger exit angle.

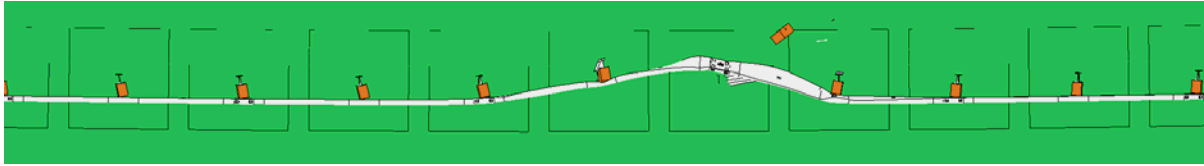


Fig. 4.106: Maximum dynamic deflection of the front-side, convex horizontal curvature 29-inch guardrail on a 2.5H:1V slope at 62 mph (100 km/hour) and 25° and impacted by a Dodge Neon.

Figure 4.107 shows the detailed views of vehicle-barrier interactions while the Dodge Neon impacts the 29-inch single-faced guardrail with convex horizontal curvature. The guardrail had very minor engagement with the vehicle's bumper cover and fender. Instead, the Dodge Neon intruded under the rail, engaged with the rail on its hood, and dragged the rail forward, resulting in a large, but localized, transverse deflection of the guardrail.



Fig. 4.107: Simulations of Dodge Neon impacting the front-side, convex horizontal curvature 29-inch guardrail on a 2.5H:1V slope at 62 mph (100 km/hour) and 25°.

Figure 4.108 shows the time histories of transverse displacements and velocities measured at the CG point of the Dodge Neon impacting the 29-inch single-faced guardrail with convex horizontal curvature at 62 mph (100 km/hour) and 25°. The transverse velocity of the vehicle after impacting the guardrail was approximately 5 mph (2.2 m/s) towards the travel lane. In this case, since the vehicle was snagged on the guardrail and spun around a post before losing contact with the guardrail, it had with a large exit angle and was likely to be involved in a secondary collision. The results in Figs. 4.104 to 4.108 indicated that the 29-inch guardrail with convex horizontal curvature placed on a 2.5H:1V slope could prevent a small car from penetration but the vehicle would have a small probability of being involved in a secondary collision.

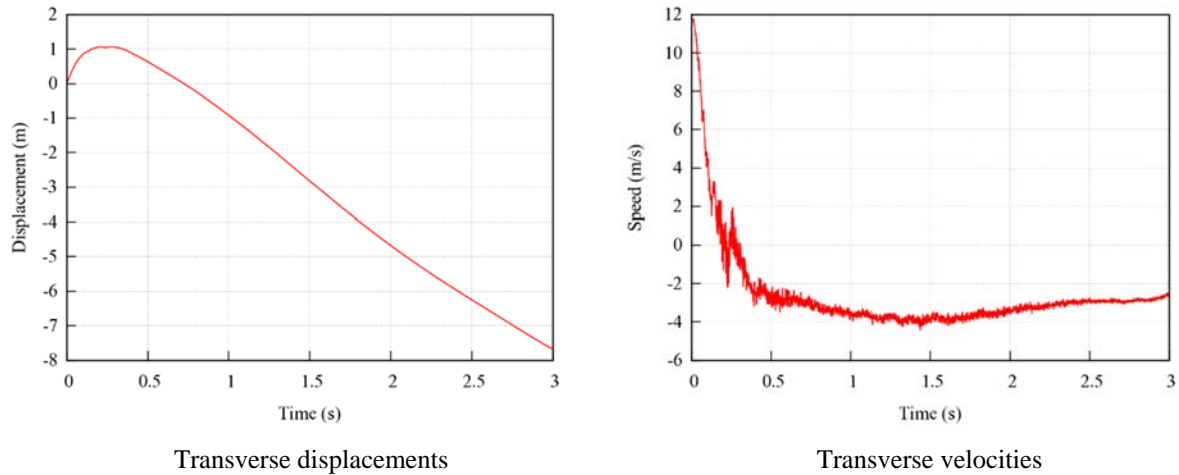


Fig. 4.108: Transverse displacements and velocities of the Dodge Neon impacting the front-side, convex horizontal curvature 29-inch guardrail on a 2.5H:1V slope at 62 mph (100 km/hour) and 25°.

Figure 4.109 shows the vehicle trajectory of the Ford F250 impacting the 29-inch single-faced W-beam guardrail with convex horizontal curvature. In this case, the vehicle impacted the guardrail and spun around the post but did not lose contact with the guardrail during the entire simulation; therefore, the exit-box was not needed. According to the MASH evaluation criterion *N*, an acceptable post-impact behavior may be achieved if the vehicle is decelerated to a stop while vehicle-barrier contact is maintained. The vehicle’s post-impact responses in this case indicated that this criterion was met. Even though the exit-box criterion was not applicable, the case can be determined as safe without the possibility of causing a secondary collision.

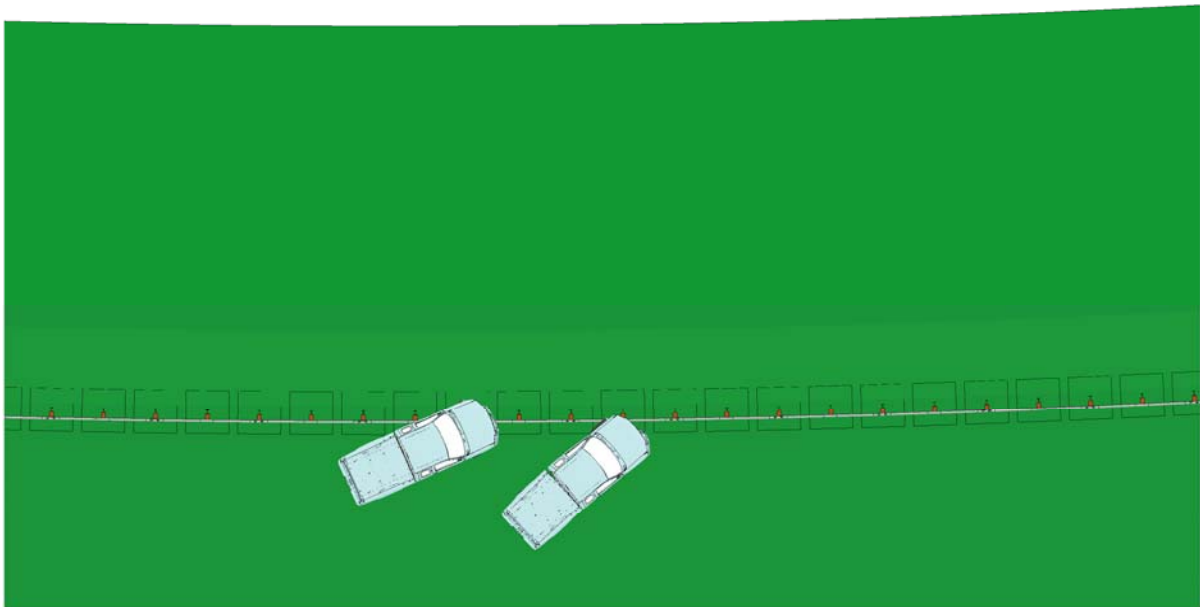


Fig. 4.109: A Ford F250 impacting the front-side, convex horizontal curvature 29-inch guardrail on a 2.5H:1V slope at 62 mph (100 km/hour) and 25°.

The yaw, pitch, and roll angles of the Ford F250 impacting the 29-inch single-faced guardrail with convex horizontal curvature is shown in Fig. 4.110. Since the vehicle did not lose contact with the guardrail, an exit angle could not be calculated. The roll and pitch angles in this impact was less than twelve degrees in either positive or negative direction and thus passed the MASH evaluation criterion F , which specified a maximum 75° roll or pitch angle.

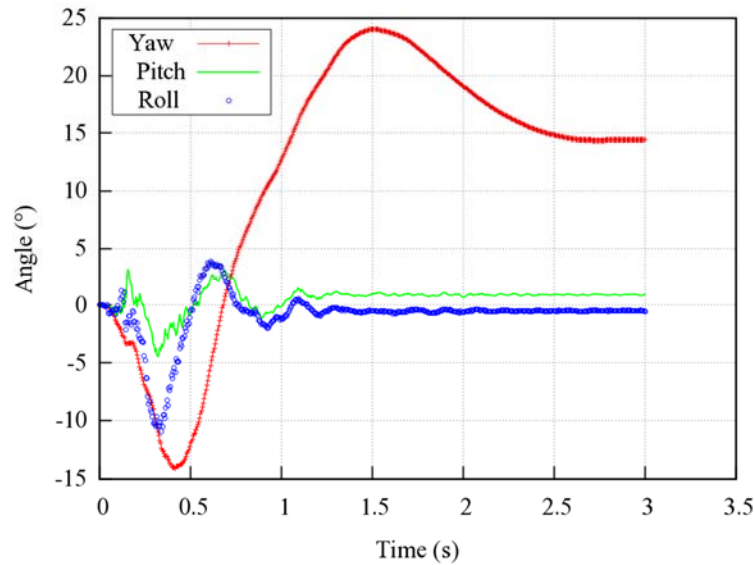


Fig. 4.110: Yaw, pitch, and roll angles of Ford F250 impacting the front-side, convex horizontal curvature 29-inch guardrail on a 2.5H:1V slope at 62 mph (100 km/hour) and 25° .

Figure 4.111 shows the maximum dynamic deflection of the 29-inch single-faced guardrail with convex horizontal curvature impacted by the Ford F250 at 62 mph (100 km/hour) and 25° . The maximum dynamic deflection of the guardrail for this impact was measured to be 3.64 ft (1.11 m). The maximum dynamic deflection in this case was more severe than previous cases due to the large amount of kinetic energy absorbed by the guardrail as compared to redirecting the vehicle with minimal contact in previous cases. The guardrail slipped behind the vehicle's tire after the front-left fender was damaged by the initial impact with the guardrail, as can be seen from the detailed view of vehicle-guardrail interaction shown in Fig. 4.112.

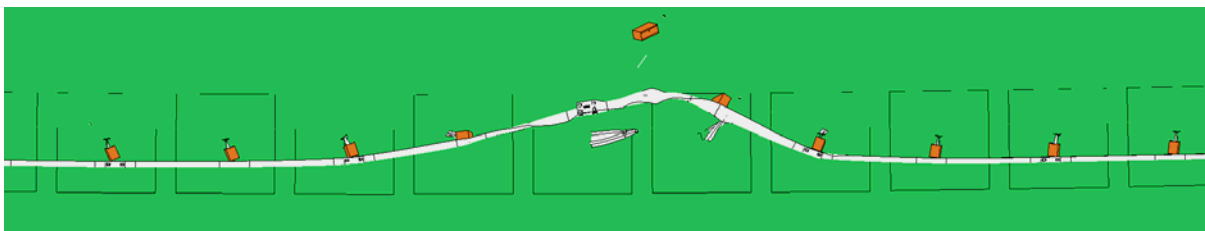


Fig. 4.111: Maximum dynamic deflection of the front-side, convex horizontal curvature 29-inch guardrail on a 2.5H:1V slope at 62 mph (100 km/hour) and 25° and impacted by a Ford F250.

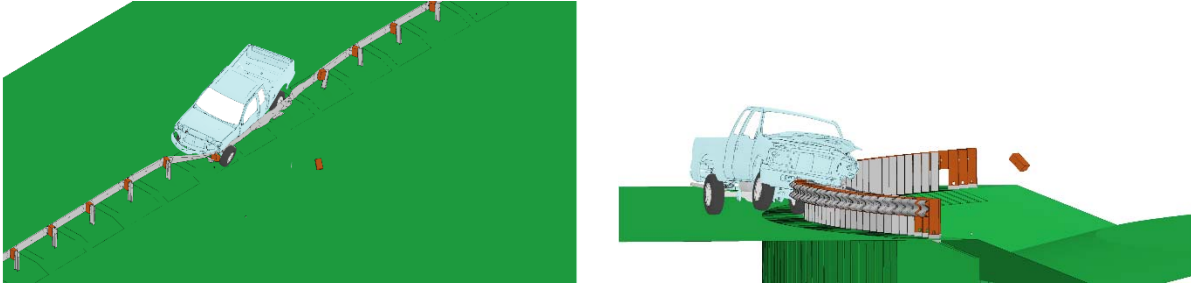


Fig. 4.112: Simulations of Ford F250 impacting the front-side, convex horizontal curvature, 29-inch guardrail on a 2.5H:1V slope at 62 mph (100 km/hour) and 25°.

Figure 4.113 show the time histories of transverse displacements and velocities measured at the CG point of the Ford F250 impacting the 29-inch single-faced guardrail with convex horizontal curvature placed on a 2.5H:1V slope. The transverse velocity was reduced to approximately zero because the vehicle remained in contact with the barrier. Considering the MASH evaluation criterion N and transverse velocity, the Ford F250 had essentially no chance of getting involved in a secondary collision.

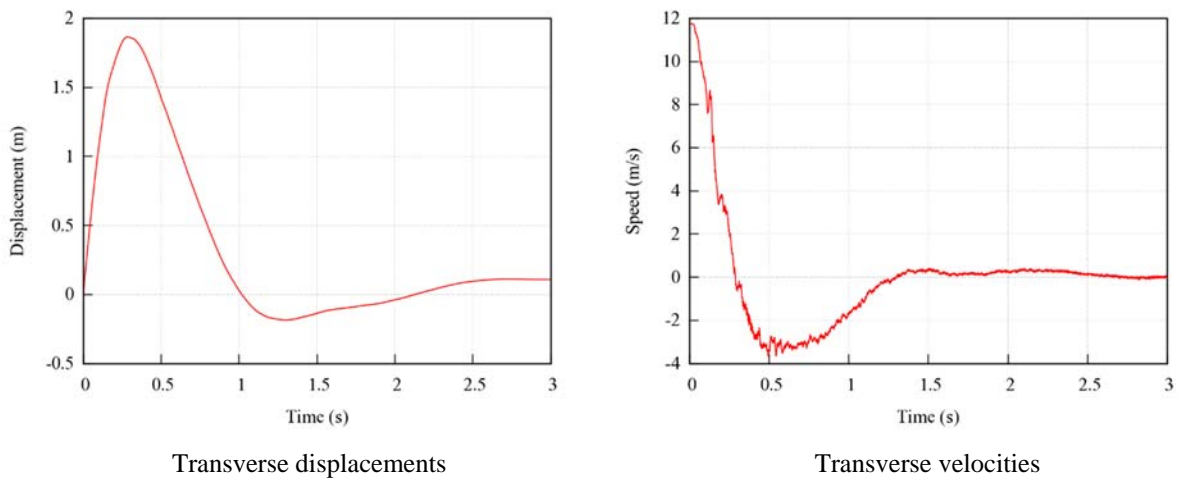


Fig. 4.113: Transverse displacements and velocities of the Ford F250 impacting the front-side, convex horizontal curvature, 29-inch guardrail on a 2.5H:1V slope at 62 mph (100 km/hour) and 25°.

4.4.2 The Single-faced 31-inch Guardrail with convex horizontal curvature – Front-side Impact

Figure 4.114 shows the top view vehicle trajectory of the Dodge Neon impacting the 31-inch single-faced guardrail with convex horizontal curvature at 62 mph (100 km/hour) and 25°. The W-beam guardrail, placed on a 2.5H:1V slope, is shown in its original undeformed shape and the exit-box, placed at the last point of contact of the vehicle’s wheel tracks to the initial guardrail face, is shown by the yellow dotted rectangle. It was observed from the simulation results that the vehicle experienced tire snagging on the guardrail post, causing pocketing and snagging on the front part of the vehicle. The vehicle had a continuous spin after losing contact with the guardrail and left the exit-box before traversing the length of the exit-box. Therefore, the MASH exit-box criterion was not met in this case.

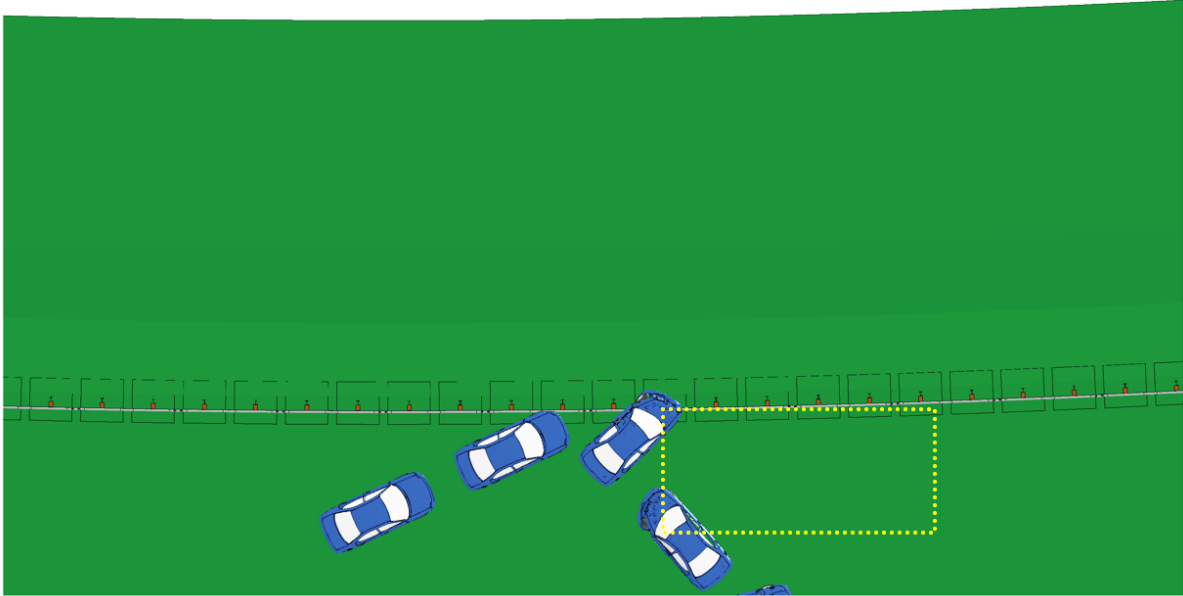


Fig. 4.114: A Dodge Neon impacting the front-side, convex horizontal curvature, 31-inch guardrail on a 2.5H:1V slope at 62 mph (100 km/hour) and 25°.

The yaw, pitch, and roll angles of the Dodge Neon in this impact are shown in Fig. 4.115. The exit angle was determined to be 56° by adding the 25° impact angle to the yaw angle at exit (i.e., 31°). The steadily increasing yaw angle indicates a counter-clockwise rotation of the vehicle away from the guardrail. The vehicle was not safely redirected due to the continuous spin after prematurely leaving the exit-box, as seen in Fig. 4.114. The roll and pitch angles were less than twenty degrees in either positive or negative direction which passed the MASH evaluation criterion F , which specified a maximum 75° roll or pitch angle.

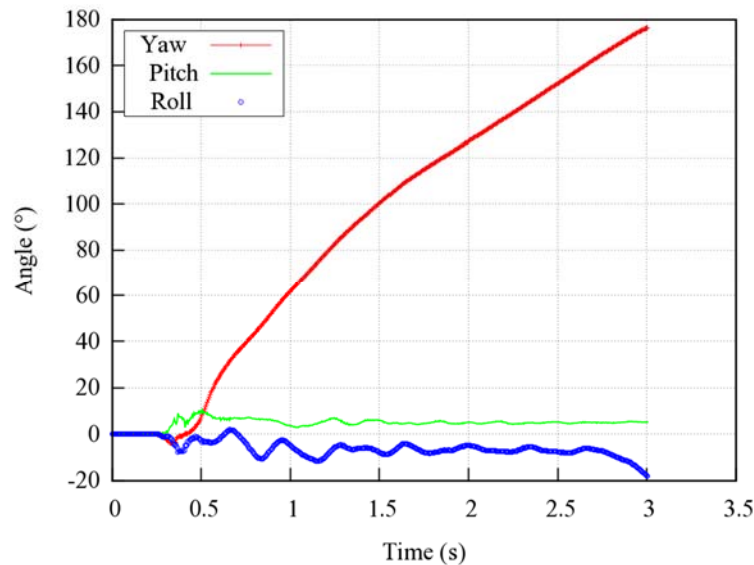


Fig. 4.115: Yaw, pitch, and roll angles of Dodge Neon impacting the front-side, convex horizontal curvature, 31-inch guardrail on a 2.5H:1V slope at 62 mph (100 km/hour) and 25°.

Figure 4.116 shows the maximum dynamic deflection of the 31-inch single-faced guardrail with convex horizontal curvature impacted by the Dodge Neon at 62 mph (100 km/hour) and 25°. The maximum dynamic deflection of the guardrail in this case was 1.87 ft (0.57 m). Compared to the case of 31-inch single-faced guardrail without horizontal curvature (see Fig. 4.15a), the maximum dynamic deflection and exit angle in this impact were both significantly smaller.

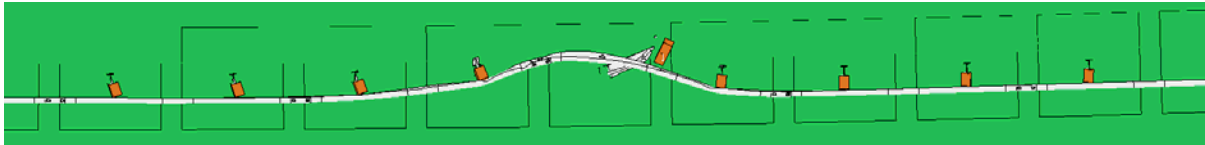


Fig. 4.116: Maximum dynamic deflection of the front-side, convex horizontal curvature, 31-inch guardrail on a 2.5H:1V slope at 62 mph (100 km/hour) and 25° and impacted by a Dodge Neon.

Figure 4.117 shows the detailed views of vehicle-barrier interactions while the Dodge Neon impacts the 31-inch single-faced guardrail with convex horizontal curvature. The guardrail had very small engagement with the vehicle's bumper cover and fender. Instead, the Dodge Neon intruded under the rail, engaged with the rail on its hood, and impacted a guardrail post, resulting in a small, but localized, transverse deflection of the guardrail.



Fig. 4.117: Simulations of Dodge Neon impacting the front-side, convex horizontal curvature, 31-inch guardrail on a 2.5H:1V slope at 62 mph (100 km/hour) and 25°.

Figure 4.118 shows the time histories of transverse displacements and velocities measured at the CG point of the Dodge Neon impacting the 31-inch single-faced guardrail with convex horizontal curvature placed on a 2.5H:1V slope. The transverse velocity of the vehicle after impact was approximately 5 mph (2.2 m/s) away from the guardrail, indicating a chance of further displacement towards the travel lane. In this case, since the vehicle had a continuous spin after losing contact with the guardrail, it would be possible to get involved in a secondary collision.

Figure 4.119 shows the vehicle trajectory of the Ford F250 impacting the 31-inch single-faced guardrail with convex horizontal curvature at 62 mph (100 km/hour) and 25°. Since the vehicle impacted the guardrail and spun around the post without losing contact with the guardrail during the entire simulation, the exit-box was not needed for this case. The MASH evaluation criterion N was satisfied since the vehicle remained in contact with the guardrail while decelerating to stop. Even though the exit-box criterion was not applicable, the impact can be determined as a safe case without the possibility of causing a secondary collision.

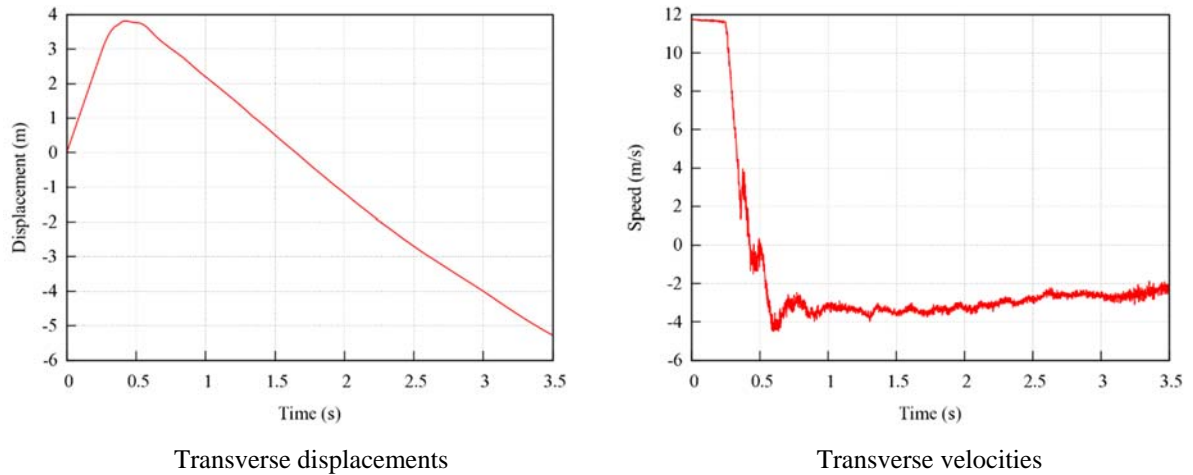


Fig. 4.118: Transverse displacements and velocities of the Dodge Neon impacting the front-side, convex horizontal curvature, 31-inch guardrail on a 2.5H:1V slope at 62 mph (100 km/hour) and 25°.

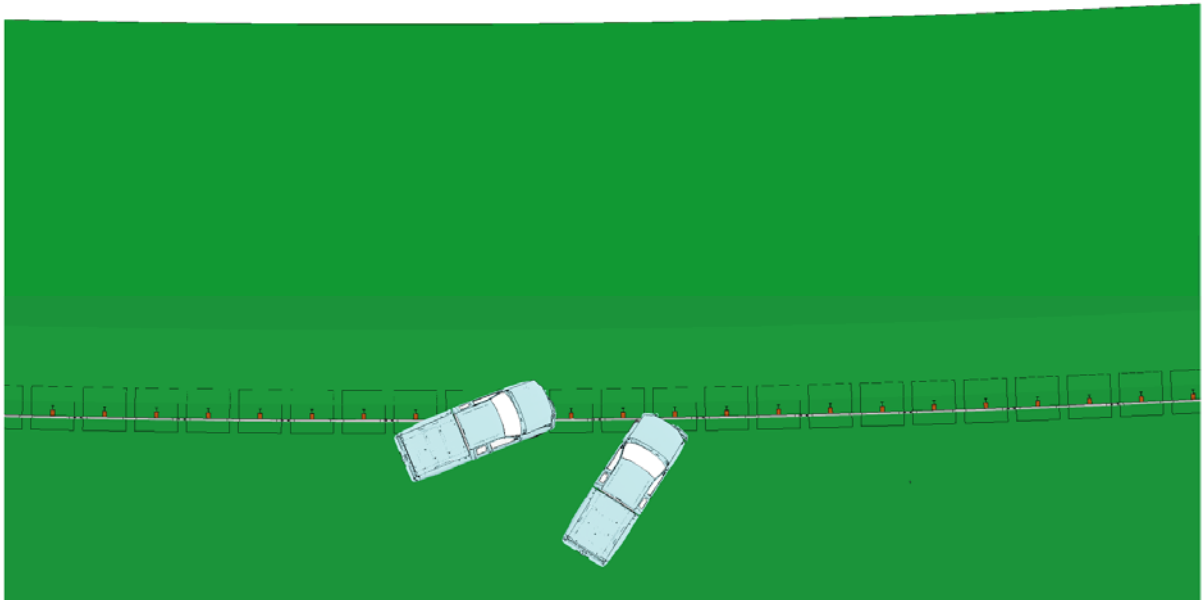


Fig. 4.119: A Ford F250 impacting the front-side, convex horizontal curvature, 31-inch guardrail on a 2.5H:1V slope at 62 mph (100 km/hour) and 25°.

The yaw, pitch, and roll angles of the Ford F250 impacting the 31-inch single-faced guardrail with convex horizontal curvature is shown in Fig. 4.120. Since the vehicle did not lose contact with the guardrail, an exit angle could not be calculated. The roll and pitch angles in this impact were less than ten degrees in either positive or negative direction and thus passed the MASH evaluation criterion F , which specified a maximum 75° roll or pitch angle.

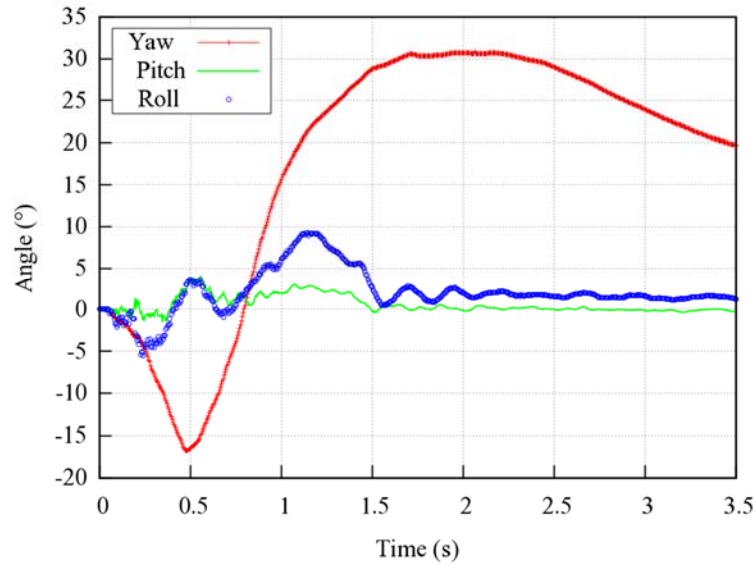


Fig. 4.120: Yaw, pitch, and roll angles of Ford F250 impacting the front-side, convex horizontal curvature 31-inch guardrail on a 2.5H:1V slope at 62 mph (100 km/hour) and 25°.

Figure 4.121 shows the maximum dynamic deflection of the 31-inch single-faced guardrail with convex horizontal curvature impacted by the Ford F250 at 62 mph (100 km/hour) and 25°. The maximum dynamic deflection of the guardrail for this impact was measured to be 3.94 ft (1.20 m). The maximum dynamic deflection was more severe than previous cases due to the large amount of kinetic energy absorbed by the guardrail as compared to previous cases in which the vehicle was redirected with minimal contact with the guardrail. The guardrail slipped behind the vehicle’s tire after the front-left fender was damaged by the initial impact with the guardrail, as can be seen from the detailed view of vehicle-guardrail interaction shown in Fig. 4.122.

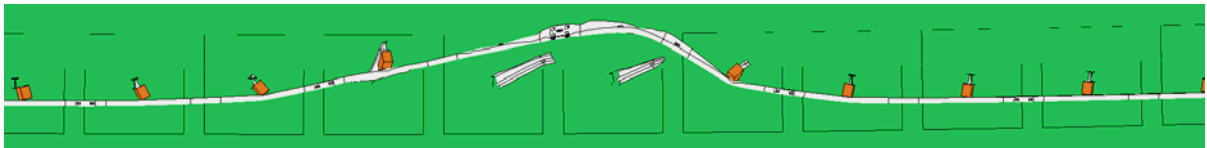


Fig. 4.121: Maximum dynamic deflection of the front-side, convex horizontal curvature, 31-inch guardrail on a 2.5H:1V slope at 62 mph (100 km/hour) and 25° and impacted by a Ford F250.

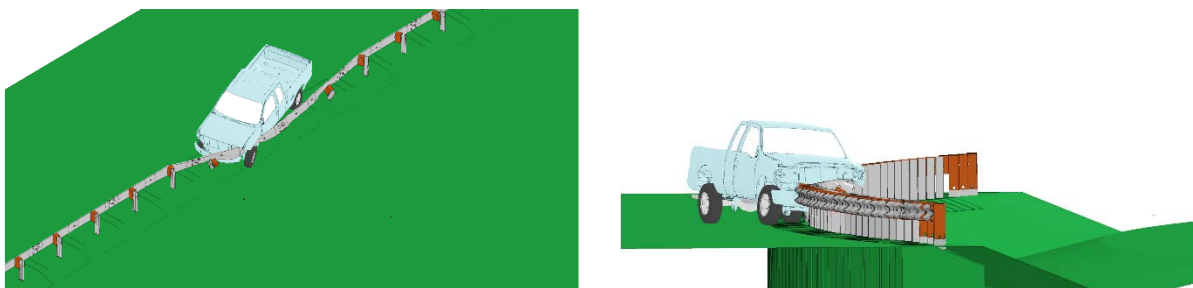


Fig. 4.122: Simulations of Ford F250 impacting the front-side, convex horizontal curvature, 31-inch guardrail on a 2.5H:1V slope at 62 mph (100 km/hour) and 25°.

Figure 4.123 show the time histories of transverse displacements and velocities measured at the CG point of the Ford F250 impacting the 31-inch single-faced guardrail with convex horizontal curvature. The transverse velocity was reduced to approximately zero because the vehicle remained in contact with the guardrail. Considering the MASH evaluation criterion N and transverse velocity, the Ford F250 had essentially no chance of getting involved in a secondary collision.

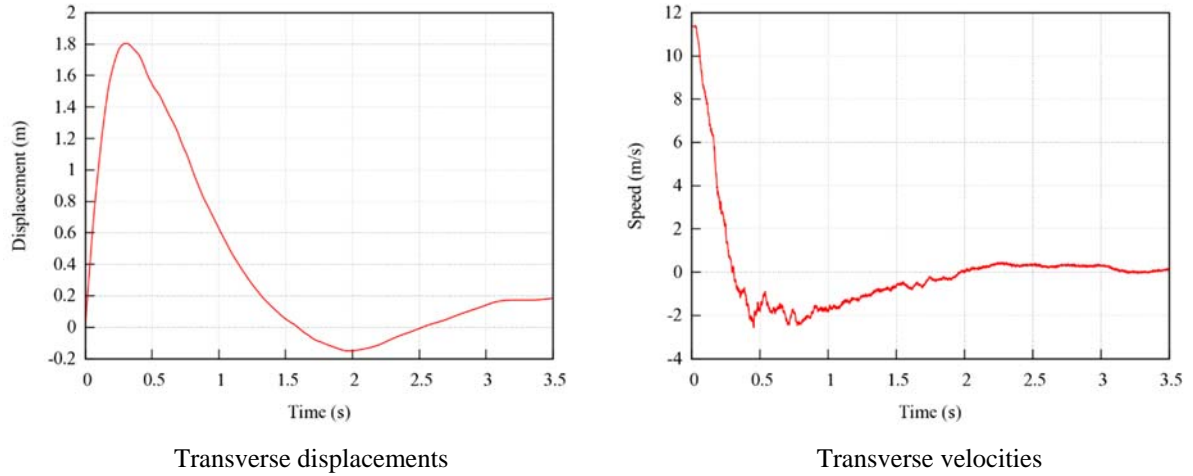


Fig. 4.123: Transverse displacements and velocities of the Ford F250 impacting the front-side, convex horizontal curvature 31-inch guardrail on a 2.5H:1V slope at 62 mph (100 km/hour) and 25°.

4.5 Case 5: Single-faced Guardrail with Concave Horizontal Curvature Placed on a 4H:1V Slope

In this case, the 29- and 31-inch single-faced guardrails with concave horizontal curvature were evaluated when placed on a 4H:1V slope and impacted by both the Dodge Neon and Ford F250. The impact speed and impact angle were 62 mph (100 km/hour) and 25°, respectively, for all simulations in Case 5. Table 4.7 gives a summary of the simulation results that were used to evaluate guardrail performance in terms of vehicular responses.

Table 4.7: Simulation results of Case 5 (Single-faced Guardrail with Concave Horizontal Curvature Placed on a 4H:1V Slope)

Impact side	Guardrail Height	Test Vehicle	Simulation Results
Front-side	29 inch	Dodge Neon	The vehicle failed the exit-box criterion caused by vehicle spin-out and a large exit angle
		Ford F250	The vehicle remained in contact with guardrail due to tire snagging on guardrail post
	31 inch	Dodge Neon	The vehicle failed the exit-box criterion caused by vehicle spin-out and a large exit angle
		Ford F250	The vehicle was redirected but failed the exit-box criterion with a low exit angle

4.5.1 The 29-inch Single-faced Guardrail with concave horizontal curvature – Front-side Impact

Figure 4.124 shows the top view vehicle trajectory of the Dodge Neon impacting the 29-inch single-faced guardrail with concave horizontal curvature at 62 mph (100 km/hour) and 25°. The W-beam guardrail, placed on a 4H:1V slope, is shown in its original undeformed shape and the exit-box is shown by the yellow dotted rectangle. It can be seen that the vehicle experienced tire snagging on the guardrail post, causing vehicle spin-out with a large exit angle. Since the vehicle left the exit-box before traversing the length of the exit-box, the MASH exit-box criterion was not met.

Figure 4.125 shows the yaw, pitch, and roll angles for the Dodge Neon impacting the 29-inch single-faced guardrail with concave horizontal curvature placed on a 4H:1V slope. The exit angle was determined to be 61° by adding the 25° impact angle to the yaw angle at exit (i.e., 36°). The steadily increasing yaw angle indicated a counter-clockwise rotation of the vehicle away from the guardrail. The vehicle was not safely redirected due to the continuous spin after leaving the exit-box, as indicated by the increasing yaw angle. It was observed from the simulation results that the Dodge Neon partially under-rode the guardrail and crashed directly on a post, causing pocketing and snagging on the front part of the vehicle. The roll and pitch angles were less than fifteen degrees in either positive or negative direction which passed the MASH evaluation criterion F , which specified a maximum 75° roll or pitch angle.

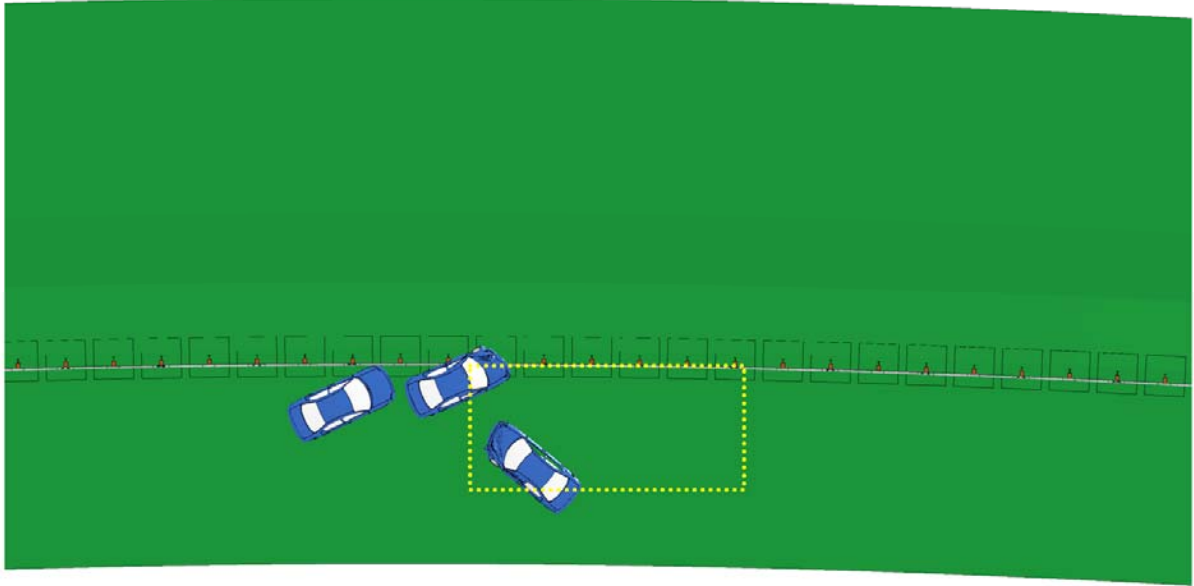


Fig. 4.124: A Dodge Neon impacting the front-side, concave horizontal curvature, 29-inch guardrail on a 2.5H:1V slope at 62 mph (100 km/hour) and 25°.

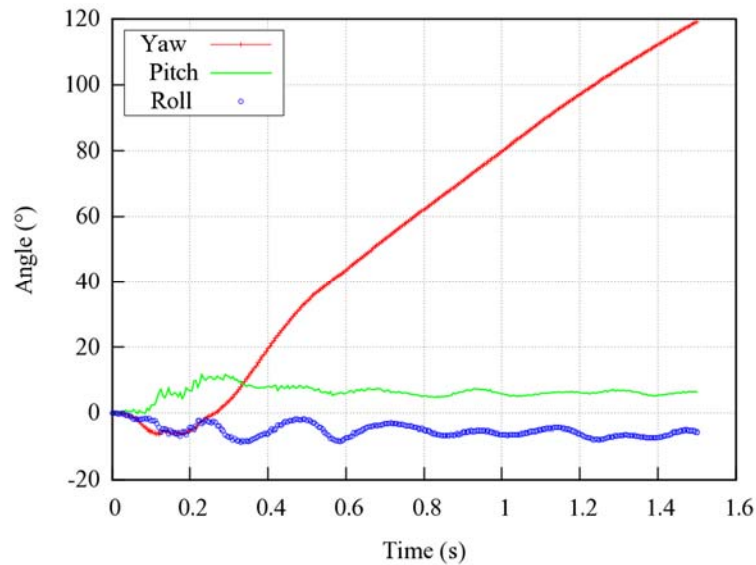


Fig. 4.125: Yaw, pitch, and roll angles of Dodge Neon impacting the front-side, concave horizontal curvature, 29-inch guardrail on a 2.5H:1V slope at 62 mph (100 km/hour) and 25°.

The maximum dynamic deflection of the 29-inch single-faced guardrail with concave horizontal curvature impacted by the Dodge Neon at 62 mph (100 km/hour) and 25° is shown in Fig. 4.126. The maximum dynamic deflection of the guardrail in this case was 2.49 ft (0.76 m). Compared to the case of the 29-inch single-faced guardrail without horizontal curvature, (see Fig. 4.4a) and impacted by the Dodge Neon at 62 mph (100 km/hour), the maximum dynamic deflections were identical and exit angle in this impact was 13° larger than the case without horizontal curvature.

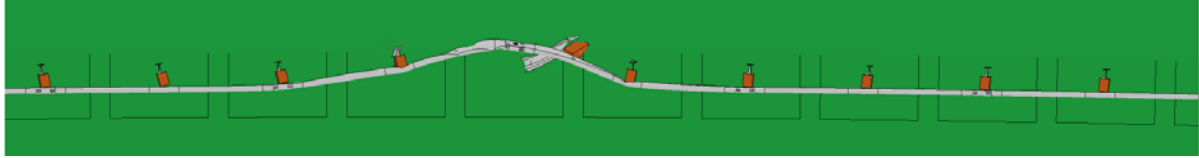


Fig. 4.126: Maximum dynamic deflection of the front-side, concave horizontal curvature, 29-inch guardrail on a 2.5H:1V slope at 62 mph (100 km/hour) and 25° and impacted by a Dodge Neon.

Figure 4.127 shows the detailed views of vehicle-barrier interactions while the Dodge Neon impacts the front-side of the 29-inch single-faced guardrail with concave horizontal curvature at 62 mph (100 km/hour) and 25°. The guardrail had very small engagement with the vehicle's bumper cover and fender. Instead, the Dodge Neon intruded under the rail, engaged with the rail on the vehicle's hood and impacted a guardrail post, resulting in a small, but localized, transverse deflection of the guardrail.

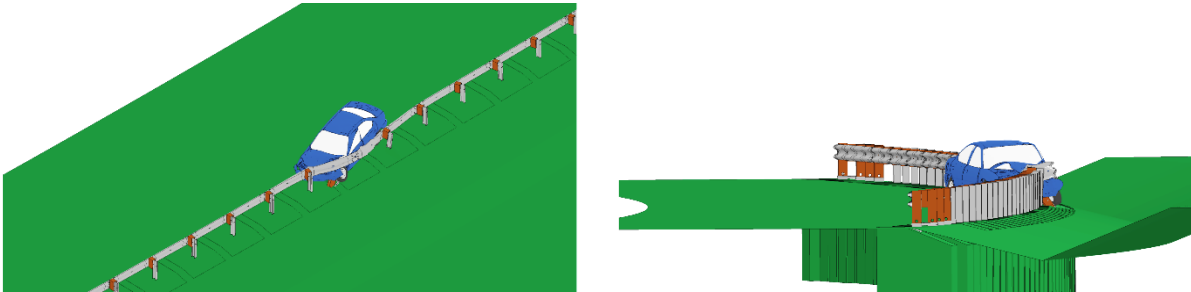


Fig. 4.127: Simulations of Dodge Neon impacting the front-side, concave horizontal curvature, 29-inch guardrail on a 2.5H:1V slope at 62 mph (100 km/hour) and 25°.

Figure 4.128 shows the time histories of transverse displacements and velocities measured at the CG point of the Dodge Neon impacting the front-side of the 29-inch single-faced guardrail with concave horizontal curvature at 62 mph (100 km/hour) and 25°. The transverse velocity of the vehicle after impact was approximately 5 mph (2.2 m/s) away from the guardrail, indicating a chance of further displacement towards the travel lane. In this case, since the vehicle was snagged on the guardrail and spun around a post before losing contact with the guardrail, it would be possible to get involved in a secondary collision.

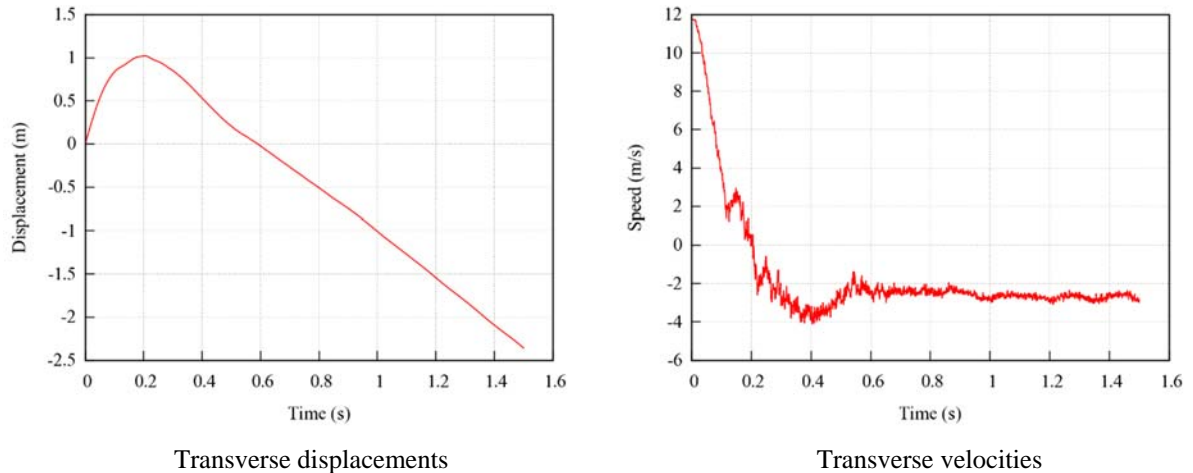


Fig. 4.128: Transverse displacements and velocities of the Dodge Neon impacting the front-side, concave horizontal curvature, 29-inch guardrail on a 2.5H:1V slope at 62 mph (100 km/hour) and 25°.

Figure 4.129 shows the vehicle trajectory for the Ford F250 impacting the front-side of the single-faced 29-inch W-beam guardrail with concave horizontal curvature at 62 mph (100 km/hour) and 25°. It can be seen that the vehicle impacted the guardrail and spun around the post but did not lose contact with the guardrail during the entire simulation. In this situation, the exit-box was not needed. From the MASH evaluation criterion *N*, an acceptable post-impact behavior may be achieved if the vehicle is decelerated to a stop while vehicle-barrier contact is maintained, indicating this criterion was met. Even though the exit-box criterion was not applicable, the impact can be determined as a safe case without the possibility of causing a secondary collision.

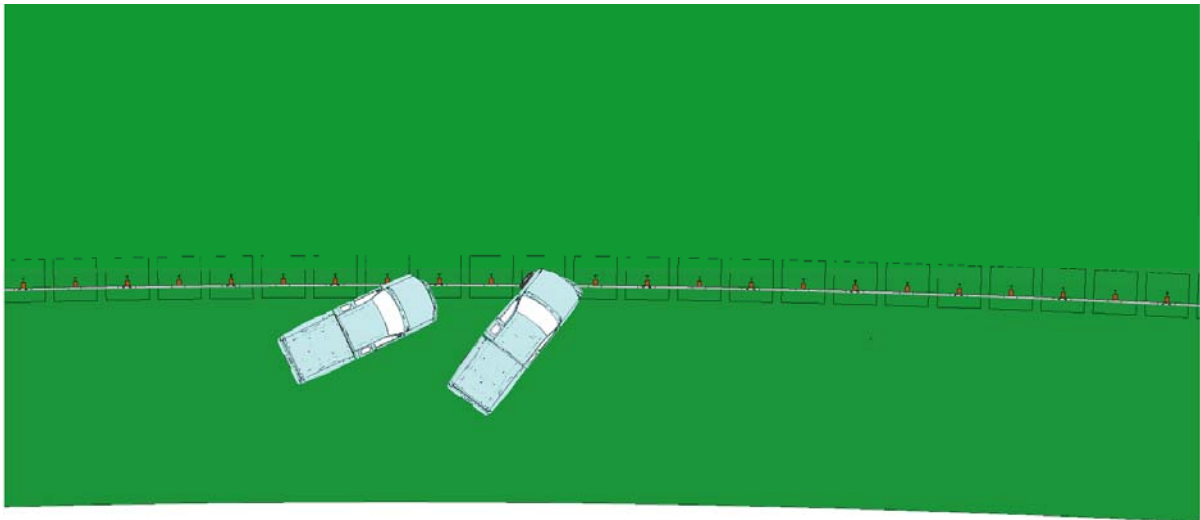


Fig. 4.129: A Ford F250 impacting the front-side, concave horizontal curvature 29-inch guardrail on a 2.5H:1V slope at 62 mph (100 km/hour) and 25°.

The yaw, pitch, and roll angles of the Ford F250 impacting the front-side of the 29-inch single-faced guardrail with concave horizontal curvature is shown in Fig. 4.130. Since the

vehicle did not lose contact with the guardrail, an exit angle could not be calculated. The roll and pitch angles in this impact were less than twelve degrees in either positive or negative direction and thus passed the MASH evaluation criterion F , which specified a maximum 75° roll or pitch angle.

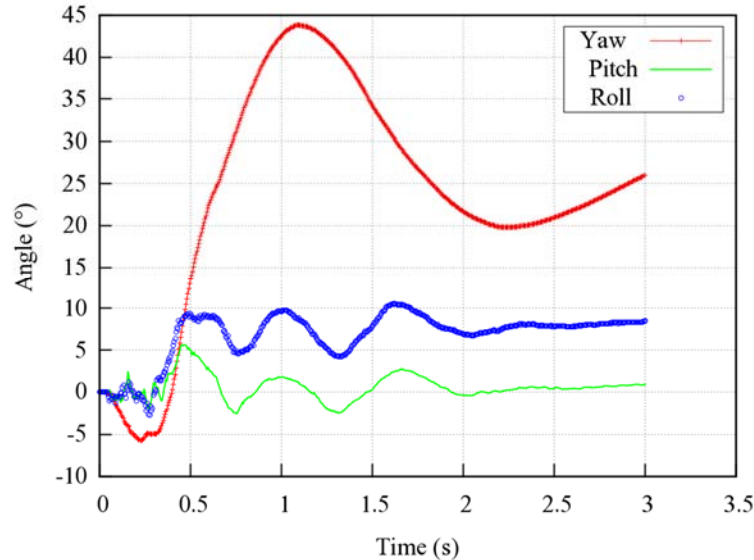


Fig. 4.130: Yaw, pitch, and roll angles of Ford F250 impacting the front-side, concave horizontal curvature, 29-inch guardrail on a 2.5H:1V slope at 62 mph (100 km/hour) and 25° .

The maximum dynamic deflection of the 29-inch single-faced guardrail with concave horizontal curvature under impact by the Ford F250 at 62 mph (100 km/hour) and 25° is shown in Fig. 4.131. The maximum dynamic deflection of the guardrail for this impact was measured to be 3.74 ft (1.14 m). The maximum dynamic deflection was more severe than other impacts on the single-faced guardrail due to the large amount of kinetic energy absorbed by the guardrail as compared to redirecting the vehicle with minimal contact in other cases. The guardrail slipped behind the vehicle's tire after the front-left fender was damaged by the initial impact with the guardrail, as can be seen from the detailed vehicle-guardrail interaction shown in Fig. 4.132.

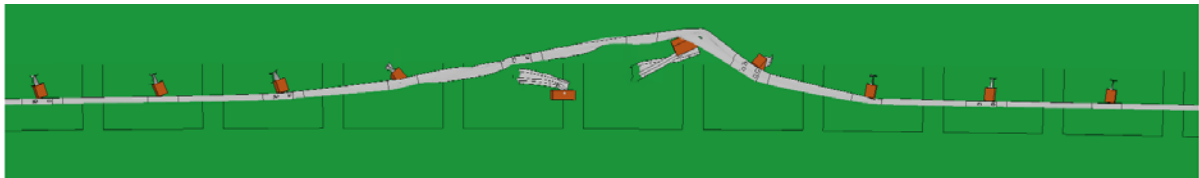


Fig. 4.131: Maximum dynamic deflection of the front-side, concave horizontal curvature, 29-inch guardrail on a 2.5H:1V slope at 62 mph (100 km/hour) and 25° and impacted by a Ford F250.

Figure 4.133 show the time histories of transverse displacements and velocities measured at the CG point of the Ford F250 impacting the front-side of the 29-inch single-faced guardrail with concave horizontal curvature. The transverse velocity was reduced to essentially zero because the vehicle remained in contact with the barrier. Considering the MASH evaluation

criterion N and transverse velocity, the Ford F250 had essentially no chance of getting involved in a secondary collision.



Fig. 4.132: Simulations of Ford F250 impacting the front-side, concave horizontal curvature, 29-inch guardrail on a 2.5H:1V slope at 62 mph (100 km/hour) and 25°.

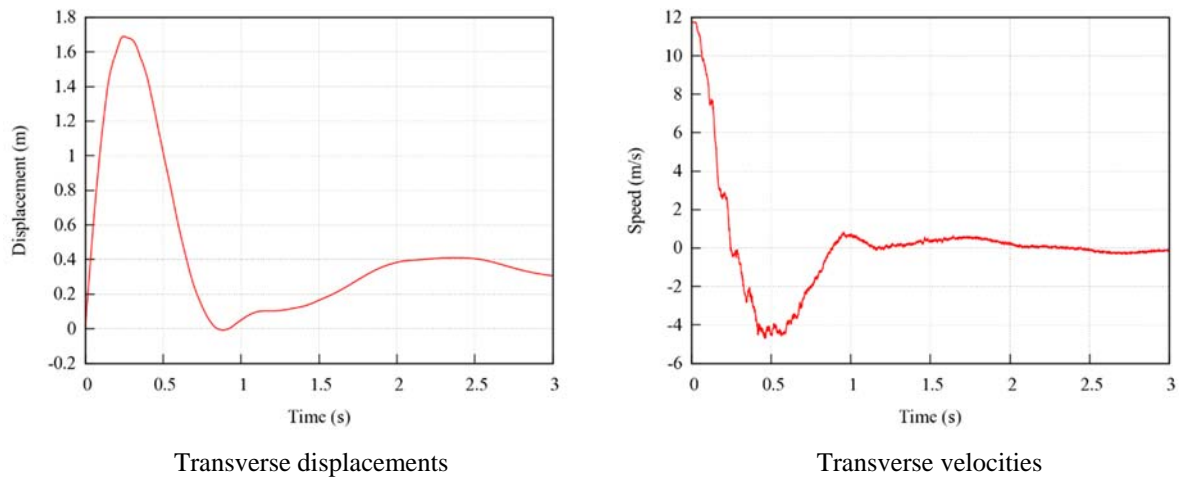


Fig. 4.133: Transverse displacements and velocities of the Ford F250 impacting the front-side, concave horizontal curvature, 29-inch guardrail on a 2.5H:1V slope at 62 mph (100 km/hour) and 25°.

4.5.2 The Single-faced 31-inch Guardrail with concave horizontal curvature – Front-side Impact

Figure 4.134 shows the top view vehicle trajectory of the Dodge Neon impacting the 31-inch single-faced guardrail with concave horizontal curvature at 62 mph (100 km/hour) and 25°. The W-beam guardrail, placed on a 4H:1V slope, is shown in its original undeformed shape and the exit-box is shown by the yellow dotted rectangle. It can be seen that the vehicle experienced tire snagging on the guardrail post, causing vehicle spin-out with a large exit angle. Since the vehicle left the exit-box before traversing the length of the exit-box, the MASH exit-box criterion was not met.

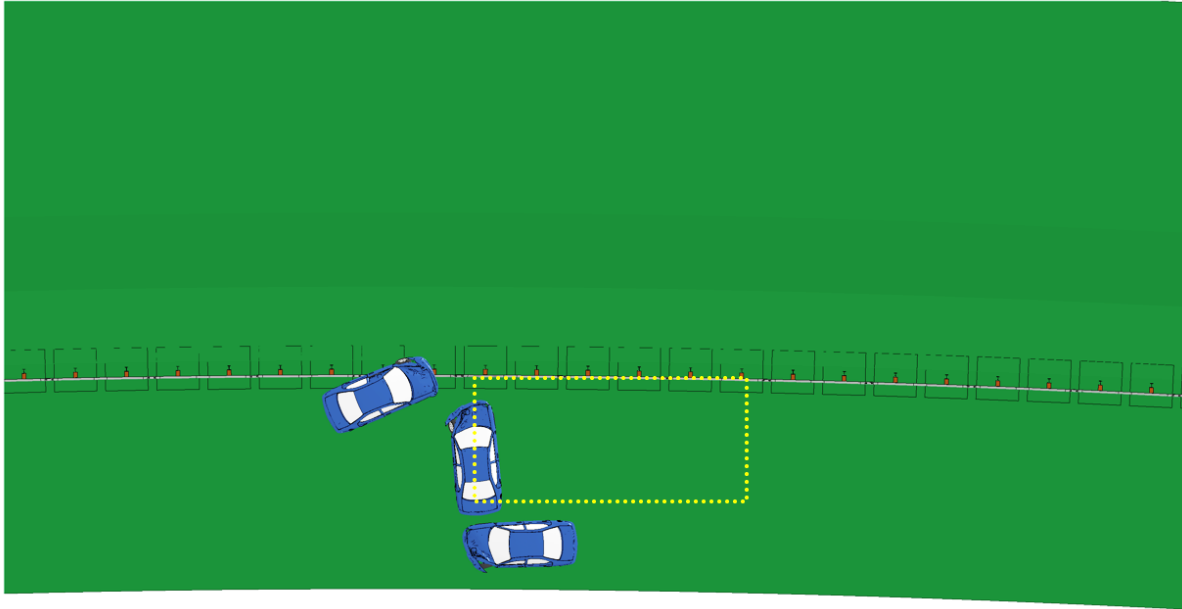


Fig. 4.134: A Dodge Neon impacting the front-side, concave horizontal curvature, 31-inch guardrail on a 2.5H:1V slope at 62 mph (100 km/hour) and 25°.

The yaw, pitch, and roll angles of the Dodge Neon impacting the 31-inch single-faced guardrail with concave horizontal curvature is shown in Fig. 4.135. The exit angle was determined to be 67° by adding the 25° impact angle to the yaw angle at exit (i.e., 42°). The steadily increasing yaw angle indicated a counter-clockwise rotation of the vehicle away from the guardrail. The vehicle was not safely redirected due to the continuous spin after prematurely leaving the exit-box as indicated by the increasing yaw angle. It was observed from the simulation results that the Dodge Neon partially under-rode the guardrail and crashed directly into a post, causing pocketing and snagging on the front part of the vehicle. The roll and pitch angles were less than fifteen degrees in either positive or negative direction which passed the MASH evaluation criterion *F*. It has a specified a maximum 75° roll or pitch angle.

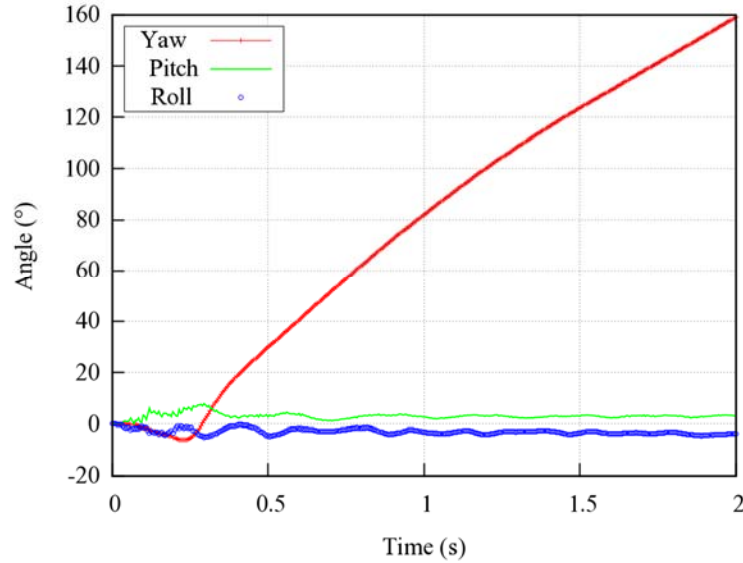


Fig. 4.135: Yaw, pitch, and roll angles of Dodge Neon impacting the front-side, concave horizontal curvature, 31-inch guardrail on a 2.5H:1V slope at 62 mph (100 km/hour) and 25°.

The maximum dynamic deflection of the 31-inch single-faced guardrail with concave horizontal curvature impacted by the Dodge Neon at 62 mph (100 km/hour) and 25° is shown in Fig. 4.136. The maximum dynamic deflection of the guardrail in this case was 2.62 ft (0.8 m). Compared to the case of the 31-inch single-faced guardrail without horizontal curvature (see Fig. 4.14) impacted by the Dodge Neon, the maximum dynamic deflection was larger whereas the exit angle in this impact was 16° smaller.

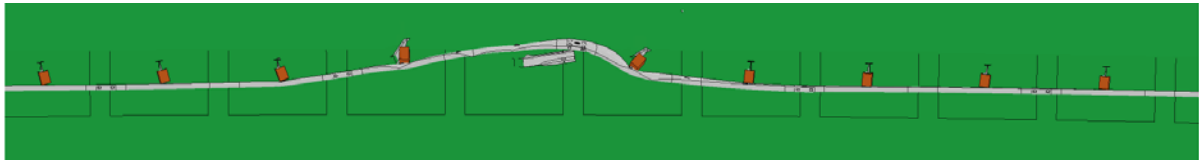


Fig. 4.136: Maximum dynamic deflection of the front-side, concave horizontal curvature, 31-inch guardrail on a 2.5H:1V slope at 62 mph (100 km/hour) and 25° and impacted by a Dodge Neon.

Figure 4.137 shows the detailed views of vehicle-barrier interactions while the Dodge Neon impacts the front-side of the 31-inch single-faced guardrail with concave horizontal curvature placed on a 4H:1V slope. The guardrail had very small engagement with the vehicle's bumper cover and fender. Instead, the Dodge Neon intruded under the rail, engaged with the rail on its hood, and impacted a guardrail post, resulting in a small, but localized, transverse deflection of the guardrail.

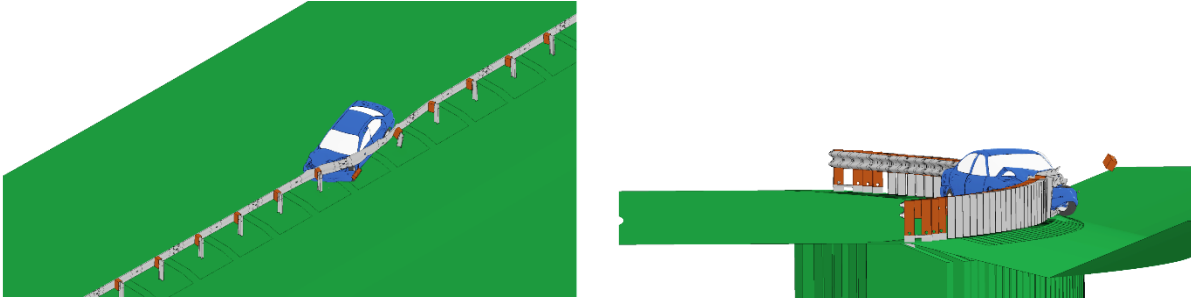


Fig. 4.137: Simulations of Dodge Neon impacting the front-side, concave horizontal curvature, 31-inch guardrail on a 2.5H:1V slope at 62 mph (100 km/hour) and 25°.

Figure 4.138 shows the time histories of transverse displacements and velocities measured at the CG point of the Dodge Neon impacting the 31-inch single-faced guardrail with concave horizontal curvature. The transverse velocity of the vehicle after impact was approximately 7 mph (3.1 m/s) away from the guardrail but was reduced to approximately zero towards the end of the simulation, indicating a low probability of further displacement towards the travel lane. However, since the vehicle traversed more than 26 feet (8 meters) away from the guardrail and thus would enter the travel lane, it would be possible to get involved in a secondary collision.

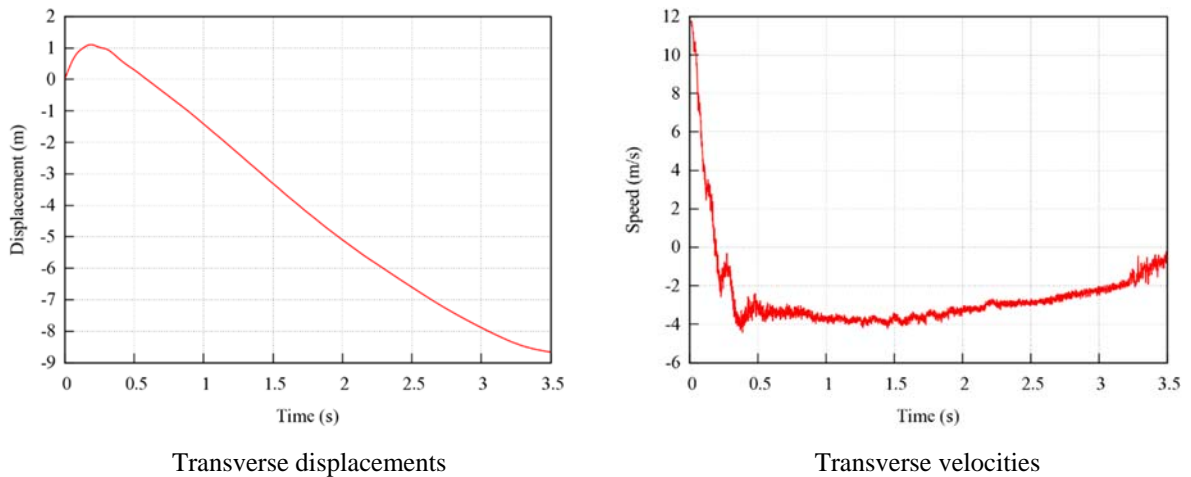


Fig. 4.138: Transverse displacements and velocities of the Dodge Neon impacting the front-side, concave horizontal curvature, 31-inch guardrail on a 2.5H:1V slope at 62 mph (100 km/hour) and 25°.

Figure 4.139 shows the top view vehicle trajectory of the Ford F250 impacting the 31-inch single-faced guardrail with concave horizontal curvature at 62mph (100 km/hour) and 25°. The W-beam guardrail, placed on a 4H:1V slope, is shown in its original undeformed shape and the exit-box is shown by the yellow dotted rectangle. The MASH exit-box criterion was not satisfied because the vehicle did not traverse the length of the exit-box before leaving the box. Due to the low exit angle of the post-impact trajectory, the chances of a secondary collision is relatively low even though the exit-box criterion was not met.

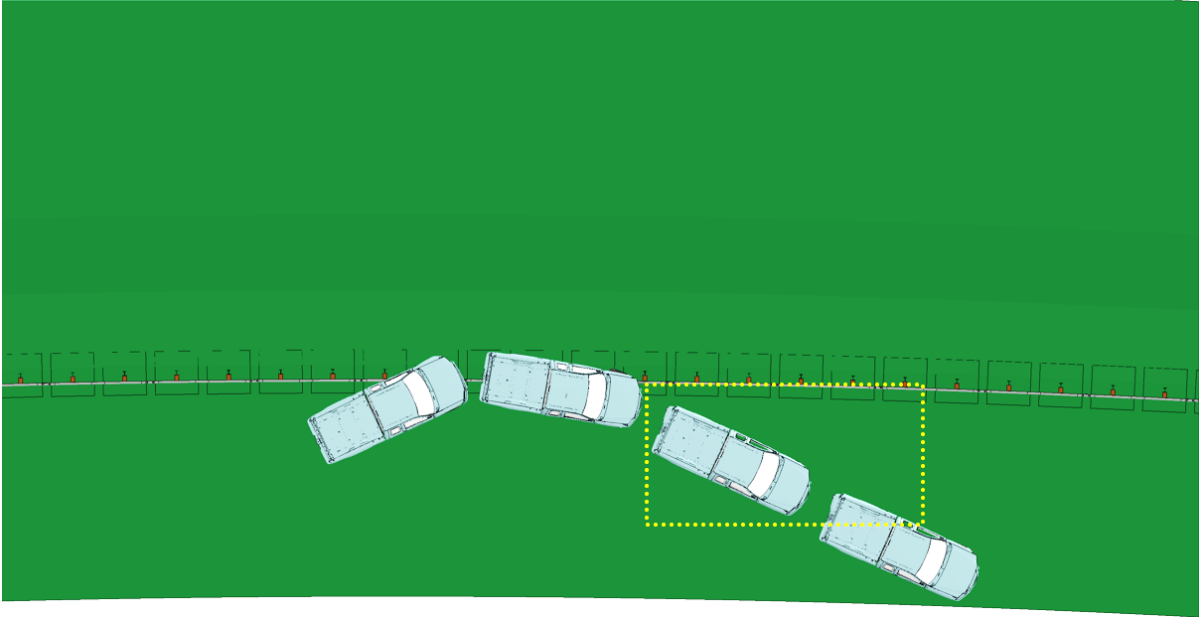


Fig. 4.139: A Ford F250 impacting the front-side, concave horizontal curvature 31-inch guardrail on a 2.5H:1V slope at 62 mph (100 km/hour) and 25°.

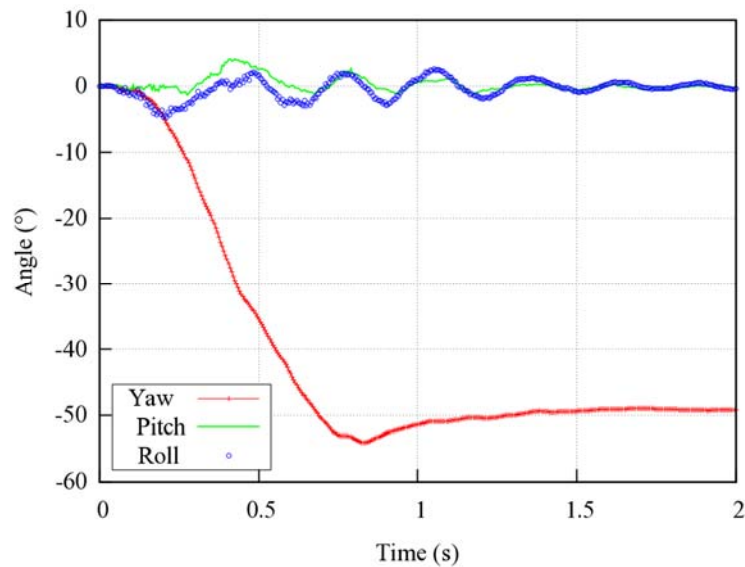


Fig. 4.140: Yaw, pitch, and roll angles of Ford F250 impacting the front-side, concave horizontal curvature 31-inch guardrail on a 2.5H:1V slope at 62 mph (100 km/hour) and 25°.

The yaw, pitch, and roll angles of the Ford F250 impacting the single-faced 31-inch guardrail with concave horizontal curvature is shown in Fig. 4.140. Since the vehicle was redirected by the guardrail instead of snagging on a post, the exit angle was determined to be 28° by subtracting the impact angle, 25° from the yaw angle at exit (i.e., 53°). This calculation would provide more useful information in this case specifically. The roll and pitch angles were less than six degrees in either positive or negative direction and thus passed the MASH evaluation criterion F , which specified a maximum 75° roll or pitch angle.

The maximum dynamic deflection of the 31-inch single-faced guardrail with concave horizontal curvature impacted by the Ford F250 at 62 mph (100 km/hour) and 25° is shown in Fig. 4.141. The maximum dynamic deflection was determined to be 4.72 ft (1.44 m). It was observed that this impact had the largest maximum dynamic deflection of all the impacts in this study. Compared to the case of the single-faced guardrail without horizontal curvature impacted by the Ford F250, the maximum dynamic deflection in this impact is considerably higher. The vehicle's front bumper and side fender had good interaction with the guardrail, resulting in a safe redirection with a relatively low exit angle, as can be seen from the detailed vehicle-guardrail interaction shown in Fig. 4.142.

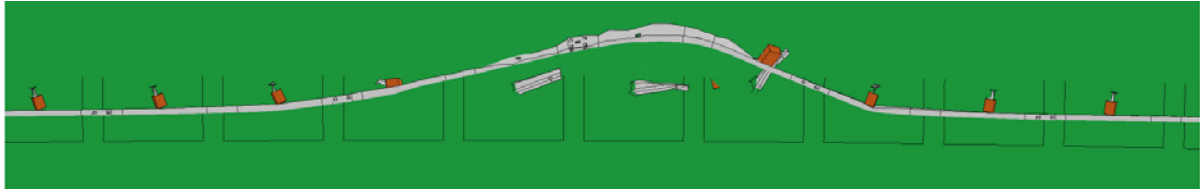


Fig. 4.141: Maximum dynamic deflection of the front-side, concave horizontal curvature 31-inch guardrail on a 2.5H:1V slope at 62 mph (100 km/hour) and 25° and impacted by a Ford F250.

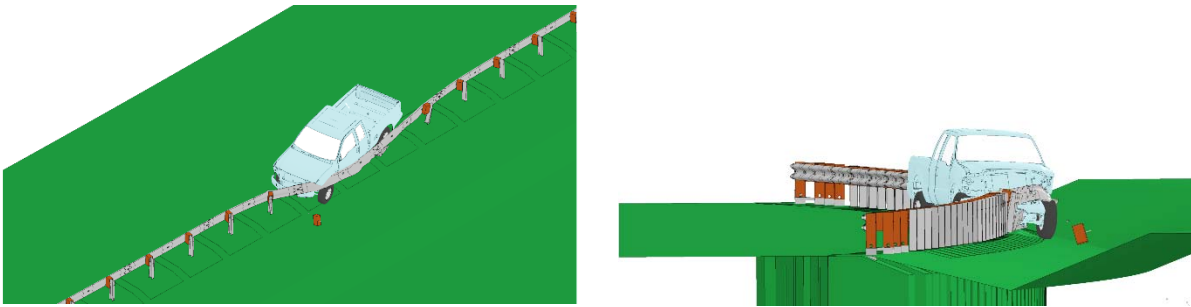
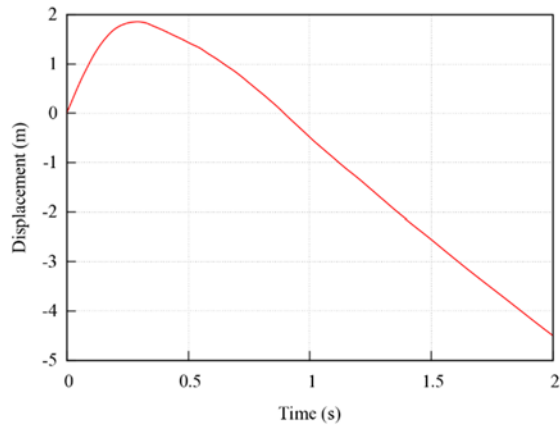
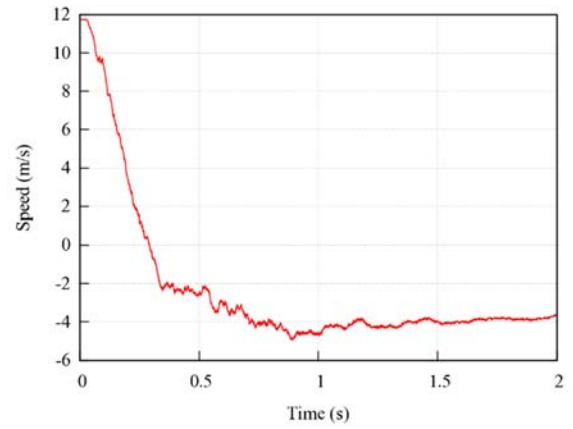


Fig. 4.142: Simulations of Ford F250 impacting the front-side, concave horizontal curvature 31-inch guardrail on a 2.5H:1V slope at 62 mph (100 km/hour) and 25°.

Figure 4.143 shows the time histories of the transverse displacements and velocities measured at the CG point of the Ford F250 impacting the 31-inch single-faced guardrail with concave horizontal curvature placed on a 4H:1V slope. The transverse velocity traveling away from the guardrail was determined to be approximately 8 mph (3.6 m/s) towards the travel lane. Considering the exit-box criterion, exit angle, and transverse velocity, the Ford F250 had a relatively small chance of getting involved in a secondary collision.



Transverse displacements



Transverse velocities

Fig. 4.143: Transverse displacements and velocities of the Ford F250 impacting the front-side, concave horizontal curvature, 31-inch guardrail on a 2.5H:1V slope at 62 mph (100 km/hour) and 25°.

4.6 Comparison of 29-inch and 31-inch Guardrail Splice Location

In Sections 4.1 to 4.5, the performance of single- and double-faced W-beam guardrails at 29- and 31-inch placement heights with and without horizontal curvature were evaluated. In this section, the performance of each guardrail is summarized and compared based on guardrail height. It should be noted that there is a difference between the splice locations of the 29- and 31-inch guardrails. The 29-inch guardrail has the splice located at a post and the 31-inch guardrail has the splice located at the midspan between two adjacent posts. Tables 4.6, 4.7, and 4.8 give a summary of the vehicle redirection characteristics of the 29- and 31-inch single-faced guardrails, double-faced guardrails under front-side impacts, and double-faced guardrails under backside impacts, respectively. In tables 4.6-4.8, all simulation cases were run with an impact speed of 62 mph (100 km/hour) unless otherwise noted under the “Test Vehicle” column of the aforementioned tables.

Table 4.8 below summarizes the results of the 29- and 31-inch single-faced guardrails with and without horizontal curvature. The Dodge Neon impacted the single faced guardrail without horizontal curvature at two impact speeds, 62 mph (100 km/hour) and 70 mph (112.6 km/hour). The rest of the simulations in Table 4.8 were all at a speed of 62 mph (100 km/hour).

It can be seen from the results that tire snagging was a common issue for the single-faced W-beam guardrail, with and without horizontal curvature, under impacts by both the Dodge Neon and Ford F250. The only case without tire snagging was the 31-inch single-faced guardrail with concave horizontal curvature under impact of the Ford F250.

- In regards to the Dodge Neon simulations, due to its low front profile, the vehicle did not engage well with the guardrails at both 29- and 31-inch rail heights. Instead, the vehicle intruded under the rail, impacted on a post, and spun out while losing contact with the guardrail. This was true to all single-faced guardrails with or without horizontal curvature. Due to vehicle spin-out, all Dodge Neon simulations on the single-faced guardrails with and without horizontal curvature had large exit angles and did not pass the MASH exit-box criterion.
- For the Ford F250 simulations, tire snagging occurred in all the cases except for the 31-inch single-faced guardrail with concave curvature, which was the only case of redirecting the Ford F250. The other single-faced guardrails with horizontal curvature performed slightly better than the guardrail without curvature. In these cases, the vehicle snagged on a guardrail post, spun around the post, and slid forward without losing contact with the guardrail. Although the MASH exit box criterion was not applicable, the MASH evaluation criterion N was met and the vehicle would likely not be involved in a secondary collision. For the 31-inch single-faced guardrail with concave horizontal curvature, although the vehicle was redirected, the concave curvature caused a slightly large exit angle that did not meet the MASH exit box criterion.

Table 4.8: Vehicle redirection characteristics of single-faced guardrails with and without horizontal curvature


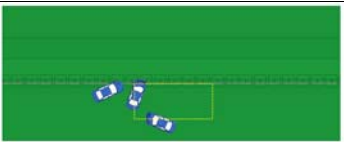


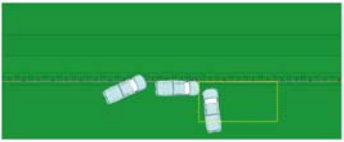





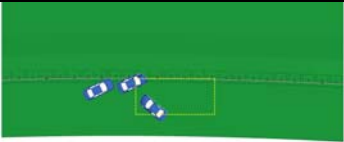


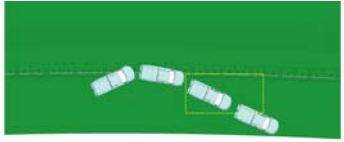



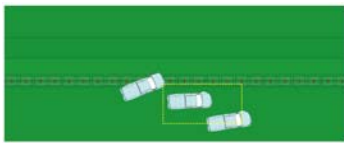


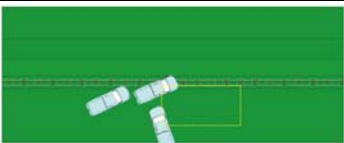
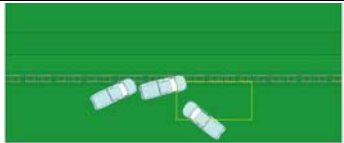
Guardrail Model	Test Vehicle	Guardrail Height	
		29-inch	31-inch
Single-faced	Dodge Neon		
	Dodge Neon (70 mph)		
	Ford F250		
Single-faced with Convex Horizontal Curvature	Dodge Neon		
	Ford F250		
Single-faced with Concave Horizontal Curvature	Dodge Neon		
	Ford F250		

Table 4.9 summarizes vehicle trajectories for the front-side impacts on the 29- and 31-inch double-faced guardrails with and without a lowered backside rail. In all the simulations, the impact speed was 62 mph (100 km/hour) and the impact angle was 25°.

It can be seen from the results in Table 4.9 that the double-faced guardrail, particularly at 31-inch rail height, had reduced the severity of tire snagging for both Dodge Neon and Ford F250, compared to the single-faced guardrails. In regards to the Dodge Neon simulations, although tire snagging was not as severe as seen on the single-faced guardrail, the vehicle spin-out still existed and the MASH exit box criterion was not met for all Dodge Neon simulations.

Table 4.9: Vehicle redirection characteristics of front-side impacts on double-faced guardrails

Guardrail Model	Test Vehicle	Guardrail Height	
		29-inch	31-inch
Double-faced	Dodge Neon		
	Ford F250		
Double-faced with lowered backside rail	Dodge Neon		
	Ford F250		

For the Ford F250 impacting the front-side rail of the 29-inch double-faced guardrail without a lowered backside rail, the vehicle remained in contact with the guardrail and passed the MASH evaluation criterion *N*. For the 31-inch guardrail without a lowered backside rail, the vehicle was successfully redirected by the guardrail with a small exit angle but did not pass the MASH exit-box criterion (vehicle left exit box before traversing through the full length of the exit box). For the double-faced guardrails with lowered backside rails, the Ford F250 snagged on a post and spun away from the guardrail. There is a possibility of the vehicle being involved in a secondary collision.



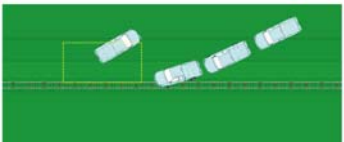



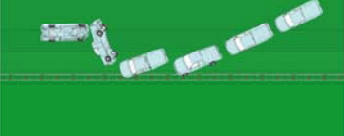

Table 4.10 summarizes vehicle trajectories of the backside impacts on the 29- and 31-inch double-faced guardrails with and without a lowered backside rail. In all the simulations, the impact speed was 62 mph (100 km/hour) and the impact angle was 25°.

It can be seen from the results in Table 4.10 that the double-faced guardrails at both 29- and 31-in rail heights, when impacted from the backside, could safely redirect the Dodge Neon and retain the Ford F250 within the sloped median. The double-faced guardrails with a lowered backside rail were able to retain both vehicles within the sloped median, but caused both vehicles to roll over at 29-inch rail height and caused the Dodge Neon to roll over at 31-inch rail height.

- In regards to the Dodge Neon simulations, the double-faced guardrails without a lowered backside rail passed the MASH exit-box criterion at both 29- and 31-inch rail heights. In the simulations with a lowered backside rail, both the MASH evaluation criterion *F* and evaluation criterion *N* were not met due to the large roll angles of the vehicle.

- For the Ford F250 impacting the backside rail of double-faced guardrails with and without a lowered backside rail, the MASH exit box criterion was either not met or not applicable (due to vehicle rollover). For the 29-inch guardrail with a lowered backside rail, the MASH evaluation criterion F and evaluation criterion N were not met due to the vehicle failing to remain upright. In all the four simulation cases, the double-faced guardrails were able to retain the Ford F250 within the sloped median. Therefore, it is unlikely the Ford F250 would be involved in a secondary collision.

Table 4.10: Vehicle redirection characteristics of backside impacts on double-faced guardrails

Guardrail Model	Test Vehicle	Guardrail Height	
		29-inch	31-inch
Double-faced	Dodge Neon		
	Ford F250		
Double-faced with lowered backside rail	Dodge Neon		
	Ford F250		

In summary, the double-faced guardrails without a lowered backside rail, were shown to have improved performance over single-faced guardrails at both 29- and 31-inch rail heights. The double-faced guardrails with a lowered backside rail, however, tend to cause vehicle rollover when struck from the backside .

5. Findings and Conclusions

In this project, finite element simulations were conducted to study the performance of single- and double-faced W-beam guardrails on a sloped median at 29- and 31-inch guardrail heights. The single-faced guardrail designs were evaluated using impact cases with and without horizontal curvature; whereas, the double-faced guardrail designs had impact cases with and without a lowered backside rail. The single-faced guardrails without horizontal curvature as well as all of the double-faced guardrails were evaluated when placed on a 2.5H:1V slope. For the single-faced guardrails with horizontal curvature, the guardrail with convex horizontal curvature was placed on a 2.5H:1V slope and the guardrail with concave horizontal curvature was placed on a 4H:1V slope. The first double-faced guardrail design had the front-side and backside rails installed at the same elevation; thus the backside ground-to-rail-top height was slightly higher than the placement height due to the slope of the median. The second double-faced guardrail design had the backside rail lowered by 2.1 in (53.3 mm) to allow the ground-to-rail-top height of backside rail to match the ground-to-rail-top height of the front-side rail. All single-faced guardrails were evaluated using front-side impacts only, and all double-faced guardrails were evaluated for both front-side and backside impacts. In the backside impacts, the test vehicles were placed on the opposite side of the sloped median and traversed through both sides of the sloped median before impacting the backside rail. The impact simulations were performed using a 1996 Dodge Neon passenger car and a 2006 Ford F250 pickup truck at an impact speed of 62 mph (100 km/hour) and at an impact angle of 25°. Two additional simulations were performed to evaluate the single-faced guardrail without horizontal curvature at both guardrail heights, impacted by the Dodge Neon at an impact speed of 70 mph (112.6 km/hour) and 25°. The simulation results provided insight into the vehicle redirection characteristics as well as guardrail performance in relation to guardrail heights when placed on a sloped median. Some of the major research findings are summarized as follows.

- In the cases of the single-faced guardrails with and without horizontal curvature and the cases of front-side impacts of the double-faced guardrails with and without a lowered backside rail, the Dodge Neon experienced tire snagging and undesirable post-impact trajectories (e.g., high exit angles) in all cases and failed to meet the MASH exit-box criterion. This was true for both 29- and 31-inch rail heights. For the Ford F250 impacts on the same guardrail designs specified above, the vehicle had three post-impact responses: 1) tire snagging and undesirable high exit angles; 2) tire snagging and remaining in contact with the guardrail; and 3) being redirected by the guardrail with a large exit angle failing the MASH exit-box criterion.
- In the two additional Dodge Neon simulations, the 29- and 31-inch single-faced guardrails without horizontal curvature were evaluated at an impact speed of 70 mph (112.6 km/hour) and found to have similar post-impact behavior to the 62 mph (100 km/hour) impacts. The 29-inch single-faced guardrail had a larger exit angle and maximum dynamic deflection in the 70 mph (112.6 km/hour) impact than the 62 mph (100 km/hour) impact. For the 31-inch guardrail, the exit angle was 3° smaller but the maximum dynamic deflection was larger for the 70 mph (112.6 km/hour) impact than the 62 mph (100 km/hour) impact.

- For the backside impacts of the 29- and 31-inch double-faced guardrails without a lowered backside rail, the guardrails could safely redirect the Dodge Neon and met the MASH exit-box criterion. For the Ford F250, both 29- and 31-inch guardrails without a lowered backside rail caused tire snagging, resulted in large exit angles, and failed to meet the MASH exit-box criterion. Nevertheless, the guardrails were able to retain the Ford F250 within the sloped median, which would likely prevent the vehicle from being in a secondary collision. The double-faced guardrails, although capable of redirecting or retaining the vehicle within the sloped median, had a large chance of causing vehicle rollover.
- It was observed that the maximum dynamic deflection of the guardrails were relatively small and localized in all the impacts. The guardrail deflections were generally larger on the 31-inch guardrails than those on the 29-inch guardrails for the same vehicle. With the exception of a few impacts in which the vehicle remained in contact with the guardrail due to tire snagging and caused the largest maximum dynamic deflection of the guardrails. In cases where the vehicles were redirected with small exit angles or the vehicles were overturned, the guardrails had the smallest maximum dynamic deflections. It was observed that for impacts by the same vehicle, the maximum dynamic deflections on all double-faced guardrails were smaller than those on the single-faced guardrails. A possible reason for the reduced dynamic deflection could be due to the added rigidity and support gained from the backside rail. Under impacts of the Dodge Neon, the single-faced guardrails at both guardrail heights (i.e., 29 and 31 inches) had the smallest maximum dynamic deflections in the cases with convex horizontal curvature and the largest in the cases with concave horizontal curvature. Under impacts of the Ford F250, the single-faced guardrails with and without horizontal curvature generally had smaller maximum dynamic deflections at 29-inch rail height than the 31-inch rail height. For impacts on the double-faced guardrails at both guardrails heights (i.e., 29 and 31 inches), the guardrail designs with a lowered backside rail had larger maximum dynamic deflections than the double-faced guardrail designs without a lowered backside rail.
- The MASH evaluation criterion F , which specified a maximum roll or pitch angle of 75° , was satisfied in all the simulations except for three cases: two Dodge Neon simulations and one Ford F250 simulation of backside impacts on the double-faced guardrails with a lowered backside rail.
- In all the impact cases evaluated in this study, the vehicles were retained on the impacting side of the guardrail without fully over-riding or under-riding the guardrail, which would eliminate the possibility of a vehicle penetrating into oncoming travel lanes and causing a head on collision.

The simulation results suggest that the double-faced W-beam guardrails at 29- and 31-inch placement heights installed on a 2.5H:1V slope could safely redirect the Dodge Neon impacting the guardrail at 25° and satisfied the MASH exit-box criterion. In both cases, the vehicles were safely redirected with small exit angles. The 29-inch guardrail resulted in slightly better vehicle redirection characteristics (i.e., smaller exit angle and maximum

dynamic deflection) than the 31-inch guardrail under the same impact conditions. The Ford F250 was redirected by the guardrail in two impacts: the front-side impact on the 31-inch double-faced guardrail and the 31-inch single-faced guardrail with concave horizontal curvature. Although, the MASH exit-box criterion was not satisfied due to the post-impact trajectories, these two cases can be considered safe due to the small chance of the vehicle being involved in a secondary collision. In four separate simulations using the Ford F250, the guardrail was conveyed behind vehicle's tire during the impact and remained in contact for the duration of the simulation till the vehicle's velocity was reduced to zero. The four simulations were: front-side impact on the 29-inch double-faced guardrail, both the 29- and 31-inch single-faced guardrails with convex horizontal curvature, and the 29-inch single-faced guardrail with concave horizontal curvature.

It should be noted that in most of the simulation results the vehicles experienced spin-out caused by tire snagging or pocketing. This common outcome can be attributed to the fact that the impact location for all of the simulations in this study represents the worst-case scenario by impacting directly on a guardrail post. The simulation results of this project can be used to interpret the performance trends of W-beam guardrails. They should not be used to draw definitive conclusions about their performance for a specific crash event because some factors that could affect the performance were not considered in the simulations for this project. These factors included, but were not limited to, impact locations along the longitudinal axis of the barriers, soil conditions, and driver behaviors. Nevertheless, finite element analysis has demonstrated to be a useful tool in crash analysis and could be used in future investigations of other research issues.

6. Recommendations

Based on the simulation results for this project, it was determined that all guardrail designs were able to retain the vehicle on the impacting side of the guardrail. The 29- and 31-inch double-faced W-beam guardrails without a lowered backside rail were shown to reduce tire snagging and improve the post-impact vehicle trajectories when impacted by the pickup truck from the front-side. These two guardrails could also safely redirect the Dodge Neon and retain the Ford F250 in backside impacts. Based on the evaluation considering the post-impact vehicle trajectory, MASH exit-box criterion, MASH evaluation criteria F and N , transverse velocity, and maximum dynamic deflection of the guardrail, the 29- and 31-inch guardrail without a lowered backside rail are recommended over the double-faced guardrail with a lowered backside rail.

In this study, the double-faced guardrails were evaluated at locations along the shoulder line next to the median slope. It is recommended that other types and/or sizes of blockout be investigated to solve or alleviate the tire snagging problem.

7. Implementation and Technology Transfer Plan

The simulation results of this project will be submitted to NCDOT for consideration in future projects to install or retrofit W-beam guardrails when allowed by site conditions and deemed necessary by NCDOT personnel. Detailed simulation results will be provided to NCDOT engineers for a comprehensive understanding in evaluating proposed roadside features and/or improving the safety performance of the current system. The modeling and simulation work, along with research findings, will be presented at technical conferences and submitted for publication in technical journals to help researchers and DOT engineers nationwide with similar needs. The research results of this project will be distributed to the public through this report, which will be made available by NCDOT.

References

1. AASHTO (2011). *Roadside Design Guide*, 4th edition, American Association of State Highway and Transportation Officials, Washington, D.C.
2. Abu-Odeh, A. Y., Bligh, R. P., Bullard, D. L., Menges, W. L., (2008). "Crash Testing and Evaluation of the Modified G4(1S) W-beam Guardrail on 2:1 Slope." *Report 405160-4-1*, Texas A&M Transportation Institute, College Station, TX.
3. Abu-Odeh, A. Y., Albin R. B., and Olson, D. K., (2013). "A new MASH Compliant Guardrail System for Placement on Slope." *2013 TRB Annual Meeting*, Washington, D.C.
4. Abu-Odeh, A. Y., Bligh, R. P., Odell, W., Meza, R., Manges, W. L., (2013). "A MASH Compliant W-Beam Median Guardrail System." *2014 TRB Annual Meeting*, Washington, D.C.
5. Alluri, P., Haleem, K., and Gan, A., (2012). "In-Service Performance Evaluation (ISPE) for G4 (1S) Type of Strong-Post W-Beam Guardrail System and Cable Median Barrier: Volume I." *Final Report FDOT BDk80 977-19*, State of Florida Department of Transportation, Tallahassee, FL.
6. Atahan, A. O., (2002). "Finite element simulation of a strong-post W-beam guardrail system." *Simulation*, 78(10), 587-599.
7. Atahan, A. O., (2003). "Impact behavior of G2 steel weak-post W-beam guardrail on nonlevel terrain." *International Journal of Heavy Vehicle Systems*, 10(3), 209-223.
8. Bligh, R. P., and Mak, K. K., (1999). "Crashworthiness of roadside features across vehicle platforms." *Transportation Research Record*, 1690, 68-77.
9. Bligh, R. P., Abu-Odeh, A. Y., Hamilton, M. E., and Seckinger, N. R., (2004). "Evaluation of roadside safety devices using finite element analysis." *Report 0-1816-1*, Texas A&M Transportation Institute, College Station, TX.
10. Bligh, R. P., Miaou, S.-P., Lord, D., and Cooner, S., (2006). "Median barrier guidelines for Texas." *Report 0-4254-1*, Texas A&M Transportation Institute, College Station, TX.
11. Donnell, E. T., Harwood, D. W., Bauer, K. M., Mason, J. M., and Pietrucha, M. T., (2002). "Cross-median collisions on Pennsylvania interstates and expressways." *Transportation Research Record*, 1784, 91-99.
12. Dorcely, J., and McKyes, E., (2010). "Post-Soil Interactions on Guardrails Near the Crown of a Slope." *Transportation Research Record: Journal of the Transportation Research Board*, 2186, 147-153.
13. Fang, H., Li, N., Tian, N., (2010). "Median barrier placement on six-lane, 46-foot median divided freeways." *Final Report NCDOT 2009-04*, North Carolina Department of Transportation, Raleigh, NC.
14. Fang, H., Gutowski, M., Li, N., DiSogra, M., (2013). "Performance Evaluation of NCDOT W-beam Guardrails under MASH TL-2 Conditions." *Final Report NCDOT 2012-11*, North Carolina Department of Transportation, Raleigh, NC.
15. Ferdous, M. R., Abu-Odeh, A., Bligh, R. P., Jones, H. L., Sheikh, N. M., (2011). "Performance limit analysis for common roadside and median barriers using LS-DYNA." *International Journal of Crashworthiness*, 16(6), 691-706.

16. Ferdous, M. R., Abu-Odeh, A., Bligh, R. P., Jones, H. L., (2013). "Placement of traffic barriers on roadside and median slopes – guidelines based on numerical simulations." *International Journal of Crashworthiness*, 18(2), 110-125.
17. Findley, D. J., Cunningham, C. M., Schroeder, B. J., Vaughan, C. L., Fowler, T. J., (2012). "Structural and safety investigation of statewide performance of weathered steel beam guardrail in North Carolina" *Transportation Research Record: Journal of the Transportation Research Board*, 2309, 63-72.
18. Gabauer, D. J., Kusano, K. D., Marzougui, D., Opiela, K., Hargrave, M., Gabler, H. C., (2010). "Pendulum testing as a means of assessing the crash performance of longitudinal barrier with minor damage." *International Journal of Impact Engineering*, 37(11), 1121-1137.
19. Gabler, H. C., Gabauer, D. J., and Bowen, D., (2005). "Evaluation of cross median crashes." *Final Report FHWA-NJ-2005-004*, Rowan University, Glassboro, NJ.
20. Gabler, H. C. and Gabauer, D. J., (2006). "Safety audit of fatalities and injuries involving guide rail." *Final Report FHWA-NJ-2007-001*, Virginia Tech, Blacksburg, VA.
21. Graham, J. L., Harwood, D. W., Richard, K. R., O'Laughlin, M. K., Donnell, E. T., Brennan, S. N., (2014). "NCHRP Report 794, Median Cross-Section Design for Rural Divided Highways." *Transportation Research Board's National Cooperative Highway Research Program*, Washington D.C.
22. Hampton, C. E., Gabauer, D. J., Gabler, H. C., (2010). "Limits of acceptable rail-and-post deflection in crash-damaged strong-post W-beam guardrail" *Transportation Research Record: Journal of the Transportation Research Board*, 2195, 95-105.
23. Hampton, C. and Gabler, H., (2013). "Development of a missing post repair guideline for longitudinal barrier crash safety." *Journal of Transportation Engineering*, 139(6), 549–555.
24. Hiser, N. R., and Reid, J. D., (2005). "Modeling slip base mechanisms." *International Journal of Crashworthiness*, 10(5), 463-472.
25. Hiss, J. G. F., Jr., and Bryden, J. E. (1992). "Traffic barrier performance." *Report 155*, New York State Department of Transportation, Albany, NY.
26. Hu, W., Donnell, E. T., (2010). "Median barrier crash severity: some new insights" *Accident Analysis & Prevention*, 42(6), 1697-1704.
27. Hughes, W. E., (2004). "Improved guidelines for median safety." *NCHRP 17-14*, Transportation Research Board, National Research Council, Washington, D.C.
28. Kan, C.-D., Marzougui, D., Bahouth, G. T., and Bedewi, N. E., (2001). "Crashworthiness evaluation using integrated vehicle and occupant finite element models." *International Journal of Crashworthiness*, 6, 387-398.
29. Lewis, B. A., (2004). "Manual for LS-DYNA soil material model 147." *FHWA-HRT-04-095*, U.S. Department of Transportation, Federal Highway Administration, McLean, VA.
30. LSTC (2013). "LS-DYNA Keyword User's Manual – Volume I, Version R7.0." Livermore Software Technology Corporation (LSTC), Livermore, CA.
31. Lynch, J. M., Crowe, N. C., and Rosendahl, J. F., (1993). "Interstate across median accident study: a comprehensive study of traffic accidents involving errant vehicles which cross the median divider strips on North Carolina interstate highways." *1993 AASHTO Annual Meeting Proceedings*, AASHTO, 125-133.

32. Mackerle, J., (2003). "Finite element crash simulations and impact-induced injuries: an addendum. A bibliography (1998–2002)." *The Shock and Vibration Digest*, 35(4), 273-280.
33. Mak, K.K., and Bligh, R.P., (2002). "Assessment of NCHRP Report 350 test conditions." *Transportation Research Record 1797*, 38-43.
34. Mak, K. K., and Sicking, D. L., (2003). "NCHRP Report 492 roadside safety analysis program (RSAP) – engineer's manual." *Transportation Research Board*, 7-28.
35. Marzougui, D., Bahouth, G., Eskandarian, A., Meczkowski, L., and Taylor, H. (2000). "Evaluation of portable concrete barriers using finite element simulation." *Transportation Research Record*, 1720, 1-6.
36. Marzougui, D., Zink, M., Zaouk, A. K., Kan, C.-D., and Bedewi, N. E. (2004). "Development and validation of a vehicle suspension finite element model for use in crash simulations." *International Journal of Crashworthiness*, 9(6), 565-576.
37. Marzougui, D., Mohan, P., Kan, C.-D., and Opiela, K. S. (2007). "Evaluation of rail height effects on the safety performance of W-beam barriers." *2007 TRB Annual Meeting*, Washington, D.C.
38. Marzougui, D., Mohan, P., Kan, C.-D., and Opiela, K. S. (2012). "Assessing options for improving barrier crashworthiness using finite element models and crash simulations." *Final Report NCAC-2012-W-008*, National Crash Analysis Center, George Washington University, Washington, D.C.
39. Marzougui, D., Opiela, K. S., and Kan, C.-D. (2015). "Analyses of Vehicle Trajectories when Leaving the Traveled Way on Curved, Superelevated Road Sections." *Transportation Research Board 94th Annual Meeting*, No. 15-5838.
40. MASH (2009). "Manual for assessing safety hardware (MASH)." American Association of State Highway and Transportation Officials (AASHTO), Washington D.C.
41. Miaou, S.-P., Bligh, R. P., and Lord, D., (2005). "Developing guidelines for median barrier installation: benefit-cost analysis with Texas data." *Transportation Research Record*, 1904, 3-19.
42. Mohan, P., Marzougui, D., and Kan, C.-D., (2007). "Validation of a single unit truck model for roadside hardware impact." *International Journal of Vehicle Systems Modelling and Testing*, 2(1), 1-15.
43. Mongiardini, M., and Reid, J. D. (2013). "Investigation of a series of relevant phenomena for modeling the full-scale crash test of a small vehicle with a guardrail system." *International Journal of Computer Aided Engineering and Technology*, 5(1), 58-75.
44. Murray, Y. D., Reid, J. D., Faller, R. K., Bielenberg, B. W., and Paulsen, T. J., (2005). "Evaluation of LS-DYNA wood material model 143." *FHWA-HRT-04-096*, U.S. Department of Transportation, Federal Highway Administration, McLean, VA.
45. Murray, Y. D., (2007). "User manual for LS-DYNA concrete material model 159." *FHWA-HRT-05-062*, U.S. Department of Transportation, Federal Highway Administration, McLean, VA.
46. NCAC (web1). "NCAC Finite Element Models." <<http://www.ncac.gwu.edu/vml/models.html>>.
47. NCAC (web2). "NCAC Publications." <<http://www.ncac.gwu.edu/filmlibrary/publications.html>>.
48. NCAC (2008). "Technical Summary – NCAC 2008-T-003: Development & Validation of a Finite Element Model for the 2006 Ford F250 Pickup Truck." <<http://www.ncac.gwu.edu/research/pubs/NCAC-2008-T-003.pdf>>

49. NCAC (2007a). "Technical Summary – NCAC 2007-T-007: Development & Validation of a Finite Element Model for the 1996 Dodge Neon Passenger Sedan."
<<http://www.ncac.gwu.edu/research/pubs/NCAC-2007-T-007.pdf>>
50. NCAC (2007b). "Technical Summary – NCAC 2007-T-004: Development of a Finite Element Model for W-beam Guardrails." <<http://www.ncac.gwu.edu/research/pubs/NCAC-2007-T-004.pdf>>
51. NCHRP 22-21 (2011). "Project 22-21: median cross-section design for rural divided highways."
<<http://apps.trb.org/cmsfeed/TRBNetProjectDisplay.asp?ProjectID=694>>.
52. NCHRP 22-22 (2010). "Project 22-22: placement of traffic barriers on roadside and median slopes." <<http://apps.trb.org/cmsfeed/TRBNetProjectDisplay.asp?ProjectID=695>>.
53. NCHRP 22-27 (2012). "Project 22-27: roadside safety analysis program (RSAP) update."
<<http://apps.trb.org/cmsfeed/TRBNetProjectDisplay.asp?ProjectID=2517>>.
54. Nicol, D. A., (2010) "Roadside Design: Steel Strong Post W-beam Guardrail." *Memorandum 051710*, U.S. Department of Transportation, Federal Highway Administration, McLean, VA.
55. Ochoa, C. M., Ochoa, T. A., (2011) "Guardrail optimization for rural roads." *Transportation Research Board of the National Academies*, 2203, 71-78.
56. Orengo, F., Ray, M. H., and Plaxico, C. A., (2003). "Modeling tire blow-out in roadside hardware simulations using LS-DYNA." *IMECE2003-55057*, 2003 ASME International Mechanical Engineering Congress & Exposition, Washington, D.C.
57. Patzner, G. S., Plaxico, C. A., and Ray, M. H., (1999). "Effects of post and soil strength on performance of modified eccentric loader breakaway cable terminal." *Transportation Research Record*, 1690, 78-83.
58. Plaxico, C. A., Hackett, R. M., and Uddin, W., (1997). "Simulation of a vehicle impacting a modified thrie-beam guardrail." *Transportation Research Record*, 1599, 1-10.
59. Plaxico, C. A., Patzner, G. S., and Ray, M. H., (1998). "Finite element modeling of guardrail timber posts and the post-soil interaction." *Transportation Research Record*, 1647, 139-146.
60. Plaxico, C. A., Ray, M. H., and Hiranmayee, K., (2000). "Impact performance of the G4(1W) and G4(2W) guardrail systems: comparison under NCHRP Report 350 test 3-11 conditions." *Transportation Research Record*, 1720, 7-18.
61. Plaxico, C. A., Mozzarelli, F., and Ray, M. H., (2003). "Tests and simulation of a w-beam rail-to-post connection." *International Journal of Crashworthiness*, 8(6), 543-551.
62. Ray, M. H., (1996a). "Repeatability of full-scale crash tests and criteria for validating simulation results." *Transportation Research Record*, 1528, 155-160.
63. Ray, M. H., (1996b). "Use of finite element analysis in roadside hardware design." *Transportation Research Circular*, 453, 61-71.
64. Ray, M. H., and McGinnis, R. G., (1997). "Guardrail and median barrier crashworthiness: synthesis of highway practice." Transportation Research Board, Washington, D.C.
65. Ray, M. H., and Patzner, G. S., (1997). "Finite element model of modified eccentric loader terminal (MELT)." *Transportation Research Record*, 1599, 11-21.
66. Ray, M. H., and Weir, J. A., (2001). "Unreported collisions with post-and-beam guardrails in Connecticut, Iowa, and North Carolina." *Transportation Research Record*, 1743, 111-119.

67. Ray, M. H., Weir, J., and Hopp, J., (2003). "In-service performance of traffic barriers." *NCHRP Report 490*, Transportation Research Board, National Research Council, Washington, D.C.
68. Ray, M. H., Oldani, E., and Plaxico, C. A., (2004). "Design and analysis of an aluminum F-shape bridge railing." *International Journal of Crashworthiness*, 9(4), 349-363.
69. Reid, J. D., (1996). "Towards the understanding of material property influence on automotive crash structures." *Thin-Walled Structures*, 24, 285-313.
70. Reid, J. D., (1998). "Admissible modeling errors or modeling simplifications?" *Finite Elements in Analysis and Design*, 29, 49-63.
71. Reid, J. D., (2004). "LS-DYNA simulation influence on roadside hardware." *Transportation Research Record*, 1890, 34-41.
72. Reid, J. D., and Bielenberg, B. W., (1999). "Using LS-DYNA simulation to solve a design problem: bullnose guardrail example." *Transportation Research Record*, 1690, 95-102.
73. Reid, J. D., and Marzougui, D., (2002). "Improved truck model for roadside safety simulations: Part I - structural modeling." *Transportation Research Record*, 1797, 53-62.
74. Reid, J. D., Coon, B. A., Lewis, B. A., Sutherland, S. H., and Murray, Y. D., (2004). "Evaluation of LS-DYNA soil material model 147." *FHWA-HRT-04-094*, U.S. Department of Transportation, Federal Highway Administration, McLean, VA.
75. Reid, J. D., and Hiser, N. R., (2004). "Friction modelling between solid elements." *International Journal of Crashworthiness*, 9(1), 65-72.
76. Reid, J. D., and Hiser, N. R., (2005). "Detailed modeling of bolted joints with slippage." *Finite Elements in Analysis and Design*, 41, 547-562.
77. Reid, J. D., Kuipers, B. D., Sicking, D. L., and Faller, R. K., (2009). "Impact performance of W-beam guardrail installed at various flare rates." *International Journal of Impact Engineering*, 36, 476-485.
78. Ross, H. E. Jr., and Sicking, D. L., (1984). "Guidelines for placement of longitudinal barriers on slopes." *Transportation Research Record*, 970, 3-9.
79. Ross, H. E. Jr., Sicking, D. L., Zimmer, R. A., and Michie, J. D., (1993). "Recommended procedures for the safety performance evaluation of highway features." *NCHRP Report 350*, Transportation Research Board, National Research Council, Washington, D.C.
80. Schrum, K.D., Lechtenberg, K.A., Bielenberg, R.W., Rosenbaugh, S.K., Faller, R.K., Reid, J.D., and Sicking, D.L., (2013). "Safety performance evaluation of the non-blocked midwest guardrail system (MGS)." Midwest Roadside Safety Facility. TRP-03-262-12.
81. Tiso, P., Plaxico, C., and Ray, M., (2002). "Improved truck model for roadside safety simulations: Part II - suspension modeling." *Transportation Research Record*, 1797, 63-71.
82. Whitworth, H. A., Bendidi, R., Marzougui, D., and Reiss, R., (2004). "Finite element modeling of the crash performance of roadside barriers." *International Journal of Crashworthiness*, 9(1), 35-43.
83. Zaouk, A. K., Bedewi, N. E., Kan, C.-D., and Marzougui, D., (1997). "Development and evaluation of a C-1500 pickup truck model for roadside hardware impact simulation." *FHWA-RD-96-212*, Federal Highway Administration, Washington, D.C.
84. Zaouk, A. K., Marzougui, D., and Bedewi, N. E., (2000a). "Development of a detailed vehicle finite element model, Part I: methodology." *International Journal of Crashworthiness*, 5(1), 25-36.

85. Zaouk, A. K., Marzougui, D., and Kan, C.-D., (2000b). "Development of a detailed vehicle finite element model, Part II: material characterization and component testing." *International Journal of Crashworthiness*, 5(1), 37-50.
86. Zweden, J. V., and Bryden, J. E., (1977). "In-service performance of highway barriers." *Report NYSDOT-ERD-77-RR51*, New York State Department of Transportation, Albany, NY.